REPUBLIQUE DU CAMEROUN
Paix – Travail – Patrie
****
UNIVERSITE DE YAOUNDE I
FACULTE DES SCIENCES
DEPARTEMENT DE PHYSIQUE
****

REPUBLIC OF CAMEROUN
Peace – Work – Fatherland
****
UNIVERSITY OF YAOUNDE I
FACULTY OF SCIENCE
DEPARTMENT OF PHYSICS
****

DISCRETE EXCITON DYNAMICS OF THE DAVYDOV MODEL WITH SATURABLE NONLINEARITIES

THESIS
Submitted in partial fulfillment of the requirements for the award of the degree of Doctorat/PhD in Physics

Par : **TCHINANG TCHAMEU JOËL DUREL**
Master in Physics

Sous la direction de
TCHAWOUA Clément
Professor
University of Yaounde I

Année Académique : 2019

UNIVERSITE DE YAOUNDE I
UNIVERSITY OF YAOUNDE I

FACULTE DES SCIENCES
FACULTY OF SCIENCE

DEPARTEMENT DE PHYSIQUE
DEPARTMENT OF PHYSICS

ATTESTATION DE CORRECTION DE LA THESE DE DOCTORAT/Ph.D

Nous, Professeur **SIEWE SIEWE Martin** et Professeur **NDJAKA Jean-Marie Bienvenu**, respectivement Examinateur et Président du jury de la Thèse de Doctorat/Ph.D de Monsieur **TCHINANG TCHAMEU Joël Durel**, Matricule **03Z374,** préparée sous la direction du Professeur **TCHAWOUA Clément,** intitulée : **«DISCRETE EXCITON DYNAMICS OF THE DAVYDOV MODEL WITH SATURABLE NONLINEARITIES»**, soutenue le **Vendredi 20 Décembre 2019**, en vue de l'obtention du grade de Docteur/Ph.D en Physique, Spécialité **Mécanique, Matériaux et Structures** option **Mécanique Fondamentale et Systèmes Complexes,** attestons que toutes les corrections demandées par le jury de soutenance ont été effectuées.

En foi de quoi, la présente attestation lui est délivrée pour servir et valoir ce que de droit.

Fait à Yaoundé, le 21 JAN 2020

Examinateur

SIEWE SIEWE Martin
Maître de Conférences

Le Président du jury

NDJAKA Jean-Marie Bienvenu
Professeur

Le Chef de Département de Physique

UNIVERSITE DE YAOUNDE I ★ FACULTE DES SCIENCES ★ DEPARTEMENT DE PHYSIQUE
Le Chef de Département

Ndjaka Jean-Marie Bienvenu
Professeur

Contents

List of Figures

List of Tables

Dedication

In loving memory of my Father, ***Pierre TCHINANG*** (1957-2016).

Acknowledgments

I would like to express my gratitude to all those who gave me the possibility to complete this thesis. First, I give thanks to Pr. NDJAKA Jean-Marie Bienvenu, Head of the Department of Physics, for having provided me with all the facilities to carry out this research work.

I am so grateful to Pr. KOFANE Timoléon, head of the laboratory of Mechanics, for making it possible for me to study here.

I am deeply indebted to my advisor Pr. TCHAWOUA Clément for supporting me over the years; for his patience, motivation, enthusiasm, and editing skills in helping me to structure this thesis and to publish articles from this research work. Apart from this thesis topic, I learnt a lot from him like the soft skills. Without You my doctoral research would not have seen the light of the day. Thank you, so very much.

I extend my sincere thanks to all members of the jury: Pr. NDJAKA Jean-Marie Bienvenu, Pr. TCHAWOUA Clément, Pr. WOAFO Paul, Pr. MOHAMADOU ALIDOU, Pr. FEWO Serge Ibraïd, and Pr. SIEWE SIEWE Martin for agreeing to read the manuscript and to participate in the defense of this thesis.

I am also very grateful to all the teaching staff of the Department of Physics at the University of Yaounde I that have provided me with basic tools required for the postgraduate studies. Pr. NJOMO Donatien and Pr. ZEKENG Serges Sylvain are two of them.

I would also like to thank Pr. MOUKAM KAKMENI François Marie, Dr. TOGUEU MOTCHEYO Alain Bertrand, Dr. MANDENG MANDENG Lucien and Dr. GUEMKAM Patrick for their thorough reading of this thesis, for their helpful comments, and for creating a nice working atmosphere in the lab with regard to some of them.

I thank my fellow labmates and/or my juniors in the research team: Dr. NONO Buckjohn, Dr. TATCHIM David, Dr. NDJOMATCHOUA Thomas Frank, Dr. DJOMO, Dr. MOKEM, FOUPOUAPOUOGNIGNI, FEUZE, DJAKO for their lively company and support which made my working on the research thesis in a non-stressful way.

I would especially like to thank my amazing family for the love, support, and constant encouragement. In particular, I would like to thank the large MBEU PANANG Family and among them: Ngambou Emile, Lefanda, Tchame Chantal, Tchame Pauline, and Tchame Suzanne. I would also like in

this direction to thank the large MBAH ZEFFEU NANA Family and among them: Taphop Njomo Daniel, Ngongang Augustin, Njomo Ghislain, Fosso Simo Cedric, Njomo Kemegni Marcelle, and Tameghe Brenda.

My heart felt regard goes to my father-in-law Djomgoue Emmanuel, mother-in-law Christine, and brother-in-law Teabe Boris for their love and moral support.

Warm thanks to a social welfare organisation named "PHY52" for their friendly supports.

I owe thanks to a very special persons, my first wife and mother, Tchinang Rebecca, as well as my children Tchinang Tatiana, Tchinang Didier, Tchinang Elodie, and Tchinang Laetitia for their continued and unfailing loves, support and understanding during my pursuits.

Last, but not least, I would like to thank my second wife and supportive wife Astrid for her patience and motherly tenderness during all these years. Thanks for your emotional support. Your support has meant more to me than you could possibly realize.

Of course, thanks are due to the ancestors for their various protective shields.

List of Abbreviations

bc: bond-centered

DB: Discrete Soliton

DMHS: Discrete Multihump Soliton

DMRW: Discrete Multi-rogue Waves

DNLS: Discrete Nonlinear Schrödinger

MI: Modulational Instability

next-NNI: next-Nearest-Neighbor Interactions

sc: site-centered

Abstract

In this thesis, we show that the state of amide-I excitations in α-helical proteins is modeled by the discrete nonlinear Schrödinger (DNLS) equation with saturable nonlinearities. This is done by extending the Davydov model to take into account the competition between local compression and local dilatation of the lattice, thus leading to the interplay between self-focusing and defocusing saturable nonlinearities. Site-centered (sc) mode and/or bond-centered (bc) mode like discrete multihump soliton (DMHS) solutions are found numerically and their stability is analyzed. As a result, we obtained the existence and stability diagrams for all observed types of sc DMHS solutions. We also note that the stability of sc DMHS solutions depends not only on the value of the interpeak separation but also on the number of peaks, while their counterpart having at least one intersite soliton is instable. A study of mobility is achieved and it appears that, depending on the higher-order saturable nonlinearity, DMHS-like mechanism for vibrational energy transport along the protein chain is possible.

Subsequently, the influence of next-nearest-neighbor interactions (next-NNI) of dipole-dipole type is analyzed in Davydov model with saturable nonlinearities. We analytically study the regions of discrete modulational instability (MI) of plane carrier waves and it appears that this region decreases as the number of nearest neighbors, m, increases. We also show via the instability growth rate (gain) that when m increases, bandwidth of instability decreases. Otherwise, it is noted that the saturation also has an antagonistic effect on the gain. Numerical simulations indicate that the presence of next-NNI induced downward corrections of the time of onset of MI. After having sought Discrete Soliton (DS) and Discrete Multihump soliton (DMHS) numerically with $m = 1$; 2; 3, the next-nearest neighbor dependence of the width and height of these solutions is discussed. A study of mobility is achieved and it results that next-NNI increase the speed of DMHS. Furthermore, the collisions of two DMHS are performed and it emerges mainly that next-NNI lead to the formation of large stationary solitons.

As a second step, we show that the transport of vibrational energy in protein chains modeled by the DNLS equation with saturable nonlinearities can be done through the nonlinear supratransmission phenomenon: we find numerically and semi-analytically threshold amplitudes beyond which the wave propagation takes place within the molecular chains. Subsequently, it is

shown that the saturable higher order nonlinearity parameter reduces the supratransmission threshold amplitude. We also prove that the discrete gap multibreathers can be transmitted or supratransmitted according to the frequency belonging to the lower forbidden band gap. More precisely, the discrete gap multibreathers are supratransmitted close to the edge of the lower forbidden band.

Thereafter the discrete multi-rogue waves (DMRW) as solution of the discrete nonlinear Schrödinger (DNLS) equation with saturable nonlinearities and small disorder is studied numerically. These biological rogue waves represent the complex probability amplitude of finding an amide-I vibrational quantum at a site. We observe that the growth in the higher order saturable nonlinearity implies the formation of DMRW including an increase in the short-living DMRW and a decrease in amplitude of the long-living DMRW.

And finally, we report numerical observations of scattering process of moving multibreathers by isolated impurities in the discrete nonlinear Schrödinger lattice representing the vibrational energy transport along the protein chain. It is found that, except for the multibreather passing, internal collision phenomenon support all types of scattering outcomes for both attractive and repulsive impurities. Furthermore, for large strength of attractive impurity the scattering of two-hump soliton can give rise to a trapping on a site other than the one containing the impurity. As concerns three-hump soliton, the passing, trapping and reflection are simultaneously carried out for some parameters. In the case of three-hump soliton introduced between two repulsive impurity sites, back and forth are observed as well as increasingly individualistic behavior of humps over time. Nonetheless, two-hump soliton launched under the same conditions results in large stationary single breather.

keywords: DNLS equation, Saturable nonlinearity, Discrete Multibreathers, Soliton collisions, Next-NNI, Supratransmission, Discrete multi-rogue waves.

Résumé

Dans cette thèse, nous montrons que l'état vibrationnel du mode amide-I des protéines hélices alpha est modélisé par l'équation discrète de Schrödinger non linéaire (DSNL) avec des non-linéarités saturables. Ceci est obtenu par une extension du modèle de Davydov permettant de prendre en compte la compétition entre la compression et la dilatation locale du réseau, et par suite, la compétition entre les non-linéarités saturables focalisante et défocalisante. Les solitons discrets centrés sur un site, sur deux sites, ainsi que les solitons discrets à plusieurs bosses (SDPB) sont trouvés numériquement et leurs stabilités analysés. A l'issu de cela, nous obtenons les diagrammes d'existence et de stabilité de tous les types de SDPB centrées sur un site. Nous notons aussi que la stabilité des SDPB centrées sur un site dépend non seulement de la distance entre deux pics mais aussi du nombre de pics, pendant que leurs homologues ayant au moins une bosse centrée sur deux sites sont instables. Une étude de la mobilité est réalisée et il apparaît que, en fonction de la non-linéarité saturable d'ordre supérieur, le SDPB comme mécanisme de transport d'énergie vibrationnelle le long de la chaîne de protéine est envisageable.

Par la suite, l'influence de l'interaction dipolaire à longue portée est analysée sur le modèle de Davydov avec des non-linéarités saturables. Dans ce sillage, nous étudions analytiquement les régions d'une instabilité modulationnelle (IM) discrète des ondes planes et il en découle que ces régions décroissent au fur et à mesure que le nombre de plus proches voisins (m) dans les interactions augmente. Nous montrons aussi à travers le gain que lorsque m augmente, la largeur de la bande de l'instabilité décroît. En outre, il est noté que la saturation a aussi un effet antagoniste sur le gain. Les simulations numériques indiquent que la présence des interactions au-delà des premiers voisins (APV) induit une correction à la baisse du temps d'apparition de l'IM. Après avoir trouvé les solitons discrets (SD) et SDPB numériquement pour m=1,2,3 ; la dépendance de la largeur et de la hauteur de ces solutions en fonction de m est discutée. Une étude de la mobilité est ensuite réalisée et il en résulte que les interactions APV accroissent la vitesse des SDPB. Bien plus, la collision de deux SDPB est effectuée et il en ressort principalement que les interactions APV conduisent à la formation de larges solitons stationnaires.

Dans un second temps, nous montrons que le transport de l'énergie vibrationnelle dans une chaîne de protéine modélisée par l'équation DSNL avec des non-linéarités saturables peut être fait à travers le phénomène de supra-

transmission non linéaire : nous cherchons numériquement et semi analytiquement les amplitudes seuils au-dessus desquelles la propagation des ondes prend place dans la chaîne de molécule. Subséquemment, il est établi que le paramètre de non-linéarité saturable d'ordre supérieur réduit l'amplitude seuil de supratransmission. Nous prouvons également que les multibreathers discrets de gap peuvent être transmis ou supratransmis selon que la fréquence appartient au gap inférieur. Plus précisément, les multibreathers discrets de gap sont supratransmis près du bord du gap inférieur.

Bien après, la solution de type onde extrême discrète (OED) découlant de l'équation DSNL avec des non-linéarités saturables et un faible désordre est étudiée numériquement. Cette onde extrême biologique représente l'amplitude de probabilité complexe associée à la probabilité de trouver l'état vibrationnel du mode amide-I dans un site particulier. Nous observons que l'augmentation du coefficient de non-linéarité saturable d'ordre supérieur favorise la formation des multiples OED (MOED), allant de pair avec une promotion des MOED de courtes durées de vie et une décroissance en amplitude des MOED de longues durées de vie.

Finalement, nous répertorions numériquement les différentes interactions entre les SDPB en mouvement et des impuretés ponctuelles dans les réseaux DSNL représentant le transport de l'énergie vibrationnelle dans une chaîne de protéine. Il est démontré que, mis à part le cas de la transmission totale du SDPB, le phénomène de collision interne accompagne tous les types de scénarii liés aux interactions sus-évoquées, aussi bien pour des impuretés attractives que répulsives. De surcroît, pour des fortes valeurs du coefficient de l'impureté attractive, l'interaction entre soliton à deux bosses et impureté peut donner lieu à un piégeage sur un site autre que celui abritant l'impureté. S'agissant des solitons à trois bosses, la transmission, le piégeage et la réflexion sont simultanément enregistrés pour certains paramètres. Dans le cas du soliton à trois bosses introduit entre deux impuretés ponctuelles répulsives, des va-et-vient sont observés ainsi qu'un comportement individualiste croissant des bosses à travers le temps. Toutefois, le soliton à deux bosses lancé dans les mêmes conditions débouche sur un soliton stationnaire de grande amplitude et à une bosse.

Mots-Clefs: Equation DSNL, Non-linéarité saturable, Multibreathers discrets, Collision de solitons, Interactions APV, Supratransmission, Multiple ondes extrêmes discrètes.

General Introduction

During many biological processes, such as muscle contraction, DNA reduplication, neuroelectric pulse transfer on the neurolemma and work of calcium or sodium pump, the bio-energy needed is provided by the hydrolysis of Adenosine TriPhosphate (ATP). This energy has important significance and the comprehension of their storage and transport has been a challenge to scientists. In 1977, Davydov [1] suggested a mechanism based on soliton to contribute to elucidate the problem. Since the previous mentioned work, the possible existence of solitons in bio-molecular systems has been widely studied (see Ref. [2] and references therein). Following Davydov's idea, energy released during ATP hydrolysis is stored in the form of a vibrational energy of the C = O stretching (amide I) oscillators. This energy is transported from one peptide group to the next because of the dipole-dipole coupling between the adjacent groups. Experimentally, the model of Scott and Davydov was tested through the crystalline polymer acetalinide ($(CH_3CONHC_6H_5)_X$), or ACN, which is an organic solid close to a biological molecule [3].

At low temperature it has been shown that Davydov's theory for the alpha-helix gives rise to Discrete Nonlinear Schrödinger (DNLS) equation [4], which is one of the basic lattice models appearing in various contexts of physics and biology. During the past decade, DNLS equations as well as one of their solutions called discrete breather (alias intrinsic localized modes) have been intensively studied [5, 6]. Discrete breather has a bell-shaped form while ones possessing an arbitrary number of extrema is called multibreather. Proof of the existence of the latter is given in Ref. [7], and since this work a great deal of effort has been invested to show their existence in Salerno equation [8], DNLS equation with cubic nonlinearity [9], and Klein-Gordon chain [10]. More recently, multibreathers have been predicted theoretically in realistic systems [11] and observed experimentally [12]. In spite the fact that multihump soliton have been observed in saturable dispersive nonlinear medium [13], their study is not yet done in purely discrete saturable nonlinear equation. **The first purpose of this thesis is to explore the possible existence of multibreathers in DNLS equation with saturable nonlinearities**.

At the beginning of the year 2000, the stability of multibreathers was an open problem (see Ref. [14]). Up to now much effort has gone into their stabilization [10–12, 15], and it's well clear that stable multibreathers can be found. **Could we obtain stable multibreathers in the exciton dynamics modeled**

by DNLS equation with competitive nonlinearities? The answer to this question is the second purpose of this thesis.

It has been observed for several years that discrete breathers could be mobile in some models [16–24]. To the best of our knowledge, a study related to the mobility of multibreathers is not yet done. **As other aims of this thesis, we look for the possible mobile multibreathers in the system**.

One of the most important problems most studied in the field of biomolecular processes is the storage and transport of biological energy in $\alpha-$helical proteins. Davydov, through a soliton mechanisms [25], was the first to offer an answer. Thus, according to him, the formation of soliton results from the balance between the effects of dispersion caused by the resonance interaction of adjacent peptide groups and the interaction of the amide-I excitation with the lattice vibrations (self-localization or self-trapping mechanism). Since then, this model has been refined from now taking into account the effect of temperature [26, 27, 29–31, 98], the geometry [32] of the protein, higher order excitations or coupling interactions [33, 34], the interaction of a charge with intrinsic localized mode [35] and long range interactions [36]. Indeed, in most studies, the dispersive interactions are assumed to be short ranged leading to the nearest neighbor approximation. It turns out that this approximation does not always reflect the physical or biological reality. Thus in an environment where transition dipole-dipole interaction exists with $1/r^3$ dependence on the distance, r, the nearest neighbor approximation no longer holds. It is in this framework that the investigations on the excitation transfer in molecular crystals [25] and energy and charge transport in biological molecules [4, 37] were conducted. The influence of long-range interactions (LRI) has been observed in various fields of physics [38–42] through the study of soliton solutions. In effect, the fundamental question that motivates studies on LRI remains how it can affect the stability and dynamics of soliton solutions?

In the last few years, Aguero et al. [43], in the continuum limit, have shown that collective excitations in a molecular chain like proteins were modeled by the saturable NLS (SNLS) equation. In order to determine the distribution of these excitations, this equation has been simplified leading to the Cubic-Quintic Nonlinear Schrödinger Equation (CQNSE). To the best of our knowledge, the interest of LRI has not registered in biological macromolecule systems by means of DMHS. In the case where the previous purposes were achieved, **the other aim of this thesis is to study the influence of next-**

NNI on DMHS solutions of a DNLS equation with saturable nonlinearities.

The discrete nonlinear Schrödinger equation (DNSE) in its many versions plays a key role in different fields of science, such as biology [1], nonlinear optics [44], solid-state physics [45], and Bose-Einstein condensates [46]. The version of DNSE with saturable nonlinearity represents a vast class of physical systems, ranging from optical pulse propagation in various doped fibres [47, 48], to waveguide arrays in photorefractive strontium barium niobate crystals [49]. Since 1975 where Vinetskii-Kukhtarev model [50] has been introduced, it is recently that a great deal of interest has been drawn to Saturable DNSE [51]. The existence and properties of discrete Solitons (which are also known as intrinsic localized modes) has been considered in preceding studies [51]. Moreover, as an effect of nonlinear modes, gap Solitons in a periodic structure have modeled the wave propagation in the forbidden band of the linear spectrum [53, 87]. This phenomenon has been called nonlinear supratransmission and widely used in many models such as coupled pendulum chain [54], discrete nonlinear electrical transmission lattice [55], birefringent quadratic medium [56], waveguide arrays [57, 58], Frenkel-Kontorova model [59], granular chains [60] and nanostructured multiferroics [61]. From the perspective of nonlinear supratransmission, this phenomenon has technological applications like terahertz frequency selection devices [62] and binary signal transmissions of information [63]. All the above mentioned works study the gap transmission of single hump breathers. Up to now, no work concerning the study of supratransmission phenomenon using multibreathers has been presented in literature in our knowledge. Supratransmitted mutibreather could presumably bring better understanding of energy transport in the proteins within our model. **Study the possibility of supratransmission of the multibreathers is also the purpose of this thesis**.

As indicated above, the Discrete Nonlinear Schrödinger (DNLS) equation is involved in the modeling of several phenomena. These phenomena resulting from interplay between nonlinearity and discreteness such as energy localization in discrete condensed matter and biological systems. Moreover, this energy localization occurs by means of intrinsic localized modes (ILM) or discrete breathers [4, 32, 64] which are spatially localized oscillations of large

amplitude. Among the classes of localized structure, the rigorous proof of existence of ILM having an arbitrary number of extrama and called multi-brethers was done [7]. In this direction the study of their existence has continued in Salerno equation [8], DNLS equation with cubic nonlinearity [9], and Klein-Gordon chain [15]. In addition, multibreathers have been observed in a realistic systems by means of numerical experiment [55].

Besides these localized modes, it is established that there is mode with a double spatio-temporal localization known as Peregrine soliton and solution of the NLS equation [65]. This solution has a particular characteristic in that it maximum wave amplitude exceeds the background amplitude by a factor of 3, and consequently, is qualified as a Rogue Wave (RW) [66]. The name RW or extreme waves owe its origin to the fact that it was previously met in the ocean and described by fishermen like solid walls of water appearing from nowhere and higher than 30 m. Since then, beyond the hydrodynamics, RW have been mentioned in other systems such as optics [67, 68] in order to generate an hight amplitude optical pulse (Optical RW) [69]. In the Bose-Einstein condensates, vector RW have been constructed [70]. Moreover, multi-rogue waves solutions have been obtained analytically for a higher-order nonlinear Schrödinger equation in optical fibers [71].

On the other hand, when the discreteness of the system is taken into account, RW are also noted for Ablowitz-Ladik equation, Hirota equation [72,73], cubic DNLS equation [74] with a small degree of disorder [75]. Recently, it has been shown that the localization and vibrational energy in $\alpha-$helical protein molecules could be modeled by DNLS equation with saturable nonlinearities in continuous medium [43]. Following Bludov's idea who showed that discrete RW can give rise to a localization of all energy into a single (or a few) waveguide(s) of a network [74] and knowing that RW implies a high nonlinearity of the system [76], questions emerge. **Could Discrete Multi-rogue waves (DMRW) be solution of DNLS equation with saturable nonlinearities and randomly distributed molecules around the peptide groups chain? Does biological rogue wave exist in the framework where the dynamic variable is a complex probability amplitude at the n^{th} peptide group? The answers to these questions include aims of this thesis.**

Many problems in solid-state physics are relative to nonlinear localized waves propagation in disordered media (see e.g., Ref. [77] and references therein) because a considerable number of structures in nature are non-

crystalline. However, understanding of such problems requires the study of the interaction of soliton with a single impurity. Due to its numerous applications, solitons play a significant role for the dynamics of ferro- and antiferromagnetic materials [78], phase changes in solids [79], dielectric relaxation in crystalline polyethylene [80], dislocations in crystals, fluxons in Josephson contacts and junctions, etc [81]. Moreover, localized inhomogeneity hit by a soliton can correspond to mass discontinuity in lattice [82, 83], base-pair inhomogeneity [84], sheath ions in plasma [85], electric or magnetic impurities [86], parity-time-symmetric defects [87–89]. Solitary waves involved in the interaction with localized impurity are governed by a variety of equation such as nonlinear sine-Gordon (SG) equation [90], Discrete Nonlinear Schrödinger (DNLS) equation [91–95]. With particular regard to breather, these equations generally highlight four outcomes in the case of an unexcited impurity: passing, trapping, partial and total reflection [96]. It therefore appears that this outcomes play an important role in transport properties of breathers.

Pointing out the transport in condensed matter systems, Davydov showed that, under adiabatic approximation, Hamilton's equations corresponding to exciton-phonon interaction is reduced to the DNLS equation [4]. In addition, a more realistic modeling of the main polypeptide chain provides the need to take into account diagonal disorder standing for the side groups on the geometry of this chain [4, 97, 98].

On the other hand, we intend to show that multibreathers-like mechanism for vibrational energy transport along the protein chain is possible. All in a framework of perfect lattice and particularly at a time when a great deal of attention is paid to the study of multibreathers [13, 55]. Drawing on this, a question arises. Does the impurity can modify the multibreathers dynamics? If so, in what ways? Indeed, to our knowledge, there is no report on the study of the multibreathers scattering by impurities. Although the topic relating to the interaction of breathers with impurity is old, there is an intrinsic difficulty of the problem in the case of multibreathers-impurity interactions due to the lack of analytical expression of multibreathers in discrete systems at this time. It is in this context that our concern is to explore the problem of multibreathers-impurity interactions in DNLS model from a qualitative standpoint, and to a lesser extent from a quantitative standpoint. Motivated by this, **the ultimate objective of the present thesis is to analyze the interaction of moving multibreathers with an isolated impurity in the discrete nonlinear Schrödinger model representing the vibrational energy transport along the protein chain.**

In order to achieve the above-mentioned aims, this manuscript is organized as follows:

- Chapter 1 provides a bief review of the literature on the protein, the bioenergy transport in protein molecules, and localized modes.
- Chapter 2 is devoted to the models that describe the localization and transport of vibrational energy in protein, as well as to numerical methods used to obtain some solutions of these models.
- Chapter 3 presents the results and discussions obtained for each case study.

Concluding remarks and perspectives are given at the end of this manuscript.

CHAPTER 1

Review of literature

1.1 Overview of Protein

1.1.1 Protein Function

Physically, proteins are polymers whose units are the amino acids. Amino acids are simple organic compounds. Their physical and chemical properties can be explained by the presence of both acidic and basic groups in the same molecule. We can distinguish α-amino acids (in which the amino and carboxylic functions are both linked to the same carbon atom) from β, γ, δ, ε-amino acids, which have a greater distance between the functional groups.

$$\begin{aligned} \cdots CH_2 - CH(NH_2) - COOH \qquad & \alpha - amino \quad acid \\ \cdots CH_2 - CH(NH_2) - CH_2 - COOH \qquad & \beta - amino \quad acid \\ \cdots CH(NH_2) - CH_2 - CH_2 - CH_2 - CH_2 - COOH \qquad & \varepsilon - amino \quad acid \end{aligned}$$

The α-amino acids are the most common form found in nature. There are 20 different of amino acids in proteins that are coded for directly in an organism's DNA, each with different properties (table1.1). The peptide bond links amino acids together to form proteins. Proteins are therefore also known as polypeptides. Amino acids play central roles as building blocks of proteins which (like the nucleic acid) are particularly prominent among the molecules essential to life. Their importance stems from the remarkable diversity of their functional roles. This diversity can be illustrated by listing a few of the major groups within each of these molecular families. Proteins are molecules that act to build the structural elements of organisms and to provide the energy necessary for life processes. Enzymes are proteins that catalyze biochemical reactions. Familiar examples include the digestive enzymes that degrade foodstuffs to simple, assimilable compounds; the biosynthetic enzymes that build complex molecules from simpler compounds; and muscle proteins that produce mechanical work from chemical reactions. Transport proteins such as hemoglobin facilitate the movement of molecular oxygen and other essential

Amino acid name	three-letter Abbreviation	one-letter abbreviation
Arginine	Arg	R
Histidine	His	H
Lysine	Lys	K
Aspartic acid	Asp	D
Glutamic acid	Glu	E
Asparagine	Asn	N
Cysteine	Cys	C
Glutamine	Gln	Q
Glycine	Gly	G
Serine	Ser	S
Threonine	Thr	T
Tyrosine	Tyr	Y
Alanine	Ala	A
Isoleucine	Ile	I
Leucine	Leu	L
Methionine	Met	M
Phenylalanine	Phe	F
Proline	Pro	P
Tryptophan	Trp	W
Valine	Val	V

Table 1.1: 20 coded amino acids.

compounds to their sites of utilization. Antibodies are proteins that bind to and neutralize foreign materials that may be harmful to an organism. Other proteins are responsible for maintaining the structures of cells, organs, and organisms, while still others play essential roles in genetic expression, nerve conduction, and all other biological processes. The functional diversity of proteins ultimately reflects the large amount of information that is stored in these molecules [99].

1.1.2 Protein Architecture

Proteins are all composed of one or more polypeptide chains, each containing from several to hundreds or even thousands of the 20 amino acids. The backbone of the polypeptide is given by the repeated sequence of three atoms of each residue in the chain: the amide N, the alpha Carbon and the Carbonyl Carbon. The 20 different amino acid side chains, that give each amino acid its unique properties, are not involved in making a peptide bond (Fig. 1.1).

Protein structure is usually described at four different levels. Primary structure is the basic level of the hierarchy. Moreover, *primary structure* is the particular linear sequence of amino acids in which the amino acids are

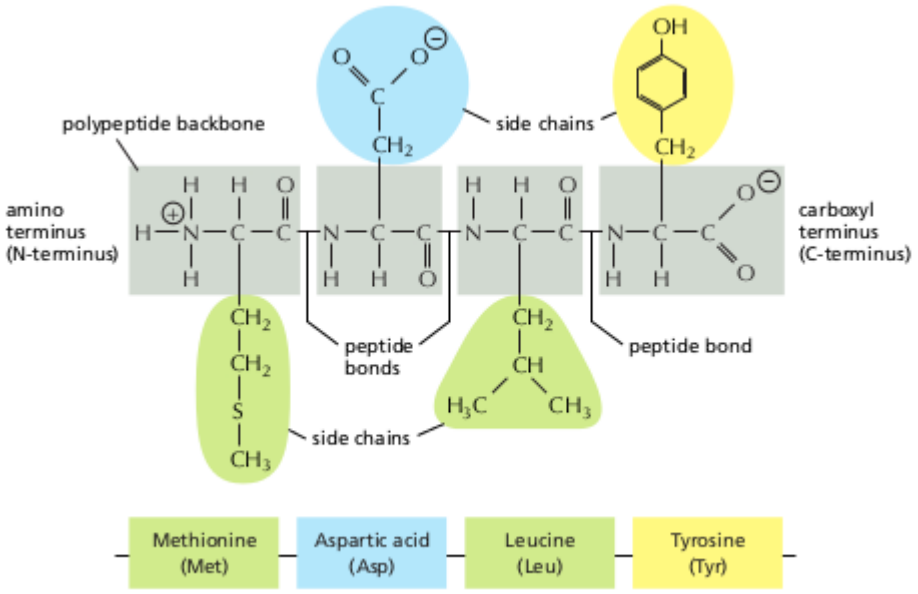

Figure 1.1: A polypeptide backbone with attached side chains

covalently linked together and that comprises one polypeptide chain. *Secondary structure* is a local regulary occuring structure in proteins and is mainly formed through hydrogen bonds between the carbonyl oxygen and the amide hydrogen of the peptide bond. There are two types of stable secondary structures: Alpha helices and beta-sheets (see Fig. 1.2 and Fig. 3.19, respectively). Alpha-helices and beta-sheets are preferably located at the core of the protein, whereat loops prefer to reside in outer regions. Geometrically, a alpha-helix is formed with a definite number of units per turn ($n = 3.6$), a characteristic pitch of the helix ($h = 5.4$ Å), and a specific distance traveled parallel to the helix axis per residue ($d = 1.5$ Å). So-called random coils, loops or turns don't have a stable secondary structure.

The *tertiary structure* is the next higher level of organization, the overall arrangement of secondary structural elements. *Quaternary structure* only exists, if there is more than one polypeptide chain present in a complex protein. Then quaternary structure describes the spatial organization of the chains. This whole hierarchy in protein structure is summarized in the Fig. 1.4.

Amongst the levels above-mentioned, only one will draw our attention.

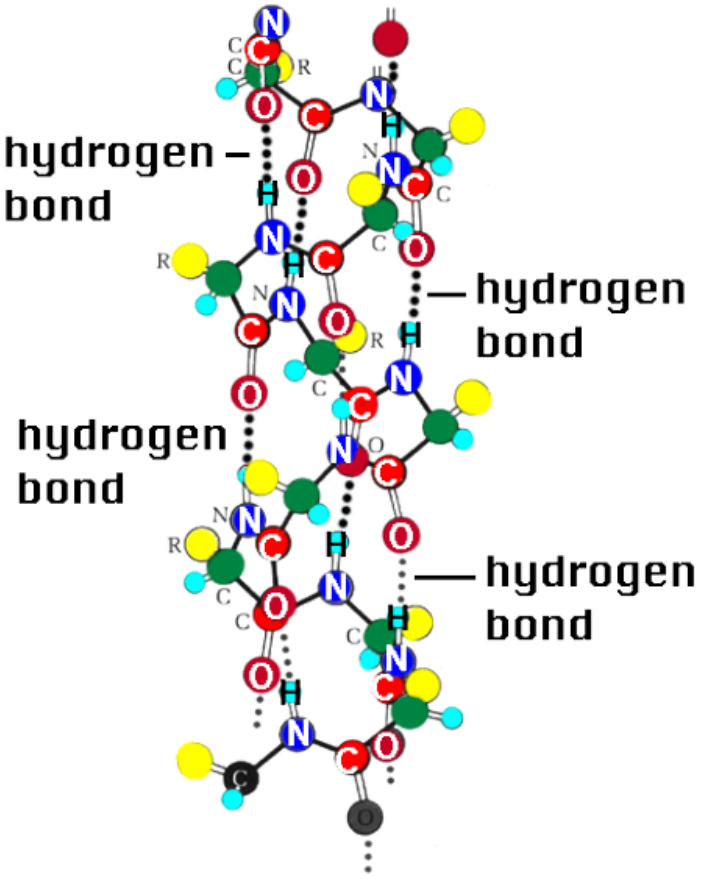

Figure 1.2: An alpha helix structure in protein with intrachain hydrogen bonds that stabilized the helix.

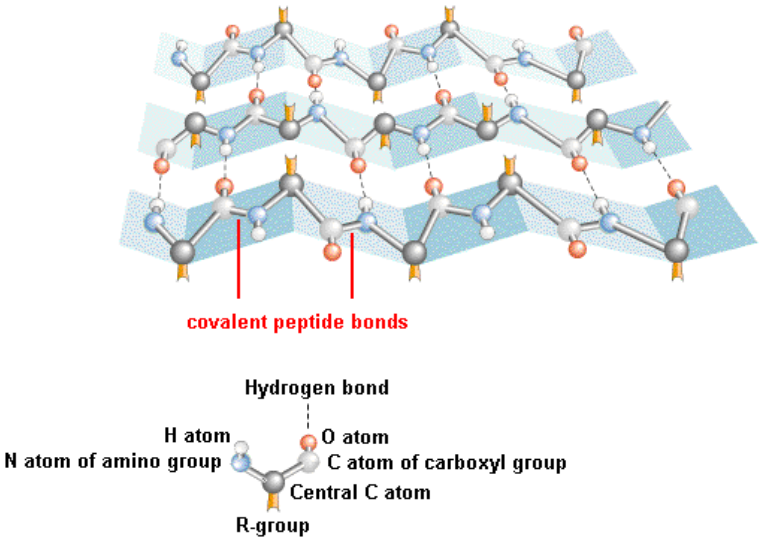

Figure 1.3: An antiparallel beta sheet. These chains are said to be antiparallel because they run in the opposite directions. The beta pleated sheet structure is stabilized by hydrogen bonds between the different chains

1.1.3 The emphasis on the alpha-helix structure in protein

The choice of alpha-helix is justified by the fact that the helical configuration is the most common of protein structures. Alpha-helical proteins are found in both the membrane and cytoskeletal fractions of cells. It has been estimated that up to one third of membrane proteins are in the helical configuration, with the remainder of proteins in a random coil form. The helix is also a common structural motif in the cytoskeleton, where there are at least three important classes of contractile proteins that are highly alpha-helical: spectrin, tropomyosin and myosin. In addition to the contractile system, the extensive network of intermediate filaments in the cytoskeleton also demonstrates predominant helical character [100]. Furthermore, alpha-helix has a quasi-one-dimensional structure.

Some proteins can bind to Adenosine triphosphate (ATP) in order to fulfil its function.

1.1.4 ATP and biological energy

ATP is an abbreviation for adenosine triphosphate, a small molecule used in cells as a coenzyme (Fig. 1.5). It is often referred by biologists to be the energy currency of life. The ATP is used for many cell functions including transport work moving substances across cell membranes. It is also used for

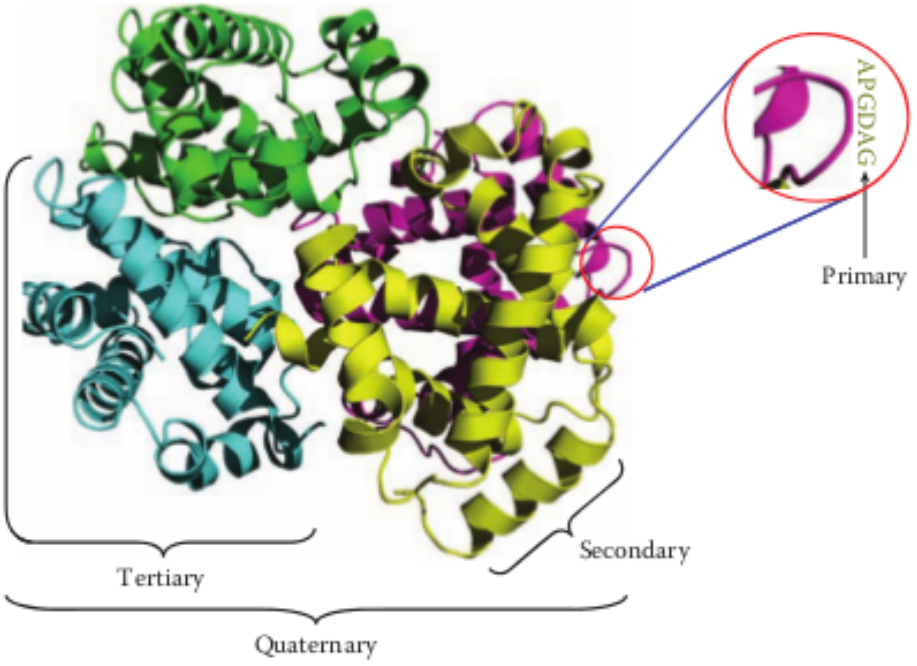

Figure 1.4: A ribbon model (*Ribbon model is generated by interpolating a smooth curve through the polypeptide backbone.*) of hemoglobin protein which includes four levels of protein structure (shown in different colors). The first level is the amino acid sequence of the chains, depicted here as an olive-colored one-letter code (enlarged image on the figure's top right side). The second level includes the helical segments of the protein, as well as the connecting loops. Other proteins include additional secondary elements, mainly the extended conformation. The third level includes the complete three-dimensional organization of each of the chains. Finally, the fourth level includes the arrangement of the different chains [101].

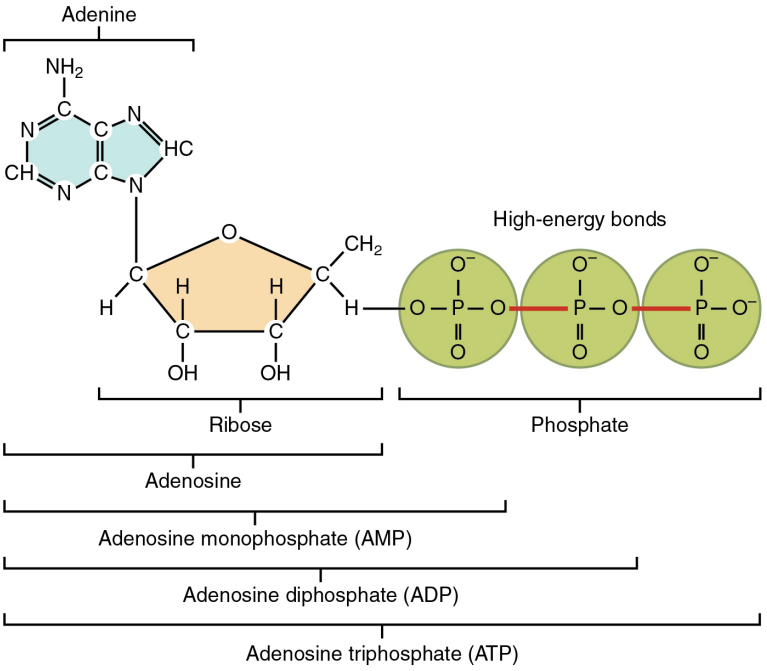

Figure 1.5: The two-dimensional stick model of the adenosine phosphate family of molecules, showing the atom and bond arrangement.

mechanical work, supplying the energy needed for muscle contraction. A major role of ATP is in chemical work, supplying the needed energy to synthesize the multi-thousands of types of macromolecules that the cell needs to exist. The above-mentioned energy comes from he hydrolysis of ATP into adenosine diphosphate (ADP) by the reaction

$$ATP^{4-} + H_2O \longrightarrow ADP^{3-} + HPO_4^{2-} + H^+. \tag{1.1}$$

Under normal physiological conditions approximately 10 kcal/mole or 0.42 eV of free energy is released by this reaction which involve protein molecules. These protein molecules are generally of a very large size and the site where hydrolysis occurs is often separated by a considerable distance from the site where the energy is used [102]. The ensuing question is whether mechanism governing localization and transport of energy in protein. But before we deal with this mechanism, let us address the possible ways for storage of metabolic energy in protein.

1.1.5 Vibrational energy in proteins

As the structural repeat units of proteins, the peptide bond exhibits a number of infrared (IR)-active amide bands. Nine normal modes are allowed for the amide band of proteins. These are called A, B, and I-VII in order of decreasing frequency. The amide A band (about 3500 cm^{-1}) and amide B (about 3100 cm^{-1}) originate from a Fermi resonance between the first overtone of amide II and and the N-H stretching vibration. Amide I is the most intense absorption band in proteins. It is primilary goverend by the stretching vibrations of the C=O (70-85%) and C-N groups (10-20%). Its frequency is found in the range between 1600 and 1700 cm^{-1}. Amide II results from the N-H bending vibration (40-60%) and from the C-N stretching vibration (18-40%). This band is conformationally sensitive. Amide III and IV are very complex bands resulting from a mixture of several coordinate displacements. The out-of-plane motions are found in amide V, VI and VIII [103]. It seems that an interesting candidate for transport and storage of metabolic energy is the amide-I (or CO stretching) vibration in proteins. This is due to the fact that this vibration has a quantum energy of about 0.2 eV (1650 cm^{-1}) which is appropriate to store or transport the 0.43 eV of free energy released in the hydrolysis of ATP.

1.2 Overview of bio-energy transport in protein molecules

1.2.1 Davydov's original model

An important biological problem is the mechanism of energy transfer and storage in proteins [104]. Interactions of intramolecular excitations with lattice vibrations in one-dimensional systems were first studied by Rashba [105]. Following that, Davydov and Kislukha built up the coupled equations for both the wave function of the excitation of the amide groups at site n coupled with the phonon motion caused by the elastic motion of the hydrogen bonds [25, 64]. This reasoning was based on the fact that the dipole-dipole interaction between the adjacent peptide groups situated along a hydrogen-bonded chain in the alpha-helical protein molecules is an order of magnitude higher than a similar interaction between the nearest groups of neighbouring chains. In view of this, the excitations of the three chains may thus be considered independently [1, 25]. That is how Davydov's original model is based on the infinite discrete chain consists of peptide groups ($H-N-C=O$) with a mass M, regularly spaced by a distance R, and weakly bound according to the following sequence: $\cdots H-N-C=O\cdots H-N-C=O\cdots H-N-C=$

$O\cdots H-N-C=O\cdots$. The dotted lines represent the hydrogen bonding. In addition, the interaction is assumed to work only between nearest-neighbors molecules. Moreover, effects due to the interactions between hydrogen bonds, which stabilize the helix and covalent bonds, other than the amide-I, which constitute the protein backbone, are neglected. The Hamiltonian of the chain thus described is

$$H = T + U + \sum_n [(\varepsilon - D_n)B_n^+ B_n - J(B_{n+1}^+ B_n + B_{n+1}B_n^+)], \tag{1.2}$$

where T is kinetic energy and U is the potential energy. The first part of the third term, $\varepsilon B_n^+ B_n$, defines the amide−I excitation energy, and the fourth term stands for the resonance dipole interaction between nearest neighbors. This interaction is characterized by the dipole−dipole interaction energy J. Notice that B_n^+ (B_n) is the creation (annihilation) operator of the amide−I excitation in the nth group. In the second part of the third term, the function $-D_n$ represents the deformation excitation energy of the nth peptide group with its nearest neighbours and can be written as

$$D_n = \mathcal{D}_n(\mid x_{n+1} - x_n \mid) + \mathcal{D}_n(\mid x_n - x_{n-1} \mid), \tag{1.3}$$

Then,$-D_n B_n^+ B_n$ describes the interaction between the intra-molecular excitation and the lattice displacements. Taking into account the interaction with nearest neighbors we have, Eq. (1.3) can be written in the form

$$D_n \approx \left(1 + \frac{\beta}{R}\rho_n\right) D, \tag{1.4}$$

where

$$\rho_n = R - |x_n - x_{n-1}| \tag{1.5}$$

denotes the relative distances between two neighboring groups from equilibrium and x_n, the small displacement of the nth peptide groups. Add that β is adjustable positive parameter of the deformation excitation energy while $D = 2\mathcal{D}(R)$.

Within this framework, Davydov suggested that the energy released in the hydrolysis of ATP molecules can be transferred in the form of vibration solitons along a alpha-helical protein molecules.

1.2.2 The Takeno soliton model

Takeno soliton model [108] differs from the previous one in the fact that it deals with more complex systems, and used a vibron model to denote the vibration of amide-I, the amide-I energy is coupled to both acoustic and optic phonons. Namely, the principal difference of Eq.(1.2) from Takeno's model is as follows: The Takeno Hamiltonian contains the factor $(B_n^+ B_m^+ + B_n B_m)$ in addition to $(B_n^+ B_m + B_m^+ B_n)$. In addition, in studying the amide-I vibration, Takeno took the normal coordinate or displacement field q_n as a relevant field variable, while the corresponding one in Davydov theory is the probability amplitude a_n for finding a vibrational quantum in nth amide-I oscillator subject to the constraint $\sum_n |a_n|^2 = 1$. Further, by using the continuum approximation, Davydov directly arrived at the Nonlinear Schrödinger equation for $a_n \longrightarrow a(x,t)$ while the equations of motion derived from Takeno's Hamiltonian are the coupled nonlinear Klein-Gordon equations for dynamic coordinate. Even as the latter finally leads to a Nonlinear Schrödinger equation through rotating-wave approximation.

1.2.3 Yomosa's model

With respect to Yomosa's model [109], he introduced also another classical soliton model in protein molecules in general (especially muscle proteins). Since the H-bonding interaction between peptide groups has a remarkable nonlinearity due to its charge-transfer interaction, Yomosa found a H-bonded chain of peptide groups as a one-dimensional nonlinear lattice. Indeed, he wrote the potential of nth H-bond approximately as follows

$$V_n(r_n) = Ar_n^2 - Br_n^3, \quad r_n = y_{n+1} - y_n \tag{1.6}$$

where r_n is the elongation of the nth peptide bond, y_n is the displacement of the nth peptide group, A and B are the constants. It follows that the Yomosa's Lagrangian is written as

$$L = \frac{1}{2}\sum_n \left(\frac{dy_n}{dt}\right)^2 - \sum_n \left[A(y_n - y_{n-1})^2 - B(y_n - y_{n-1})^3\right] \tag{1.7}$$

where m is a mass of a peptide group plus residue. Further to that, Yomosa introduced the continuum limit and arrived to a Korteweg-de Vries equation. However, the resulting one-soliton solutions are supersonic, unlike those of Davydov and Takeno.

1.2.4 The improved models of Davydov's theory

Many studies have been done on this Davydov's original model [100, 106, 107] and the subsequent improvements are relying on the effects of disorders, temperature, long-range interaction and interchain coupling, the foundation and accuracy of the theory, the quantum and classical properties and the thermal stability and lifetimes of the Davydov soliton [34, 97, 110–116, 118, 131].

As will be later noted in this manuscript, an improvement of Davydov's theory can be seen by taking into account the higher order exciton-phonon interaction. Once made, special attention will be paid to localized states as collective excitations traveling along protein molecules.

1.3 Localized states

1.3.1 Multibreathers

For more than two decades, attention has been paid to spatially localized and time-oscillatory excitations also called discrete breathers (DBs) or intrinsic localized modes (ILMs), which emerge due to nonlinearity and discreteness of system. These breathers have a bell-shaped form (Fig. 1.6(a)). Apart from these excitations and in the early 2000s, efforts were stepped up in order to study localized patterns possessing an arbitrary number of extrema (multibreathers) as depicted by Fig. 1.6. The latter were initially discussed in [119]. Since that pioneering work, the resulting studies are backed by existence and stability of multibreathers [15, 120–122]. So, the existence and stability of single/multi-site breathers have been studied in diatomic FPU lattices. Next, the study the existence and stability of multibreathers in Klein-Gordon chains with interactions that are not restricted to nearest neighbors has been completed. Futhermore, multibreathers have been predicted theoretically in realistic systems such as discrete electrical transmission line [11] and observed experimentally [12]. However, the existing knowledge on properties and especially on the stability and mobility of the multibreathers is rather limited or even nonexistent.

1.3.2 Nonlinear Supratransmission

It is well known that plane waves with frequency components within particular intervals (known as pass bands) travel through the structure unattenuated, whereas all other frequency components (belonging to the forbidden

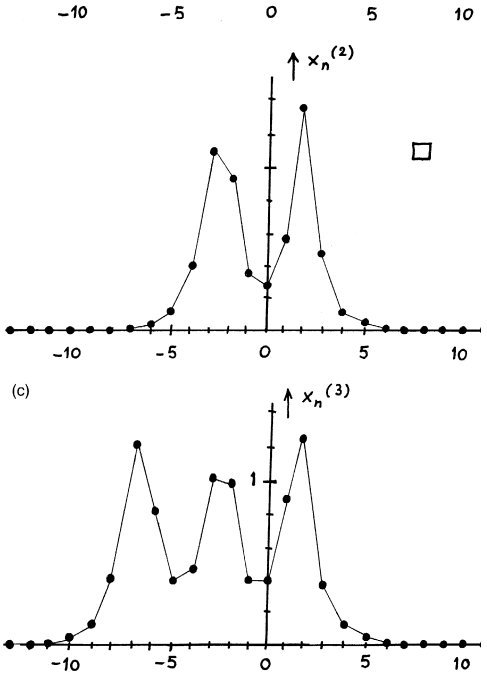

Figure 1.6: Examples of profiles of single-hump (a), two-hump (b), and three-hump solitons (c) .

band gap) are spatially attenuated as they propagate through the structure. On the other hand, it was recently discovered that, for frequency in the forbidden band gap, waves could generate a sequence of nonlinear modes propagating in the medium. This phenomenon is called nonlinear supratransmission and is observed above some amplitude threshold (Fig. 1.7).

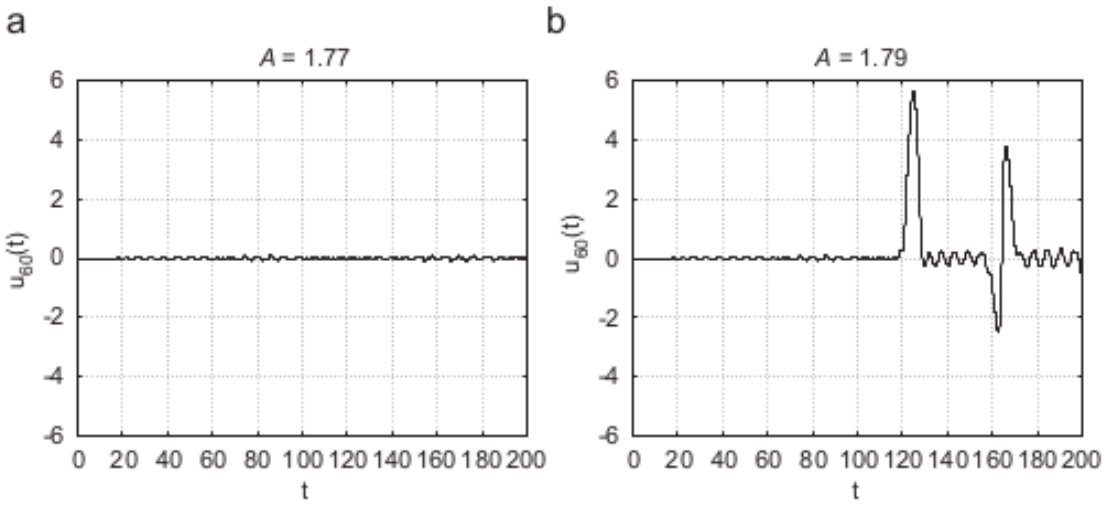

Figure 1.7: Numerical solution of a sine-Gordon system for a driving frequency of 0.9 and the site $n = 60$ (out of a total of 200). The left and right panels describe the dynamics of the sine-Gordon's equations for the driving amplitudes $A = 1.77$ and $A = 1.79$, respectively [123].

The nonlinear supratransmission was first discovered in coupled pendulum chain described by coupled sine-Gordon and Klein-Gordon equations [54], and then studied in other nonlinear models [124–127]. This phenomenon is also widely used in many others models such as discrete nonlinear electrical transmission lattice [55], birefringent quadratic medium [56], waveguide arrays [57, 58], Frenkel-Kontorova model [59], granular chains [60] and nanostructured multiferroics [61]. That being so, it is important to note that the above mentioned works have focused on the gap transmission of single hump breathers.

1.3.3 Rogue Waves

Freak, rogue, or giant waves are localized in both space and time, which seems to appear from nowhere and disappear without a trace [66]. These waves have received much attention in recent years. Initiated first in the context of oceanic waves, where there is the commonly used statistical definition

of a wave that is 2-3 times larger than the significant wave height, the notion of rogue waves have been recently identified in other fields. In this way, "optical rogue waves" was first observed in nonlinear optics by Solli et *al.* [69]. Since then, rogue waves have been mentioned in nonlinear optics [67, 68], Bose-Einstein condensates [70], plasmas, etc. [128].

On the other hand, we should mention that one of the major models for the rogue waves is the nonlinear Schrödinger equation. The first-order rational solution derived by Peregrine is there to remind us of that [65]. Discrete systems are not exempt from this kinds of solutions. It has been demonstrated that the Ablowitz-Ladik equation, which is an integrable form of the DNLS equation, has rogue wave solutions in the form of the rational solutions [73]. Figure 1.8 is an illustration of this rogue waves, in an array of nonlinear waveguides, where their maximums are higher than three times the background level. Moreover, through experimental imperfection, a very small degree of disorder has a deep effect on the formation of discrete rogue waves in cubic DNLS lattice [75]. In any event it must be pointed out that the case of saturable nonlinearities remains open.

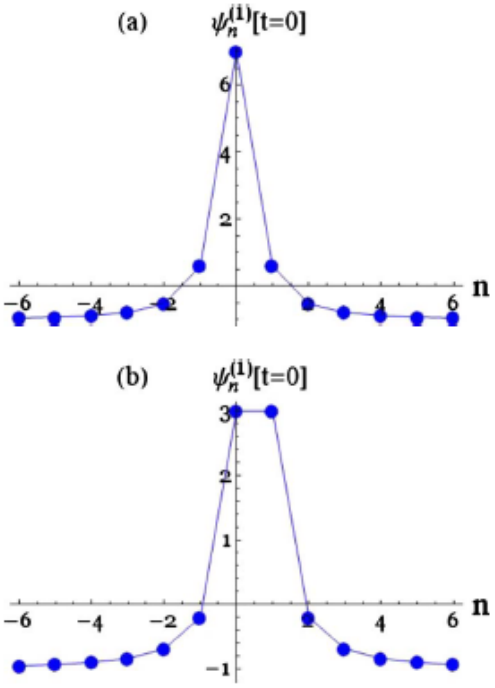

Figure 1.8: The first-order rational solutions $\psi_n^{(1)}$ of the Ablowitz-Ladik equation for $t = 0$, t being a longitudinal spacial variable. This solutions start at $t = -\infty$ and increase until they reach their maximum value at $t = 0$ and decreases symmetrically afterward. The offsets are 0 (a) and $1/2$ (b) [73].

CHAPTER 2

Methodology: Modeling and Numerical methods

After outlining the biological background of the DNLS equation with saturable or cubic nonlinearities, we will further see the numerical methods used to obtain some solutions for the above-mentioned equation, as well as its properties.

2.1 Modeling

2.1.1 DNLS equation with saturable nonlinearities

Let us start by pointing out that our model forms an extension of the Davydov's original model discussed in subsection 1.2.1. This being so, we assume here that the interaction between the intra-molecular excitation and the lattice displacements is strong, because it has been shown [129] that auto-localized excitation solitons appear in the system due to the nonlinear and strong exciton-phonon interaction. Eq. (1.3) can then be written in the form

$$D_n \approx \left(1 + \frac{\beta}{R}\rho_n - \frac{\gamma}{2R^2}\rho_n^2\right) D, \tag{2.1}$$

where

$$\rho_n = R - |x_n - x_{n-1}| \tag{2.2}$$

denotes the relative distances between two neighboring groups from equilibrium and x_n, the small displacement of the nth peptide groups. Add that β and γ are adjustable positive parameters of the deformation excitation energy while $D = 2\mathcal{D}(R)$. Comparing Eq. (2.1) to one used in Ref. [43], the choice of the negative sign of the last term here is to take into account the competition between local compression and local dilation of lattice.

The use of Born-Oppenheimer approximation leads us to consider the lattice displacements as classical variables. This is justified by the fact that the

effective mass M of the peptide group is large, thus leading acoustic vibrations to be slow compared to the excitonic modes. In order to establish the equations of motion, we define the soliton wave function as

$$|\psi>=\sum_n a_n(t)B_n^+|0>, \tag{2.3}$$

where $|0>$ is the vacuum state and a_n is the complex probability amplitude of the exciton wave, which satisfies the normalization condition

$$<\psi|\psi>=\sum_n |a_n(t)|^2=1. \tag{2.4}$$

Let us determine the Hamiltonian function in our system by the equality

$$\Xi=<\psi|H|\psi>=\sum_n\{\left[\varepsilon+T+U-\left(1+\frac{\beta}{R}\rho_n-\frac{\gamma}{2R^2}\rho_n^2\right)D\right]a_n a_n^*-Ja_n^*\left(a_{n+1}+a_{n-1}\right)\}, \tag{2.5}$$

that depends on a_n, ρ_n and on their canonically conjugate variables $i\hbar a_n^*$ and π_n. $T=\frac{M}{2}\sum_n\left(\frac{\partial x_n}{\partial t}\right)^2$ and $U=\frac{\omega}{2}\sum_n\rho_n^2$ where ω is the spring constant. Knowing that $\pi_n=\frac{\partial T}{\partial\dot{\rho_n}}$, we have

$$T=\frac{1}{2M}\sum_n\left(\pi_n-\pi_{n-1}\right)^2. \tag{2.6}$$

Taking the Hamiltonian function Ξ, we get the Hamiltonian equation

$$i\hbar\frac{\partial a_n}{\partial t}=\frac{\partial\Xi}{\partial a_n^*}, \tag{2.7}$$

$$\frac{\partial\rho_n}{\partial t}=\frac{\partial\Xi}{\partial\pi_n}, \tag{2.8}$$

$$\frac{\partial\pi_n}{\partial t}=-\frac{\partial\Xi}{\partial\rho_n}. \tag{2.9}$$

The exploitation of the previous system of equations leads to the system of coupled equations

$$i\hbar\frac{\partial a_n}{\partial t}=\left[\varepsilon+T+U-\left(1+\frac{\beta}{R}\rho_n-\frac{\gamma}{2R^2}\rho_n^2\right)D\right]a_n-J\left(a_{n+1}+a_{n-1}\right), \tag{2.10}$$

$$M\frac{\partial^2\rho_n}{\partial t^2}=-\omega\left(2\rho_n-\rho_{n+1}-\rho_{n-1}\right)+\frac{\beta D}{R}\left(2|a_n|^2-|a_{n+1}|^2-|a_{n-1}|^2\right)$$

$$-\frac{\gamma D}{R^2}\left(2\rho_n|a_n|^2-\rho_{n+1}|a_{n+1}|^2-\rho_{n-1}|a_{n-1}|^2\right). \tag{2.11}$$

It should be noted that $H_{ph}=T+U$ is just a c-number in Eq. (2.10). The great value of M leads to the adiabatic approximation [4]

$$\frac{\partial^2\rho_n}{\partial t^2}\approx 0. \tag{2.12}$$

Neglecting the inertia term, we solve Eq. (2.11) and obtain the following relation:

$$\rho_n=\frac{\frac{\beta D}{R\omega}|a_n|^2}{1+\frac{\gamma D}{R^2\omega}|a_n|^2}. \tag{2.13}$$

Then, the substitution of Eq. (2.13) in Eq. (2.10) yields

$$i\hbar\frac{\partial a_n}{\partial t}=\left[\varepsilon+T+U-D\right]a_n-\nu_1 J\frac{|a_n|^2a_n}{1+\nu_3|a_n|^2}+\nu_2 J\frac{|a_n|^4a_n}{(1+\nu_3|a_n|^2)^2}-J\left(a_{n+1}+a_{n-1}\right), \tag{2.14}$$

where $\nu_1=\frac{\beta^2D^2}{R^2\omega J}$, $\nu_2=\frac{\gamma\beta^2D^3}{2R^4\omega^2 J}$, and $\nu_3=\frac{\gamma D}{R^2\omega}$.
Equation (2.14) is reduced in the form

$$i\frac{\partial\phi_n}{\partial\tau}=-\Delta_2\phi_n+\eta_1\frac{\phi_n}{1+|\phi_n|^2}+\eta_2\frac{|\phi_n|^2\phi_n}{(1+|\phi_n|^2)^2}, \tag{2.15}$$

if we set

$$\phi_n=\sqrt{\nu_3}a_n\exp i\tau\left[\frac{\varepsilon+T+U-D-2J-\eta_1 J}{J}\right],\ \eta_1=\nu_1/2\nu_3,\ \text{with}\ \nu_3\neq 0,\ \eta_2=-\eta_1, \tag{2.16}$$

and use the dimensionless time $\tau=Jt/\hbar$. In Eq. (2.15), η_1 and η_2 are the strength of the nonlinearities and $\Delta_2\phi_n=(\phi_{n+1}+\phi_{n-1}-2\phi_n)$.

It is well known that under adiabatic approximation, Davydov shows that the dynamics of the coupled exciton-phonon system is reduced to the DNLS equation [4]. Here, since $\eta_1>0$ and $\eta_2<0$, Eq. (2.15) is named the DNLS equation with competitive saturable nonlinearities. This equation has two conserved quantities: the Hamiltonian,

$$E=\sum_n\left[|\phi_{n+1}-\phi_n|^2+(\eta_1+\eta_2)\log(1+|\phi_n|^2)+\frac{\eta_2}{1+|\phi_n|^2}\right], \tag{2.17}$$

and the number of quanta (l^2-$norm$),

$$P=\sum_n|\phi_n|^2. \tag{2.18}$$

We also note that, due to the last term in the right-hand side, Eq. (2.15) is different from the well-known DNLS equation with photorefractive nonlinearity, widely used in optics. In the other words, the coefficient η_2 guarantees the presence of higher-order saturable nonlinearity. In order to give a physical meaning to η_2, let us set $\eta_1 = -\eta_2 = \eta$ and we consider $\chi_1 = (\beta D/R) > 0$ and $\chi_2 = -(\gamma D/2R) < 0$, the phonon−exciton coupling parameters. χ_1 and χ_2, respectively, represent the parameters of nonlinear coupling. Thus, if $\gamma = 0$ ($\chi_2 = 0$), we have through Eq. (2.14) $\nu_2 = \nu_3 = 0$, and we get the classical Davydov-Scott model, which leads to the well-known DNLS equation with cubic nonlinearity. Therefore, χ_2 contributes to the strong phonon−exciton coupling, thereby promoting the formation of soliton. Similar considerations have been used by Velarde and co-workers [130], when looking for long-living intrinsic localized solectron, they have considered an extended polaron Hamiltonian in which the electron hopping term is affected by anharmonicity. In the following, we parametrize our problem by η, which is also expressed as $\eta = (\chi_1 R/4J)\widetilde{\eta}$, with $\widetilde{\eta} = -(\chi_1/\chi_2)$. For α-helical proteins, the use of the following physical parameters [131, 132] $J = 9.67 \times 10^{-4}$eV, $\chi_1 = 8 \times 10^{-2}$eV/Å, $\omega = 0.8125$ eV/^{2}, $R = 4.5$ Å, leads to $\eta \approx 93\ \widetilde{\eta}$.

Based on the meaning of the sign of χ [133], it appears that negative coefficient means that the molecular chain is locally dilated (dilatational soliton) and a positive value represents the local compression (compressional soliton) of molecular chain due to amide−I vibrations. It follows that our model exhibits a competition of self-focusing (dilatation) and defocusing (compression) saturable nonlinearities. This is a good compromise given the fact that in the literature, the coupling parameter is taken positive or negative [134].

It is also important to recall that an equation similar to Eq. (2.14) has been obtained by Aguero [43] in a continuous medium. However, to look for the soliton structures, he has simplified the equation to cubic-qintic nonlinear Schrödinger equation in order to solve it.

2.1.2 DNLS equation with saturable nonlinearities and next-nearest-neighbor interactions

Let us consider the following Discrete Nonlinear Schrödinger equation with higher order saturable nonlinearity as described above,

$$i\frac{\partial \phi_n}{\partial t} = -\Delta_2 \phi_n + \eta_1 \frac{\phi_n}{1+|\phi_n|^2} - \eta_2 \frac{|\phi_n|^2 \phi_n}{(1+|\phi_n|^2)^2}, \tag{2.19}$$

which describes the dynamics of the state of amide-I excitations in hydrogen-bonded protein chain. In Eq.(2.19), ϕ_n is the excitation wave function at site n, $\Delta_2\phi_n = (\phi_{n+1} + \phi_{n-1} - 2\phi_n)$, η_1 and η_2 are the strengths of the nonlinearities. Eq.(2.19) has been established within the framework of nearest neighbor interaction. Hydrogen bonding in proteins can be described as an electrostatic dipole-dipole interaction [148]. Taking into account the long-range interaction due to dipole-dipole interaction [140], it can be written as:

$$i\frac{\partial\phi_n}{\partial t} = -\sum_{m(m\neq 0)} S_m(\phi_{n+m} + \phi_{n-m} - 2\phi_n) + \eta_1\frac{\phi_n}{1+|\phi_n|^2} - \eta_2\frac{|\phi_n|^2\phi_n}{(1+|\phi_n|^2)^2}, \tag{2.20}$$

where $S_m = \mid m \mid^{-3}$ and S_m represents the order of coupling between the polypeptides of the sites n and $n \pm m$. Thus, when $S_m = 0$ for $|m| > 1$, Eq.(2.20) is reduced to Eq.(2.19) where only the nearest neighbor interactions are handled.

Eq.(2.20) has two conserved quantities: the Hamiltonian,

$$H = \sum_{m,n(m\neq 0)} S_m|\phi_{n+m} - \phi_n|^2 + \sum_n(\eta_1 - \eta_2)\log(1+|\phi_n|^2) - \sum_n \frac{\eta_2}{1+|\phi_n|^2}, \tag{2.21}$$

and the number of quanta,

$$P = \sum_n \mid \phi_n \mid^2 . \tag{2.22}$$

2.1.3 DNLS equation with saturable nonlinearities and randomly distributed molecules around the peptide groups chain

We consider a one-dimensional hydrogen-bonded chain consisting of peptide groups ($H - N - C = O$), regularly spaced, and weakly bound according to the following sequence: $\cdots H - N - C = O \cdots H - N - C = O \cdots H - N - C = O \cdots H - N - C = O \cdots$. In the framework of strong exciton-phonon interaction, the normalized dynamical equations for the complex probability amplitude ϕ_n of finding an amide-I vibrational quantum at site n is given by Eq.(2.19)

$$i\frac{\partial\phi_n}{\partial t} = -(\phi_{n+1} + \phi_{n-1}) + \eta_1\frac{\phi_n}{1+|\phi_n|^2} - \eta_2\frac{|\phi_n|^2\phi_n}{(1+|\phi_n|^2)^2}, \tag{2.23}$$

where t is the time coordinate, η_1 and η_2 are the strength of the nonlinearities. Correspondingly, these coefficients exhibit a competition between local compression and local dilatation of lattice which leads to the interplay between self-focusing and defocusing saturable nonlinearities. For $\eta_2 = 0$, Eq.(2.23) reduces to a discrete version of the Vinetskii-Kukhtarev equation widely used in optics [141].

By taking into account the diagonal disorder ε_n in a site energies [97, 107], we can express Eq.(2.23) as

$$i\frac{\partial \phi_n}{\partial t} = \frac{\varepsilon_n}{J}\phi_n - (\phi_{n+1} + \phi_{n-1}) + \eta_1 \frac{\phi_n}{1+|\phi_n|^2} - \eta_2 \frac{|\phi_n|^2 \phi_n}{(1+|\phi_n|^2)^2}, \tag{2.24}$$

where $\varepsilon_n = \varepsilon\beta_n$, β_n is a random sequence, ε is the amide-I site energy without disorder, and J is the dipole-dipole interaction energy. As in Ref. [32] and those included therein, the shift of ground state energy ε_n is due to the interaction of the chain molecules with molecules of the environment. It follows that a random sequence ε_n is centered around the value 0. Notice that Eq.(2.24) is obtained after carrying a usual gauge transformation allowing us to cancel the term $(\varepsilon/J)\phi_n$ in its right side. Furthermore, Eq.(2.24) has two conserved quantities: the Hamiltonian H and the total power $P = \sum_n \mid \phi_n \mid^2$ which stand for the energy of the system and the total probability, respectively.

Although the previous DNLS equations are new as well as solutions sought thereafter, this is not the case for the following equation where only its solutions will be new.

2.1.4 DNLS equation with cubic nonlinearity and on-site potential arising from impurities [4]

Our starting point is the Davydov model with the coupled equations where $a_n(t)$ and $\rho_n(t)$ stand for the probability of finding two amide-I vibrational quanta at n^{th} peptide groups in chain and the relative changes in equilibrium distance between them, respectively [1]. By considering the Davydov model with a diagonal disorder ε_n in the site energies [97, 107], the dynamics of the system is assumed to be governed by

$$i\hbar\frac{\partial a_n}{\partial t} = \left[\varepsilon + \varepsilon_n + W - D - \chi\rho_n\right] a_n - J\left(a_{n+1} + a_{n-1}\right), \tag{2.25}$$

$$M\frac{\partial^2 \rho_n}{\partial t^2} = -\omega\left(2\rho_n - \rho_{n+1} - \rho_{n-1}\right) + 2\chi\left(2|a_n|^2 - |a_{n+1}|^2 - |a_{n-1}|^2\right); \tag{2.26}$$

where M is the mass of the peptide group, ω the elasticity constant of the chain, ε the energy of the $C = O$ stretching and W the total energy of the peptide group displacements. The constant J is the nearest neighbor dipole-dipole coupling energy along a chain, χ the exciton-phonon coupling parameter, D the energy of the hydrogen bond and t corresponds to temporal coordinate.

Since the dynamics of the coupled system described by Eqs. (2.25) and (2.26) is not obvious, we use a well known technique to simplify the system [107, 131]. Indeed, if

$$v = \frac{V_{ex\ max}}{V_{ac}} = \frac{4MJ^2}{\omega\hbar^2} \ll 1, \tag{2.27}$$

where $V_{ex\ max}$ is the maximal velocity of the exciton and V_{ac} is the velocity of sound, the inertia of Eq. (2.26) can be disregarded. Moreover, for α-helical proteins, we have [131, 132] $J = 9.67 \times 10^{-4}$eV, $\chi = 3.87 \times 10^{-2}$eV/Å, $\omega = 0.8125$ eV/^{2}, $\varepsilon = 0.205$ eV and M=114.47 amu. Thus, $v \sim 0.03$ and consequently, Eqs. (2.25) and (2.26) yield the Discrete Nonlinear Schrödinger (DNLS) equation

$$i\hbar\frac{\partial a_n}{\partial t} = [\varepsilon + \varepsilon_n + W - D]\, a_n -$$

$$2\frac{\chi^2}{\omega}|a_n|^2 a_n - J\left(a_{n+1} + a_{n-1}\right). \tag{2.28}$$

With the gauge transformation

$$\phi_n = a_n \exp it\left[\frac{\varepsilon + W - D}{\hbar}\right], \tag{2.29}$$

and the dimensionless time $t \to Jt/\hbar$, Eq. (2.28) becomes

$$i\frac{\partial \phi_n}{\partial t} + (\phi_{n+1} + \phi_{n-1}) - \frac{\varepsilon_n}{J}\phi_n + 2\nu|\phi_n|^2\phi_n = 0, \tag{2.30}$$

where $\nu = \frac{\chi^2}{J\omega} = 1.9$.

The model (2.30) has two conserved quantities: the Hamiltonian

$$E = \sum_n \left[-\frac{\nu}{2}|\phi_n|^4 - (\phi_n\phi_{n-1}^* + \phi_{n-1}\phi_n^*) - \frac{\varepsilon_n}{J}|\phi_n|^2\right], \tag{2.31}$$

with canonical conjugated variables $\{i\phi_n\}$, $\{\phi_n^*\}$ where the asterisk denotes

complex conjugate, and the l^2-$norm$

$$P = \sum_n |\phi_n|^2 = 1. \tag{2.32}$$

In this section, we have addressed some discrete equations underlying the Davydov model. The use of a set of numerical methods is required for their resolution.

2.2 Numerical methods

2.2.1 The multidimensional Newton-Raphson method

By using a suitable ansatz, it is possible to turn DNLS equation into set of coupled algebraic equations, namely

$$\mathbf{f(u)=0} \tag{2.33}$$

or, using scalar notation

$$\begin{aligned} f_1(u_1, u_2, \ldots, u_n) &= 0 \\ f_2(u_1, u_2, \ldots, u_n) &= 0 \\ &\vdots \\ f_n(u_1, u_2, \ldots, u_n) &= 0, \end{aligned} \tag{2.34}$$

where **u** denotes the entire vector of values u_j and **f** denotes the entire vector of functions f_j (j=1, 2, ..., n). To look for the stationary solutions of DNLS equation therefore comes down to find the zero of a higher-dimensional function **f**. In this regard, the system

$$\mathbf{J}(\mathbf{u}^{(k)}) \cdot (\mathbf{u}^{(k+1)} - \mathbf{u}^{(k)}) = -\mathbf{f}(\mathbf{u}^{(k)}) \tag{2.35}$$

should be solved (for the vector $\mathbf{u}^{(k+1)}$) where the superscript indicates iteration number and **J** is the Jacobian matrix of the n equations **f** with respect to the n unknowns **u** ($J_{ij} = \frac{\partial f_i}{\partial u_j}$).

The following steps are consequently required to solve Eq. (2.33)

1. Estimate the solution vector $\mathbf{u}^{(k)}$.
2. Evaluate $\mathbf{f}(\mathbf{u}^{(k)})$.

3. Compute the Jacobian matrix $\mathbf{J}(\mathbf{u}^{(k)})$.

4. Set up the simultaneous equations in Eq. (2.35) and solve for $\mathbf{u}^{(k+1)}$.

5. Let $\mathbf{u}^{(k)} \leftarrow \mathbf{u}^{(k+1)}$ and repeat steps 2-5 until $|\mathbf{u}^{(k+1)} - \mathbf{u}^{(k)}| < \varepsilon$, where ε is the error tolerance.

It should be noted that the good starting value (step 1) is suggested by the type of solution.

2.2.2 The fourth-order Runge-Kutta method

By means of fourth-order Runge-Kutta scheme, a numerical evolution of the solution obtained in step 5 above can be achieved.

Let us consider a system of n ordinary differential equations written in vector form as follows

$$\frac{d\mathbf{y}}{dt} = \mathbf{f}(t, \mathbf{y}) \tag{2.36}$$

where $\mathbf{y} = (y_1, y_2, \ldots, y_n)$ and $\mathbf{f} = (f_1, f_2, \ldots, f_n)$. Next we label our time states $t^{(k)}$, $t^{(k+1)}$ which are separated by time interval of length dt. Suppose we have the state of the simulation at time $t^{(k)}$ as $\mathbf{y}^{(k)}$. To compute the state a short time dt later and put the results into $\mathbf{y}^{(k+1)}$, the fourth-order Runge-Kutta algorithm does the following

$$\mathbf{a} = dt\ \mathbf{f}(t^{(k)}, \mathbf{y}^{(k)}), \tag{2.37}$$

$$\mathbf{b} = dt\ \mathbf{f}(t^{(k)} + \frac{dt}{2}, \mathbf{y}^{(k)} + \frac{dt}{2}\mathbf{a}), \tag{2.38}$$

$$\mathbf{c} = dt\ \mathbf{f}(t^{(k)} + \frac{dt}{2}, \mathbf{y}^{(k)} + \frac{dt}{2}\mathbf{b}), \tag{2.39}$$

$$\mathbf{d} = dt\ \mathbf{f}(t^{(k)} + dt, \mathbf{y}^{(k)} + dt\ \mathbf{c}), \tag{2.40}$$

$$\mathbf{y}^{(k+1)} = \mathbf{y}^{(k)} + \frac{1}{6}(\mathbf{a} + 2\mathbf{b} + 2\mathbf{c} + \mathbf{d}). \tag{2.41}$$

After completing the iterative process, Eq. (2.36) is thus solved numerically by the 4^{th} order Runge-Kutta method. In addition, this direct numerical integration can be used to investigate the stability of the solutions.

2.2.3 Linear stability analysis

Following the methodology of the paper [145] for the DNLS lattice, the stability of the solutions can be analyzed by taking a perturbed solution in the form

$$\phi_n = \exp(-i\Omega t)[u_n + \varepsilon(x_n \exp(\lambda t) + y_n \exp(\overline{\lambda} t))], \tag{2.42}$$

where ε is a linearization parameter around the solution u_n, and λ is the eigenvalue (x_n and y_n are the corresponding eigenvectors). Add that $\overline{\lambda}$ denotes the complex conjugate of λ, Ω being the frequency. Therefore, substituting Eq. (2.42) into the DNLS equation and keeping only the terms linear in ε yield to an eigenvalue problem:

$$i\lambda \begin{pmatrix} x_n \\ \overline{y_n} \end{pmatrix} = \mathbf{A} \cdot \begin{pmatrix} x_n \\ \overline{y_n} \end{pmatrix}, \tag{2.43}$$

where $\mathbf{A}$ is the $2N$x $2N$ matrix (N being the size of u_n). For the form of the perturbation chosen, an eigenvalue with $Re(\lambda) > 0$ and $\sum(|x_n|^2 + |y_n|^2) < \infty$ indicates instability of the discrete solution u_n. Otherwise, the solution is called weakly spectrally stable. Solving numerically Eq. (2.43), we obtain the eigenvalue spectrum for discrete solution u_n. This can be done by a standard numerical eigenvalue solver such as MATLAB. In MATLAB the eigenstructure is computed by the function eig. In particular, the command

$$>> [Y, F] = eig(A)$$

gives the matrix $\mathbf{Y}$ of eigenvectors $\mathbf{y}$ and the diagonal matrix $\mathbf{F}$ of corresponding eigenvalues λ of the matrix $\mathbf{A}$.

To conclude this chapter on the modeling and numerical methods, some discrete equations behind the localization and transport of vibrational energy in protein have been addressed in the light of the strong exciton-phonon interaction. They are DNLS equation with saturable nonlinearities, DNLS equation with saturable nonlinearities and next-nearest-neighbor interactions, DNLS equation

with saturable nonlinearities and randomly distributed molecules around the peptide groups chain. DNLS equation with cubic nonlinearity and on-site potential arising from impurities has been also mentioned. Thereafter, the multidimensional Newton-Raphson method, the fourth-order Runge-Kutta method, and linear stability analysis have been seen as numerical tools. These tools allow us to obtain and analyze solutions provided by the above equations.

CHAPTER 3

Results and Discussion

In this chapter, we present the results and discussion related to models seen in the previous chapter. More specifically, In section 3.1, we investigate the existence and stability of soliton and multisoliton solutions in a DNLS equation with competing saturable nonlinearities. This is presented in the context of Amide-I vibrational energy excitations in proteins. It follows an analysis of the effects of next-NNI for this model in section 3.2. Section 3.3 deals with the supratransmission in a DNLS equation with competing saturable nonlinearities while section 3.4 describes the biological rogues waves in the one-dimentional chain of peptide groups containing 200 elements. Finally, section 3.5 shows the collisions of multihump solitons by isolated impurities, in the framework of the DNLS equation.

3.1 Discrete multibreathers in the exciton dynamics of the Davydov model with saturable nonlinearities

3.1.1 Discrete stationary multihump soliton solutions

In order to solve Eq. (2.15) governing the evolution of the complex probability amplitude ϕ_n, we seek the stationary solutions of the form $\phi_n = u_n \exp(-i\Omega\tau)$, Ω being a frequency. Under this condition, we obtain a set of coupled algebraic equations for the real function u_n:

$$\Omega u_n + (u_{n+1} + u_{n-1} - 2u_n) - \eta \frac{u_n}{1+u_n^2} + \eta \frac{u_n^3}{(1+u_n^2)^2} = 0. \tag{3.1}$$

It should be added to the above relations, the normalization condition given by Eq. (2.4), and rewritten as

$$\sum_n u_n^2 \simeq \frac{0.043}{\widetilde{\eta}}. \tag{3.2}$$

It is well known that two-component systems with saturable nonlinearity can sustain both single-hump and multi-hump solitons (optical solitons) [135]. The idea is to investigate the presence of such solutions in our model despite being a one-component system. This is done numerically, by means of iterative multidimensional Newton-Raphson method with periodic boundary conditions and initial guess produced by the high-confinement approximation [136]. These solutions are illustrated in Fig. 3.1, where we give the profiles of single-hump, two-hump, three-hump, and four-hump solitons for $(\widetilde{\eta};\Omega)\approx$(1.1;96.706), $(\widetilde{\eta};\Omega)\approx$(1.1;100.4), $(\widetilde{\eta};\Omega)\approx$(1.1;101.75), and $(\widetilde{\eta};\Omega)\approx$(1.1;102), respectively. These discrete stationary multihump solitons are all constituted of solitons belonging to site-centered (sc) mode. Note that multihump solitons composed of solitons belonging to bond-centered (bc) mode and those belonging to bc and sc mode were also found. Figure 3.2 shows this case with the profile of two-hump and three-hump solitons for bc-sc mode, bc-bc mode and sc-bc-sc mode. We are now interested in multihump soliton solutions constituted solely of sc modes. Let ℓ_δ represents the interpeak separation, i.e., the distance between two neighbor peaks, where the subscript δ is the number of peak of the solution. In the case of two-hump solitons, we obtain $\ell_2 = 4$ while for three- and four-hump solitons, $\ell_3 = \ell_4 = 4\ell_2 = 16$ (see Fig. 3.1). This means that the localization of solution decreases when δ increases. Moreover, by noting ζ_δ as being the maximum amplitude of the δ-soliton, we have $\zeta_1 \simeq 0.19$, $\zeta_2 \simeq 0.13$, $\zeta_3 \simeq 0.077$ and $\zeta_4 \simeq 0.055$. So we also see a gradual decrease of ζ_δ as the number of peaks δ increases. It appears from these results that the system can not admit an unlimited number of peaked localized states. Recall that the normalization condition for envelope u_n ($\sum_n u_n^2 \simeq \frac{0.043}{\widetilde{\eta}}$) is satisfied for all these solutions. We can conclude that the localization of vibrational energy in protein can be in the form of single discrete solitons or a discrete multisoliton. A similar result was obtained in the past in the context of two-component solitary waves [137].

It is important to mention that $\widetilde{\eta}$ not only reflects the saturation coefficient but also the ratio between the expansion and compression terms of the molecular chain. We also want to add the following biological meaning of the phenomenon of saturation in order to show how our model is more realistic. The ATP conserves energy via glycolysis, glycogenolysis and the citric acid cycle. If the cells have sufficient supplies of ATP, then these pathways and cycles are inhibited. Under these conditions of excess ATP, the liver will attempt to convert a variety of excess glucose molecules into glycogen [138]. Thus, when ATP is too large, there is a saturation through these inhibitions. Otherwise,

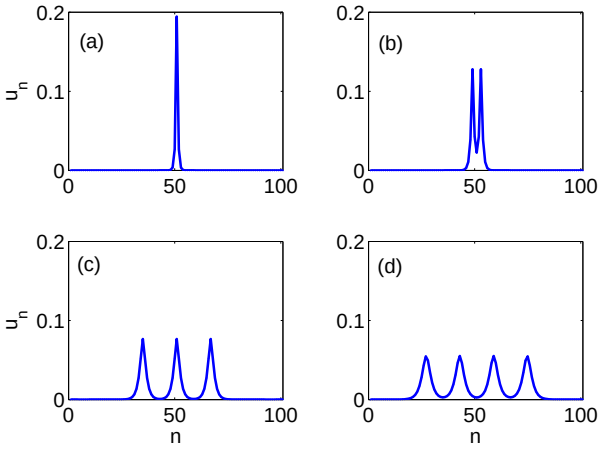

Figure 3.1: Examples of profiles of single-hump [(a), $(\widetilde{\eta};\Omega)$ ≈(1.1;96.706)], two-hump [(b), $(\widetilde{\eta};\Omega)$ ≈(1.1;100.4)], three-hump [(c), $(\widetilde{\eta};\Omega)$ ≈(1.1;101.75)], and four-hump [(d), $(\widetilde{\eta};\Omega)$ ≈(1.1;102)] solitons.

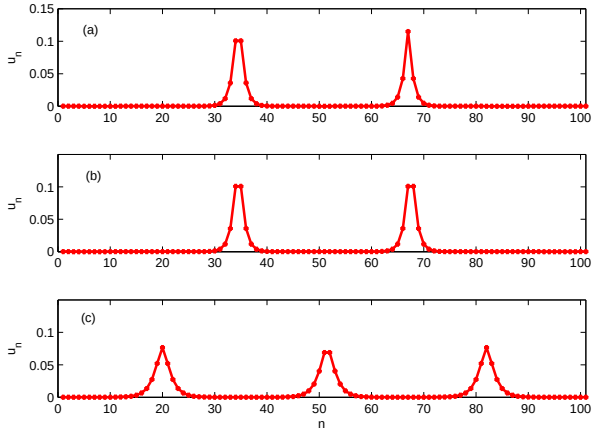

Figure 3.2: Examples of profiles of two-hump [(a), $(\widetilde{\eta};\Omega)$ ≈(1.1;100.9)], two-hump [(b), $(\widetilde{\eta};\Omega)$ ≈(1.1;100.9)] and three-hump [(c), $(\widetilde{\eta};\Omega)$ ≈(1.1;101.75)] solitons for bc-sc mode, bc-bc mode, and sc-bc-sc mode, respectively.

when the probability amplitude $|\phi_n|$ is low, the saturable nonlinearities can be reduced to a cubic nonlinearity via a Taylor expansion. Thus, the feature of our model is that it includes two cases (where ATP is produced in excess and otherwise).

For the soliton solutions previously seen to be biologically acceptable, they must be stable. Study of their stability is the purpose of the next section.

3.1.2 Stability analysis

The previous discrete solutions must be stable to be biologically acceptable for the localization and transport of vibrational energy in protein. Here, the stability of these solutions is considered from the view point of both the map orbit stability and the corresponding dynamical stability.

3.1.2.1 Mapping stability

Using the map approach technique [8, 136, 141–143], and defining $p_n = u_n$ and $q_n = u_{n-1}$. Eq.(3.1) is transformed into the following two dimensional real map:

$$\begin{cases} p_{n+1} = (2-\Omega)p_n + \eta\frac{p_n}{1+p_n^2} - \eta\frac{p_n^3}{(1+p_n^2)^2} - q_n \\ q_{n+1} = p_n. \end{cases} \tag{3.3}$$

A linearly unstable map orbit gives rise to a dynamically stable solution [141]. Moreover, to investigate the mapping stability, the study of the stability of the fixed point of the corresponding 2D map is sufficient. Then, the fixed points of Eq. (3.3), for which $p_n = q_n$, are located at:

$$p_0 = 0, \quad p_{1,2} = \pm\sqrt{\frac{-\Omega \pm \sqrt{\Omega\eta}}{\Omega}}. \tag{3.4}$$

Knowing that $\eta > 0$ with $\eta = 93\widetilde{\eta}$, $p_{1,2}$ exists if only if $\Omega > 0$ and $\eta \geq \Omega$. The Jacobian matrix $\check{J}$ of the map Eq. (3.3) is given by:

$$\begin{pmatrix} (2-\Omega) + \eta\frac{1-p_n^2}{(1+p_n^2)^2} - \eta\frac{p_n^2(3-p_n^2)}{(1+p_n^2)^3} & -1 \\ 1 & 0 \end{pmatrix} \tag{3.5}$$

The study of the stability of fixed points requires the evaluation (calculation) of the eigenvalues of the Jacobian $\check{J}$ evaluated at these points. This being done, the fixed points will be an unstable saddle point if $|\lambda_1| > 1$ and $|\lambda_2| < 1$ or vice versa. λ_1 and λ_2 being the eigenvalues of $\check{J}$. Particular attention is given to saddle fixed points due to the fact that they can support homoclinic orbits used to generate bright soliton solutions [141]. On the other hand, we recall

that the homoclinic orbits are obtained through the intersection of stable and unstable manifolds. In the top left panel of Fig. 3.17, the areas marked in blue, red and yellow are those for which p_0, p_1, and p_2 are unstable saddle nodes, respectively. When we employ the technique of residues as defined in Ref. [142], we obtain that the condition of existence of unstaggererd soliton is: $\eta \geq \Omega$, with $\eta = 93\widetilde{\eta}$. This condition is shown in the top left panel of Fig. 3.17 by the area bounded by two straight lines of black color. The condition of existence mentioned above is similar to that in the case of the discrete version of the Vinetskii-Kukhtarev equation [136]. This is probably due to the fact that our model has the same tangent map around zero as the discrete Vinetskii-Kukhtarev equation. However, properties related to non-zero fixed points are different from theirs.

Notice that the area of existence in the top left panel of Fig. 3.17 contains probably two types of spatially localized solutions: breathers and multibreathers [8]. Because the fixed point is saddle, it is not sufficient by itself to guarantee the existence of stable and unstable manifolds that intersect [9]. This is why we must determine the domain for which the stable and unstable manifolds intersect. Figure 3.18 corroborates the top left panel of Fig. 3.17 despites some nuances observed when $\Omega \lesssim 0.08$.

Another illustration of the comments that have been carried out is through the top right and bottom left panels of Fig. 3.17. From these figures, it clearly reflected that the bright soliton cannot exist without constraints on the parameters. Moreover, knowing that a much richer tangling structure is equivalent to a richer family of solitons [143], the evolution of map orbits ($\widetilde{\eta} = 0.06$) from $\Omega = 4.4$ to $\Omega = 5$ shows a dimunition of this family of soliton solutions (bottom right panel of Fig. 3.17). This dimunition continues until Ω = 5.58, where a fold bifurcation occurs. Before that, we have a pitchfork bifurcation that occurs when $\Omega \simeq 4.9$.

At this point, among the previous types (or modes) of solitons discussed, which are most likely to carry in a stable manner the energy of amide-I vibrational excitation through the protein molecules?

3.1.2.2 Linear stability analysis

In this subsection, we will study the stability of DMHS by means of linear stability analysis [145]. Here the DMHS are slightly perturbed:

$$\phi_n = \exp(-i\Omega t)[u_n + \varepsilon(x_n \exp(\lambda t) + y_n \exp(\overline{\lambda} t))], \tag{3.6}$$

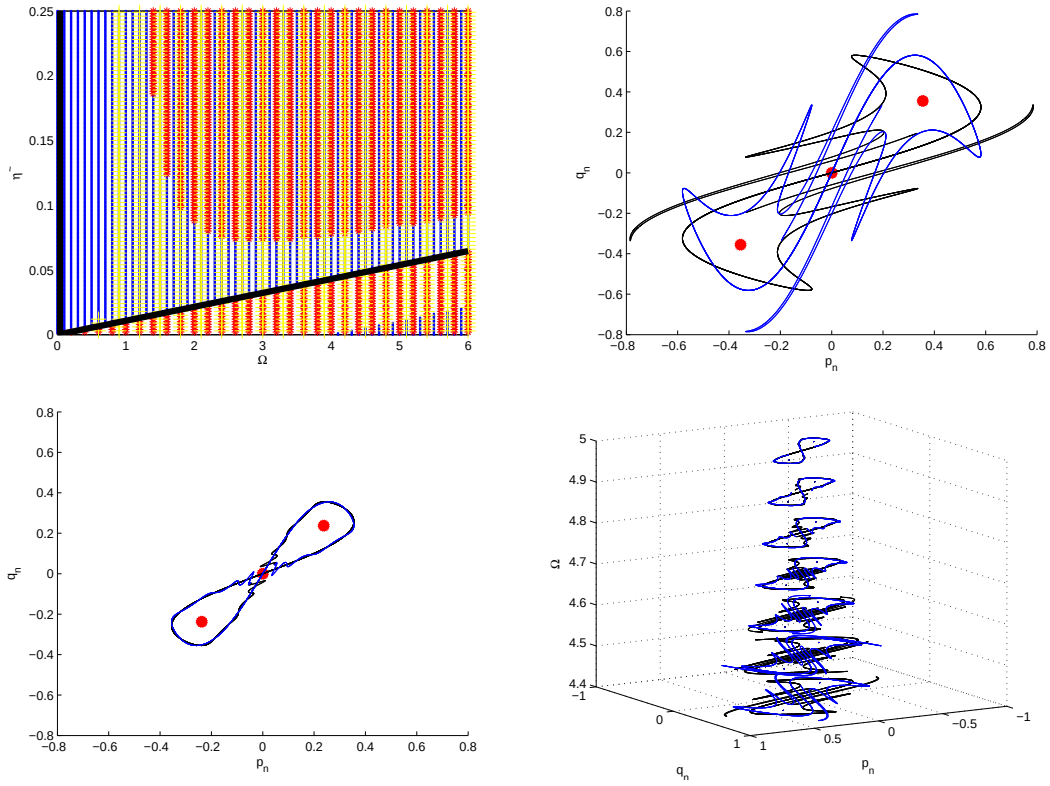

Figure 3.3: Stability diagram of the fixed points of Eq. (3.4) (top left panel) in the $\Omega - \widetilde{\eta}$ parameter plane. The areas marked in blue, red, and yellow are those for which p_0, p_1, and p_2 are, respectively, unstable saddle nodes. In the top right and bottom left panels, we have intersections of stable and unstable manifolds for (Ω, $\widetilde{\eta}$) = $(4.4, 0.06)$ and $(5, 0.06)$, respectively. The red dots being the fixed points. In the bottom right panel, we have the map orbits around the fixed point p_0 according to Ω, $\widetilde{\eta} = 0.06$.

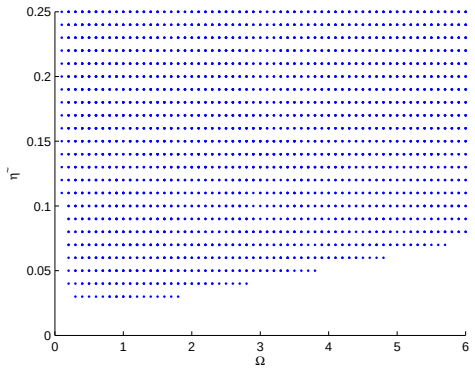

Figure 3.4: Domain of existence of the intersection of manifolds. Condition of obtaining bright soliton solution.

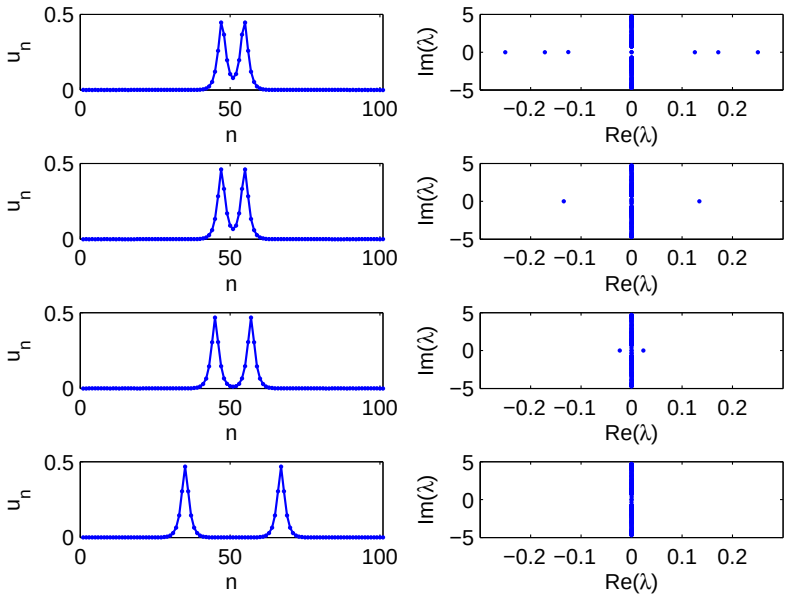

Figure 3.5: Profiles of two−hump solitons (left column) and their correponding eigenvalue spectrum (right column) with increasing (from top to bottom) values of ℓ_2: ℓ_2 =4; 8; 12 and 32. $\Omega \approx 3.6$, $\widetilde{\eta} \approx 0.0464$.

where x_n and y_n are complex, ε is a linearization parameter, and λ is the eigenvalue. Add that $\overline{\lambda}$ denotes the complex conjugate of λ, Ω being the frequency seen above. This leads to the linear stability equations:

$$i\lambda \begin{pmatrix} x_n \\ \overline{y_n} \end{pmatrix} = \begin{pmatrix} -\Omega + \frac{\eta}{1+|u_n|^2} - \frac{3\eta|u_n|^2}{(1+|u_n|^2)^2} + \frac{2\eta|u_n|^4}{(1+|u_n|^2)^3} - \Delta_2 & -\frac{2\eta u_n^2}{(1+|u_n|^2)^2} + \frac{2\eta|u_n|^2 u_n^2}{(1+|u_n|^2)^3} \\ \frac{2\eta \overline{u_n^2}}{(1+|u_n|^2)^2} - \frac{2\eta|u_n|^2 \overline{u_n^2}}{(1+|u_n|^2)^3} & \Omega - \frac{\eta}{1+|u_n|^2} + \frac{3\eta|u_n|^2}{(1+|u_n|^2)^2} - \frac{2\eta|u_n|^4}{(1+|u_n|^2)^3} + \Delta_2 \end{pmatrix} \begin{pmatrix} x_n \\ \overline{y_n} \end{pmatrix} \tag{3.7}$$

Among the $2N$ eigenvalues λ, if at least one has a strictly positive real part, a DMHS is spectrally unstable. Solving numerically Eq. (3.7), we obtain the eigenvalue spectrum for strongly localized sc and bc modes.

A linear analysis of stability of DMHS composed of soliton belonging to sc mode is carried out by solving numerically the eigenvalue problem (EVP) described by Eq. (3.7) where u_n is the solution found numerically in the previous section. The results of this analysis are shown in Figs. 3.5 and 3.6. Figure 3.5 is concerning the symmetric two-hump solitons normalized for four values of ℓ_2: 4, 8, 12 and 32. The corresponding eigenvalues spectrum shows that the intensity of the instability decreases as ℓ_2 increases. After checking

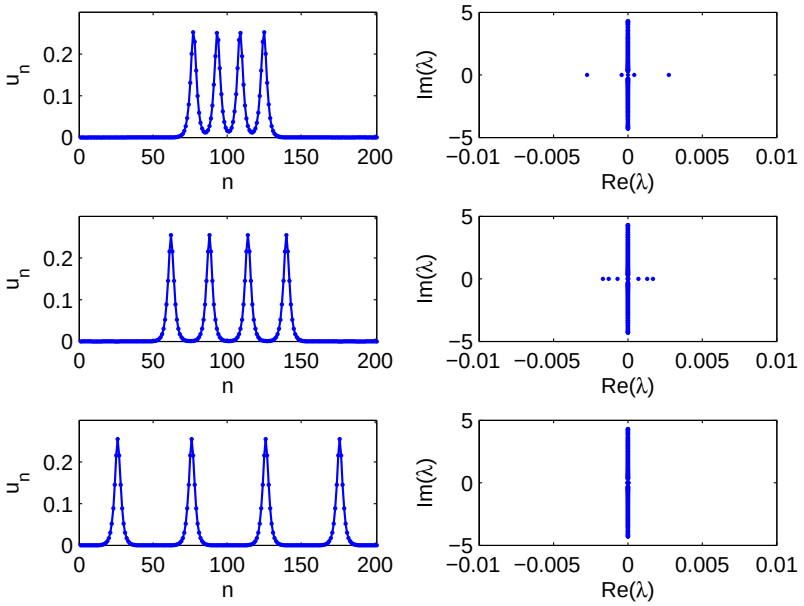

Figure 3.6: Profiles of four−hump solitons (left column) and their correponding eigenvalue spectrum (right column) with increasing (from top to bottom) values of ℓ_4: ℓ_4 =16; 26 and 50. $\Omega \approx 4.9$, $\widetilde{\eta} \approx 0.056$.

intermediate values, we note that $\ell_\delta^* \approx 32$ is the threshold value where the solution becomes stable. A similar phenomenon is observed in Fig. 3.6 for four-hump solitons when $\ell_\delta^* \approx 50$. Thus, the stability of multihump solitons depends on the value of ℓ contrary to what is observed in optics (see [135]). We further note that the stability of multisoliton depends on ℓ_δ. In fact, ℓ_δ increases as δ increases. As an explanation, we can say that the instability of our multisoliton for values of ℓ_δ below the ℓ_δ^* is probably due to interactions between the δ present solitons. This is why a large number of peaks (δ) leads to great interaction between them, hence a large distance between them to stabilize. This explains the reasons for which we have: $\ell_2^* < \ell_3^* < \ell_4^*$.

A numerical evolution of DMHS having at least one soliton with bc mode, by means of fourth-order Runge-Kutta scheme with a suitable choice of time step and absolute tolerance (10^{-10}) in order to ensure the conservation of energy and normalization condition, is performed. It appears that this type of solutions is unstable as we shown in Fig. 3.7. Indeed, the bc solition of DMHS turns on sc soliton during the evolution of DMHS. A similar fact was noted in Ref. [144], where only on-site single-hump solitons are stable.

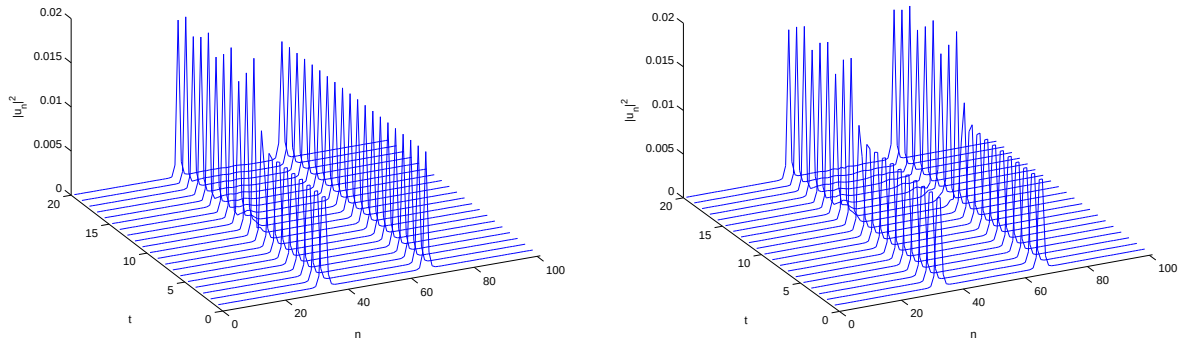

Figure 3.7: Development of instability of two-hump solitons having at least one intersite soliton for [(Ω, $\widetilde{\eta}$) = $(100.9, 1.1)$]. The left and right panels correspond to bc-sc mode and bc-bc mode, respectively.

3.1.2.3 Existence and stability diagrams of sc DMHS solutions

We proceed to exploring the existence and stability diagrams for all observed types of sc DMHS in the parameter space (Ω, $\widetilde{\eta}$). It appears from Fig. 3.8 (top left and bottom right panels) that the regions where DMHS exist decreases as the number of humps increase. For the case of four-hump solitons it is reduced to a very thin region of parameter space. Insets of these figures illustrate the case where the local compression prevails over the local dilatation ($\widetilde{\eta} > 1$). Stability of two-hump soliton with $\ell_2 = 32$ is displayed in the bottom left panel of Fig. 3.8. It emerges that the increase of interpeak separation ℓ_2 does not make all of the solution stable in the parameter space. It being understood that for $\ell_2 < 32$, almost all two-hump solitons are unstable. Similar to two-hump solitons, almost all four-hump solitons are unstable for ℓ_4 <50 and stable for $\ell_4 = 50$ (see the bottom right panel of Fig. 3.8). This fact reaffirms that interpeak separation has a stabilizing effect on the solutions. The bottom left panel of Fig. 3.8 underpins this observation. Otherwise, since the magnitude of instability decreases as the interpeak separation increases [146], the strength of higher-order nonlinearity in our saturable DNLS may enhance the stability. Indeed, it is well known that the magnitude of instability decreases by increasing the strength of nonlinearity of Cubic DNLS [146]. Here the enhancement of the stability is justified by the fact that the strength of higher order saturable nonlinearity increases the nonlinearity of cubic DNLS equation obtained by expanding in Taylor series the saturable nonlinearities.

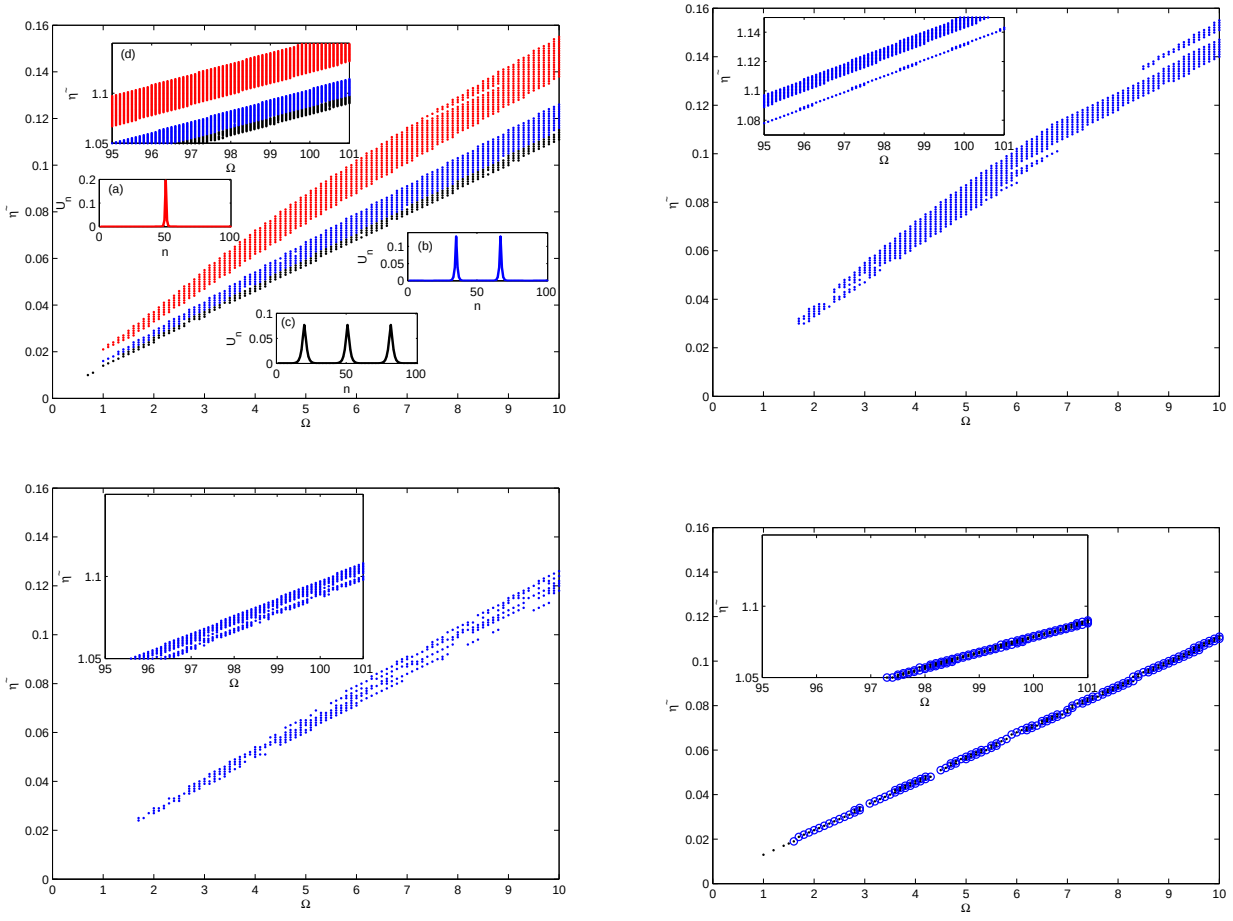

Figure 3.8: Existence and stability diagrams for all observed types of sc DMHS solutions. In the top left panel, we have the existence diagram for one-hump solitons (red), two-hump solitons (blue), and three-hump solitons (black). Inset (d) shows the case where $\widetilde{\eta} > 1$. Other inserts, (a), (b), and (c), are related to observed types of sc DMHS. The stability diagram of one-hump and two-hump ($\ell_2 = 32$) solitons is shows in the top right and bottom left panels, respectively. The bottom right figure illustrates the existence (dot) and stability (circle) diagram for four-hump ($\ell_4 = 50$) solitons. Insets show the case where $\widetilde{\eta} > 1$.

At the end of this section, as the evolution of the localized solectron states has suggested their potential as new carriers for fast electric charge transport [130], it emerges that when multi-peaked localized solutions are stable, they may be a candidate for energy transport in the protein.

3.1.3 Mobility of Discrete Multihump Solitons

In this section, we study the DMHS mobility. Note at the outset that the study of bright mobile solution in the DNLS with photorefractive nonlinearity has already been done [19, 141, 147]. However, for DNLS equation with saturable nonlinearities, mobility of multibreathers has not been yet found. We use here the energy techniques which consists "to push" the localized solution to move through the lattice by means of a variation of the solution initial phase. This is done through the following perturbation:

$$\phi_n(0) = u_n \exp(i\varpi n), \tag{3.8}$$

where u_n is a stationary solution seen above, and ϖ represents the relative strength.

By applying the kick to two-hump [[Fig. 3.9(a)], three-hump [Fig. 3.9(b)] and four-hump solitons [Fig. 3.9(c)], we obtain Figs. 3.9(d), 3.9(e), and 3.9(f), respectively. In these figures, it appears that the mobility is achieved for three-hump solitons, four-hump solitons, and to a more limited extent, two-hump solitons. This is not the case for one-hump soliton. Moreover, in our model, the mobility is achieved for $\Omega \simeq \eta_1(1 + \frac{\eta_2\alpha^2}{\eta_1(1+\alpha^2)})$, where α is the amplitude of our solutions and $\eta_2 = -\eta_1$. This new condition of mobility depends on the higher-order saturable nonlinearity. For the general case (model where η_1 and η_2 are arbitrary nonlinear coefficients), if $\eta_2 = 0$, this latter condition reduces to $\Omega \simeq \eta$, which is the condition of mobility for the single soliton in the DNLS equation with saturable nonlinearity (see Ref. [141]). In view of the existence diagram, it follows that the sc DMHS are more able to be mobile. In other words, the sc DMHS are more able (with the kick) to overcome the Peierls-Nabarro barrier (PNB).

The main conclusion to be drawn from these observations is that a discrete multihump soliton-like mechanism for vibrational energy transport along the protein chain is possible.

However, it would be advisable to dwell on the influence of long-range interactions on the above results.

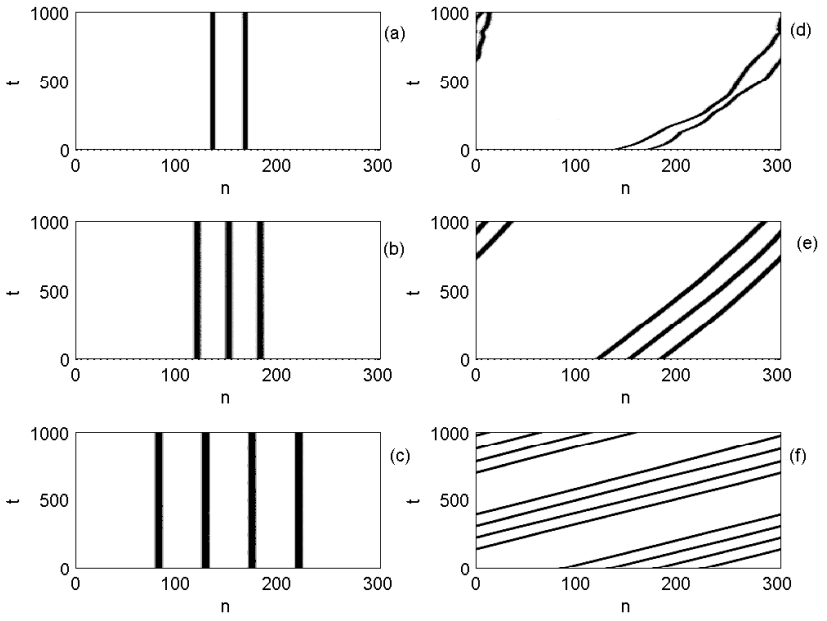

Figure 3.9: Density plot $|\phi_n|^2$ for not kicked (a) two-hump, (b) three-hump, (c) four-hump solitons and their kicked counterparts, (d), (e), and (f), respectively. We have (d) $\varpi = 0.55$, $\Omega \approx 3.6$, $\widetilde{\eta} \approx 0.0464$; (e) $\varpi = 0.3$, $\Omega \approx 5.635$, $\widetilde{\eta} \approx 0.065$; (f) $\varpi = 0.3$, $\Omega \approx 4.9$, $\widetilde{\eta} \approx 0.056$; respectively. Mobility is achieved for $\Omega \simeq \eta(\frac{1}{1+\alpha^2})$, (d) $\alpha = 0.4777$, (e) $\alpha = 0.2765$, (f) $\alpha = 0.2549$.

3.2 Effects of next-NNI on discrete multibreathers corresponding to Davydov model with saturable nonlinearities

We recall that Eq.(2.15) exhibits a competition between local compression and local dilatation of lattice which leads to the interplay between self-focusing and defocusing saturable nonlinearities (see section 3.1). Presumably the combination of these properties with next-NNI will have implications on the modulational instability of a nonlinear plane waves.

3.2.1 Discrete modulational instability

We propose here to discuss the discrete MI of DNLS equation with saturable nonlinearities. We note that a similar study was conducted in one-dimensional waveguide arrays possessing a saturable self-defocusing nonlinearity and taking into account only NNI [149].

Let us begin this study by looking for solutions of Eq.(2.20) in the form of discrete plane wave

$$\phi_n = \zeta \exp[i(qn - \omega t)], \tag{3.9}$$

where ζ is is the constant amplitude, q is the wave number, and ω is the frequency. The nonlinear dispersion relation satisfied by this frequency is given by

$$\omega = 4\sum_m S_m \sin^2(\frac{qm}{2}) + \frac{\eta_1}{1+\zeta^2} - \frac{\eta_2\zeta^2}{(1+\zeta^2)^2}. \tag{3.10}$$

The linear stability of Eq.(3.9) can be investigated by studying the stability of its amplitude as a function of sufficiently small perturbation so that, one can linearize the equation of the envelope of the carrier wave. Therefore, one introduces a small perturbation, $\delta\phi_n$, in Eq.(3.9) and checks the solution of Eq.(2.20) in the form

$$\phi_n = (\zeta + \delta\phi_n) \exp[i(qn - \omega t)]. \tag{3.11}$$

The insertion of Eq.(3.11) in Eq.(2.20), with a linearization around the unperturbed plane wave gives us the following equation

$$i\frac{\partial(\delta\phi_n)}{\partial t} = -\sum_m S_m \left[\delta\phi_{n+m}\exp(iqm) + \delta\phi_{n-m}\exp(-iqm)\right]$$

$$+ 2\sum_m S_m \cos(qm)\delta\phi_n - \Upsilon(\eta_1,\eta_2,\zeta)(\delta\phi_n + \overline{\delta\phi_n}), \tag{3.12}$$

where the overbar, $^-$, denotes complex conjugate and Υ is defined by

$$\Upsilon(\eta_1,\eta_2,\zeta) = \frac{\eta_1\zeta^2}{(1+\zeta^2)^2} - \frac{\eta_2\zeta^2(\zeta^2-1)}{(1+\zeta^2)^3}. \tag{3.13}$$

Furthermore, considering the solution of Eq.(3.12) with the wave number Q and frequency Ω in the form

$$\delta\phi_n = A_1 \exp[i(Qn-\Omega t)] + \overline{A_2}\exp[-i(Qn-\overline{\Omega}t)], \tag{3.14}$$

where $A_{1,2}$ are constants, we obtain

$$\left[\Omega - 2\sum_m S_m \sin(qm)\sin(Qm)\right]^2 = 4\left[\sum_m S_m\cos(qm)\sin^2\left(\frac{Qm}{2}\right)\right]$$

$$\times\left[4\sum_m S_m\cos(qm)\sin^2\left(\frac{Qm}{2}\right) - 2\Upsilon(\eta_1,\eta_2,\zeta)\right], \tag{3.15}$$

which represents the dispersion relation. The perturbation (Eq.(3.14)) will be unstable if the righ-hand side of Eq.(3.15) is negative. Note that the saturable medium occurs here through the function Υ while the contribution of next-NNI is made through S_m. Moreover, when $\zeta \ll 1$ and $m = 1$, we find the results obtained in [150] for the discrete cubic-quintic nonlinear Schrödinger equation where the coefficients of cubic and quintic terms are $\lambda = (\eta_1+\eta_2)$ and $\gamma = -(\eta_1 + 2\eta_2)$, respectively. In the following, we will use the dimensionless variable $\widetilde{\eta}$ knowing that $\eta = 93\widetilde{\eta}$ (see section 3.1).

Fig. 3.10(a) shows the region (dark) of modulational instability in plane (q, Q) in the case of nearest neighbor interaction ($m = 1$). When taking into account successively the second, third, fourth, tenth and twentieth neighbors, we see gradually as m increases the narrowing of the area where MI occurs (Fig. 3.10(b), (c), (d), (e), (f)). This area hardly varies for $m > 3$. For low values of the wave number of carrier wave q the MI region is cropped gradually as m increases. An analogous observation was noted in [42] where the authors used the Discrete Cubic Schrödinger equation. However, for the large value of q, there is no instability zone here. This result contrasts with the one obtained in [42] for the case $m = 2$.

By using the growth rate of MI defined by $G(Q) = Im(\Omega)$, it appears through

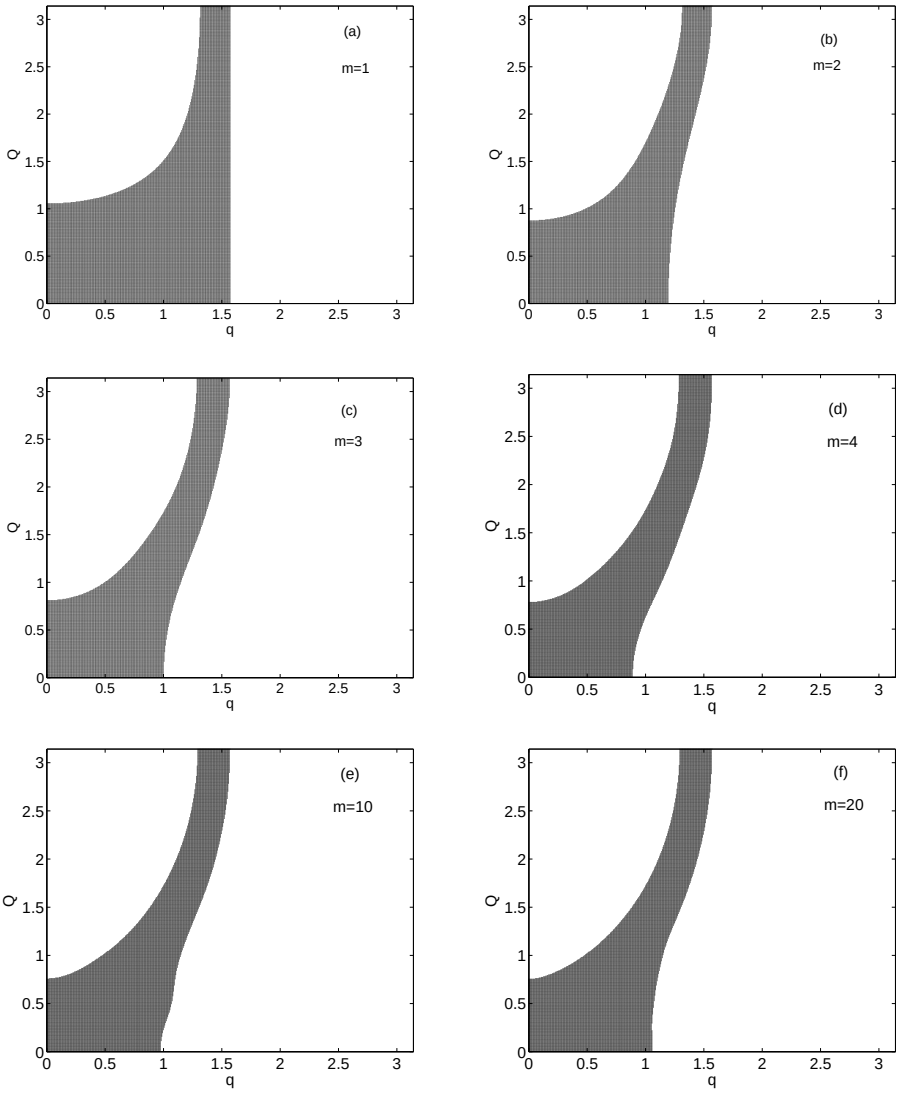

Figure 3.10: Modulational instability region (dark) in the $q-Q$ plane versus next-nearest neighbor interaction parameter m: $\widetilde{\eta}_1 = \widetilde{\eta}_2 = 1.1$ and $\zeta = 0.05$.

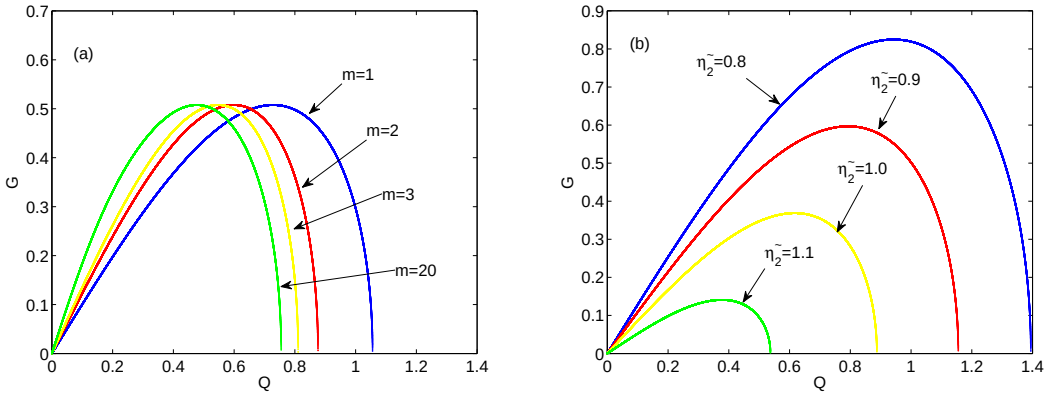

Figure 3.11: Growth rate versus the wave number of perturbation for different (a) number of next-nearest neighbors [$\zeta = 0.05$, $\widetilde{\eta}_1 = \widetilde{\eta}_2 = 1.1$] and (b) saturable higher order nonlinearity parameters [$\zeta = 6.05$, $\widetilde{\eta}_1 = 1.1$, $m = 1$].

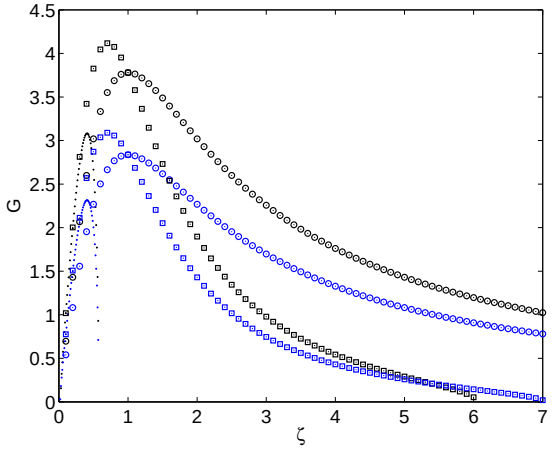

Figure 3.12: Dependence of gain with ζ for discrete cubic-quintic nonlinear Schrödinger equation [(dots), $\widetilde{\eta}_1 = \widetilde{\eta}_2 = 1.1$], discrete Vinetskii-Kukhtarev equation [(circles), $\widetilde{\eta}_1 = 1.1, \widetilde{\eta}_2 = 0$] and Eq.(1.3) [(squares), $\widetilde{\eta}_1 = \widetilde{\eta}_2 = 1.1$]. Q being 0.4. Blue markers correspond to $m = 1$ while black markers correspond to $m = 3$.

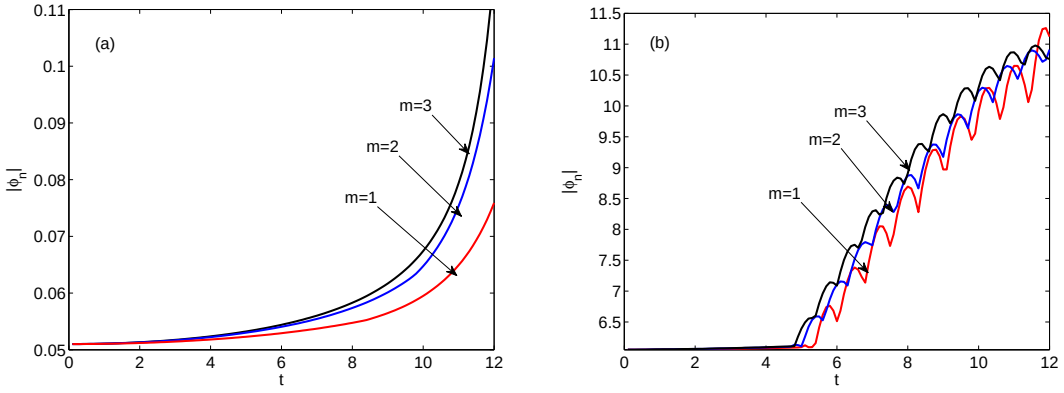

Figure 3.13: Simulated evolution of plane wave with small perturbation (Eq.(2.15)) for (a) $\zeta = 0.05$ and (b) $\zeta = 6.05$. In both cases, $\widetilde{\eta}_1 = \widetilde{\eta}_2 = 1.1$.

Fig. 3.11(a) that the inclusion of next-NNI increases the stability zone, since the maximum value of the gain remains constant when m ranges. Besides, Fig. 3.11(b) reveals that the gain decreases when the saturable higher order nonlinearity increases, $\widetilde{\eta}_1$ being fixed and $\zeta = 6.05$. It follows that the higher order saturable nonlinearity can suppress the instability. This can explain the absence of MI zone for large values of q in Fig. 3.10 and their presence in [42] for the case $m = 2$.

For a given value of Q, the dependence of the gain on the unperturbed plane wave solution is almost identical regarding the discrete cubic-quintic nonlinear Schrödinger equation (CQNS), the discrete Vinetskii-Kukhtarev (VK) equation and our model (Fig. 3.12). In fact, this is true for small values of ζ and is due to the fact that nonlinearities in the three previous mentioned models are reduced to cubic-quintic terms when the Taylor expansion is applied in the first approximation. We also note that our saturation compared to that of VK increases the maximum gain and reduces the bandwidth of amplitudes which can lead to MI. This trend is maintained when m varies. Nevertheless for a given value of Q, where m increases, the maximum value of the gain increases in our model.

It is well known that MI of plane waves predicts the formation of localized excitations. With the aim to verify that numerically, we integrate Eq.(2.20) by fourth-order Runge-Kutta method with periodic boundary conditions and taking 10^{-10} as absolute tolerance. The step is for its selected so that it ensures the conservation of P and H. The use of the following initial condition

$$\phi_n(t=0) = (\zeta + A\cos(Qn))\cos(qn) \tag{3.16}$$

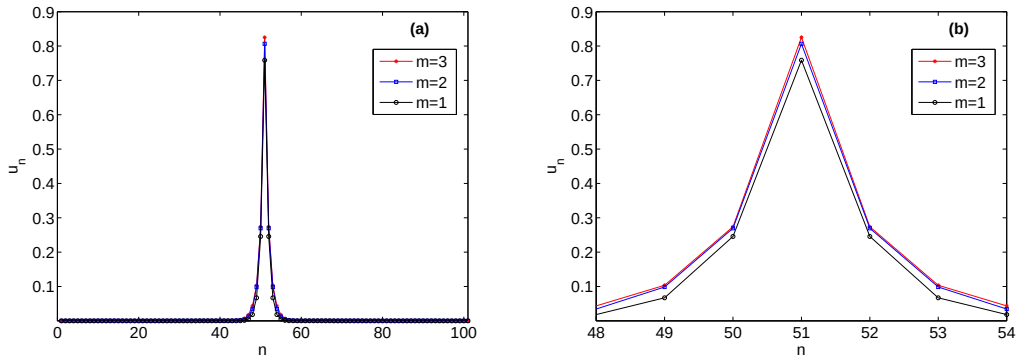

Figure 3.14: Dependence of single-hump soliton with next-NNI parameter m. $\widetilde{\eta}$=0.06, μ=3.6.

allows us to obtain the two panels of Fig. 3.13 where Q=q=0.0419. We note that the inclusion of second nearest neighbors and third nearest neighbors leads to early onset of MI for both values of the amplitude ζ ($\zeta = 0.05$ and $\zeta = 6.05$). In other words, neglecting the presence of next-NNI means overestimate the time of onset of MI.

Since the MI is the first step towards energy localization [151], let us move to the study of the effect of next-NNI on stationary localized solutions.

3.2.2 Stationary localized solutions

We focus here on unstaggered modes having their maxima in one (multiple) peptide group(s) of the alpha-helical protein chain. For this purpose, we use the steady-state ansatz $\phi_n = u_n \exp(-i\mu t)$ where μ is the frequency and u_n is the stationary amplitude and insert it in Eq.(1.3) to obtain

$$\mu u_n + \sum_{m(m\neq 0)} S_m(u_{n+m} + u_{n-m} - 2u_n) - \eta \frac{u_n}{1+|u_n|^2} + \eta \frac{|u_n|^2 u_n}{(1+|u_n|^2)^2} = 0, \tag{3.17}$$

where we set $\eta = \eta_1 = \eta_2$. Solutions of Eq.(3.17) must verify the normalization condition (see section 3.1)

$$\sum_n u_n^2 \simeq \frac{0.043}{\widetilde{\eta}}, \tag{3.18}$$

where $\widetilde{\eta}$ is the above mentioned dimensionless parameter. Using Newton-Raphson (NR) method with periodic boundary conditions to find solutions of Eq.(3.17) under the constraint of Eq.(3.18), it follows Figs. 3.14, 3.15, 3.16. The results described in these figures were obtained on a chain composed of

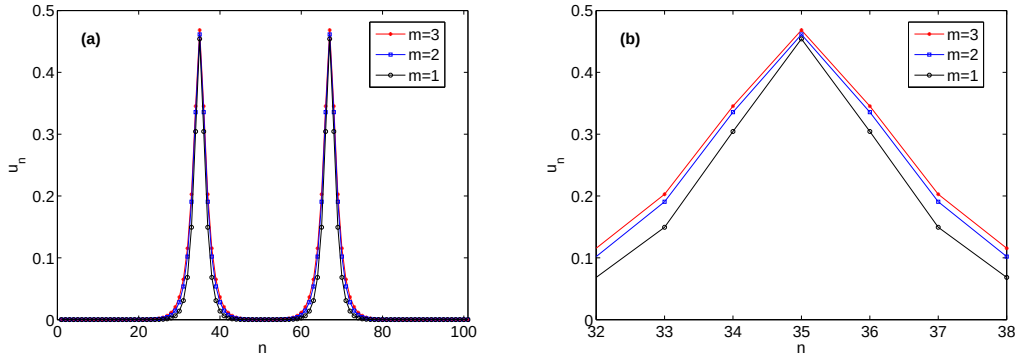

Figure 3.15: Dependence of two-hump soliton with next-NNI parameter m. $\widetilde{\eta}$=0.0464, μ=3.6.

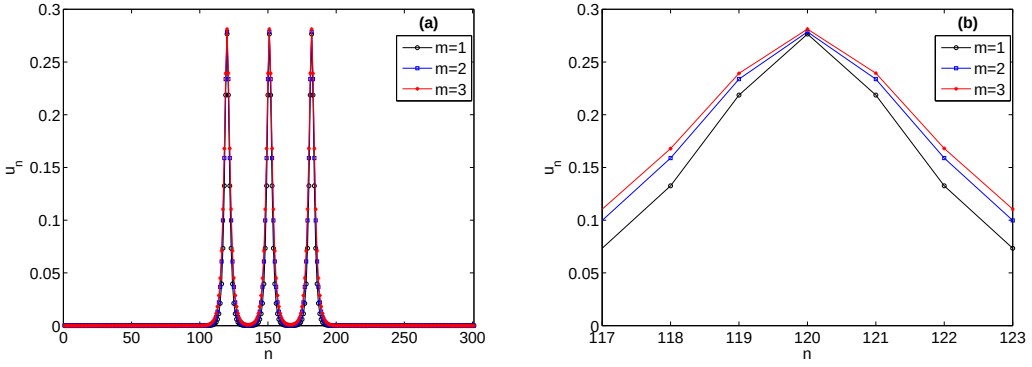

Figure 3.16: Dependence of three-hump soliton with next-NNI parameter m. $\widetilde{\eta}$=0.065, μ=5.63.

101 sites for single-hump and two-hump solitons, and 301 sites for three-hump soliton. It appears that the inclusion of second and third nearest neighbors makes corrections on DS and DMHS. More precisely, when m increases, the width and height of DS and DMHS increase. For the case of DS, Saha et al [152] has obtained similar observations on the protein-DNA dynamics in the long-wave limit. However, for a given solution, the corrections decrease as m increases (see Figs. 3.14(b), 3.15(b), 3.16(b) which are figures obtained by a zoom in Figs. 3.14(a), 3.15(a), 3.16(a), respectively). Moreover, when the number of peaks of solutions increases, the corrections of height to these solutions due to the inclusion of next-NNI decrease (see Figs. 3.14(a), 3.15(a), 3.16(a)). We recall that the next-NNI of dipole-dipole type is very important in the modeling of a realistic protein chain. Indeed, in proteins, several levels of dipoles can exist: the peptide bond is one of them. Therefore, the parallel assembly of several dipoles in an alpha helix leads to a dipole moment significantly greater [148, 153]. It appears within this framework that, according to the results seen above, energy localization in proteins can be mediated by DMHS.

3.2.3 Mobility and Collisional interactions

We study here numerically the DMHS mobility and the collision between two DMHS taking into account the next-NNI. For performing this, we use as initial condition

$$\phi_{n,\pm}(0) = u_{n,\pm}\exp(\pm i\varpi n) \tag{3.19}$$

where the subscripts $\pm$ stand for the DMHS coming into collision, u_n is a stationary solution and ϖ represents the relative strength. The numerical simulations presented in this framework use $N = 301$ sites for the mobility and $N = 602$ sites for the collision, a collision center being at $N_0 = 301$.

Following the observations made in previous section where it seems that the mobility is achieved for three-hump and four-hump solitons in short ranged limit, we apply the kick on these modes but this time around we consider the next-NNI. From Fig. 3.17(a), three-hump soliton ($\mu = 5.635$; $\widetilde{\eta} = 0.065$) has traveled 367 peptide groups for $m = 1$. When m is increased to two (Fig. 3.17(b)), the number of peptide groups traveled raised to 511. The number of peptide groups is 540 when $m = 3$ (Fig. 3.17(c)). Regarding four-hump soliton ($\mu = 4.9$ and $\widetilde{\eta} = 0.056$), the number of peptide groups traveled by this wave is 506, 700, 732 for $m = 1$ (Fig. 3.17(d)), $m = 2$ (Fig. 3.17(f)) and $m = 3$ (Fig. 3.17(f)), respectively. The interpretation we draw from this observations is

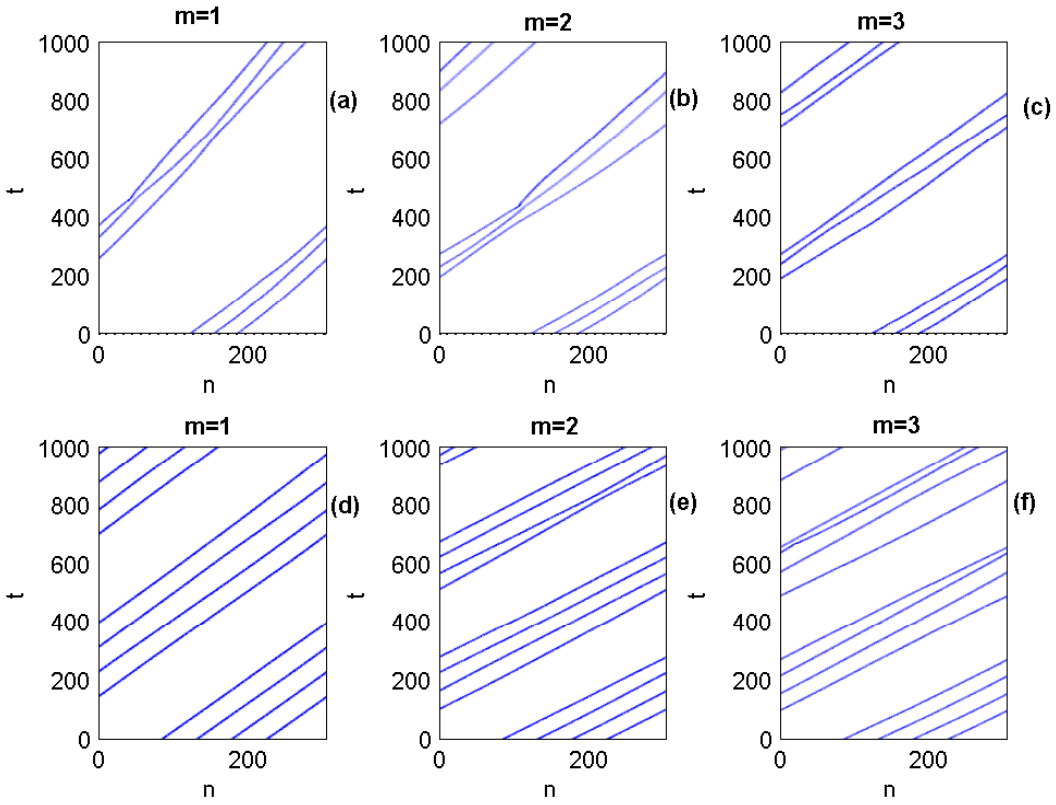

Figure 3.17: Density plot $|\phi_n|^2$ for kicked three-hump soliton ((a), (b) and (c)) and four-hump solitons ((d), (e) and (f)) for $\varpi = 0.3$. We have $\mu = 5,635$ and $\widetilde{\eta} = 0.065$ for three-hump soliton while $\mu = 4,9$ and $\widetilde{\eta} = 0.056$ for four-hump soliton.

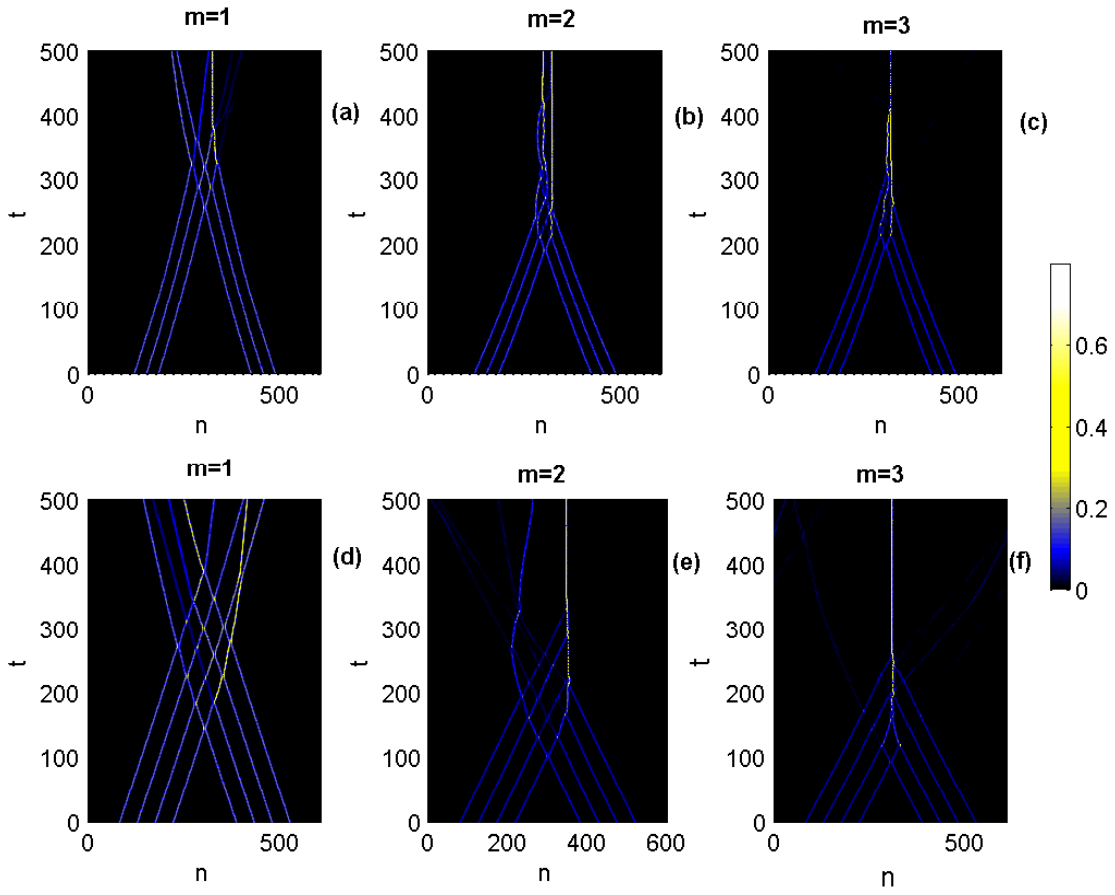

Figure 3.18: Head-on collision of two three-hump solitons ((a), (b) and (c)) and two four-hump solitons ((d), (e) and (f)) for $\varpi = 0.3$. We have $\mu = 5.635$ and $\widetilde{\eta} = 0.065$ for three-hump soliton while $\mu = 4.9$ and $\widetilde{\eta} = 0.056$ for four-hump soliton.

that the inclusion of next-NNI increases the speed of the DMHS and therefore the speed of energy transport along the protein chain. Furthermore, for given m, four-hump soliton is faster than three-hump soliton.

As regards the collision, note that the major part of the studies on collisions of solitons in saturable media was performed in optics. Generally, they are done in multi-component nonlinear systems [154]. Moreover, the study of the collisions of Davydov solitons was carried out [155] in two-component nonlinear systems. We focus here, for some examples, on interactions between multihump solitons that propagate in opposite directions with the same kick.

The simulations reveal through Fig. 3.18(a) the collision between two three-hump solitons. From this collision arises mainly a stationary solution.

It was also observed an internal reflection during this collision. This reflection leads a small fraction of energy to continue his career. When we increase the number of nearest neighbors m, this contributes to the formation of a large stationary solution after the collision (Fig. 3.18(b) and (c)). For the collision of two four-hump solitons, we observe in short ranged limit (Fig. 3.18(d)), a set of reflection. The inclusion of the second and third nearest neighbors (Fig. 3.18(e) and (f)) leads to the major reduction of reflections and formation of large stationary solutions. The salient feature that emerges here when considering next-NNI is that the collision between two DMHS leads mainly to the formation of a large stationary soliton.

Fair enough, do DMHS are transmitted or "supratransmitted"?

3.3 Nonlinear supratransmission of multibreathers in DNLS equation with saturable nonlinearities

Let us consider a one-dimensional ring of peptide groups (H-N-C=O) regularly positioned and coupled by hydrogen bonds. In dimensionless variables (ϕ_n), the state of amide-I excitations associated with this network is described by the DNSE with higher order saturable nonlinearity (section 3.1) given by

$$i\frac{\partial \phi_n}{\partial t} = -(\phi_{n+1} + \phi_{n-1} - 2\phi_n) + \eta_1 \frac{\phi_n}{1+|\phi_n|^2} - \eta_2 \frac{|\phi_n|^2 \phi_n}{(1+|\phi_n|^2)^2}, \tag{3.20}$$

for $n = 0, \ldots, N-1$, where N is the number of peptide groups. The real parameters η_1 and η_2 account for the nonlinearities and t corresponds to temporal coordinate.

There are two integrals of motion in Eq.(3.20). The first is the Hamiltonian

$$H = \sum_n \left[|\phi_{n+1} - \phi_n|^2 + (\eta_1 - \eta_2)\log(1+|\phi_n|^2) - \frac{\eta_2}{1+|\phi_n|^2} \right]. \tag{3.21}$$

The second constant is the number of quanta (l^2-$norm$), which is given by

$$P = \sum_n |\phi_n|^2. \tag{3.22}$$

The interest for the Eq.(3.20) model arises from the fact that it exhibits a competition between local compression and local dilatation of lattice which leads to the interplay between self-focusing and defocusing saturable nonlinearities.

In order to obtain allowed linear band of Eq.(3.20), we approximate a solution as the discrete plane wave

$$\phi_n = \zeta \exp[i(qn - \omega t)], \tag{3.23}$$

with ζ, q and ω representing amplitude, wave number, and frequency, respectively. Therefore we obtain the dispersion relation

$$\omega = 4\sin^2(\frac{q}{2}) + \eta_1, \tag{3.24}$$

having the phonon band $[\eta_1, \eta_1 + 4]$ in the frequency. For a frequency ω in the forbidden band, the linear theory predicts that a plane wave becomes evanescent.

Moreover, in the case where $\eta_2 = 0$, Eq.(1.2) reduced to DNSE with saturable nonlinearity for which the existence of supratransmission has been

performed by Susanto and Karjanto [57]. Could we abtain the transmission of plane wave in the forbidden band gap when $\eta_2 \neq 0$?

3.3.1 Threshold of supratransmission phenomena

To check supratransmission phenomena in our model, we will impose the launch of the wave by submitting Eq.(3.20) to the following conditions

$$\phi_0(t) = Ae^{-i\mu t}, \quad \phi_n(0) = 0 \quad for \quad n > 0 \tag{3.25}$$

where A is a the driving amplitude and μ is a driving frequency belonging to the lower forbidden band gap. By putting $A \to A(1 - e^{(-t/50)})$ and adding a damping with intensity linearly varying from 0 to 10 on the last 10 peptide groups, we avoid the initial shock wave and edge reflection respectively [54, 125].

The numerical integration of Eq.(3.20), by means fourth-order Runge-Kutta method and boundary conditions seen above, yields Fig. 3.19. This figure bring out the norm of the fiftieth particle $|\phi_{50}|^2$ for $\mu = 2$ belonging to the lower forbidden band gap and η_1 remaining fixed at 20. Being in the gap, it appears that there is a threshold amplitudes beyond which the wave propagation takes place within the molecular chain $(N = 100)$. This threshold values decrease gradually as the saturable higher order nonlinearity parameters η_2 increase. Indeed we have the threshold amplitudes 9.96 (Fig. 3.19 (a)), 7.84 (Fig. 3.19 (b)) and 6.47 (Fig. 3.19 (c)) for $\eta_2 = 0$, 10 and 20, respectively. Furthermore, the norm of the complex-valued amplitudes $\phi_{n=50}$ decrease as η_2 increase.

In order to obtain a systematic analysis of the threshold amplitudes versus μ, let us consider stationary solutions to Eq.(1.2) in the form $\phi_n = u_n e^{-i\mu t}$. We obtain subsequently a set of N coupled algebraic equation for the real-valued function u_n

$$\mu u_n + (u_{n+1} + u_{n-1} - 2u_n) - \eta_1 \frac{u_n}{1 + u_n^2} + \eta_2 \frac{u_n^3}{(1 + u_n^2)^2} = 0. \tag{3.26}$$

Following Ref. [58] and therefore making the approximation that the system is reduced to a few neighboring site only, Eq.(3.26) takes the form

$$f = [(\mu - 2)u_1 + A](1 + u_1^2)^2 - \eta_1 u_1(1 + u_1^2) + \eta_2 u_1^3 = 0. \tag{3.27}$$

These considerations (Eqs.(3.26) and (3.27)) are due to the fact that it has been shown in Ref. [58] using discrete Vinetskii-Kukhtarev equation that a threshold amplitude for supratransmission corresponds to a saddle-node bi-

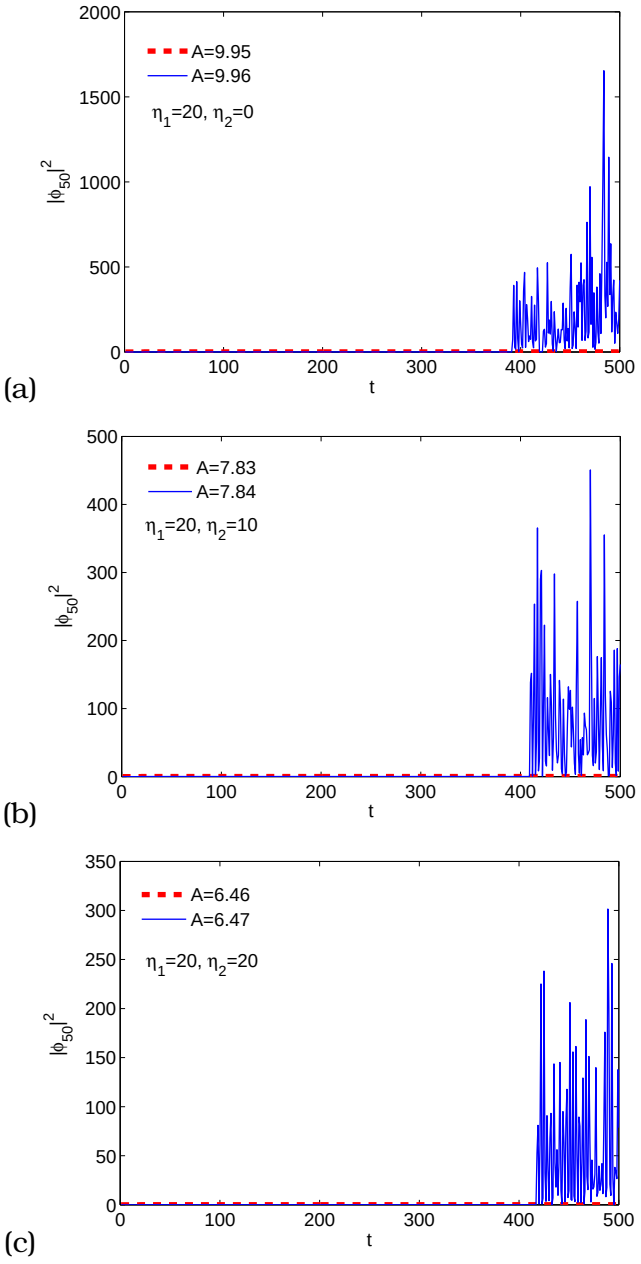

Figure 3.19: Plot of $|\phi_{n=50}|^2(t)$ for $\mu = 2$ and $\eta_1 = 20$. The red dashed line corresponds to $A = 9.95$ (a), $A = 7.83$ (b), $A = 6.46$ (c) while the solid blue line corresponds to $A = 9.96$ (a), $A = 7.84$ (b) and $A = 6.47$ (c). Thus the threshold amplitudes for $\eta_2 = 0$ (a), $\eta_2 = 10$ (b), $\eta_2 = 20$ (c) are 9.96, 7.84 and 6.47, respectively.

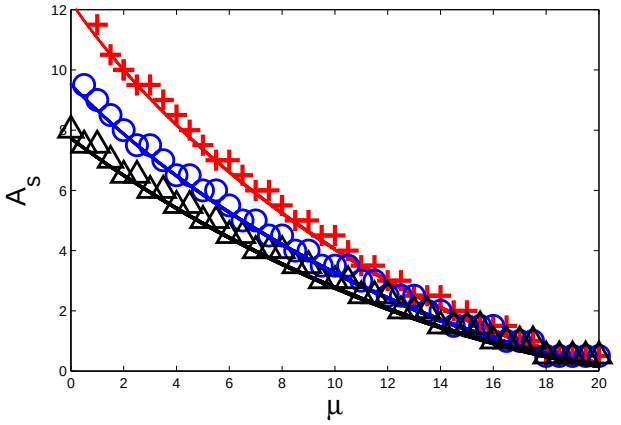

Figure 3.20: Threshold amplitude A_s versus driving frequency μ for $\eta_2 = 0$ (solid red line), $\eta_2 = 10$ (solid blue line) and $\eta_2 = 20$ (solid black line). The cross markers ($\eta_2 = 0$), the circle markers ($\eta_2 = 10$) and triangle markers ($\eta_2 = 20$) are relative to numerical method while the solid lines correspond to semi-analytical method. The results of numerical simulation were obtained by computing Eqs.(3.20) and (3.25) over the time interval [0, 500] with $N = 100$ and $\eta_1 = 20$.

furcation in the stationary solution. This bifurcation occurs when the local minimum of the function f for u_1 becomes a root of f with respect to A.

By searching analytically the minimum of f for u_1 and numerically a root of this one for A, we get in Fig. 3.20 the rule of change of threshold amplitude A_s versus frequency μ in the forbidden band gap. Fig. 3.20 shows the threshold amplitude A_s above which supratransmission occurs.

In this figure, the solid red line, the solid blue line and solid black line correspond to $\eta_2 = 0$, 10 and 20, respectively. Note that when $\eta_2 = 0$ and η_1 being set to 20, threshold amplitude versus frequency reduces to that found in Ref. [57]. Furthermore, there emerges from Fig. 3.20 that the saturable higher order nonlinearity parameter η_2 lowers the threshold amplitude A_s for supratransmission. Besides this semi-analytical method, numerical simulations of Eqs.(3.20) and (3.25) confirm the above-mentioned observations. In fact, the sequence of cross signs ($\eta_2 = 0$), circle signs ($\eta_2 = 10$) and triangle signs ($\eta_2 = 20$) correspond to numerical simulations. As another observations, we find that the required critical amplitude for supratransmission tends to zero close to the band edge, whatever the value of η_2. This finding joins that made by Leon et $al.$ in Bragg medium under nonlinear continuous wave excitation [126].

Recall that above some threshold amplitude, a sequence of nonlinear modes propagating in the medium [156].

On the other hand, it has been shown that our model (Eq.(3.20)) admits discrete multibreathers solutions as nonlinear modes (see section 3.1). The question that emerges from these previous observations is whether among the nonlinear modes propagate in the framework of supratransmission, can discrete multibreathers be one of them?

3.3.2 Discrete gap multibreathers

Let's start by noticing that it has been experimentally proved that the supratransmission does occur by means of gap soliton trains in Bragg gratings [157]. Here the concern is to show that the supratransmission can occur by means of discrete gap multibreathers that are intrinsic localized modes possessing an arbitrary number of humps. To carry out this work, let us consider Eq.(3.26) with following constraint

$$\sum_n u_n^2 \simeq \frac{4}{\eta}, \tag{3.28}$$

representing the normalization condition for a single quantum state when we set $\eta_1 = \eta_2 = \eta$ (as discussed above in section 3.1). The resolution of the Eqs.(3.26) and (3.28) in order to seek discrete stationary multibreathers solutions, oscillating with frequency belonging to the forbidden band, is done by means of iterative multidimensional Newton-Raphson method with periodic boundary conditions and initial guess produced by the high-confinement approximation [136].

It is worth noticing that, in our model, the mobility of discrete multisoliton is achieved for

$$\mu \simeq \eta_1 \left[1 - \frac{\eta_2 \alpha^2}{\eta_1(1+\alpha^2)}\right] \tag{3.29}$$

where α is the amplitude of our solutions (see section 3.1). Eq.(3.29) is an extension of what has been done for $\eta_2 = 0$ corresponding to discrete version of the Vinetskii-Kukhtarev equation and using mapping analysis [141]. A comparative study of the threshold amplitude for supratransmission and the mobility condition of discrete multibreathers yields Fig. 3.21(a) and (b). In these figures, mobility curve of discrete multibreathers has common parts with the area where the supratransmission occurs. Besides that, the discrete gap multibreathers can be transmitted or "supratransmitted" according to the frequency. Moreover, the discrete gap multibrathers are "supratransmitted" when we are close to the edge of the lower forbidden band. It emerges from Fig. 3.21 that the supratransmission can take the form of a discrete gap

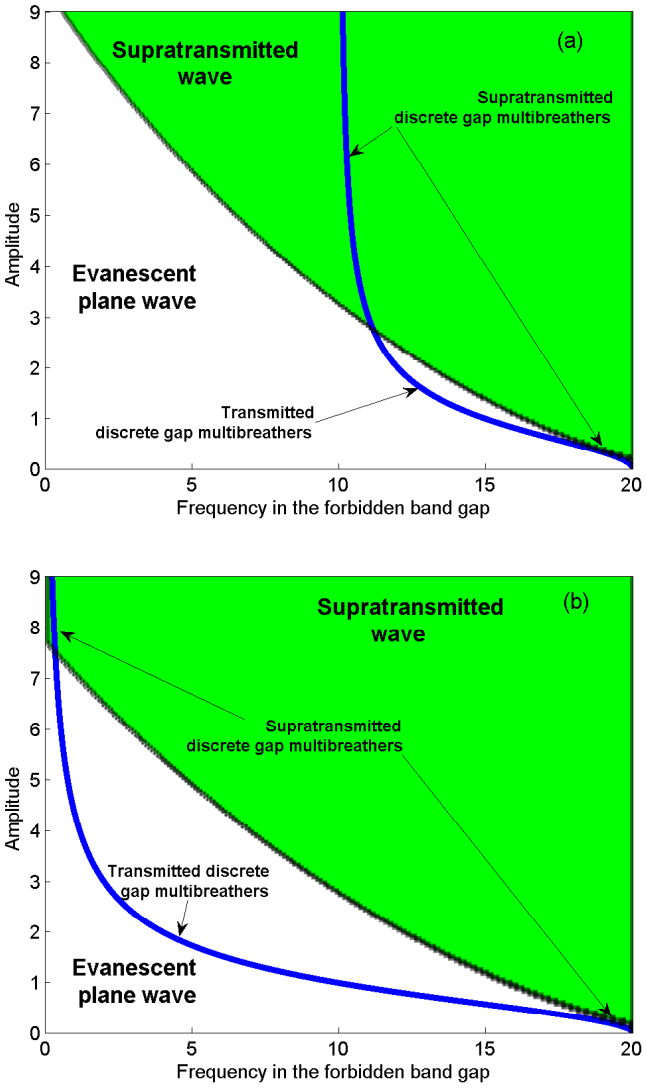

Figure 3.21: Graphs of threshold amplitude versus frequency (black line), above which supratransmission occurs (green zone), compared to the mobility curve of discrete multisolitons (blue line) governed by Eq. (2.13). The saturable higher order nonlinearity parameter is $\eta_2 = 10$ for (a) and $\eta_2 = 20$ for (b), η_1 remaining fixed at 20.

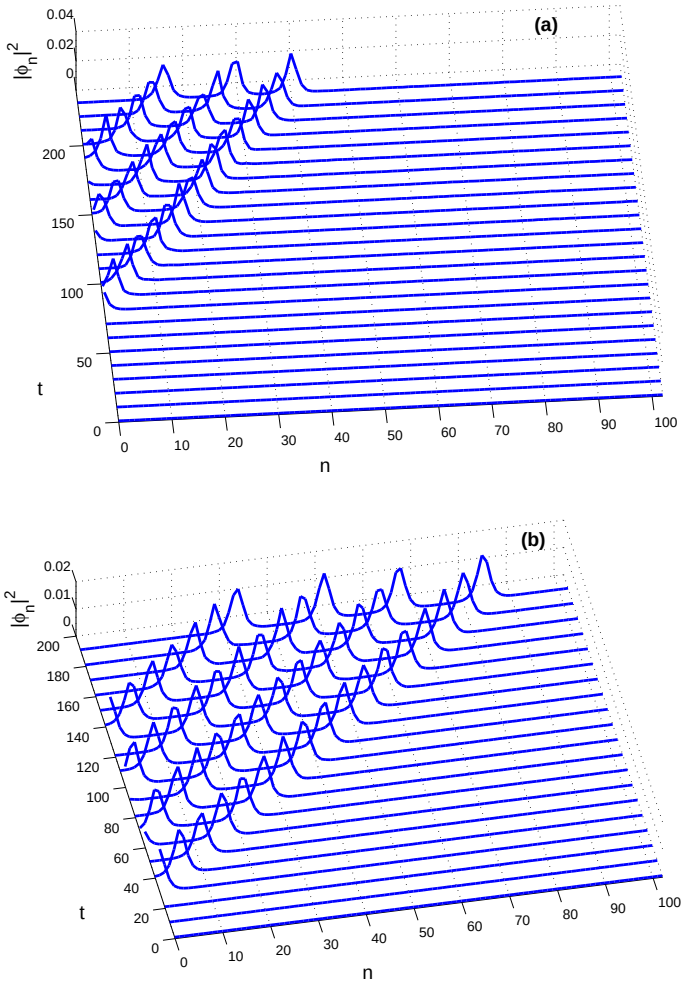

Figure 3.22: Propagations of discrete gap three-hump solitons ((a) for ($\xi = 0.27$, $\eta_1 = \eta_2 = 20$, $\alpha = 0.16$, $\mu = 19.50$)) and four-hump soliton ((b) for ($\xi = 0.56$, $\eta_1 = \eta_2 = 20$, $\alpha = 0.12$, $\mu = 19.71$)) in protein chains consisting of 101 peptide groups.

multibreathers. By the way, the following boundary condition has been used for Eq.(3.20)

$$\phi_{n=0}(t) = u(\xi t)e^{-i\mu t} \tag{3.30}$$

where μ is a driving frequency belonging to the lower forbidden band gap. u emulates the discrete stationary multibreathers (breathers with three and four humps) found numerically. Thus, the forcing amplitude u is molded by the shape of the discrete stationary multibreathers. Hence, ξ is the shaken frequency relating to the generation of the humps of the multibreathers. The numerical integration of Eq.(3.20) with Eq.(3.30), on a molecular lattice chain consisting of 101 peptide groups, yields Fig. 3.22(a) and (b) for three-hump soliton ($\xi = 0.27$, $\eta_1 = \eta_2 = 20$, $\alpha = 0.16$, $\mu = 19.50$) and four-hump soliton ($\xi = 0.56$, $\eta_1 = \eta_2 = 20$, $\alpha = 0.12$, $\mu = 19.71$), respectively. The normalization condition, namely Eq.(3.28), was monitored during the integration procedure.

On the other hand, the normalization condition implies that the amplitudes of the discrete multihump solitons decrease as the number of peaks increases. Thus, the discrete multihump solitons require less energy, for frequencies close to the lower band edge, compared to single solitons.

We should also add that during the nonlinear supratransmission, Leon and co-worker [126] think that the one-soliton tail provides an adiabatic deformation of the evanescent plane wave, and that any higher gap soliton trains would require more energy to be generated. This is probably due, besides the fact that Leon were in a continuum limit, to the fact that the discrete multihump soliton is a solution of DNSE while a soliton train is a group of solutions. From that perspective and in the framework where the normalization condition prevails, the nonlinear supratransmission can occur through the discrete gap multibreathers, particularly for frequencies close to the lower band edge.

That being so, what happens when we take into account the discreteness of the system and a small degree of disorder?

3.4 Biological multi-rogue waves in DNLS equation with saturable nonlinearities

3.4.1 Discrete Multi-rogue waves

The idea is to look for the discrete Multi-rogue waves by means of numerical experiments. To accomplish this, the following physical parameters are used [131, 132]: $J = 9.67 \times 10^{-4}$eV, $\varepsilon = 0.205$ eV. The random quantity β_n is taken as $|\beta_n| \leq 10^{-3}$. Our experiments are carried out on a chain with $N = 200$ peptide groups. By using a fourth-order Runge-Kutta method with periodic boundary conditions and taking 10^{-10} as absolute tolerance for the purpose of the conservation of P and H, we integrate Eq.(2.24). Unlike rational solutions generally used to obtain RW and following the idea of Ref. [75], a uniform probability amplitude is applied as the initial condition of Eq.(2.24). This is all the more physically relevant since the normalization condition requires $\sum_n \mid \phi_n \mid^2 = P$. P being a constant. Therefore $\phi_n(t=0) = \sqrt{\frac{P}{N}}$. Without loss of generality, let $P = 1$. Then the integration of Eq.(2.24), for $\eta_1 = 102.3$ and $\eta_2 = 0$, leads to Fig. 3.23(a). We observe that, with a initial uniform probability amplitude ($\phi_n(t=0) \simeq 0.0707$), the system selforganizes as a result of both disorder and nonlinearity. This selforganization is carried out in two ways. Firstly, we note that a short-living peaks appear on different sites. Secondly, as the time evolves, we remark the start (from $t \simeq 401$) of long-living peaks along the chain of peptide groups while the number and intensity of the short-living peaks decrease. Based on the precise definition of RW which stipulates that a wave is seen as extreme if its height is higher than the average wave amplitude plus eight times its corresponding standard deviation (see [76] and references therein), we can analyze the statistical distribution of maximum peak amplitudes. Then, Fig. 3.24(a) shows that, through each site n, 39.5 percent of absolute maximum amplitudes over time are rogue waves. In addition, the highest value of the maxima is 0.3. Inset of Fig. 3.24(a) shows the DMRW profile where we can see seven long-living peaks. Recall nevertheless that the normalization condition of amplitude ϕ_n is satisfied ($P \simeq 1$) when $t = 4000$. It therefore follows that the biological rogue waves as complex probability amplitude are not disastrous like rogue waves in the ocean. By increasing the strength of nonlinearity $\eta_2 = 51.15$ in Fig. 3.23(b), and $\eta_2 = 102.3$ in Fig. 3.23(c), we observe that the appearance of short-living peaks grows whereas the amplitude of long-living peaks decreases slightly. This is best seen in Fig. 3.24(b) and Fig. 3.24(c) where we find that 66.5 percent and 100 percent of absolute (the greatest) maximum peak amplitudes along the lattice,

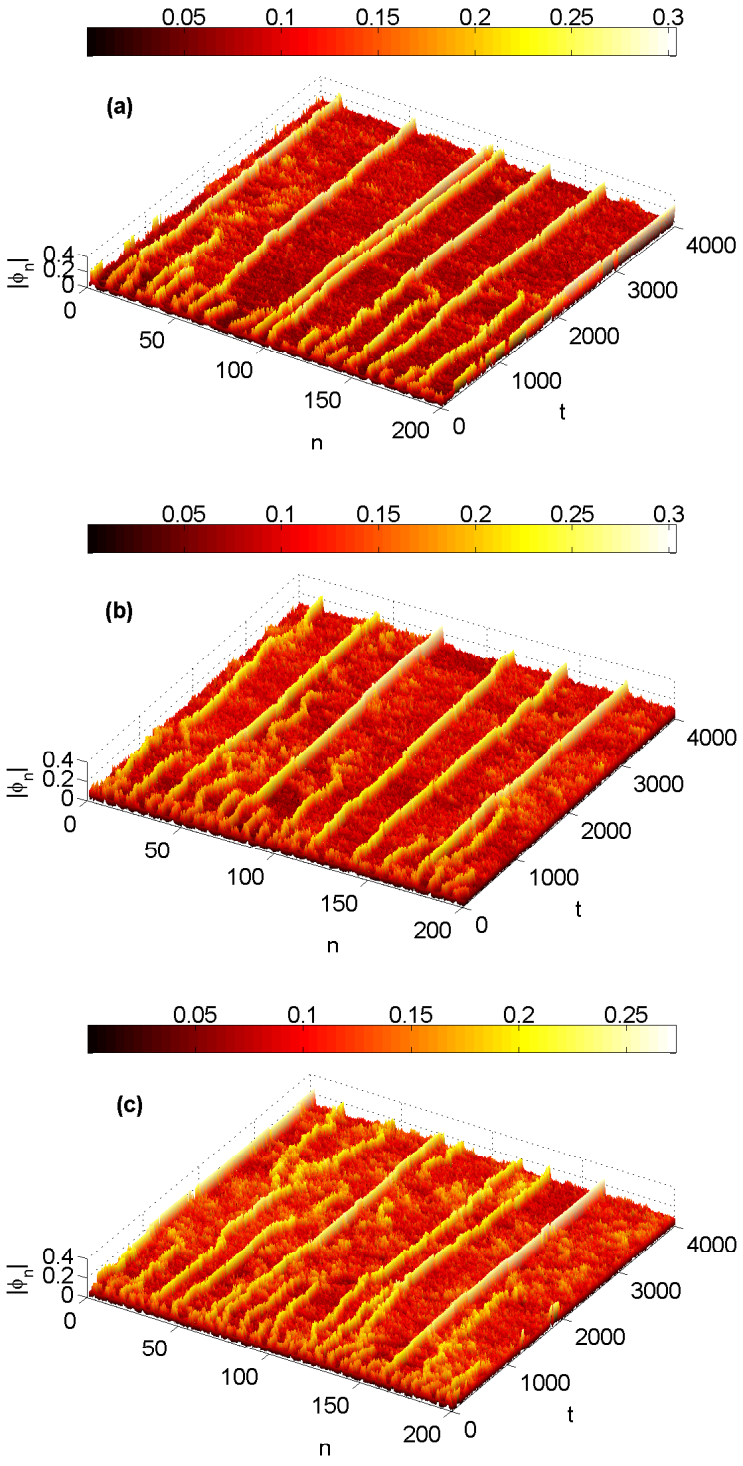

Figure 3.23: Discrete multi-rogue waves for $\eta_1 = 102.3$, $\eta_2 = 0$ (a), $\eta_2 = 51.15$ (b), and $\eta_2 = 102.3$ (c). These figures are the results of the integration of Eq.(2.24) with periodic boundary conditions and a chain of 200 peptide groups. The initial condition of Eq.(2.24) is taken in the form of uniform probability amplitude $\phi_n(t=0) \simeq 0.0707$. The random sequence β_n has zero-mean distribution in the interval $[-10^{-3}, 10^{-3}]$.

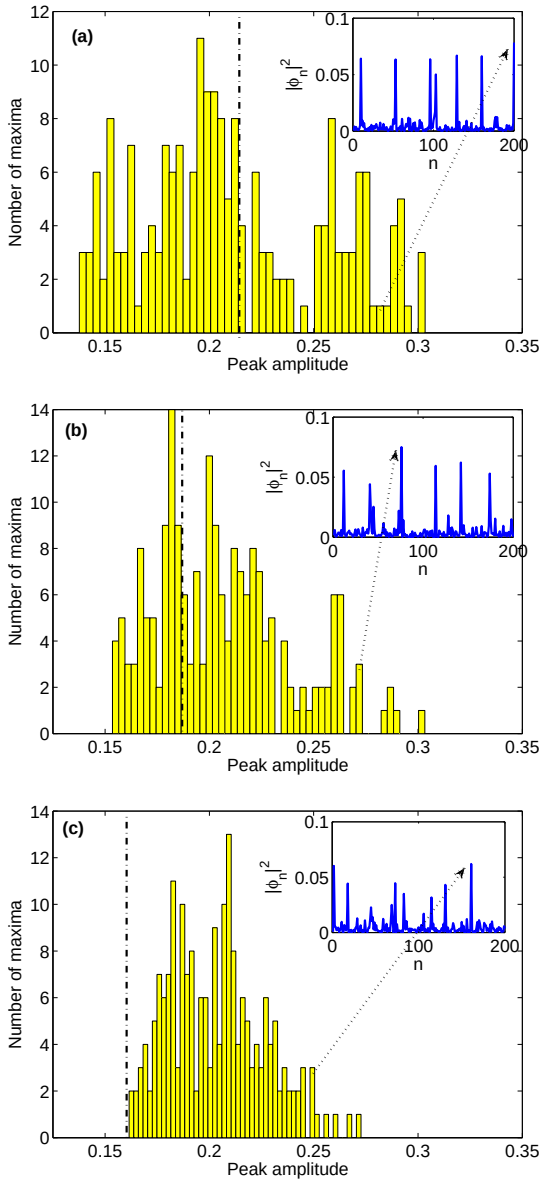

Figure 3.24: Statistical distributions of the absolute maximum amplitudes recorded through each peptide group, as a function of their numbers, over the time period [0, 4000] for $\eta_1 = 102.3$, $\eta_2 = 0$ (a), $\eta_2 = 51.15$ (b), and $\eta_2 = 102.3$ (c). For a given peptide group (200 in total), the greatest peak amplitude is retained among 4000 amplitudes after having integrated Eq.(2.24). The width of the 50 bins is 0.0035 (a), 0.003 (b), and 0.002 (c). The vertical dashed lines stand for a threshold amplitudes beyond which the greatest maximum peak amplitude can be seen as discrete rogue wave. The insets show the DMRW profiles (blue lines) when $t = 4000$.

recorded over the time period [0, 4000], are rogue waves, respectively. Subsequently, the higher order saturable nonlinearity promotes the formation of DMRW including an increase in the short-living RW and a decrease in amplitude of the long-living RW. Also indicated in Fig. 3.24(b) and Fig. 3.24(c), we have a reduction of the highest value of the maxima which changes from 0.3 to 0.27.

3.4.2 Discussions

Through study of discrete rogue waves in discrete nonlinear Schrödinger lattice with cubic nonlinearity, it has been recently obtained three sharp peaks from uniform initial condition [75]. Here, with saturable nonlinearity which can be emulated by cubic-quintic nonlinearity, we get seven sharp peaks on average. This observation illustrates that the saturable nonlinearity exhibit more extreme events than cubic nonlinearity. Moreover, in light of what has been done in continuum medium of the ocean surface [158], these peaks can be explained as follows. The instability of a uniform initial condition leads first to the creation of a chain of discrete solitons with small amplitudes. As time continues forward, inelastic interactions among each other promote the growth of the larger excitation. Note as well that disorder considerably enhances the instability and, thus, the growth of the larger excitation that could lead to discrete rogue waves when the required criterion in term of the standard deviation is satisfied. As a matter of fact, these explanations join those reported in [75]. DMRW-like mechanism for the localization of vibrational energy in protein chain is therefore possible. On that point, Daumont et al [151] have presented modulational instability as first step towards energy localization in nonlinear lattices. In the latter work, while taking into account the discreteness, localized modes arising from the modulational instability (MI) have not lead to rogue waves. This is probably because the lack of small disorder which enhances the instability and thus allow for the excitation of discrete rogue waves. As such, the fact that rogue waves are excited when MI develops from noise is consistent with the previous works [159].

As regards the biological nature of our DMRW as probability amplitude of finding a quantum of amide-I, the effect of normalization ($\sum_n \mid \phi_n \mid^2 = 1$) on this solution is of paramount importance. Building on the normalize uniform initial condition, the DMRW is found by means of numerical experiments. This initial condition means that, although low, the probability amplitude is uniform at the beginning on all peptide groups. Thereafter, there is a sudden redistribution of probabilities accompanied by a large one at least two times

higher than uniform background probability amplitude in some sites at the expense of other (Fig. 3.23), due to the conservation of energy which is monitored during the integration procedure. This conservation avoids the system to have unlimited and catastrophic amplitudes and, therefore, to have a great molecular bond distortion that can cause a breakage of the molecular chain (with the understanding that there is a phonon-exciton coupling (see section 3.1 and [107]).

Spatiotemporal evolution of the DMRW arising from system depends on the strengths of higher order saturable nonlinearity. By using colormaps which vary smoothly from black through shades of red, orange, and yellow, to white; it appears from Fig. 3.23(a) that long-living DMRW are promoted. Between crests of DMRW in bright yellow, furrows are red. 39.5 percent of absolute maximum amplitudes of $|\phi_n|$ through each peptide group are RW (Fig. 3.24(a)). The increasing of the strengths of higher order saturable nonlinearity is associated with a reduction of the amplitude of the long-living DMRW and the short-living DMRW development. The latter appears from nowhere and disappears without a trace as illustrated by the rise of probability "clumps", in yellow, on the furrows (Figs. 3.23(b) and (c)) when η_2 increases from 51.15 to 102.3. Simultaneously, the percentage of absolute maximum amplitudes of $|\phi_n|$ through each peptide group, recorded over the time period [0, 4000], which are RW increases from 66.5 to 100 (Figs. 3.24(b) and (c)). The higher order saturable nonlinearity is responsible for the small localization in space of DMRW.

In any event, it appears that DNLS equation with saturable nonlinearities can sustain DMRW as complex probability amplitude. Then DMRW-like mechanism for the localization of vibrational energy in protein chain is possible.

However, having said that, what is happening when only the central peptide group of a chain length is disordered?

3.5 Multibreathers-impurity interactions in the DNLS model

Let us consider stationary solutions to (2.30) of the form $\phi_n = u_n \exp(i\Omega t)$, Ω being a frequency and u_n, the real-valued amplitudes. The amplitudes u_n satisfy a set of coupled algebraic equations

$$-\Omega u_n + (u_{n+1} + u_{n-1}) - \frac{\varepsilon_n}{J} u_n + \nu u^3 = 0. \tag{3.31}$$

Use of iterative multidimensional Newton-Raphson method, starting from trivial solutions of the anti-continuous limit depending on the desired localized stationary solution (two-hump and three-hump with the corresponding interpeak separation), and application of the concept of continuation [119] give us the discrete stationary multihump soliton solutions of Eq. (3.31) (see section 3.1 and [146]). In order to check the stability of these solutions, we have added the perturbation

$$\zeta_n = \exp(i\Omega t)(x_n \exp(\lambda t) + y_n \exp(\lambda^* t)) \tag{3.32}$$

to stationary solutions ϕ_n and linearized Eq. (2.30) with respect to small perturbation modes x_n and y_n. The ensuing eigenvalue problem was solved by a standard numerical eigenvalue solver. Stationary soliton solutions are linearly unstable if at least one eigenvalue has a strictly positive real part. Once the steps mentioned above is verified, the discrete multihump soliton can be launched along the protein chain with diagonal disorder. In this case, only the central peptide group at n_0 from a chain length of 400 units is disordered. Thus $\varepsilon_n = \varepsilon\sigma_0\delta_{nn_0}$ where δ_{nn_0} is the Kronecker delta symbol, σ_0 is the parameter impurity which can be negative (attractive impurity) or positive (repulsive impurity) and $\varepsilon = 0.205$ eV. Such a diagonal impurity is used for the modeling of different amino acid side groups and local geometric distortions to these groups in proteins [97, 116].

In order to get an information about the interaction of discrete multibreathers with a linear point-defect impurity, we perform a numerical integration of Eq. (2.30) using the 4th order Runge-Kutta scheme with a suitable choice of time step and absolute tolerance (10^{-10}) for the purpose of the conservation of energy and norm.

It is well known that stationary discrete multibreathers can be put into mouvement by adding a thrust q to it so that $\phi_n(0) = u_n \exp(iqn)$(see section 3.1 and references therein). During the propagation, the interaction of mov-

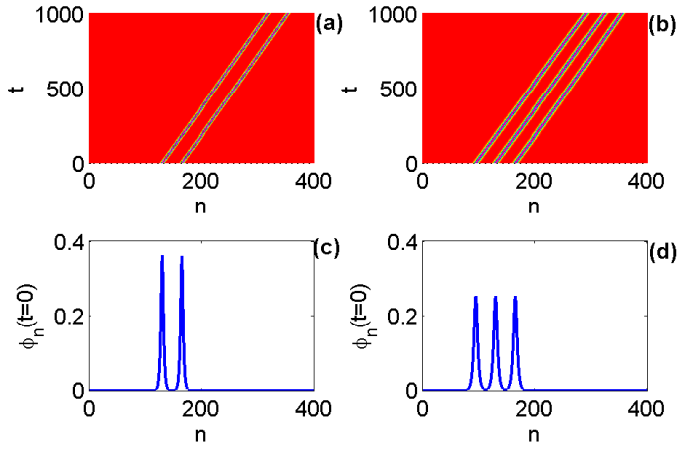

Figure 3.25: Discrete (a) two-hump soliton and (b) three-hump soliton passing through the impurity located at $n_0 = 200$ for $\sigma_0 = 0.0001$, $q = 0.1$, $\Omega = 2.24$ (a) and $\Omega = 2.12$ (b). Initial profiles are shown in panels (c) and (d), respectively.

ing discrete multihump soliton with a linear point-defect impurity is observed. Well before that, it should be noted that the stability of propagating discrete multihump soliton has been checked. Indeed, with discrete multibreathers, it has been shown that the intensity of instability decreases as interpeak separation increases (see section 3.1 and [146]). It seems that for interpeak separation of 35, two-hump solitons and three-hump soliton becomes stable with frequencies $\Omega = 2.24$ and $\Omega = 2.12$, respectively. Therefore, we can achieve the mobility of discrete multibreathers. For $\sigma_0 = 0.0001$ and $q = 0.1$, we observe a smooth propagation of the incident two-hump soliton passing through the impurity site located at $n_0 = 200$ (Figs. 3.25(a) and (c)). A similar observation is made for three-hump soliton in Fig. 3.25(b) and (d). However, for $\sigma_0 = 0.0002$ and the same thrust, the discrete multibreather is reflected. Fig. 3.26(a) indicates also the quasi-elastic character of the collision of this one with the impurity. Another striking effet of multibreather-impurity interactions is what may be called *internal collision* of discrete two-hump soliton that leaves reflected multibreather which is identical to the incident one. In the case of attractive impurity ($\sigma_0 = -0.0005$) and kick $q = 0.1$, we obtain an unusual *partial transmission* where the impurity capture a part of the discrete multibreather and allows the other part of it to escape (Fig. 3.26(b)). Even in this case, it should be noted that collision phenomenon is an inherent element of the multibreather scattered by impurity. Taking $\sigma_0 = -0.0009$ and $q = 0.1$, we get a partial reflection as shown in Fig. 3.26(c). Increasing the value of

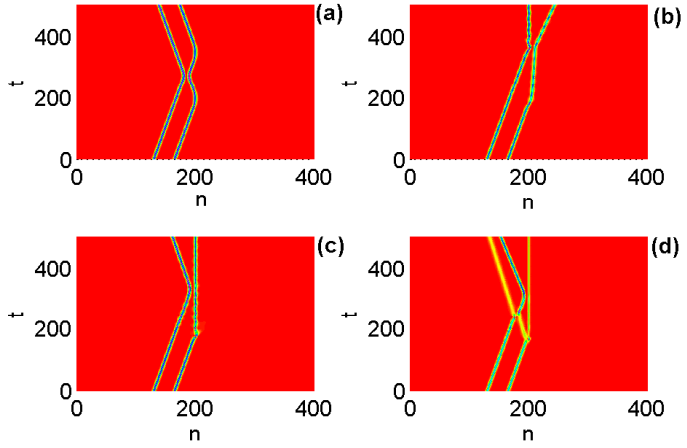

Figure 3.26: Typical results of the interaction of two-hump soliton (density plot) with an isolated impurity: reflection (a), partial transmission (b), and partial reflections [(c) and (d)]. The multibreather parameters are: $q = 0.1$, $\Omega = 2.24$, $\sigma_0 = 0.0002$ (a), $\sigma_0 = -0.0005$ (b), $\sigma_0 = -0.0009$ (c), $\sigma_0 = -0.0030$ (d) and the impurity is located at $n_0 = 200$.

σ_0 to -0.0030, we still get a partial reflection (Fig. 3.26(d)). But this time the multibreather scattered by an attractive impurity gives rise to the formation of a complex pattern involving multiple collisions.

In order to better understand the role of σ_0 and q, we define the reflection coefficient R, capture (trapping) coefficient C, and transmission coefficient T as follows

$$R = \sum_{n=1}^{197} |\phi_n(t_f)|^2, \tag{3.33}$$

$$C = \sum_{n=198}^{202} |\phi_n(t_f)|^2, \tag{3.34}$$

and

$$T = \sum_{n=203}^{400} |\phi_n(t_f)|^2, \tag{3.35}$$

where t_f is the time chosen long after the multibreather-impurity interactions has taken place. After calculation of these coefficients, it appears that for σ_0-values of the same absolute values but opposite signs the behaviors of discrete two-hump soliton with regard to impurity are not the same. This result is contrary to those obtained by Förner [97]. Our findings are evidenced by Fig. 3.27(a) and Fig. 3.28(a) for $q = 0.1$ and $q = 0.2$, respectively. We

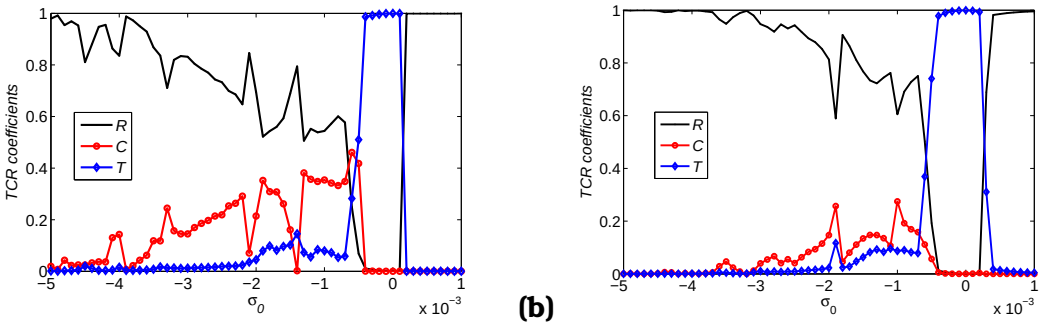

Figure 3.27: Reflection (black line), transmission (blue line), and capture (red line) diagrams for discrete two-hump (a) and three-hump (b) soliton solutions. The thrust is $q = 0.1$, the frequencies are $\Omega = 2.24$ (a), and $\Omega = 2.12$ (b).

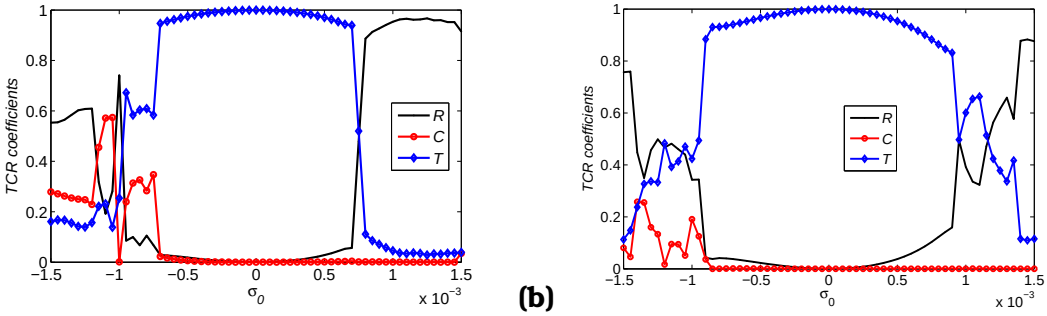

Figure 3.28: Reflection (black line), transmission (blue line), and capture (red line) diagrams for discrete two-hump (a) and three-hump (b) soliton solutions. The thrust $q = 0.2$ and the frequency $\Omega = 2.24$ (a), and $\Omega = 2.12$ (b).

can also see that the interval of the strength of inhomogeneity σ_0 for sharp transmission increases as q increases. Therefore, this interval jumps from $[-0.0004, 0.0001]$ to $[-0.0007, 0.0007]$ as the thrust q changes from 0.1 to 0.2. Furthermore, for $q = 0.3$, the interval of sharp transmission is $[-0.0012, 0.0011]$. This is expected since q acts like the velocity. Therefore, the increase of the kinetic energy of multibreathers leads to the increase of sharp transmission window. Another highlight has drawn our attention. For large strength of attractive impurity ($\sigma_0 = -0.0060$ for example), in contrast to the discrete one-hump soliton, the scattering of a discrete two-hump soliton can gives rise to a trapping on a site ($n = 183$) other than the one containing the impurity ($n_0 = 200$), as Fig. 3.29 shows. Given this observation for large strength of attractive impurity, the calculation of the reflection coefficient, capture coefficient, and transmission coefficient is strenuous by means of Eqs. (3.33), (3.34), and (3.35).

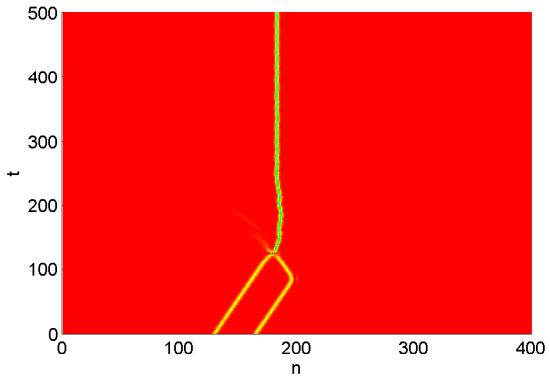

Figure 3.29: Density plot of the multibreather-impurity interactions giving rise to a trapping on a site ($n = 183$) other than the one containing the impurity ($n_0 = 200$). The thrust $q = 0.2$, the parameter of inhomogeneity $\sigma_0 = -0.0060$ and the frequency $\Omega = 2.24$.

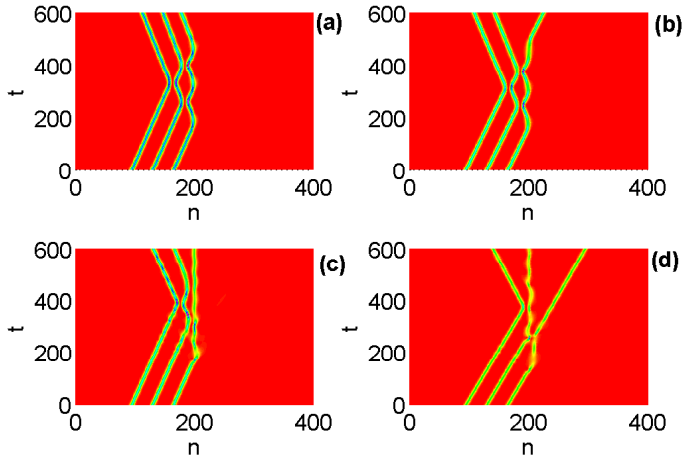

Figure 3.30: Typical results of the interaction of three-hump soliton (density plot) with an isolated impurity: reflection (a), reflection and transmission (b), and partial reflection (c), and reflection-capture-transmission (d). The multibreather parameters are: $\Omega = 2.12$; $q = 0.10, \sigma_0 = 0.0004$ (a); $q = 0.11$, $\sigma_0 = 0.0004$ (b); $q = 0.100$, $\sigma_0 = -0.0007$ (c); and $q = 0.133$, $\sigma_0 = -0.0007$ (d). The impurity is located at $n_0 = 200$.

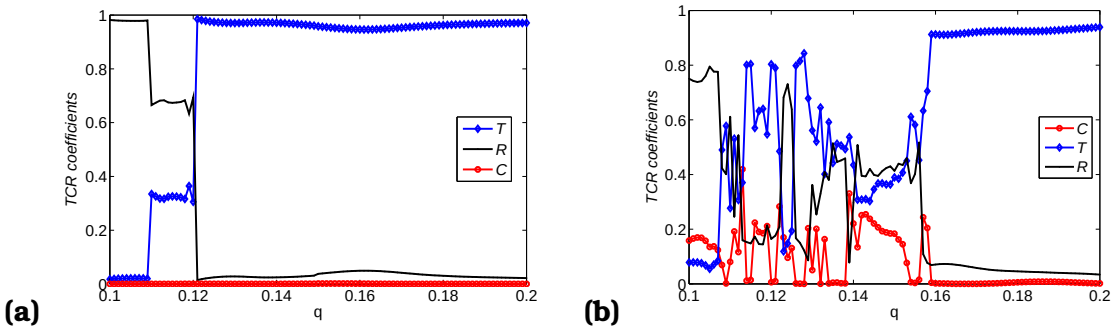

Figure 3.31: Reflection (black line), transmission (blue line), and capture (red line) coefficients versus thrust q for discrete three-hump soliton solutions. The parameters of inhomogeneity $\sigma_0 = 0.0004$ (a) and $\sigma_0 = -0.0007$ (b), the frequency $\Omega = 2.12$.

Concerning in particular three-hump soliton, they can interact in various ways among which, those present in Fig. 3.30. Clearly, the three-hump soliton can be reflected by an impurity as shown in Fig. 3.30(a) for $q = 0.1$ and $\sigma_0 = 0.0004$. The main feature of this interaction is that the reflection is accompanied by *internal collision* phenomenon, like for two-hump soliton. *Internal collision* phenomenon described here, leading to multiple collisions, feels like what is happening in Ref. [160] where we have collisions between two supersolitons. With $\sigma_0 = -0.0007$, we observe that the three-hump soliton hitting the impurity is partially captured, allowing two-hump soliton to be reflected (see Fig. 3.30(c)). Systematically, the transmission window as function of the parameter impurity is presented in Fig. 3.27(b) for $q = 0.1$. Compared to the scattering of two-hump soliton, it appears that the sharp transmission window for three-hump soliton is slightly higher: $-0.0004 \leq \sigma_0 \leq 0.0002$. Moreover, the increase in the thrust to $q = 0.2$ of three-hump soliton involves the expansion of this sharp transmission window (see Fig. 3.28(b)). Although the role played by thrust q is obvious, the transmission window as function of it in Fig. 3.31 reveals that the transition from reflection to sharp transmission over the increase in thrust is done without having a capture for repulsive impurity (see, e.g., Figs. 3.30(a), (b), and 3.31(a) with $\sigma_0 = 0.0004$). This observation is known in literature for a single breather. This is not the case for attractive impurity where this transition comes with an unusual pattern (see, e.g., Figs. 3.30(c), (d), and 3.31(b) with $\sigma_0 = -0.0007$). It follows from these multibreather-impurity interactions new outcomes as shown in Fig. 3.30(d). This figure describes simultaneously a reflection (41 %), a capture (19 %) and transmission (40 %) with a very small loss of radiation. This kind of interaction has not been reported in previous works relating to single-hump

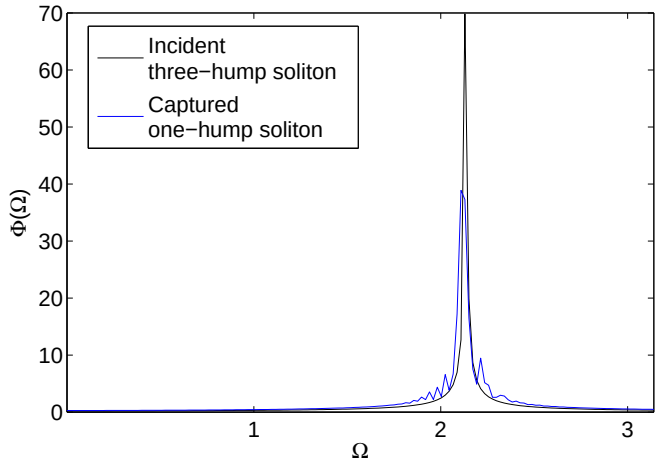

Figure 3.32: Fourier spectra $\Phi(\Omega)$ of the incident three-hump breather (black) and the captured one-hump breather (blue) involved in the interaction shown in Fig. 3.30(d).

soliton [92]. In order to understand this interaction of three-hump breathers with an impurity, recall that it is well known that trapping of single-hump breathers on a potential well is observed when the resonant transfer of translational energy from this wave to the linear impurity mode arises [91,92]. The Fourier spectra (see Fig. 3.32) of the incident three-hump breather and the captured one-hump breather may confirm the resonant transfer, since the frequency responses contain a spike at $\Omega = 2.129$ and $\Omega = 2.108$, respectively. Qualitatively, this new outcome can be explained, in addition, by the fact that the well defect is deep enough to hold a part of the miltibreather, thus leaving another part transmitted and reflected. However, for large values of strength of local impurity potential, the multibreather trapping decreases, just like for the single-hump breathers [91].

Knowing that single breather can be trapped between two repulsive impurity sites in the form of multiple reflections [161], what about multibreathers? Figs. 3.33(a) and (b) try to provide answers to this question. A multiple reflections are found for the case of three-hump soliton (Fig. 3.33(b)) with $\sigma_0 = 0.0001$, $q = 0.1$ and $\Omega = 2.12$. On top of that, we note an increasingly individualistic behavior of three-hump soliton's hump over time. Fig. 3.33(a) rather reveals a large stationary single breather when we introduce two-hump soliton between two repulsive impurity sites with $\sigma_0 = 0.0001$, $q = 0.1$ and $\Omega = 2.24$. This is likely due to the parity of the multibreather.

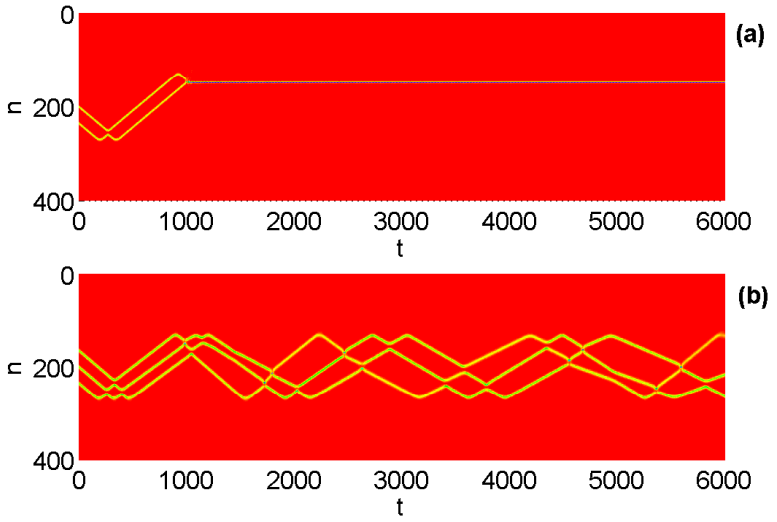

Figure 3.33: Traping of two-hump soliton (a) and three-hump soliton (b) between two impurity sites located at $n = 130$ and $n = 270$ for $\sigma_0 = 0.0001$, $q = 0.1$, $\Omega = 2.24$ (a) and $\Omega = 2.12$ (b).

In this chapter, we have studied a DNLS-type equation with competing staurable nonlinearities in the context of Amide-I vibrational energy excitations in proteins. Site-centered and bond-centered single-hump stationary solutions, as well as multi-hump states, and their stability were discussed. Mobile multi-breathers have been also examined. Thereafter, the influence of next-NNI of dipole-dipole type has been taken into account. In addition, the possibility of transport in a DNLS equation with saturable onsite nonlinearities, harmonically driven at the edge, in the form of moving multibreathers, has been explored. Then, Using uniform initial conditions to solve the DNLS equation with saturable nonlinearities and small disorder, we have simulated spatiotemporal evolution of the waves and after statistical processing, we have reported the existence of DMRW. And finally, we have studied the one-dimensional DNLS equation with point impurities. The interaction of multi-hump solitary waves and the impurity has been studied numerically. We looked for reflection, transmission and trapping phenomena, as well as interactions between the humps. These phenomena has been measured in terms of reflected, captured and transmitted power. A full conclusion is conducted in the next section.

General Conclusion

The aims of this thesis were to answer the following questions:

- Can we obtain stable and mobile multibreathers in the exciton dynamics modeled by DNLS equation with competitive nonlinearities?
- What is the influence of next-NNI on DMHS solutions of a DNLS equation with saturable nonlinearities?
- Can we get a supratransmission of the multibreathers?
- Does biological rogue wave exist in the framework where the dynamic variable is a complex probability amplitude at the n^{th} peptide group?
- What are the different outcomes in the case of multibreathers-impurity interactions in the DNLS model representing the vibrational energy transport along the protein chain?

This was done. Let us now summarize the main results of this thesis and conclude with an outlook for future studies.

Main results

After a general introduction which has enabled us to express the aims of this thesis, we have begun the Chapter 1 by providing background information about protein, localization and transport of vibrational energy in protein, and some nonlinear modes.

Immediately after that, the models and numerical methods used to analyze the subsequent solutions were presented in Chapter 2. In particular, we have shown that the DNLS equation with saturable nonlinearities models the localization and transport of vibrational energy in protein, when a nonlinear and strong exciton-phonon interaction is taken into account. Thus, the model includes conditions of excess ATP and the opposite case. In the absence of the higher-order saturable nonlinearity, the equation model is reduced to the DNLS equation with

photorefractive nonlinearity widely used in optics. Further, the next-NNI an small disorder have been variously taken into consideration, as well as point impurities for the case of cubic nonlinearity.

In Chapter 3, the multihump (two-hump, three-hump and four-hump) solitons having site-centered (sc) mode and/or bond-centered (bc) mode were sought as solutions of the DNLS equation with saturable nonlinearities and their stability was examined. The linear stability analysis that followed the stability diagram established reveals that the stability of multihump solitons depends not only on the value of the interpeak separation but also on the number of peaks of the solution. The results concerning the existence and stability of the sc DMHS solutions are consolidated in parameter space. A numerical evolution of DMHS having at least one intersite soliton reveals their instability. Finally, the study of the mobility of our solutions has led us to the main conclusion that, depending on the higher-order saturable nonlinearity, a multihump soliton-like mechanism for vibrational energy transport along the protein chain is possible.

Concerning the influence of next-NNI, we have studied in detail the discrete modulational instability of DNLS equation with higher order saturable nonlinearities. This equation has been studied in the framework of power dependence r^{-3} on the distance, r, of the dispersive interactions. It appears that the regions of MI of nonlinear plane waves shrink with increasing the number of nearest neighbor m. Furthermore, through the instability growth rate (gain), we note that when m increases, bandwidth of instability decreases. It has also been shown analytically that the higher order saturable nonlinearity can suppress the instability. Besides, the saturation of our model compared to that of Vinetskii-Kukhtarev increases the maximum gain and reduces the bandwidth of amplitudes which can lead to MI. This observation is unchanged when m varies. Using numerical simulations, it appears that the inclusion of second and third nearest neighbors leads to early onset of MI and this, whatever the value of the amplitude of the nonlinear plane waves. The numerical determination of DS and DMHS was accompanied by some remarks: when m increases, the width and height of DS and DMHS increase. However, for a given solution, the correc-

tions decrease as m increases. Moreover, when the number of peaks of solutions increases, the corrections of height to these solutions due to the inclusion of next-NNI decrease. The mobility of DMHS is achieved and we note that the next-NNI increase the speed of energy transfer along the protein molecules mediated by DMHS. Finally, after having carried out a collision between two DMHS, the main feature stands out is that next-NNI contribute significantly to the formation of large stationary solitons.

Note as well that we have highlighted supratransmission phenomena in DNLS equation with saturable nonlinearities modeling the localization and transport of vibrational energy in protein chains. Thus, a threshold amplitudes beyond which the wave propagation takes place within the molecular chains were established numerically. A semi-analytical method is also carried out to find this critical value and it follows in accordance with numerical method that the saturable higher order nonlinearity parameter lowers the threshold amplitude for supratransmission, although this critical amplitude tends to zero close to the band edge. In order to see if the supratransmission can occur by means of discrete gap multibreathers, we have drawn for some cases the graph of amplitude vs frequency for which mobility of discrete multisolitons takes place and graph of threshold amplitude vs frequency above which supratransmission occurs. Subsequently, it appears that the discrete gap multibreathers can be transmitted or "supratransmitted" according to the frequency belonging to the lower forbidden band gap. Moreover, the discrete gap multibreathers are "supratransmitted" when we are close to the edge of the lower forbidden band. Interestingly, for some parameter of saturable nonlinearities, the propagation of this type of solution has been emphasized. This shows that the nonlinear supratransmission of discrete gap multibreathers is possibly a mechanism of bio-energy transport in protein chains.

It has been shown that DNLS equation with saturable nonlinearities and small disorder admits DMRW as solution. Indeed, using uniform initial conditions we have simulated spatiotemporal evolution of the waves and after statistical processing reported the existence of DMRW. These biological rogue waves stand for the complex probability amplitude ϕ_n of finding an amide-I vibrational quantum at site n. Moreover, it has been observed that the higher order saturable nonlinearity

promotes the formation of DMRW including an increase in the short-living RW and a decrease in amplitude of the long-living RW. Therefore, DMRW opens the way towards a localization of vibrational energy in protein chain.

Finally, the influence of impurities on moving multibreathers in DNLS lattice was numerically analyzed. It emerged from this analysis that, excluding the transmission case, the phenomenon of internal collision of multibreathers accompanies all types of scattering outcomes, regardless of sign of the impurity. We have also recorded the formation of a complex pattern involving multiple collisions for the case of two-hump soliton scattered by an attractive impurity. Moreover, contrary to previous studies related to breather-impurity interactions, the scattering of a discrete two-hump soliton can lead to a trapping on a site other than the one containing the impurity, after one collision. In particular with regard to three-hump soliton, numerical simulations demonstrate for attractive impurity a reflection, a capture, a transmission with a very small loss of radiation and all this at the same time. A multiple reflections have been found for the case of three-hump soliton introduced between two repulsive impurity sites, including an increasingly individualistic behavior of humps over time. However, for two-hump soliton, we have not seen the solution moving back and forth between repulsive impurities but rather a large stationary single breather.

Outook

As future work, one could extend our work to view the effects of physiological temperature (310 K). Also, we have not yet considered the three channels of alpha-helix (one is cross-hatched in Fig. 1.2), as well as the interactions of amino acid with their local environment.

Moreover, in the framework of DNLS lattice, it might be useful to study the mobility of DMRW.

Bibliography

[1] A. S. Davydov, J. theor. Biol. **66**, 379 (1977). (Cited on pages 9, 11, 22 and 34.)

[2] P. Xiao-feng, Prog. Biophys. Mol. Bio. **108**, 1 (2012). (Cited on page 9.)

[3] G. Careri, U. Buontempo, F. Galluzzi, A. C. Scott, E. Gratton, and E. Shyamsunder, Phys. Rev. B **30**, 4689 (1984). (Cited on page 9.)

[4] A. C. Scott, Phys. Rep. **217**, 1 (1992). (Cited on pages ii, 9, 10, 11, 13, 31 and 34.)

[5] S. Flach and C. R. Willis, Phys. Rep. **295**, 181 (1998). (Cited on page 9.)

[6] S. Flach and A. V. Gorbach, Phys. Rep. **467**, 1 (2008). (Cited on page 9.)

[7] T. Ahn, Nonlinearity **11**, 965 (1998). (Cited on pages 9 and 12.)

[8] T. Bountis, H. W. Capel, M. Kollmann, J. C. Ross, J. M. Bergamin, and J. P. van derWeele, Phys. Lett. A **268**, 50 (2000). (Cited on pages 9, 12, 43 and 44.)

[9] P. G. Kevrekidis, *Discrete Nonlinear Schr¨odinger Equation: Mathematical Analysis, Numerical Computations and Physical Perspectives, Springer TractsModern Phys.*, (Springer, Berlin, 2009). (Cited on pages 9, 12 and 44.)

[10] V. Koukouloyannis, P. G. Kevrekidis, J. Cuevas, and V. Rothos, Physica D **16**, 242 (2013). (Cited on page 9.)

[11] A.B. Togueu Motcheyo, C. Tchawoua, M. Siewe Siewe, J.D. Tchinang Tchameu, Phys. Lett. A **375**, 1104 (2011). (Cited on pages 9 and 25.)

[12] F. Palmero, L. Q. English, J. Cuevas, R. Carretero-Gonzàlez, and P. G. Kevrekidis, Phys. Rev. E **84**, 026605 (2011). (Cited on pages 9 and 25.)

[13] M. Mitchell, M. Segev, and D. N. Christodoulides, Phys. Rev. Lett. **80**, 4657 (1998). (Cited on pages 9 and 13.)

[14] P. G. Kevrekidis, K.Ø. Rasmussen, and A. R. Bishop, Int J Modern Phys B **15**, 21 (2001); **15**, 2833 (2001). (Cited on page 9.)

[15] V. Koukouloyannis, S. Ichtiaroglou, Phys. Rev. E **66**, 066602 (2002); Int. J. Bifurcation Chaos **16** 1823 (2006). (Cited on pages 9, 12 and 25.)

[16] V. M. Burlakov, S. A. Kiselev, V. N. Pyrkov, Phys. Rev. B **42**, 4921 (1990). (Cited on page 10.)

[17] K. W. Sandusky, J. B. Page, K. E. Schmidt, Phys. Rev. B **46**, 6161 (1992). (Cited on page 10.)

[18] M. Öster, M. Johansson, A. Eriksson, Phys. Rev. E **67**, 056606 (2003). (Cited on page 10.)

[19] T.R.O. Melvin, A.R. Champneys, P.G. Kevrekidis, J. Cuevas, Phys. Rev. Lett **97**, 124101 (2006). (Cited on pages 10 and 50.)

[20] J. Cuevas , J.C. Eilbeck, Phys. Lett. A **358**, 15 (2006). (Cited on page 10.)

[21] R. A. Vicencio, M. Johansson, Phys. Rev . E **73**, 046602 (2006). (Cited on page 10.)

[22] H. Susanto, P. G. Kevrekidis, R. Carretero-Gonzàlez, B. A. Malomed, D. J. Frantzeskakis, Phys. Rev. Lett **99**, 214103 (2007). (Cited on page 10.)

[23] T.R.O. Melvin, A.R. Champneys, P.G. Kevrekidis, J. Cuevas, Physica D **237**, 551 (2008). (Cited on page 10.)

[24] C. Mejia-Cortes, R. A. Vicencio, and B. A. Malomed, Phys. Rev . E **88**, 052901 (2013). (Cited on page 10.)

[25] A. S. Davydov, J. theor. Biol. **38**, 559 (1973). (Cited on pages 10 and 22.)

[26] W. Forner, J. Phys. Condens. Matter **3**, 4333 (1991). (Cited on page 10.)

[27] A.V. Savin, A.V. Zolotaryuk, Physica D **68**, 59 (1993). (Cited on page 10.)

[28] W. Forner, Physica D **68**, 68 (1993). (Cited on pages 10 and 13.)

[29] L. Cruzeiro-Hansson, V.M. Kenkre, Phys. Lett. A **203**, 362 (1995). (Cited on page 10.)

[30] Yi Xiao, Phys. Lett. A **243**, 174 (1998). (Cited on page 10.)

[31] J. Herrera, M.A. Maza, A.A. Minzoni, N.F. Smyth, A.L. Worthy, Physica D **191**, 156 (2004). (Cited on page 10.)

[32] A.V. Zolotaryuk, K.H. Spatschek, O. Kluth, Phys. Rev. B **47**, 7827 (1993). (Cited on pages 10, 11 and 34.)

[33] A.V. Zolotariuk, Physica D **46**, 295 (1990). (Cited on page 10.)

[34] M. Daniel, M.M. Latha, Physica A **298** 526 (2001); Phys. Lett. A **302** 94 (2002). (Cited on pages 10 and 25.)

[35] O. G. Cantu Ros, L. Cruzeiro, M. G. Velarde, W. Ebeling, Eur. Phys. J. B **80**, 545 (2011). (Cited on page 10.)

[36] L. Cruzeiro-Hansson, Phys. Lett. A **249**, 465 (1998). (Cited on page 10.)

[37] S.F. Mingaleev, P.L. Christiansen, Y.B. Gaididei, M. Johansson, K.Ø. Rasmussen, J. Biol. Phys. **25**, 41 (1999). (Cited on page 10.)

[38] A. Neuper, Y. Gaididei, N. Flytzanis, F. Mertens, Phys. Lett. A **190**, 165 (1994). (Cited on page 10.)

[39] P. Woafo, T.C. Kofane, A.S. Bokosah, Phys. Rev. B **48**, 10153 (1993). (Cited on page 10.)

[40] C. Tatuam Kamga, T.C. Kofane, Phys. Rev. E **50**, 2257 (1994). (Cited on page 10.)

[41] C. Tchawoua, T.C. Kofane, A.S. Bokosah, J. Phys. A: Math. Gen. **26**, 6477 (1993). (Cited on page 10.)

[42] D. Hennig, Eur. Phys. J. B **20**, 419 (2001). (Cited on pages 10, 53 and 56.)

[43] M. Aguero, R. García-Salcedo, J. Socorro, E. Villagran, Int. J. Theor. Phys. **48**, 670 (2009). (Cited on pages 10, 12, 29 and 32.)

[44] D. N. Christodoulides, R. I. Joseph, Opt. Lett. **13**, 794 (1988). (Cited on page 11.)

[45] W. P. Su, J. R. Schieffer, A. J. Heeger, Phys. Rev. Lett. **42**, 1698 (1979); (Cited on page 11.)

A. J. Sievers and S. Takeno, Phys. Rev. Lett. **61**, 970 (1988).

[46] A. Trombettoni, A. Smerzi, Phys. Rev. Lett. **86**, 2353 (2001). (Cited on page 11.)

[47] S. Gatz, J. Herrmann, J. Opt. Soc. Amer. B **8**, 2296 (1991). (Cited on page 11.)

[48] S. Gatz, J. Herrmann, Opt. Lett. **17**, 484 (1992). (Cited on page 11.)

[49] M. Segev, G.C. Valley, B. Crosignani, P. DiPorto, A. Yariv, Phys. Rev. Lett. **73**, 3211 (1994). (Cited on page 11.)

[50] V.O. Vinetskii, N.V. Kukhtarev, Sov. Phys. Solid State **16**, 2414 (1975). (Cited on page 11.)

[51] M. Stepić, D. Kip, L. Hadžievski, A. Maluckov, Phys. Rev E **69**, 066618 (2004); (Cited on page 11.)

L. Hadžievski, A. Maluckov, M. Stepić, D. Kip, Phys. Rev. Lett. **93**, 033901 (2004);

A. Khare, K.Ø. Rasmussen, M.R. Samuelsen, A. Saxena, J. Phys. A **38**, 807 (2005);

R.A. Vicencio, M. Johansson, Phys. Rev. E **73**, 046602 (2006);

T.R.O. Melvin, A.R. Champneys, P.G. Kevrekidis, J. Cuevas, Phys. Rev. Lett. **97**, 124101 (2006).

[52] W. Chen, D.L. Mills, Phys Rev Lett **58**, 160 (1987). (Cited on pages 11 and 13.)

[53] D.L. Mills, S.E. Trullinger, Phys Rev B **36**, 947 (1987). (Cited on page 11.)

[54] F. Geniet, J. Leon, Phys. Rev. Lett. **89**, 134102 (2002). (Cited on pages 11, 27 and 64.)

[55] A. B. Togueu Motcheyo, C. Tchawoua, M. Siewe Siewe, and J. D. Tchinang Tchameu, Commun. Nonlinear. Sci. Numer. Simul. **18**, 946 (2013); (Cited on pages 11, 12, 13 and 27.)

A. B. Togueu Motcheyo, C. Tchawoua, and J. D. Tchinang Tchameu, Phys. Rev. E **88**, 040901(R) (2013);

K. Tse Ve Koon, J. Leon, P. Marquié, P. Tchofo-Dinda, Phys. Rev. E **75**, 066604 (2007);

F. Tao, W. Chen, J. Pan, W. Xu, S. Du, Chaos, Solitons & Fractals **45**, 810 (2012);

K. Tse Ve Koon, P. Marquié, P. Tchofo Dinda, Phys. Rev. E **90**, 052901 (2014);

F. Kenmogne, G. B. Ndombou, D. Yemélé and A. Fomethe, Chaos, Solitons & Fractals **75**, 263 (2015).

[56] P. Anghel-Vasilescu, J. Dorignac, F. Geniet, J. Leon, M. Taki, Phys. Rev. Lett. **105**, 074101 (2010). (Cited on pages 11 and 27.)

[57] H. Susanto, N. Karjanto, J. Nonlinear Opt. Phys. Mater. **17**, 159 (2008). (Cited on pages 11, 27, 64 and 66.)

[58] H. Susanto, SIAM J. Appl. Math. **69**, 111 (2008). (Cited on pages 11, 27 and 64.)

[59] J.E. Macías-Díaz, Wave Motion **48**, 13 (2011). (Cited on pages 11 and 27.)

[60] J. Lydon, G. Theocharis, C. Daraio, Phys. Rev. E **91**, 023208 (2015). (Cited on pages 11 and 27.)

[61] R. Khomeriki, L. Chotorlishvili, B. A. Malomed, and J. Berakdar, Phys. Rev. B **91**, 041408(R) (2015). (Cited on pages 11 and 27.)

[62] S. Savel'ev, V. A. Yampol'skii, A. L. Rakhmanov, F. Nori, Phys. Rev. B **75**, 184503 (2007). (Cited on page 11.)

[63] J. E. Macías-Díaz, A. Puri, Phys. D **228**, 112 (2007); (Cited on page 11.)

J. E. Macías-Díaz, A. Puri, Phys. Lett. A **366**, 447 (2007).

[64] A.S. Davydov, N.I. Kislukha, Phys. Status Solidi (b) **59**, 465 (1973). (Cited on pages 11 and 22.)

[65] D.H. Peregrine, J. Aust. Math. Soc. B **25**, 16 (1983). (Cited on pages 12 and 28.)

[66] N. Akhmediev, A. Ankiewicz, M. Taki, Phys. Lett. A **373**, 675 (2009). (Cited on pages 12 and 27.)

[67] B.G.E. Onana, J. Atangana, F. M. Biya, B. Mokhtari, N.E. Cherkaoui, T.C. Kofane, Phys. Rev. E **90**, 032911 (2014). (Cited on pages 12 and 28.)

[68] D.E. Temgoua, T.C. Kofane, Phys. Rev. E **91**, 063201 (2015).

[69] D. R. Solli, C. Ropers, P. Koonath, B. Jalali, Nature **450**, 1054 (2007). (Cited on pages 12 and 28.)

[70] F. Baronio, A. Degasperis, M. Conforti, S. Wabnitz, Phys. Rev. Lett. **109**, 044102 (2012). (Cited on pages 12 and 28.)

[71] F. Yu, Applied Mathematics and Computation **220**, 176 (2013). (Cited on pages 12 and 28.)

[72] N. Akhmediev, A. Ankiewicz, Phys. Rev.E **83**, 046603 (2011). (Cited on page 12.)

[73] A. Ankiewicz, N. Akhmediev, J. M. Soto-Crespo, Phys. Rev.E **82**, 026602 (2010). (Cited on page 12.)

[74] Y. V. Bludov, V. V. Konotop, N. Akhmediev, Opt. Lett. **34**, 3015 (2009). (Cited on pages iii, 12 and 28.)

[75] S. Efe, C. Yuce, Phys. Lett. A **379**, 1251 (2015). (Cited on page 12.)

[76] C. Bonatto, M. Feyereisen, S. Barland, M. Giudici, C. Masoller, J.R. Leite, J.R. Tredicce, Phys. Rev. Lett. **107**, 053901 (2011). (Cited on pages 12, 28, 71 and 74.)

[77] Yu. S. Kivshar, S. A. Gredeskul, A. Sanchez, and L. Vázquez, Phys. Rev. Lett. **64**, 1693 (1990). (Cited on pages 12 and 71.)

[78] O. M. Braun, Y. S. Kivshar, Phys. Rep. **306**, 1 (1998). (Cited on page 12.)

[79] S. Aubry, J. Chem. Phys **64**, 3392 (1976). (Cited on page 13.)

(Cited on page 13.)

[80] K. J. Wahlstrand, J. Chem. Phys. **82**, 5247 (1985). (Cited on page 13.)

[81] *The Sine-Gordon Model and Its Applications: From Pendula and Josephson Junctions to Gravity and High-Energy Physics*, edited by Cuevas-Maraver, P. G. Kevrekidis, and F. Williams, (Springer, Berlin, 2014). (Cited on page 13.)

[82] T. Iizuka, H. Amie, T. Hasegawa, C. Matsuoka, Phys. Lett. A **220**, 97 (1996). (Cited on page 13.)

[83] S. Shadkhoo, R. Bruinsma, Phys. Rev. Lett. **115**, 159903 (2015). (Cited on page 13.)

[84] F. Palmero, J. F. R. Archilla, D. Hennig, F. R. Romero, New Journal of Physic **6**, 13 (2004). (Cited on page 13.)

[85] T. Watanabe, Y. Kanamori, N. Yajima, J. Phys. Soc. Jpn. **58**, 1273 (1989). (Cited on page 13.)

[86] D. Tong, K. Wong, Phys. Rev. D **91**, 026007 (2015). (Cited on page 13.)

[87] Z. Chen, J. Huang, J. Chai, X. Zhang, Y. Li, B. A. Malomed, Phys. Rev. A **91**, 053821 (2015). (Cited on pages 11 and 13.)

[88] S. V. Suchkov, A. A. Sukhorukov, S. V. Dmitriev, Y. S. Kivshar, Europhys. Lett. **100**, 54003 (2012). (Cited on page 13.)

[89] F. K. Abdullaev, V. A. Brazhnyi, M. Salerno, Phys. Rev. A **88**, 043829 (2013). (Cited on page 13.)

[90] D. Saadatmand, S. V. Dmitriev, D. I. Borisov, P. G. Kevrekidis, Phys. Rev. E **90**, 052902 (2014). (Cited on page 13.)

[91] L. Morales-Molina, R. A. Vicencio, Opt Lett **31**, 966 (2006). (Cited on pages 13 and 82.)

[92] F. Palmero, R. Carretero-Gonzalez, J. Cuevas-Maraver, P. G. Kevrekidis, W. Krolikowski, Phys. Rev. E **77**, 036614 (2008). (Cited on pages 13 and 82.)

[93] S. M. Al-Marzoug, Inter. J. Mod. Phys. B **28**, 1450214 (2014). (Cited on page 13.)

[94] H. Yue, M. I. Molina, P. G. Kevrekidis, N. I. Karachalios, J. Math. Phys. **55**, 102703 (2014). (Cited on page 13.)

[95] V. A. Brazhnyi, C. P. Jisha, A. S. Rodrigues, Phys. Rev. A **87**, 013609 (2013). (Cited on page 13.)

[96] A. Adamatzky, *Computing in nonlinear media and automata collectives, Springer TractsModern Phys.*, (IoP Publishing, Bristol and Philadelphia, 2001). (Cited on page 13.)

[97] W. Förner, Phys. Rev. A **44**, 2694 (1991). (Cited on pages 13, 25, 34, 76 and 78.)

[98] W. Forner, J. Phys.: Condens. Matter **3**, 3235 (1991). (Cited on pages 10 and 13.)

[99] J. A. McCammon, S. C. Harvey, *Dynamics of proteins and nucleic acids*, (Cambridge Univ. Press, Cambridge, 1987).

[100] *Nonlinear electrodynamics in biological systems*, edited by W. R. Adey, A. F. Lawrence, (Plenum Press, New York, 1984). (Cited on page 16.)

[101] A. Kessel, N. Ben-Tal, *Introduction to proteins: structure, function, and motion*, (CRC Press, Taylor & Francis Group, London, 2010). (Cited on pages 19 and 25.)

(Cited on pages iii and 20.)

[102] *Bioelectrodynamics and biocommunication (Vol. 6)*, edited by M. W. Ho, F. A. Popp, U. Warnke, (World Scientific, London, 1994). (Cited on page 21.)

[103] S. Krimm, J. Bandekar, Advances in protein chemistry **38**, 181 (1986). (Cited on page 22.)

[104] A. Szent-Györgyi, Nature **148**, 157 (1941). (Cited on page 22.)

[105] E. I. Rashba, Optika i Spektroskopiya **2**, 75 (1957). (Cited on page 22.)

[106] *Coherence in biology. In Coherent Excitations in Biological Systems*, edited by H. Fröhlich and F. Kremer, (Springer- Verlag GmbH & Co., Heidelberg, Berlin, 1983). (Cited on page 25.)

[107] A. C. Scott, Phys. Lett. A **86**, 60 (1981); Phys. Rev. A. **26**, 578 (1982); Physica Scripta **25**, 651 (1982). (Cited on pages 25, 34, 35 and 75.)

[108] S. Takeno , Prog. Theo. Phys. **69**, 1798 (1983); Prog. Theo. Phys. **71**, 395 (1984); Prog. Theo. Phys. **75**, 853 (1985). (Cited on page 24.)

[109] S. Yomosa , J. Phys. Soc. Jpn **53**, 3692 (1984); Phys. Rev. A **32**, 1752 (1985). (Cited on page 24.)

[110] A. Mvogo, G. H. Ben-Bolie, T. C. Kofané, Eur. Phys. J. B **86** 217 (2013); Eur. Phys. J. B **86** 413 (2013); Chaos **25** 063115 (2015); Chin. Phys. B **23** 098701 (2014); Int. J. Mod. Phys. B **28** 1450109 (2014). (Cited on page 25.)

[111] H. Motschmann, W. Förner, J. Ladik, J. Phys. Condens. Matter **1** 5083 (1989). (Cited on page 25.)

[112] *Davydov's Soliton Revisited*, edited by P.L. Christiansen and A.C. Scott, (Plenum, New York, 1990). (Cited on page 25.)

[113] D.W. Brown , B.J. West , K. Lindenberg, Phys. Rev. A **33** 4104 (1986); Phys. Rev. A **33** 4110 (1986). (Cited on page 25.)

[114] L. Cruzeiro-Hansson, Phys. Rev. Lett. **73** 2927 (1994); Phys. Rev. A **45** 4111 (1992). (Cited on page 25.)

[115] J.C. Eibeck , P.S. Lomdahl , A.C. Scott, Phys. Rev. B **30** 4703 (1984). (Cited on page 25.)

[116] Pang Xiao-feng, J. Phys.: Condens. Matter **2** 9541 (1990); Phys. Rev. B **49** 4747 (1994). (Cited on pages 25 and 76.)

[117] K. Kundu, Phys. Rev. E **61** 5839 (2000). (Cited on pages 25, 32, 35 and 71.)

[118] E. Simo, T.C. Kofane, Phys. Rev. E **56** 4751 (1997); Phys. Rev. E **54** 2071 (1996). (Cited on page 25.)

[119] R.S. MacKay, S. Aubry, Nonlinearity **7** 1623 (1994). (Cited on pages 25 and 76.)

[120] T. Ahn, R.S. MacKay, J-A. Sepulchre, Nonlinear Dynamics **25**, 157 (2001). (Cited on page 25.)

[121] J.F.R. Archilla, J. Cuevasa, B. Sanchez-Rey, A. Alvarez, Physica D **180**, 235 (2003). (Cited on page 25.)

[122] V. Koukouloyannis, Phys. Rev. E **69**, 046613 (2004). (Cited on page 25.)

[123] J.E. Macías-Díaz, A. Puri, J. Comput. Appl. Math. **214**, 393 (2008). (Cited on pages iii and 27.)

[124] F. Geniet, J. Leon, J. Phys.: Condens. Matter **15**, 2933 (2003). (Cited on page 27.)

[125] R. Khomeriki, Phys. Rev. Lett. **92**, 063905 (2004). (Cited on pages 27 and 64.)

[126] J. Leon, A. Spire, Phys. Lett. A **327**, 474 (2004). (Cited on pages 27, 66 and 70.)

[127] R. Khomeriki, J. Leon, Phys. Rev. E **71**, 056620 (2005). (Cited on page 27.)

[128] N. Akhmediev, J. M. Soto-Crespo, A. Ankiewicz, Phys. Lett. A **373**, 2137 (2009). (Cited on page 28.)

[129] A.S. Davydov, *Theory of Molecular Excitons.*, (Plenum Press, New York, 1971). (Cited on page 29.)

[130] O.G. Cantu Ros, L. Cruzeiro, M. G. Velarde, W. Ebeling, Eur. Phys. J. B **80**, 545 (2011). (Cited on pages 32 and 50.)

[131] K. Kundu, Phys. Rev. E **61**, 5839 (2000). (Cited on pages 25, 32, 35 and 71.)

[132] L. MacNeil, A.C. Scott, Physica Scripta **29**, 284 (1984). (Cited on pages 32, 35 and 71.)

[133] E.A. Bartnik, J.A. Tuszynski, D. Sept, Phys. Lett. A **204**, 263 (1995). (Cited on page 32.)

[134] L. A. Cisneros-Ake and A.A. Minzoni, Phys. Rev. E **85**, 021925 (2012). (Cited on page 32.)

[135] E.A. Ostrovskaya, Yu.S. Kivshar, D.V. Skryabin, W.J. Firth, Phys. Rev. Lett. **83**, 296 (1999). (Cited on pages 41 and 47.)

[136] Lj. Hadžievski, A. Maluckov, M. Stepić, D. Kip, Phys. Rev. Lett. **93**, 033901 (2004). (Cited on pages 41, 43, 44 and 67.)

[137] E.A. Ostrovskaya, S.F. Mingaleev, Yu.S. Kivshar, Y.B. Gaididei, P.L. Christiansen, Phys. Lett. A **282**, 157 (2001). (Cited on page 41.)

[138] F. Mitchell, *Essential Biochemistry for Medicine.*, October ed. (John Wiley and Sons, New York, 2010). (Cited on page 41.)

[139] S.K. Burley, G.A. Petsko, Adv. Protein Chem. **39**, 125 (1988). (Cited on pages 33 and 59.)

[140] K.Ø. Rasmussen, P.L. Christiansen, M. Johansson, Yu.B. Gaididei, S.F. Mingaleev, Physica D **113**, 134 (1998). (Cited on page 33.)

[141] A. Maluckov, Lj. Hadžievski, M. Stepić, Physica D **216**, 95 (2006). (Cited on pages 34, 43, 50 and 67.)

[142] D. Hennig, K.Ø. Rasmussen, H. Gabriel, A. Bülow , Phys. Rev. E **54**, 5788 (1996). (Cited on pages 43 and 44.)

[143] R. Carretero-Gonzàlez, J.D. Talley, C. Chong, B.A. Malomed, Physica D **216**, 77 (2006). (Cited on pages 43 and 44.)

[144] M. Stepić, A. Maluckov, M. Stojanović, F. Chen, D. Kip, Phys. Rev. A **78**, 043819 (2009). (Cited on page 47.)

[145] A. Maluckov, Lj. Hadžievski, B. A.Malomed, Phys. Rev. E **76**, 046605 (2007). (Cited on pages 38 and 44.)

[146] G. Kalosakas, Physica D **216**, 44 (2006). (Cited on pages 48, 76 and 77.)

[147] O. Cohen, R. Uzdin, T. Carmon, J. W. Fleischer, M. Segev, S. Odoulov, Phys. Rev. Lett **89**, 133901 (2002). (Cited on page 50.)

[148] S.K. Burley, G.A. Petsko, Adv. Protein Chem. **39**, 125 (1988). (Cited on pages 33 and 59.)

[149] M. Stepić, C. E. Rüter, Detlef Kip, A. Maluckov, Ljupčo Hadžievski, Optics Communications **267**, 229 (2006). (Cited on page 52.)

[150] F.Kh. Abdullaev, A. Bouketirb, A. Messikhc, B.A. Umarova, Physica D **232**, 54 (2007). (Cited on page 53.)

[151] I. Daumont, T. Dauxois, M. Peyrard, Nonlinearity **10**, 617 (1997). (Cited on pages 57 and 74.)

[152] M. Saha and T. C. Kofane, Int. J. Mod. Phys. B **26**, 1250101 (2012). (Cited on page 59.)

[153] M. Laberge, Biophys. Acta **1386**, 305 (1998). (Cited on page 59.)

[154] A. Maluckov, Lj. Hadžievski, B. A.Malomed, Phys. Rev. E **77**, 036604 (2008). (Cited on page 61.)

[155] B. Tan, J.P. Boyd, Phys. Lett. A **240**, 282 (1998). (Cited on page 61.)

[156] J.-G. Caputo, J. Leon, A. Spire, Phys. Lett. A **283**, 129 (2001). (Cited on page 66.)

[157] D. Taverner, N. G. R. Broderick, D. J. Richardson, R. I. Laming, M. Ibsen, Opt. Lett. **23**, 328 (1998). (Cited on page 67.)

[158] A. I. Dyachenko, V. E. E. Zakharov, J. Exp. Theor. Phys. **81**, 255 (2005). (Cited on page 74.)

[159] N. Akhmediev, J. M. Soto-Crespo, A. Ankiewicz, Phys. Lett. A **373**, 2137 (2009). (Cited on page 74.)

[160] P. Li, L. Li, B. A. Malomed, Phys. Rev. E **89**, 062926 (2014). (Cited on page 81.)

[161] Shigeo Homma, Shazo Takeno, Phys. Lett. A **169**, 355 (1992). (Cited on page 82.)

List of Publications

Publications of the thesis

1. **J. D. Tchinang Tchameu**, A. B. Togueu Motcheyo, and C. Tchawoua, *Mobility of discrete multibreathers in the exciton dynamics of the Davydov model with saturable nonlinearities*, Phys. Rev. E **90**, 043203 (2014).

2. **J. D. Tchinang Tchameu**, C. Tchawoua, A. B. Togueu Motcheyo, *Effects of next-nearest-neighbor interactions on discrete multibreathers corresponding to Davydov model with saturable nonlinearities*, Phys. Lett. A **379**, 2984 (2015).

3. **J. D. Tchinang Tchameu**, C. Tchawoua, A. B. Togueu Motcheyo, *Nonlinear supratransmission of multibreathers in discrete nonlinear Schrödinger equation with saturable nonlinearities*, Wave Motion **65**, 112 (2016).

4. **J. D. Tchinang Tchameu**, A. B. Togueu Motcheyo, and C. Tchawoua, *Biological multi-rogue waves in discrete nonlinear Schrödinger equation with saturable nonlinearities*, Phys. Lett. A **38**, 3057 (2016).

5. **J. D. Tchinang Tchameu**, A. B. Togueu Motcheyo, and C. Tchawoua, *Multibreathers-impurity interactions in the discrete nonlinear Schrödinger model*, Chaos, Solitons & Fractals **99**, 180 (2017).

Other publications

1. A. B. Togueu Motcheyo, C. Tchawoua, M. Siewe Siewe, **J. D. Tchinang Tchameu**, *Multisolitons and stability of two hump solitons*

of upper cutoff mode in discrete electrical transmission line, Phys. Lett. A **375**, 1104 (2011).

2. A. B. Togueu Motcheyo, C. Tchawoua, M. Siewe Siewe, and **J. D. Tchinang Tchameu**, *Supratransmission phenomenon in a discrete electrical lattice with nonlinear dispersion*, Commun. Nonlinear. Sci. Numer. Simul. **18**, 946 (2013).

3. A. B. Togueu Motcheyo, C. Tchawoua, and **J. D. Tchinang Tchameu**, *Supratransmission induced by waves collisions in a discrete electrical lattice*, Phys. Rev. E **88**, 040901(R) (2013).

4. F. T. Ndjomatchoua, C. Tchawoua, **J. D. Tchinang Tchameu**, B. P. LeRu, H. E. Z. Tonnang, *Discrete Davydov's soliton in α-helical protein molecule with anharmonic hydrogen bond and thermal noise*, Commun. Nonlinear. Sci. Numer. Simul. **29**, 148 (2015).

5. A. B. Togueu Motcheyo, **J. D. Tchinang Tchameu**, M. Siewe Siewe, and C. Tchawoua, *Homoclinic nonlinear band gap transmission threshold in discrete optical waveguide arrays*, Commun. Nonlinear. Sci. Numer. Simul. **50**, 29 (2017).

6. A. B. Togueu Motcheyo, **J. D. Tchinang Tchameu**, S. I. Fewo, C.Tchawoua, T. C. Kofane, *Chameleon's behavior of modulable nonlinear electrical transmission line*, Commun. Nonlinear. Sci. Numer. Simul. **53**, 22 (2017).

Mobility of discrete multibreathers in the exciton dynamics of the Davydov model with saturable nonlinearities

J. D. Tchinang Tchameu,[*] A. B. Togueu Motcheyo,[†] and C. Tchawoua[‡]
Laboratory of Mechanics, Department of Physics, Faculty of Science, University de Yaounde I, P.O. Box 812, Yaounde, Cameroon
(Received 27 May 2014; published 21 October 2014)

We show that the state of amide-I excitations in proteins is modeled by the discrete nonlinear Schrödinger equation with saturable nonlinearities. This is done by extending the Davydov model to take into account the competition between local compression and local dilatation of the lattice, thus leading to the interplay between self-focusing and defocusing saturable nonlinearities. Site-centered (sc) mode and/or bond-centered mode like discrete multihump soliton (DMHS) solutions are found numerically and their stability is analyzed. As a result, we obtained the existence and stability diagrams for all observed types of sc DMHS solutions. We also note that the stability of sc DMHS solutions depends not only on the value of the interpeak separation but also on the number of peaks, while their counterpart having at least one intersite soliton is instable. A study of mobility is achieved and it appears that, depending on the higher-order saturable nonlinearity, DMHS-like mechanism for vibrational energy transport along the protein chain is possible.

DOI: 10.1103/PhysRevE.90.043203 PACS number(s): 05.45.Yv, 87.14.E−, 63.20.Pw, 71.35.−y

I. INTRODUCTION

During many biological processes, such as muscle contraction, DNA reduplication, neuroelectric pulse transfer on the neurolemma, and work of calcium or sodium pump, the bioenergy needed is provided by the hydrolysis of adenosine triphosphate (ATP). This energy has important significance and the comprehension of their storage and transport has been a challenge to scientists. In 1973, Davydov [1] suggested a mechanism based on soliton to elucidate the problem. Since the previous mentioned work, the possible existence of solitons in biomolecular systems has been widely studied (see Ref. [2], and references therein). Following Davydov's idea, energy released during ATP hydrolysis is stored in the form of a vibrational energy of the C=O stretching (amide-I) oscillators. This energy is transported from one peptide group to the next because of the dipole-dipole coupling between the adjacent groups. Experimentally, the model of Scott and Davydov was tested through the crystalline polymer acetalinide ($(CH_3CONHC_6H_5)_X$), or ACN, which is an organic solid close to a biological molecule [3].

At low temperature it has been shown that Davydov's theory for the α-helix gives rise to discrete nonlinear Schrödinger (DNLS) equation [4], which is one of the basic lattice models appearing in various contexts of physics and biology. During the past decade, DNLS equations as well as one of their solutions called discrete breather (alias intrinsic localized modes) have been intensively studied [5,6]. Discrete breather has a bell-shaped form while ones possessing an arbitrary number of extrema is called multibreather. Proof of the existence of the latter is given in Ref. [7], and since this work a great deal of effort has been invested to show their existence in Salerno equation [8], DNLS equation with cubic nonlinearity [9], and Klein-Gordon chain [10]. More recently, multibreathers have been predicted theoretically in realistic systems [11] and observed experimentally [12]. In spite the fact that multihump soliton have been observed in saturable dispersive nonlinear medium [13], their study is not yet done in purely discrete saturable nonlinear equation. The first purpose of this work is to explore the possible existence of multibreathers in DNLS equation with saturable nonlinearities.

At the beginning of the year 2000, the stability of multibreathers was an open problem (see Ref. [14]). Up to now much effort has gone into their stabilization [10–12,15], and it's well clear that stable multibreathers can be found. Could we obtain stable multibreathers in the exciton dynamics modeled by DNLS equation with competitive nonlinearities? The answer to this question is the second purpose of this work.

It has been observed for several years that discrete breathers could be mobile in some models [16–24]. To the best our knowledge, a study related to the mobility of multibreathers is not yet done. As the last aims of this work, we look for the possible mobile multibreathers in the system.

The rest of the paper is organized in the following manner. In Sec. II, the DNLS equation with saturable nonlinearities, which describes the state of amide-I excitations in proteins is derived. In Sec. III, we look for the discrete multihump solitons solutions of the previous-mentioned equation. Section IV is devoted to the mapping and linear stability analysis of these solutions. This section ends with the existence and stability diagrams for all observed types of discrete multihump soliton solutions. In Sec. V, we investigate the potential mobility of these solutions. Finally, the conclusion summarizing the different results of this work is given in the Sec. VI.

II. THE DAVYDOV MODEL AND DISCRETE NONLINEAR SCHRÖDINGER EQUATION WITH SATURABLE NONLINEARITIES

Let us consider the Davydov model with exciton-phonon coupling in hydrogen-bonded molecular chains. This infinite discrete chain consists of peptide groups (H-N-C=O) with a mass M, regularly spaced by a distance R, and

[*]jtchinang@gmail.com
[†]abtogueu@yahoo.fr
[‡]Corresponding author: ctchawa@yahoo.fr

weakly bound according to the following sequence: $\cdots$ H-N-C=O$\cdots$H-N-C=O$\cdots$H-N-C=O$\cdots$H-N-C=O$\cdots$. The dotted lines represent the hydrogen bonding. In addition, the interaction is assumed to work only between nearest-neighbor molecules.

The Hamiltonian associated with the network so described is expressed as

$$H = T + U + \sum_n [(\varepsilon - D_n)B_n^+ B_n - J(B_{n+1}^+ B_n + B_{n+1}B_n^+)], \quad (1)$$

where T is kinetic energy and U is the potential energy. The first part of the third term, $\varepsilon B_n^+ B_n$, defines the amide-I excitation energy, and the fourth term stands for the resonance dipole interaction between nearest neighbors. This interaction is characterized by the dipole-dipole interaction energy J. Notice that B_n^+ (B_n) is the creation (annihilation) operator of the amide-I excitation in the nth group. In the second part of the third term, the function $-D_n$ represents the deformation excitation energy of the nth peptide group with its nearest neighbors and can be written as [25]

$$D_n = \mathcal{D}_n(|x_{n+1} - x_n|) + \mathcal{D}_n(|x_n - x_{n-1}|). \quad (2)$$

Then, $-D_n B_n^+ B_n$ describes the interaction between the intramolecular excitation and the lattice displacements. Assuming that the coupling is strong, because it has been shown [26] that autolocalized excitation solitons appear in the system due to the nonlinear and strong exciton-phonon interaction, Eq. (2) can be written in the form

$$D_n \approx \left(1 + \frac{\beta}{R}\rho_n - \frac{\gamma}{2R^2}\rho_n^2\right)D, \quad (3)$$

where

$$\rho_n = R - |x_n - x_{n-1}| \quad (4)$$

denotes the relative distances between two neighboring groups from equilibrium and x_n, the small displacement of the nth peptide groups. Add that β and γ are adjustable positive parameters of the deformation excitation energy while $D = 2\mathcal{D}(R)$. Comparing Eq. (3) to one used in Ref. [27], the choice of the negative sign of the last term here is to take into account the competition between local compression and local dilation of lattice.

The use of Born-Oppenheimer approximation leads us to consider the lattice displacements as classical variables. This is justified by the fact that the effective mass M of the peptide group is large, thus leading acoustic vibrations to be slow compared to the excitonic modes. In order to establish the equations of motion, we define the soliton wave function as

$$|\psi\rangle = \sum_n a_n(t)B_n^+|0\rangle, \quad (5)$$

where $|0\rangle$ is the vacuum state and a_n is the complex probability amplitude of the exciton wave, which satisfies the normalization condition

$$\langle\psi|\psi\rangle = \sum_n |a_n(t)|^2 = 1. \quad (6)$$

Using time-dependent Schrödinger equation and Heisenberg equation we obtain the system of coupled equations

$$i\hbar\frac{\partial a_n}{\partial t} = \left[\varepsilon + T + U - \left(1 + \frac{\beta}{R}\rho_n - \frac{\gamma}{2R^2}\rho_n^2\right)D\right]a_n - J(a_{n+1} + a_{n-1}), \quad (7)$$

$$M\frac{\partial^2\rho_n}{\partial t^2} = -\omega(2\rho_n - \rho_{n+1} - \rho_{n-1}) + \frac{\beta D}{R}(2|a_n|^2 - |a_{n+1}|^2 - |a_{n-1}|^2) - \frac{\gamma D}{R^2}(2\rho_n|a_n|^2 - \rho_{n+1}|a_{n+1}|^2 - \rho_{n-1}|a_{n-1}|^2), \quad (8)$$

where ω is the spring constant. $T = \frac{M}{2}\sum_n(\frac{\partial x_n}{\partial t})^2$ and $U = \frac{\omega}{2}\sum_n \rho_n^2$. The great value of M leads to the adiabatic approximation [4]

$$\frac{\partial^2\rho_n}{\partial t^2} \approx 0. \quad (9)$$

Neglecting the inertia term, we solve Eq. (8) and obtain the following relation:

$$\rho_n = \frac{\frac{\beta D}{R\omega}|a_n|^2}{1 + \frac{\gamma D}{R^2\omega}|a_n|^2}. \quad (10)$$

Then, the substitution of Eq. (10) in Eq. (7) yields

$$i\hbar\frac{\partial a_n}{\partial t} = [\varepsilon + T + U - D]a_n - \nu_1 J\frac{|a_n|^2 a_n}{1 + \nu_3|a_n|^2} + \nu_2 J\frac{|a_n|^4 a_n}{(1 + \nu_3|a_n|^2)^2} - J(a_{n+1} + a_{n-1}), \quad (11)$$

where $\nu_1 = \frac{\beta^2 D^2}{R^2\omega J}$, $\nu_2 = \frac{\gamma\beta^2 D^3}{2R^4\omega^2 J}$, and $\nu_3 = \frac{\gamma D}{R^2\omega}$.

Equation (11) is reduced in the form

$$i\frac{\partial\phi_n}{\partial\tau} = -\Delta_2\phi_n + \eta_1\frac{\phi_n}{1 + |\phi_n|^2} + \eta_2\frac{|\phi_n|^2\phi_n}{(1 + |\phi_n|^2)^2}, \quad (12)$$

if we set

$$\phi_n = \sqrt{\nu_3}a_n \exp i\tau\left[\frac{\varepsilon + T + U - D - 2J - \eta_1 J}{J}\right], \quad \eta_1 = \nu_1/2\nu_3, \quad \text{with} \quad \nu_3 \neq 0,\ \eta_2 = -\eta_1, \quad (13)$$

and use the dimensionless time $\tau = Jt/\hbar$. In Eq. (12), η_1 and η_2 are the strength of the nonlinearities and $\Delta_2\phi_n = (\phi_{n+1} + \phi_{n-1} - 2\phi_n)$.

It is well known that under adiabatic approximation, Davydov shows that the dynamics of the coupled exciton-phonon system is reduced to the DNLS equation [4]. Here, since $\eta_1 > 0$ and $\eta_2 < 0$, Eq. (12) is named the DNLS equation with competitive saturable nonlinearities. This equation has

two conserved quantities: the Hamiltonian,

$$E = \sum_n \Big[|\phi_{n+1} - \phi_n|^2 + (\eta_1 + \eta_2) \times \log(1 + |\phi_n|^2) + \frac{\eta_2}{1 + |\phi_n|^2} \Big], \quad (14)$$

and the number of quanta (l^2-norm),

$$P = \sum_n |\phi_n|^2. \quad (15)$$

We also note that, due to the last term in the right-hand side, Eq. (12) is different from the well-known DNLS equation with photorefractive nonlinearity, widely used in optics. In the other words, the coefficient η_2 guarantees the presence of higher-order saturable nonlinearity. In order to give a physical meaning to η_2, let us set $\eta_1 = -\eta_2 = \eta$ and we consider $\chi_1 = (\beta D/R) > 0$ and $\chi_2 = -(\gamma D/2R) < 0$, the phonon-exciton coupling parameters. χ_1 and χ_2, respectively, represent the parameters of nonlinear coupling. Thus, if $\gamma = 0$ ($\chi_2 = 0$), we have through Eq. (11) $\nu_2 = \nu_3 = 0$, and we get the classical Davydov-Scott model, which leads to the well-known DNLS equation with cubic nonlinearity. Therefore, χ_2 contributes to the strong phonon-exciton coupling, thereby promoting the formation of soliton. Similar considerations have been used by Velarde and coworkers [28], when looking for long-living intrinsic localized solectron, they have considered an extended polaron Hamiltonian in which the electron-hopping term is affected by anharmonicity. In the following, we parametrize our problem by η, which is also expressed as $\eta = (\chi_1 R/4J)\widetilde{\eta}$, with $\widetilde{\eta} = -(\chi_1/\chi_2)$. For α-helical proteins, the use of the following physical parameters [29,30] $J = 9.67 \times 10^{-4}$ eV, $\chi_1 = 8 \times 10^{-2}$ eV/Å, $\omega = 0.8125$ eV/Å^2, $R = 4.5$ Å, leads to $\eta \approx 93\widetilde{\eta}$.

Based on the meaning of the sign of χ [31], it appears that negative coefficient means that the molecular chain is locally dilated (dilatational soliton) and a positive value represents the local compression (compressional soliton) of molecular chain due to amide-I vibrations. It follows that our model exhibits a competition of self-focusing (dilatation) and defocusing (compression) saturable nonlinearities. This is a good compromise given the fact that in the literature, the coupling parameter is taken positive or negative [32].

It is also important to recall that an equation similar to Eq. (11) has been obtained by Aguero [27] in a continuous medium. However, to look for the soliton structures, he has simplified the equation to cubic-qintic nonlinear Schrödinger equation in order to solve it. So, in the next section, we will determine discrete multisoliton (discrete multibreather) solutions of Eq. (12).

III. DISCRETE STATIONARY MULTIHUMP SOLITON SOLUTIONS

In order to solve Eq. (12) governing the evolution of the complex probability amplitude ϕ_n, we seek the stationary solutions of the form $\phi_n = u_n \exp(-i\Omega\tau)$, Ω being a frequency. Under this condition, we obtain a set of coupled algebraic equations for the real function u_n:

$$\Omega u_n + (u_{n+1} + u_{n-1} - 2u_n) - \eta \frac{u_n}{1 + u_n^2} + \eta \frac{u_n^3}{\left(1 + u_n^2\right)^2} = 0. \quad (16)$$

It should be added to the above relations, the normalization condition given by Eq. (6), and rewritten as

$$\sum_n u_n^2 \simeq \frac{0.043}{\widetilde{\eta}}. \quad (17)$$

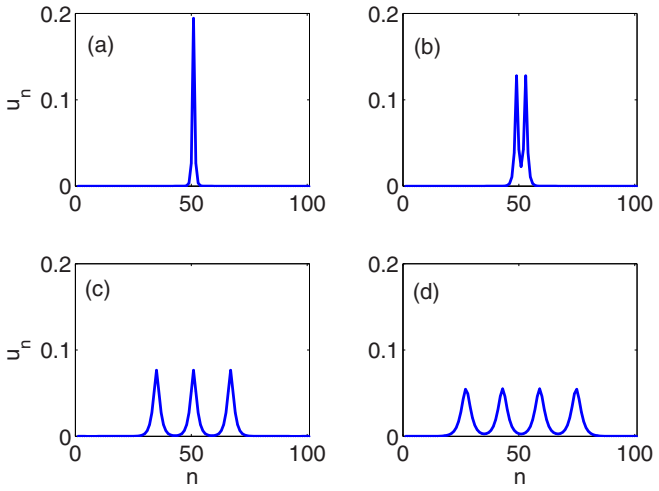

FIG. 1. (Color online) Examples of profiles of single-hump [(a) $(\widetilde{\eta};\Omega) \approx$ (1.1;96.706)], two-hump [(b) $(\widetilde{\eta};\Omega) \approx$ (1.1;100.4)], three-hump [(c) $(\widetilde{\eta};\Omega) \approx$ (1.1;101.75)], and four-hump [(d) $(\widetilde{\eta};\Omega) \approx$ (1.1;102)] solitons.

It is well known that two-component systems with saturable nonlinearity can sustain both single-hump and multihump solitons (optical solitons) [33]. The idea is to investigate the presence of such solutions in our model despite being a one-component system. This is done numerically, by means of iterative multidimensional Newton-Raphson method with periodic boundary conditions and initial guess produced by the high-confinement approximation [34]. These solutions are illustrated in Fig. 1, where we give the profiles of single-hump, two-hump, three-hump, and four-hump solitons for $(\widetilde{\eta};\Omega) \approx (1.1;96.706)$, $(\widetilde{\eta};\Omega) \approx (1.1;100.4)$, $(\widetilde{\eta};\Omega) \approx (1.1;101.75)$, and $(\widetilde{\eta};\Omega) \approx (1.1;102)$, respectively. These discrete stationary multihump solitons are all constituted of solitons belonging to site-centered (sc) mode. Note that multihump solitons composed of solitons belonging to bond-centered (bc) mode and those belonging to bc and sc mode were also found. Figure 2 shows this case with the profile of two-hump and three-hump solitons for bc-sc mode, bc-bc mode, and sc-bc-sc mode. We are now interested in multihump soliton solutions constituted solely of sc modes. Let ℓ_δ represents the interpeak separation, i.e., the distance between two neighbor peaks, where the subscript δ is the number of peak of the solution. In the case of two-hump solitons, we obtain $\ell_2 = 4$ while for three- and four-hump solitons, $\ell_3 = \ell_4 = 4\ell_2 = 16$ (see Fig. 1). This means that the localization of solution decreases when δ increases. Moreover,

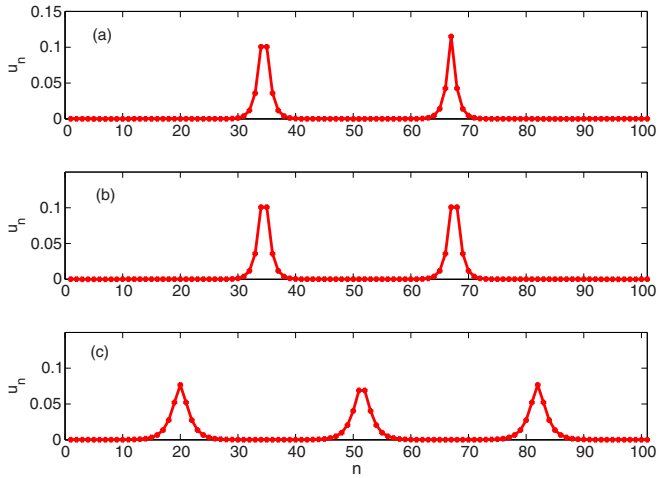

FIG. 2. (Color online) Examples of profiles of two-hump [(a) $(\widetilde{\eta};\Omega)\approx(1.1;100.9)$], two-hump [(b) $(\widetilde{\eta};\Omega)\approx(1.1;100.9)$], and three-hump [(c) $(\widetilde{\eta};\Omega)\approx(1.1;101.75)$] solitons for bc-sc mode, bc-bc mode, and sc-bc-sc mode, respectively.

by noting ζ_δ as being the maximum amplitude of the δ-soliton, we have $\zeta_1\simeq 0.19$, $\zeta_2\simeq 0.13$, $\zeta_3\simeq 0.077$, and $\zeta_4\simeq 0.055$. So we also see a gradual decrease of ζ_δ as the number of peaks δ increases. It appears from these results that the system cannot admit an unlimited number of peaked localized states. Recall that the normalization condition for envelope u_n ($\sum_n u_n^2\simeq\frac{0.043}{\widetilde{\eta}}$) is satisfied for all these solutions. We can conclude that the localization of vibrational energy in protein can be in the form of single discrete solitons or a discrete multisoliton. A similar result was obtained in the past in the context of two-component solitary waves [35].

It is important to mention that $\widetilde{\eta}$ not only reflects the saturation coefficient but also the ratio between the expansion and compression terms of the molecular chain. We also want to add the following biological meaning of the phenomenon of saturation in order to show how our model is more realistic. The ATP conserves energy via glycolysis, glycogenolysis, and the citric acid cycle. If the cells have sufficient supplies of ATP, then these pathways and cycles are inhibited. Under these conditions of excess ATP, the liver will attempt to convert a variety of excess glucose molecules into glycogen [36]. Thus, when ATP is too large, there is a saturation through these inhibitions. Otherwise, when the probability amplitude $|\phi_n|$ is low, the saturable nonlinearities can be reduced to a cubic nonlinearity via a Taylor expansion. Thus, the feature of our model is that it includes two cases (where ATP is produced in excess and otherwise).

For the soliton solutions previously seen to be biologically acceptable, they must be stable. Study of their stability is the purpose of the next section.

IV. STABILITY ANALYSIS

The previous discrete solutions must be stable to be biologically acceptable for the localization and transport of vibrational energy in protein. Here, the stability of these solutions is considered from the view point of both the map orbit stability and the corresponding dynamical stability.

A. Mapping stability

Using the map approach technique [8,34,37–39], and defining $p_n=u_n$ and $q_n=u_{n-1}$, Eq. (16) is transformed into the following two-dimensional real map:

$$\begin{aligned} p_{n+1} &= (2-\Omega)p_n+\eta\frac{p_n}{1+p_n^2}-\eta\frac{p_n^3}{\left(1+p_n^2\right)^2}-q_n \\ q_{n+1} &= p_n. \end{aligned} \tag{18}$$

A linearly unstable map orbit gives rise to a dynamically stable solution [37]. Moreover, to investigate the mapping stability, the study of the stability of the fixed point of the corresponding 2D map is sufficient. Then, the fixed points of Eq. (18), for which $p_n=q_n$, are located at

$$p_0=0,\quad p_{1,2}=\pm\sqrt{\frac{-\Omega\pm\sqrt{\Omega\eta}}{\Omega}}. \tag{19}$$

Knowing that $\eta>0$ with $\eta=93\widetilde{\eta}$, $p_{1,2}$ exists if only if $\Omega>0$ and $\eta\geqslant\Omega$. The Jacobian matrix $\check{J}$ of the map Eq. (18) is given by

$$\begin{bmatrix} (2-\Omega)+\eta\frac{1-p_n^2}{\left(1+p_n^2\right)^2}-\eta\frac{p_n^2\left(3-p_n^2\right)}{\left(1+p_n^2\right)^3} & -1 \\ 1 & 0 \end{bmatrix}. \tag{20}$$

The study of the stability of fixed points requires the evaluation (calculation) of the eigenvalues of the Jacobian $\check{J}$ evaluated at these points. This being done, the fixed points will be an unstable saddle point if $|\lambda_1|>1$ and $|\lambda_2|<1$ or vice versa. λ_1 and λ_2 being the eigenvalues of $\check{J}$. Particular attention is given to saddle fixed points due to the fact that they can support homoclinic orbits used to generate bright soliton solutions [37]. On the other hand, we recall that the homoclinic orbits are obtained through the intersection of stable and unstable manifolds. In the top left panel of Fig. 3, the areas marked in blue, red, and yellow are those for which p_0, p_1, and p_2 are unstable saddle nodes, respectively. When we employ the technique of residues as defined in Ref. [38], we obtain that the condition of existence of unstaggererd soliton is $\eta\geqslant\Omega$, with $\eta=93\widetilde{\eta}$. This condition is shown in the top left panel of Fig. 3 by the area bounded by two straight lines of black color. The condition of existence mentioned above is similar to that in the case of the discrete version of the Vinetskii-Kukhtarev equation [34]. This is probably due to the fact that our model has the same tangent map around zero as the discrete Vinetskii-Kukhtarev equation. However, properties related to nonzero fixed points are different from theirs.

Notice that the area of existence in the top left panel of Fig. 3 contains probably two types of spatially localized solutions: breathers and multibreathers [8]. Because the fixed point is saddle, it is not sufficient by itself to guarantee the existence of stable and unstable manifolds that intersect [9]. This is why we must determine the domain for which the stable and unstable manifolds intersect. Figure 4 corroborates the top left panel of Fig. 3 despite some nuances observed when $\Omega\lesssim 0.08$.

Another illustration of the comments that have been carried out is through the top right and bottom left panels of Fig. 3. From these figures, it clearly reflected that the bright soliton

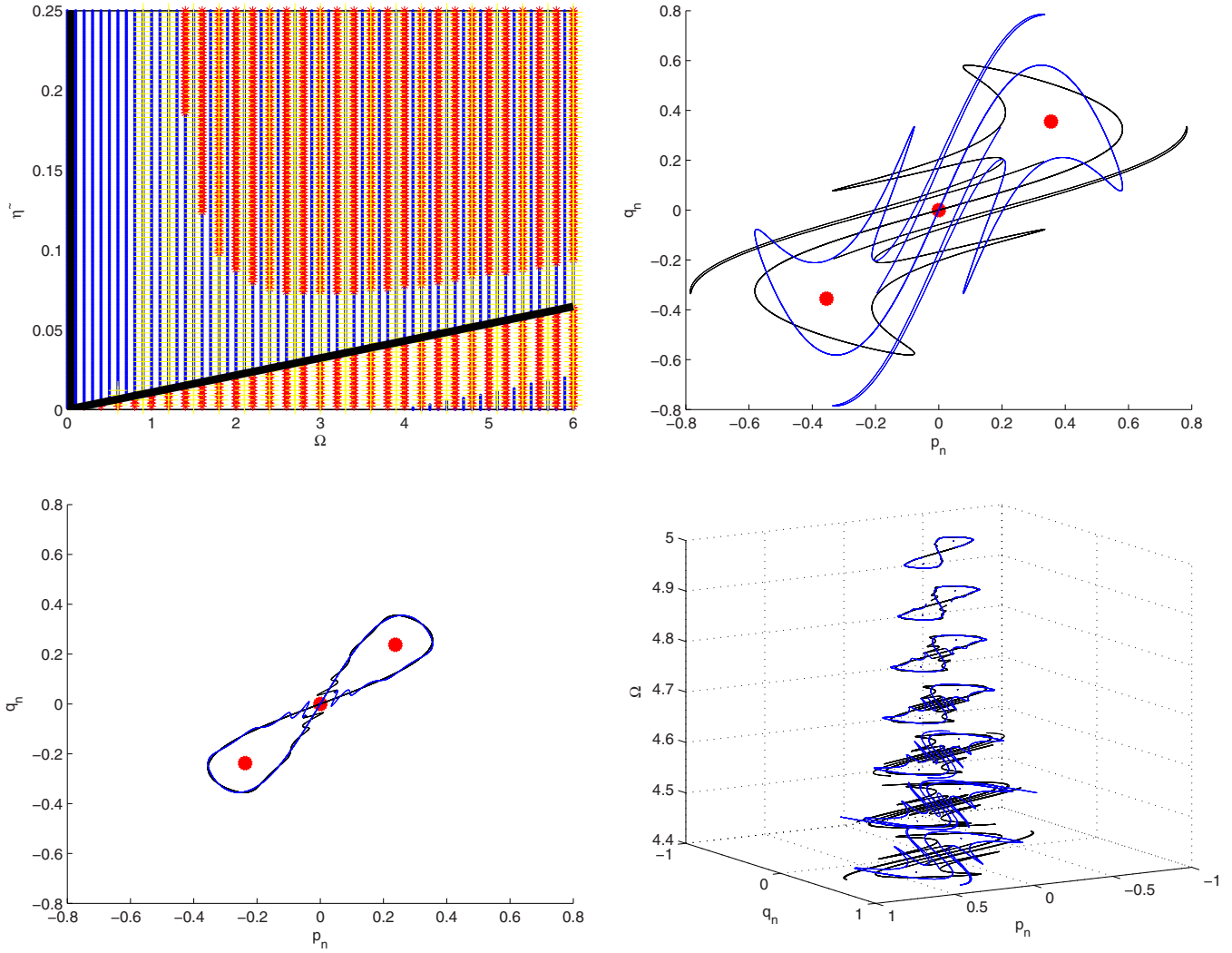

FIG. 3. (Color online) Stability diagram of the fixed points of Eq. (19) (top left panel) in the Ω-$\widetilde{\eta}$ parameter plane. The areas marked in blue, red, and yellow are those for which p_0, p_1, and p_2 are, respectively, unstable saddle nodes. In the top right and bottom left panels, we have intersections of stable and unstable manifolds for $(\Omega, \widetilde{\eta}) = (4.4, 0.06)$ and $(5, 0.06)$, respectively. The red dots being the fixed points. In the bottom right panel, we have the map orbits around the fixed point p_0 according to Ω, $\widetilde{\eta} = 0.06$.

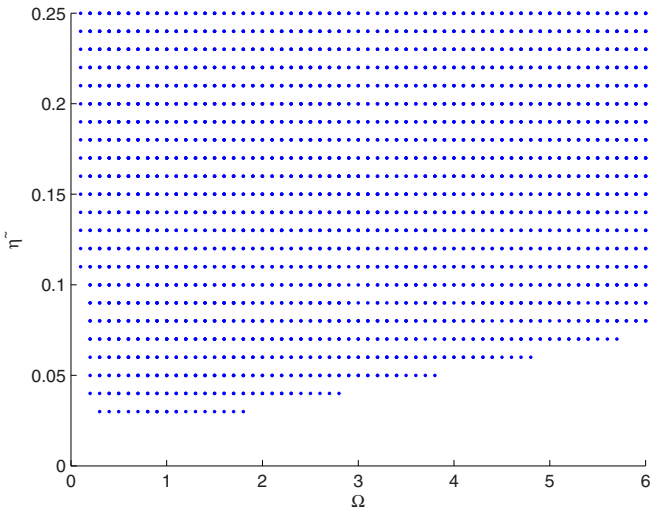

FIG. 4. (Color online) Domain of existence of the intersection of manifolds. Condition of obtaining bright soliton solution.

cannot exist without constraints on the parameters. Moreover, knowing that a much richer tangling structure is equivalent to a richer family of solitons [39], the evolution of map orbits ($\widetilde{\eta} = 0.06$) from $\Omega = 4.4$ to $\Omega = 5$ shows a dimunition of this family of soliton solutions (bottom right panel of Fig. 3). This dimunition continues until $\Omega = 5.58$, where a fold bifurcation occurs. Before that, we have a pitchfork bifurcation that occurs when $\Omega \simeq 4.9$.

At this point, among the previous types (or modes) of solitons discussed, which are most likely to carry in a stable manner the energy of amide-I vibrational excitation through the protein molecules?

B. Linear stability analysis

In this subsection, we will study the stability of DMHS by means of linear stability analysis [40]. Here the DMHS are slightly perturbed:

$$\phi_n = \exp(-i\Omega t)\{u_n + \epsilon[x_n \exp(\lambda t) + y_n \exp(\bar{\lambda} t)]\}, \quad (21)$$

where x_n and y_n are complex, ϵ is a linearization parameter, and λ is the eigenvalue. Add that $\overline{\lambda}$ denotes the complex conjugate of λ, Ω being the frequency seen above. This leads to the linear stability equations:

$$i\lambda\begin{pmatrix}x_n\\ y_n\end{pmatrix}=\begin{bmatrix}-\Omega+\frac{\eta}{1+|u_n|^2}-\frac{3\eta|u_n|^2}{(1+|u_n|^2)^2}+\frac{2\eta|u_n|^4}{(1+|u_n|^2)^3}-\Delta_2 & -\frac{2\eta u_n^2}{(1+|u_n|^2)^2}+\frac{2\eta|u_n|^2u_n^2}{(1+|u_n|^2)^3}\\ \frac{2\eta\overline{u_n^2}}{(1+|u_n|^2)^2}-\frac{2\eta|u_n|^2\overline{u_n^2}}{(1+|u_n|^2)^3} & \Omega-\frac{\eta}{1+|u_n|^2}+\frac{3\eta|u_n|^2}{(1+|u_n|^2)^2}-\frac{2\eta|u_n|^4}{(1+|u_n|^2)^3}+\Delta_2\end{bmatrix}\begin{pmatrix}x_n\\ y_n\end{pmatrix}. \quad (22)$$

Among the $2N$ eigenvalues λ, if at least one has a strictly positive real part, a DMHS is spectrally unstable. Solving numerically Eq. (22), we obtain the eigenvalue spectrum for strongly localized sc and bc modes.

A linear analysis of stability of DMHS composed of soliton belonging to sc mode is carried out by solving numerically the eigenvalue problem (EVP) described by Eq. (22) where u_n is the solution found numerically in the previous section. The results of this analysis are shown in Figs. 5 and 6. Figure 5 is concerning the symmetric two-hump solitons normalized for four values of ℓ_2: 4, 8, 12, and 32. The corresponding eigenvalues spectrum shows that the intensity of the instability decreases as ℓ_2 increases. After checking intermediate values, we note that $\ell_\delta^* \approx 32$ is the threshold value where the solution becomes stable. A similar phenomenon is observed in Fig. 6 for four-hump solitons when $\ell_\delta^* \approx 50$. Thus, the stability of multihump solitons depends on the value of ℓ contrary to what is observed in optics (see Ref. [33]). We further note that the stability of multisoliton depends on ℓ_δ. In fact, ℓ_δ increases as δ increases. As an explanation, we can say that the instability of our multisoliton for values of ℓ_δ below the ℓ_δ^* is probably due to interactions between the δ present solitons. This is why a large number of peaks (δ) leads to great interaction between them, hence a large distance between them to stabilize. This explains the reasons for which we have $\ell_2^* < \ell_3^* < \ell_4^*$.

A numerical evolution of DMHS having at least one soliton with bc mode, by means of fourth-order Runge-Kutta scheme with a suitable choice of time step and absolute tolerance (10^{-10}) in order to ensure the conservation of energy and normalization condition, is performed. It appears that this type of solutions is unstable as we shown in Fig. 7. Indeed, the bc solition of DMHS turns on sc soliton during the evolution of DMHS. A similar fact was noted in Ref. [41], where only onsite single-hump solitons are stable.

C. Existence and stability diagrams of sc DMHS solutions

We proceed to exploring the existence and stability diagrams for all observed types of sc DMHS in the parameter space $(\Omega, \widetilde{\eta})$. It appears from Fig. 8 (top left and bottom right panels) that the regions where DMHS exist decrease as the number of humps increase. For the case of four-hump solitons it is reduced to a very thin region of parameter space. Insets of these figures illustrate the case where the local compression prevails over the local dilatation ($\widetilde{\eta} > 1$). Stability of two-hump soliton with $\ell_2 = 32$ is displayed in the bottom left panel of Fig. 8. It emerges that the increase of interpeak separation ℓ_2 does not make all of the solution stable in the parameter space. It being understood that for $\ell_2 < 32$, almost all two-hump solitons are unstable. Similar to two-hump solitons, almost all four-hump solitons are unstable for $\ell_4 < 50$ and stable for $\ell_4 = 50$ (see the bottom right panel of Fig. 8). This fact reaffirms that interpeak separation has a stabilizing effect on the solutions. The bottom left panel of Fig. 8 underpins this observation. Otherwise, since the magnitude of instability decreases as the interpeak separation

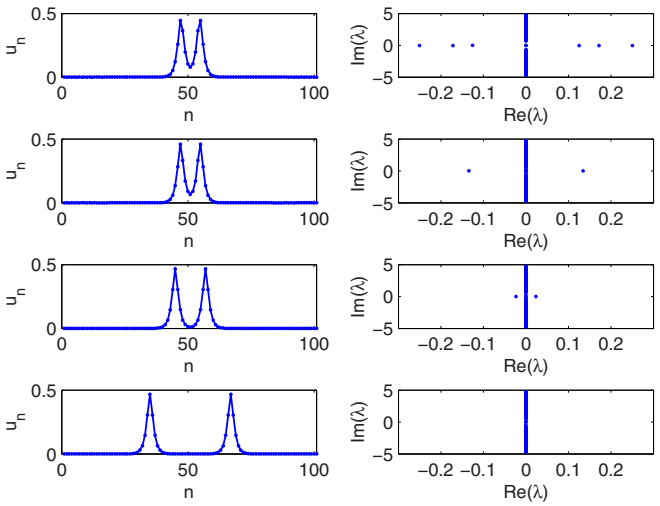

FIG. 5. (Color online) Profiles of two−hump solitons (left column) and their correponding eigenvalue spectrum (right column) with increasing (from top to bottom) values of ℓ_2: $\ell_2 = 4$; 8; 12 and 32. $\Omega \approx 3.6$, $\widetilde{\eta} \approx 0.0464$.

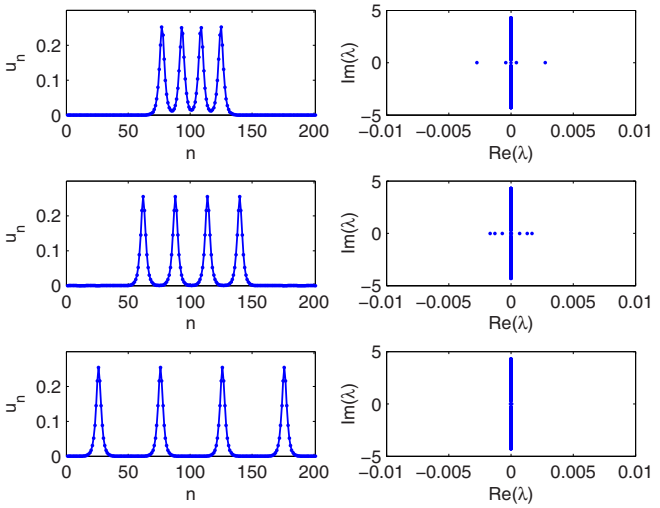

FIG. 6. (Color online) Profiles of four−hump solitons (left column) and their correponding eigenvalue spectrum (right column) with increasing (from top to bottom) values of ℓ_4: ℓ_4 =16; 26 and 50. $\Omega \approx 4.9$, $\widetilde{\eta} \approx 0.056$.

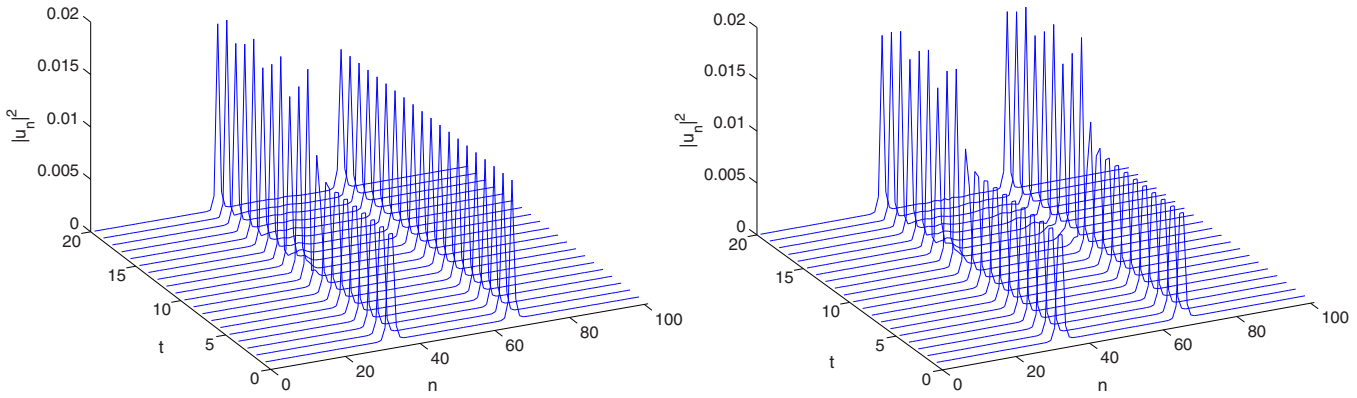

FIG. 7. (Color online) Development of instability of two-hump solitons having at least one intersite soliton for $[(\Omega,\widetilde{\eta}) = (100.9, 1.1)]$. The left and right panels correspond to bc-sc mode and bc-bc mode, respectively.

increases [42], the strength of higher-order nonlinearity in our saturable DNLS may enhance the stability. Indeed, it is well known that the magnitude of instability decreases by increasing the strength of nonlinearity of Cubic DNLS [42].

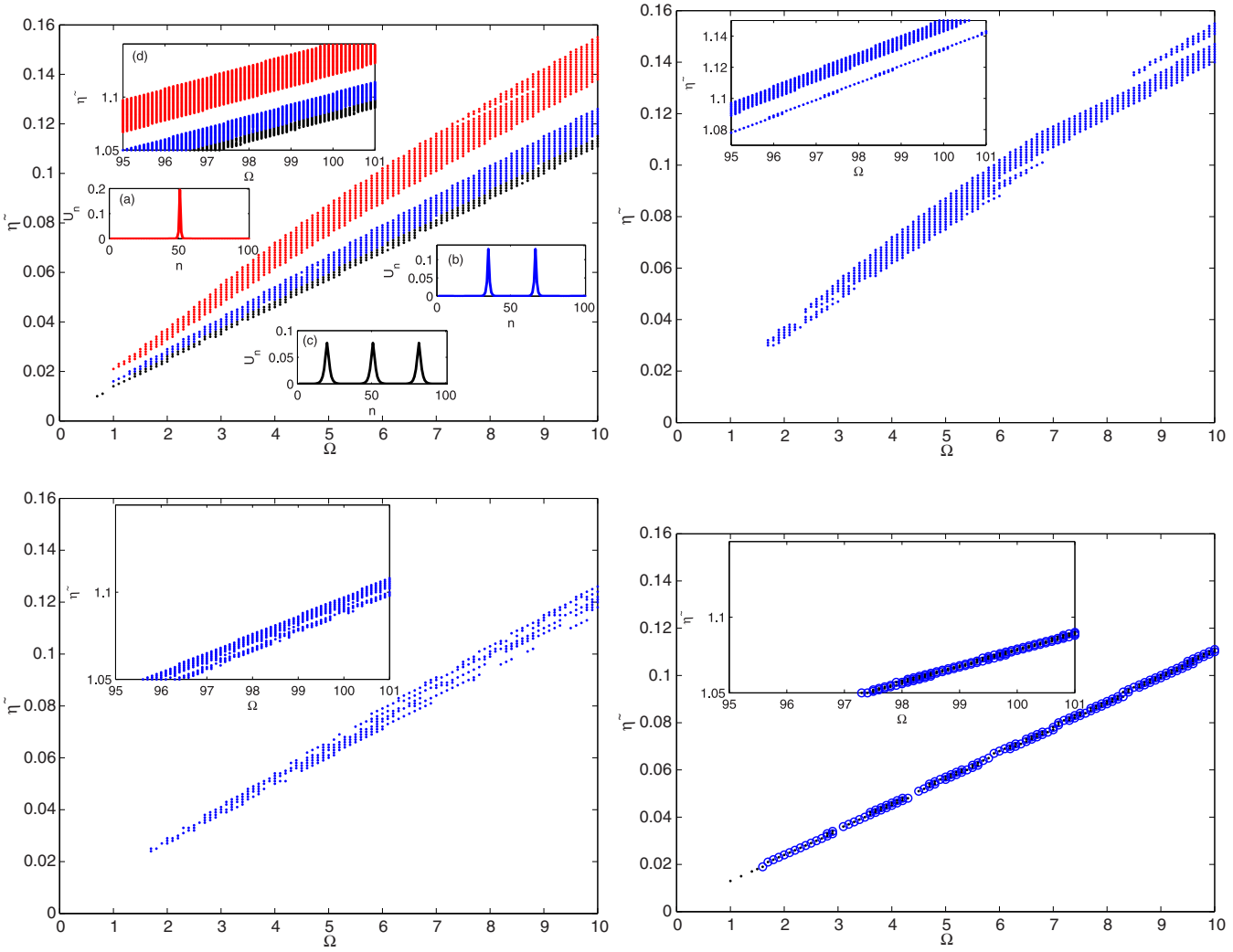

FIG. 8. (Color online) Existence and stability diagrams for all observed types of sc DMHS solutions. In the top left panel, we have the existence diagram for one-hump solitons (red), two-hump solitons (blue), and three-hump solitons (black). Inset (d) shows the case where $\widetilde{\eta} > 1$. Other insets, (a), (b), and (c), are related to observed types of sc DMHS. The stability diagram of one-hump and two-hump ($\ell_2 = 32$) solitons is shows in the top right and bottom left panels, respectively. The bottom right figure illustrates the existence (dot) and stability (circle) diagram for four-hump ($\ell_4 = 50$) solitons. Insets show the case where $\widetilde{\eta} > 1$.

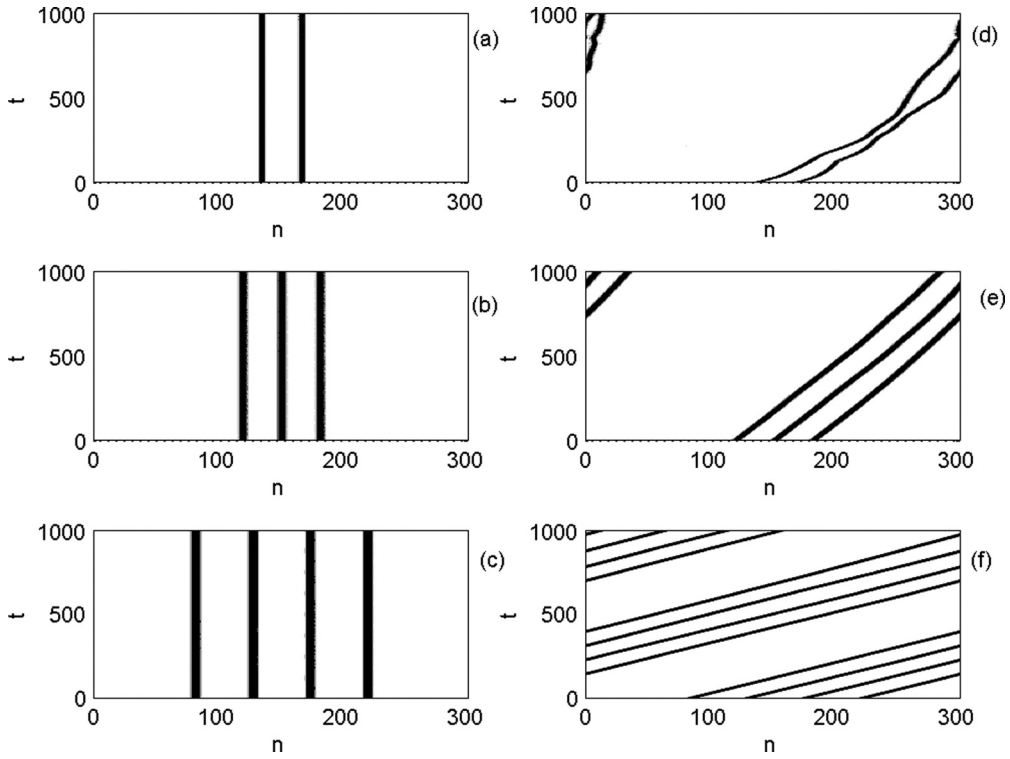

FIG. 9. Density plot $|\phi_n|^2$ for not kicked (a) two-hump, (b) three-hump, (c) four-hump solitons and their kicked counterparts, (d), (e), and (f), respectively. We have (d) $\varpi = 0.55$, $\Omega \approx 3.6$, $\widetilde{\eta} \approx 0.0464$; (e) $\varpi = 0.3$, $\Omega \approx 5.635$, $\widetilde{\eta} \approx 0.065$; (f) $\varpi = 0.3$, $\Omega \approx 4.9$, $\widetilde{\eta} \approx 0.056$; respectively. Mobility is achieved for $\Omega \simeq \eta(\frac{1}{1+\alpha^2})$, (d) $\alpha = 0.4777$, (e) $\alpha = 0.2765$, (f) $\alpha = 0.2549$.

Here the enhancement of the stability is justified by the fact that the strength of higher-order saturable nonlinearity increases the nonlinearity of cubic DNLS equation obtained by expanding in Taylor series the saturable nonlinearities.

At the end of this section, as the evolution of the localized solectron states has suggested their potential as new carriers for fast electric charge transport [28], it emerges that when multipeaked localized solutions are stable, they may be a candidate for energy transport in the protein.

V. MOBILITY OF DISCRETE MULTIHUMP SOLITONS

In this section, we study the DMHS mobility. Note at the outset that the study of bright mobile solution in the DNLS with photorefractive nonlinearity has already been done [23,37,43]. However, for DNLS equation with saturable nonlinearities, mobility of multibreathers has not been yet found. We use here the energy techniques which consist "to push" the localized solution to move through the lattice by means of a variation of the solution initial phase. This is done through the following perturbation:

$$\phi_n(0) = u_n \exp(i\varpi n), \tag{23}$$

where u_n is a stationary solution seen above, and ϖ represents the relative strength.

By applying the kick to two-hump [Fig. 9(a)], three-hump [Fig. 9(b)], and four-hump solitons [Fig. 9(c)], we obtain Figs. 9(d), 9(e), and 9(f), respectively. In these figures, it appears that the mobility is achieved for three-hump solitons, four-hump solitons, and to a more limited extent, two-hump solitons. This is not the case for one-hump solitons. Moreover, in our model, the mobility is achieved for $\Omega \simeq \eta_1[1 + \frac{\eta_2\alpha^2}{\eta_1(1+\alpha^2)}]$, where α is the amplitude of our solutions and $\eta_2 = -\eta_1$. This new condition of mobility depends on the higher-order saturable nonlinearity. For the general case (model where η_1 and η_2 are arbitrary nonlinear coefficients), if $\eta_2 = 0$, this latter condition reduces to $\Omega \simeq \eta$, which is the condition of mobility for the single soliton in the DNLS equation with saturable nonlinearity (see Ref. [37]). In view of the existence diagram, it follows that the sc DMHS are more able to be mobile. In other words, the sc DMHS are more able (with the kick) to overcome the Peierls-Nabarro barrier (PNB).

The main conclusion to be drawn from these observations is that a discrete multihump soliton-like mechanism for vibrational energy transport along the protein chain is possible.

VI. CONCLUSION

In this paper we have shown that the DNLS equation with saturable nonlinearities models the localization and transport of vibrational energy in protein, when a nonlinear and strong exciton-phonon interaction is taken into account. Thus, the model includes conditions of excess ATP and the opposite case. In the absence of the higher-order saturable nonlinearity, the equation model is reduced to the DNLS equation with photorefractive nonlinearity widely used in optics. The multihump (two-hump, three-hump, and four-hump) solitons having sc mode and/or bc mode were sought as solutions of the system and their stability was examined. The linear stability analysis

that followed the stability diagram established reveals that the stability of multihump solitons depends not only on the value of the interpeak separation but also on the number of peaks of the solution. The results concerning the existence and stability of the sc DMHS solutions are consolidated in parameter space. A numerical evolution of DMHS having at least one intersite soliton reveals their instability. Finally, the study of the mobility of our solutions has led us to the main conclusion that, depending on the higher-order saturable nonlinearity, a multihump soliton-like mechanism for vibrational energy transport along the protein chain is possible. It will be interesting to study in future works the behavior of two stable discrete multihump solitons during and after collisions.

[1] A. S. Davydov, J. Theor. Biol. **38**, 559 (1973).
[2] P. Xiao-feng, Prog. Biophys. Mol. Bio. **108**, 1 (2012).
[3] G. Careri, U. Buontempo, F. Galluzzi, A. C. Scott, E. Gratton, and E. Shyamsunder, Phys. Rev. B **30**, 4689 (1984).
[4] A. C. Scott, Phys. Rep. **217**, 1 (1992).
[5] S. Flach and C. R. Willis, Phys. Rep. **295**, 181 (1998).
[6] S. Flach and A. V. Gorbach, Phys. Rep. **467**, 1 (2008).
[7] T. Ahn, Nonlinearity **11**, 965 (1998).
[8] T. Bountis, H. W. Capel, M. Kollmann, J. C. Ross, J. M. Bergamin, and J. P. van der Weele, Phys. Lett. A **268**, 50 (2000).
[9] P. G. Kevrekidis, *Discrete Nonlinear Schrödinger Equation: Mathematical Analysis, Numerical Computations and Physical Perspectives*, Springer Tracts Modern Phys., Vol. 232 (Springer, Berlin, 2009).
[10] V. Koukouloyannis, P. G. Kevrekidis, J. Cuevas, and V. Rothos, Physica D **242**, 16 (2013).
[11] A. B. Togueu Motcheyo, C. Tchawoua, M. Siewe Siewe, and J. D. Tchinang Tchameu, Phys. Lett. A **375**, 1104 (2011).
[12] F. Palmero, L. Q. English, J. Cuevas, R. Carretero-Gonzàlez, and P. G. Kevrekidis, Phys. Rev. E **84**, 026605 (2011).
[13] M. Mitchell, M. Segev, and D. N. Christodoulides, Phys. Rev. Lett. **80**, 4657 (1998).
[14] P. G. Kevrekidis, K. Ø. Rasmussen, and A. R. Bishop, Int. J. Mod. Phys. B **15**, 2833 (2001).
[15] V. Koukouloyannis and S. Ichtiaroglou, Phys. Rev. E **66**, 066602 (2002).
[16] V. M. Burlakov, S. A. Kiselev, and V. N. Pyrkov, Phys. Rev. B **42**, 4921 (1990).
[17] K. W. Sandusky, J. B. Page, and K. E. Schmidt, Phys. Rev. B **46**, 6161 (1992).
[18] M. Öster, M. Johansson, and A. Eriksson, Phys. Rev. E **67**, 056606 (2003).
[19] T. R. O. Melvin, A. R. Champneys, P. G. Kevrekidis, and J. Cuevas, Phys. Rev. Lett. **97**, 124101 (2006).
[20] J. Cuevas and J. C. Eilbeck, Phys. Lett. A **358**, 15 (2006).
[21] R. A. Vicencio and M. Johansson, Phys. Rev. E **73**, 046602 (2006).
[22] H. Susanto, P. G. Kevrekidis, R. Carretero-Gonzàlez, B. A. Malomed, and D. J. Frantzeskakis, Phys. Rev. Lett. **99**, 214103 (2007).
[23] T. R. O. Melvin, A. R. Champneys, P. G. Kevrekidis, and J. Cuevas, Physica D **237**, 551 (2008).
[24] C. Mejía-Cortés, R. A. Vicencio, and B. A. Malomed, Phys. Rev. E **88**, 052901 (2013).
[25] A. S. Davydov, J. Theor. Biol. **66**, 379 (1977).
[26] A. S. Davydov, *Theory of Molecular Excitons* (Plenum Press, New York, 1971).
[27] M. Aguero, R. García-Salcedo, J. Socorro, and E. Villagran, Int. J. Theor. Phys. **48**, 670 (2009).
[28] O. G. Cantu Ros, L. Cruzeiro, M. G. Velarde, and W. Ebeling, Eur. Phys. J. B **80**, 545 (2011).
[29] K. Kundu, Phys. Rev. E **61**, 5839 (2000).
[30] L. MacNeil and A. C. Scott, Phys. Scr. **29**, 284 (1984).
[31] E. A. Bartnik, J. A. Tuszynski, and D. Sept, Phys. Lett. A **204**, 263 (1995).
[32] L. A. Cisneros-Ake and A. A. Minzoni, Phys. Rev. E **85**, 021925 (2012).
[33] E. A. Ostrovskaya, Yu. S. Kivshar, D. V. Skryabin, and W. J. Firth, Phys. Rev. Lett. **83**, 296 (1999).
[34] Lj. Hadžievski, A. Maluckov, M. Stepić, and D. Kip, Phys. Rev. Lett. **93**, 033901 (2004).
[35] E. A. Ostrovskaya, S. F. Mingaleev, Yu. S. Kivshar, Y. B. Gaididei, and P. L. Christiansen, Phys. Lett. A **282**, 157 (2001).
[36] F. Mitchell, *Essential Biochemistry for Medicine*, October ed. (John Wiley and Sons, New York, 2010).
[37] A. Maluckov, Lj. Hadžievski, and M. Stepić, Physica D **216**, 95 (2006).
[38] D. Hennig, K. Ø. Rasmussen, H. Gabriel, and A. Bülow, Phys. Rev. E **54**, 5788 (1996).
[39] R. Carretero-Gonzàlez, J. D. Talley, C. Chong, and B. A. Malomed, Physica D **216**, 77 (2006).
[40] A. Maluckov, Lj. Hadžievski, and B. A. Malomed, Phys. Rev. E **76**, 046605 (2007).
[41] M. Stepić, A. Maluckov, M. Stojanović, F. Chen, and D. Kip, Phys. Rev. A **78**, 043819 (2008).
[42] G. Kalosakas, Physica D **216**, 44 (2006).
[43] O. Cohen, R. Uzdin, T. Carmon, J. W. Fleischer, M. Segev, and S. Odoulov, Phys. Rev. Lett. **89**, 133901 (2002).

Physics Letters A 379 (2015) 2984–2990

Contents lists available at ScienceDirect

Physics Letters A

www.elsevier.com/locate/pla

Effects of next-nearest-neighbor interactions on discrete multibreathers corresponding to Davydov model with saturable nonlinearities

J.D. Tchinang Tchameu, C. Tchawoua *, A.B. Togueu Motcheyo

Laboratory of Mechanics, Department of Physics, Faculty of Science, University of Yaounde I, P.O. Box 812, Yaounde, Cameroon

ARTICLE INFO

Article history:
Received 20 May 2015
Received in revised form 10 August 2015
Accepted 25 August 2015
Available online 1 September 2015
Communicated by A.P. Fordy

Keywords:
Discrete modulational instability
Saturable nonlinearity
Discrete solitons
Multihump solitons
Soliton collisions
Next-nearest-neighbor interactions

ABSTRACT

The influence of next-nearest-neighbor interactions (next-NNI) of dipole–dipole type is analyzed in Davydov model with saturable nonlinearities. We analytically study the regions of discrete modulational instability (MI) of plane carrier waves and it appears that this region decreases as the number of nearest neighbors, m, increases. We also show via the instability growth rate (gain) that when m increases, bandwidth of instability decreases. Otherwise, it is noted that the saturation also has an antagonistic effect on the gain. Numerical simulations indicate that the presence of next-NNI induced downward corrections of the time of onset of MI. After having sought Discrete Soliton (DS) and Discrete Multihump soliton (DMHS) numerically with $m = 1; 2; 3$, the next-nearest neighbor dependence of the width and height of these solutions is discussed. A study of mobility is achieved and it results that next-NNI increase the speed of DMHS. Furthermore, the collisions of two DMHS are performed and it emerges mainly that next-NNI lead to the formation of large stationary solitons.

1. Introduction

One of the most important problems most studied in the field of biomolecular processes is the storage and transport of biological energy in α-helical proteins. Davydov, through a soliton mechanisms [1], was the first to offer an answer. Thus, according to him, the formation of soliton results from the balance between the effects of dispersion caused by the resonance interaction of adjacent peptide groups and the interaction of the amide-I excitation with the lattice vibrations (self-localization or self-trapping mechanism). Since then, this model has been refined from now taking into account the effect of temperature [2–7], the geometry [8] of the protein, higher order excitations or coupling interactions [9,10], the interaction of a charge with intrinsic localized mode [11] and long range interactions [12]. Indeed, in most studies, the dispersive interactions are assumed to be short ranged leading to the nearest neighbor approximation. It turns out that this approximation does not always reflect the physical or biological reality. Thus in an environment where transition dipole–dipole interaction exists with $1/r^3$ dependence on the distance, r, the nearest neighbor approximation no longer holds. It is in this framework that the investigations on the excitation transfer in molecular crystals [13] and energy and charge transport in biological molecules [14,15] were conducted. The influence of long-range interactions (LRI) has been observed in various fields of physics [16–20] through the study of soliton solutions. In effect, the fundamental question that motivates studies on LRI remains how it can affect the stability and dynamics of soliton solutions?

In the last few years, Aguero et al. [21], in the continuum limit, have shown that collective excitations in a molecular chain like proteins were modeled by the saturable NLS (SNLS) equation. In order to determine the distribution of these excitations, this equation has been simplified leading to the Cubic-Quintic Nonlinear Schrödinger Equation (CQNSE). Following Aguero's idea, Tchinang et al. [22] have recently established that the localization and vibrational energy in α-helical protein molecules could be modeled by Discrete Nonlinear Schrödinger (DNLS) equation with saturable nonlinearities. In addition, they have studied in detail the existence, stability and dynamics of DS and DMHS of this equation within the framework of NNI. To the best of our knowledge, the interest of LRI has not registered in biological macromolecule systems by means of DMHS. The aim of the present work is to study the influence of next-NNI on DMHS solutions of a DNLS equation with saturable nonlinearities.

The organization of the paper is as follows. In Section 2, we describe our model. Section 3 is devoted to analyze the effects

* Corresponding author.
E-mail addresses: jtchinang@gmail.com (J.D. Tchinang Tchameu), ctchawa@yahoo.fr (C. Tchawoua), abtogueu@yahoo.fr (A.B. Togueu Motcheyo).

http://dx.doi.org/10.1016/j.physleta.2015.08.036
0375-9601/

of next-NNI on the discrete modulational instability of nonlinear plane waves. The effects of next-NNI on stationary localized solutions (DS and DMHS) are proved in Section 4. In Section 5, we talk about the mobility of DMHS and collision between two DMHS when next-NNI are taken into account. In the final Section 6 we summarize our main results.

2. The model

Let us consider the following Discrete Nonlinear Schrödinger equation with higher order saturable nonlinearity [22],

$$i\frac{\partial\phi_n}{\partial t} = -\Delta_2\phi_n + \eta_1\frac{\phi_n}{1+|\phi_n|^2} - \eta_2\frac{|\phi_n|^2\phi_n}{(1+|\phi_n|^2)^2}, \tag{1}$$

which describes the dynamics of the state of amide-I excitations in hydrogen-bonded protein chain. In Eq. (1), ϕ_n is the excitation wave function at site n, $\Delta_2\phi_n = (\phi_{n+1} + \phi_{n-1} - 2\phi_n)$, η_1 and η_2 are the strengths of the nonlinearities. Eq. (1) has been established within the framework of nearest neighbor interaction. Hydrogen bonding in proteins can be described as an electrostatic dipole–dipole interaction [23]. Taking into account the long-range interaction due to dipole–dipole interaction [24], it can be written as:

$$i\frac{\partial\phi_n}{\partial t} = -\sum_{m(m\neq 0)} S_m(\phi_{n+m} + \phi_{n-m} - 2\phi_n) + \eta_1\frac{\phi_n}{1+|\phi_n|^2} - \eta_2\frac{|\phi_n|^2\phi_n}{(1+|\phi_n|^2)^2}, \tag{2}$$

where $S_m = |\,m\,|^{-3}$ and S_m represents the order of coupling between the polypeptides of the sites n and $n \pm m$. Thus, when $S_m = 0$ for $|m| > 1$, Eq. (2) is reduced to Eq. (1) where only the nearest neighbor interactions are handled.

Eq. (2) has two conserved quantities: the Hamiltonian,

$$H = \sum_{m,n(m\neq 0)} S_m|\phi_{n+m} - \phi_n|^2 + \sum_n(\eta_1 - \eta_2)\log(1+|\phi_n|^2) - \sum_n\frac{\eta_2}{1+|\phi_n|^2}, \tag{3}$$

and the number of quanta,

$$P = \sum_n |\,\phi_n\,|^2\,. \tag{4}$$

We recall that Eq. (1) exhibits a competition between local compression and local dilatation of lattice which leads to the interplay between self-focusing and defocusing saturable nonlinearities [22]. Presumably the combination of these properties with next-NNI will have implications on the modulational instability of a nonlinear plane waves.

3. Discrete modulational instability

We propose here to discuss the discrete MI of DNLS equation with saturable nonlinearities. We note that a similar study was conducted in one-dimensional waveguide arrays possessing a saturable self-defocusing nonlinearity and taking into account only NNI [25].

Let us begin this study by looking for solutions of Eq. (2) in the form of discrete plane wave

$$\phi_n = \zeta\exp[i(qn - \omega t)], \tag{5}$$

where ζ is the constant amplitude, q is the wave number, and ω is the frequency. The nonlinear dispersion relation satisfied by this frequency is given by

$$\omega = 4\sum_m S_m\sin^2(\frac{qm}{2}) + \frac{\eta_1}{1+\zeta^2} - \frac{\eta_2\zeta^2}{(1+\zeta^2)^2}. \tag{6}$$

The linear stability of Eq. (5) can be investigated by studying the stability of its amplitude as a function of sufficiently small perturbation so that, one can linearize the equation of the envelope of the carrier wave. Therefore, one introduces a small perturbation, $\delta\phi_n$, in Eq. (5) and checks the solution of Eq. (2) in the form

$$\phi_n = (\zeta + \delta\phi_n)\exp[i(qn - \omega t)]. \tag{7}$$

The insertion of Eq. (7) in Eq. (2), with a linearization around the unperturbed plane wave gives us the following equation

$$i\frac{\partial(\delta\phi_n)}{\partial t} = -\sum_m S_m\left[\delta\phi_{n+m}\exp(iqm) + \delta\phi_{n-m}\exp(-iqm)\right] + 2\sum_m S_m\cos(qm)\delta\phi_n - \Upsilon(\eta_1,\eta_2,\zeta)(\delta\phi_n + \overline{\delta\phi_n}), \tag{8}$$

where the overbar, $^-$, denotes complex conjugate and Υ is defined by

$$\Upsilon(\eta_1,\eta_2,\zeta) = \frac{\eta_1\zeta^2}{(1+\zeta^2)^2} - \frac{\eta_2\zeta^2(\zeta^2-1)}{(1+\zeta^2)^3}. \tag{9}$$

Furthermore, considering the solution of Eq. (8) with the wave number Q and frequency Ω in the form

$$\delta\phi_n = A_1\exp[i(Qn - \Omega t)] + \overline{A_2}\exp[-i(Qn - \overline{\Omega}t)], \tag{10}$$

where $A_{1,2}$ are constants, we obtain

$$\left[\Omega - 2\sum_m S_m\sin(qm)\sin(Qm)\right]^2 = 4\left[\sum_m S_m\cos(qm)\sin^2\left(\frac{Qm}{2}\right)\right] \times\left[4\sum_m S_m\cos(qm)\sin^2\left(\frac{Qm}{2}\right) - 2\Upsilon(\eta_1,\eta_2,\zeta)\right], \tag{11}$$

which represents the dispersion relation. The perturbation (Eq. (10)) will be unstable if the righ-hand side of Eq. (11) is negative. Note that the saturable medium occurs here through the function Υ while the contribution of next-NNI is made through S_m. Moreover, when $\zeta \ll 1$ and $m = 1$, we find the results obtained in [26] for the discrete cubic-quintic nonlinear Schrödinger equation where the coefficients of cubic and quintic terms are $\lambda = (\eta_1 + \eta_2)$ and $\gamma = -(\eta_1 + 2\eta_2)$, respectively. In the following, we will use the dimensionless variable $\widetilde{\eta}$ knowing that $\eta = 93\widetilde{\eta}$ (see [22]).

Fig. 1(a) shows the region (dark) of modulational instability in plane (q, Q) in the case of nearest neighbor interaction ($m = 1$). When taking into account successively the second, third, fourth, tenth and twentieth neighbors, we see gradually as m increases the narrowing of the area where MI occurs (Fig. 1(b), (c), (d), (e), (f)). This area hardly varies for $m > 3$. For low values of the wave number of carrier wave q the MI region is cropped gradually as m increases. An analogous observation was noted in [20] where the authors used the Discrete Cubic Schrödinger equation. However, for the large value of q, there is no instability zone here. This result contrasts with the one obtained in [20] for the case $m = 2$.

By using the growth rate of MI defined by $G(Q) = Im(\Omega)$, it appears through Fig. 2(a) that the inclusion of next-NNI increases the stability zone, since the maximum value of the gain remains constant when m ranges. Besides, Fig. 2(b) reveals that the gain decreases when the saturable higher order nonlinearity increases, $\widetilde{\eta}_1$ being fixed and $\zeta = 6.05$. It follows that the higher order saturable nonlinearity can suppress the instability. This can explain the absence of MI zone for large values of q in Fig. 1 and their presence in [20] for the case $m = 2$.

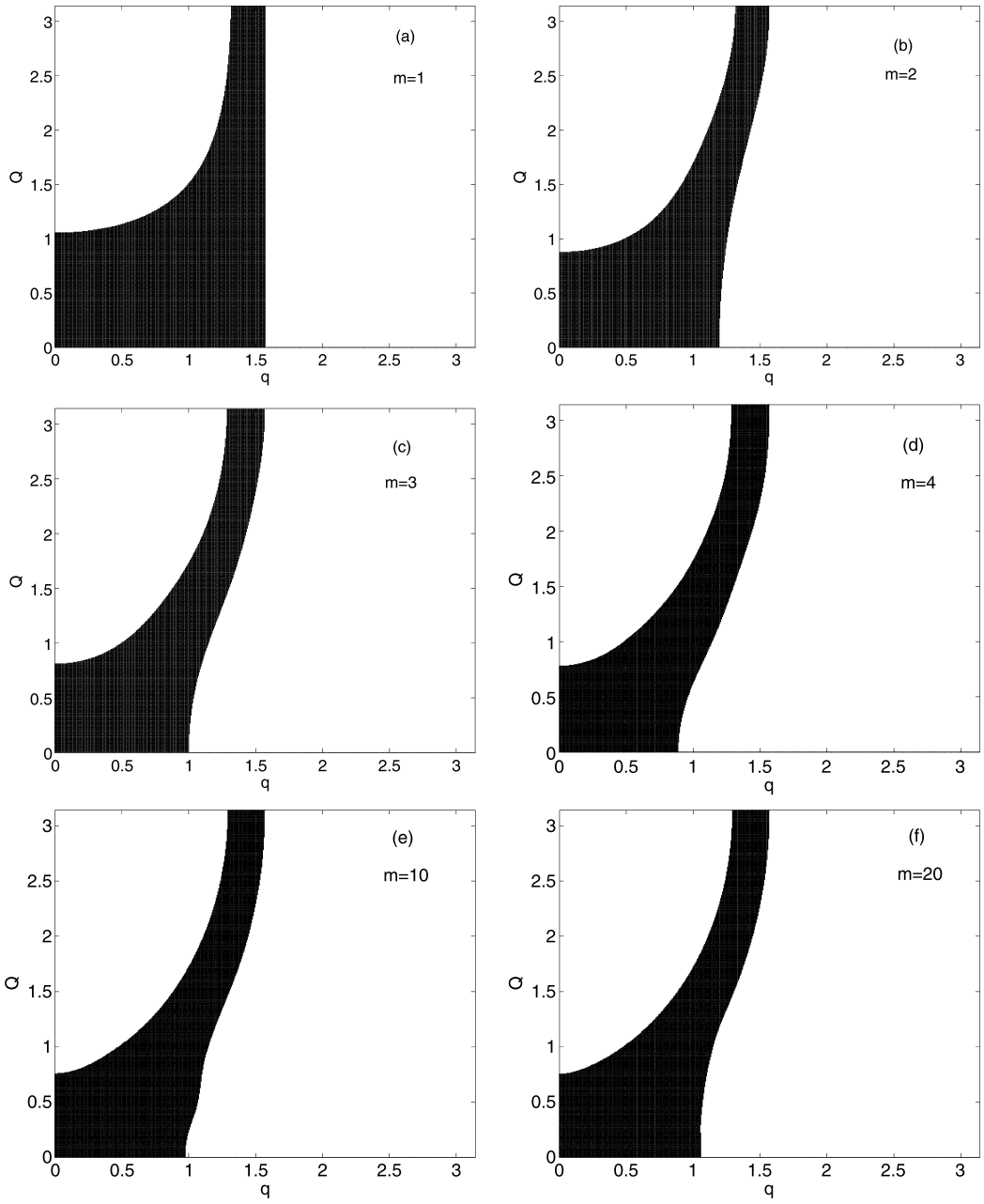

Fig. 1. Modulational instability region (dark) in the q–Q plane versus next-nearest neighbor interaction parameter m: $\widetilde{\eta}_1 = \widetilde{\eta}_2 = 1.1$ and $\zeta = 0.05$.

For a given value of Q, the dependence of the gain on the unperturbed plane wave solution is almost identical regarding the discrete cubic-quintic nonlinear Schrödinger equation (CQNS), the discrete Vinetskii–Kukhtarev (VK) equation and our model (Fig. 3). In fact, this is true for small values of ζ and is due to the fact that nonlinearities in the three previous mentioned models are reduced to cubic-quintic terms when the Taylor expansion is applied in the first approximation. We also note that our saturation compared to that of VK increases the maximum gain and reduces the bandwidth of amplitudes which can lead to MI. This trend is maintained when m varies. Nevertheless for a given value of Q, where m increases, the maximum value of the gain increases in our model.

It is well known that MI of plane waves predicts the formation of localized excitations. With the aim to verify that numerically, we integrate Eq. (2) by fourth-order Runge–Kutta method with periodic boundary conditions and taking 10^{-10} as absolute tolerance. The time step is selected so that it can ensure the conservation of P and H. The use of the following initial condition

$$\phi_n(t=0) = (\zeta + A\cos(Q\,n))\cos(qn) \tag{12}$$

allows us to obtain the two panels of Fig. 4 where $Q = q = 0.0419$. We note that the inclusion of second nearest neighbors and third nearest neighbors leads to early onset of MI for both values of the amplitude ζ ($\zeta = 0.05$ and $\zeta = 6.05$). In other words, neglecting the presence of next-NNI means overestimate the time of onset of MI.

Since the MI is the first step towards energy localization [27], let us move to the study of the effect of next-NNI on stationary localized solutions.

4. Stationary localized solutions

We focus here on unstaggered modes having their maxima in one (multiple) peptide group(s) of the alpha-helical protein chain.

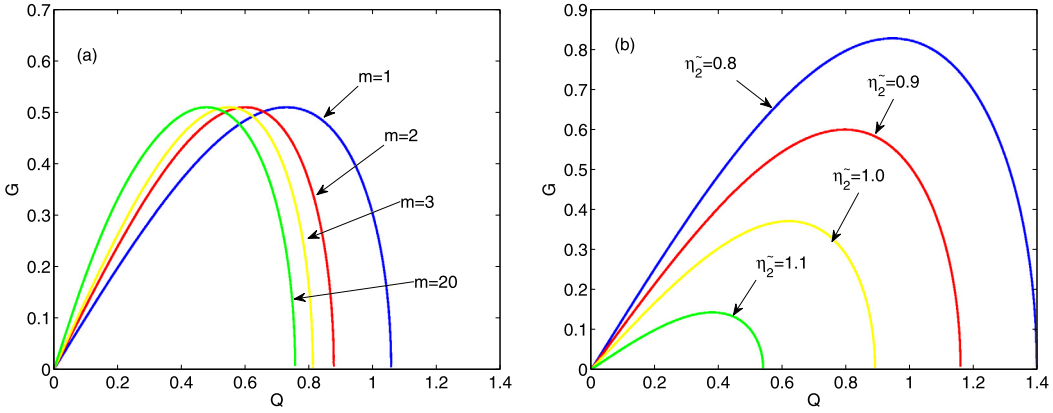

Fig. 2. Growth rate versus the wave number of perturbation for different (a) number of next-nearest neighbors [$\zeta = 0.05$, $\widetilde{\eta}_1 = \widetilde{\eta}_2 = 1.1$] and (b) saturable higher order nonlinearity parameters [$\zeta = 6.05$, $\widetilde{\eta}_1 = 1.1$, $m = 1$].

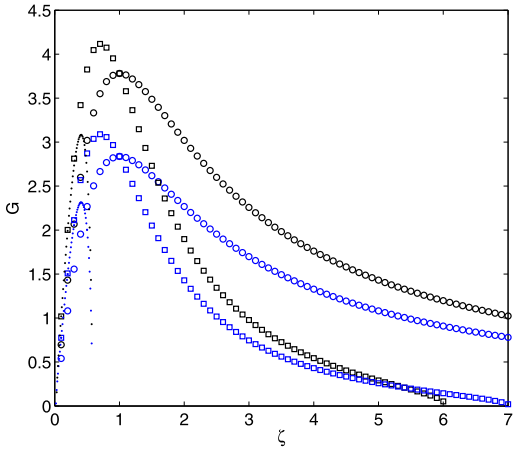

Fig. 3. Dependence of gain with ζ for discrete cubic-quintic nonlinear Schrödinger equation [(dots), $\widetilde{\eta}_1 = \widetilde{\eta}_2 = 1.1$], discrete Vinetskii–Kukhtarev equation [(circles), $\widetilde{\eta}_1 = 1.1, \widetilde{\eta}_2 = 0$] and Eq. (2) [(squares), $\widetilde{\eta}_1 = \widetilde{\eta}_2 = 1.1$]. Q being 0.4. Blue markers correspond to $m = 1$ while black markers correspond to $m = 3$. (For interpretation of the references to color in this figure legend, the reader is referred to the web version of this article.)

For this purpose, we use the steady-state ansatz $\phi_n = u_n \exp(-i\mu t)$ where μ is the frequency and u_n is the stationary amplitude and insert it in Eq. (2) to obtain

$$\mu u_n + \sum_{m(m\neq 0)} S_m(u_{n+m} + u_{n-m} - 2u_n) - \eta \frac{u_n}{1+|u_n|^2} + \eta \frac{|u_n|^2 u_n}{(1+|u_n|^2)^2} = 0, \tag{13}$$

where we set $\eta = \eta_1 = \eta_2$. Solutions of Eq. (13) must verify the normalization condition [22]

$$\sum_n u_n^2 \simeq \frac{0.043}{\widetilde{\eta}}, \tag{14}$$

where $\widetilde{\eta}$ is the above mentioned dimensionless parameter. By using Newton–Raphson (NR) method with periodic boundary conditions to find solutions of Eq. (13) under the constraint of Eq. (14), it follows Figs. 5, 6, 7. The results described in these figures were obtained on a chain composed of 101 sites for single-hump and two-hump solitons, and 301 sites for three-hump soliton. It appears that the inclusion of second and third nearest neighbors makes corrections on DS and DMHS. More precisely, when m increases, the width and height of DS and DMHS increase. For the case of DS, Saha et al. [28] has obtained similar observations on the protein-DNA dynamics in the long-wave limit. However, for a given solution, the corrections decrease as m increases (see Figs. 5(b), 6(b), 7(b) which are figures obtained by a zoom in Figs. 5(a), 6(a), 7(a), respectively). Moreover, when the number of peaks of solutions increases, the corrections of height to these solutions due to the inclusion of next-NNI decrease (see Figs. 5(a), 6(a), 7(a)). We recall that the next-NNI of dipole–dipole type is very important in the modeling of a realistic protein chain. Indeed, in proteins, several levels of dipoles can exist: the peptide bond is one of them. Therefore, the parallel assembly of several dipoles in an alpha helix leads to a dipole moment significantly greater [23,29]. It appears within this framework that, according to the results seen above, energy localization in proteins can be mediated by DMHS.

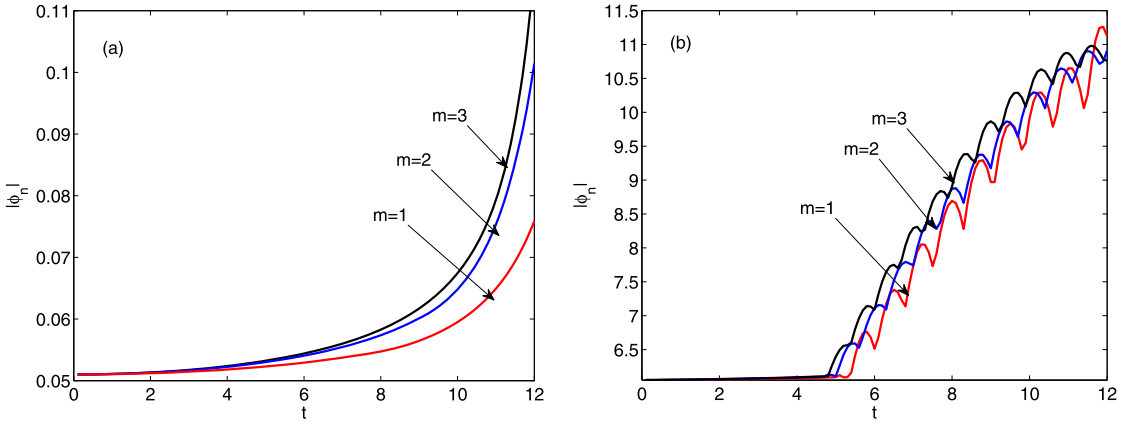

Fig. 4. Simulated evolution of plane wave with small perturbation (Eq. (12)) for (a) $\zeta = 0.05$ and (b) $\zeta = 6.05$. In both cases, $\widetilde{\eta}_1 = \widetilde{\eta}_2 = 1.1$.

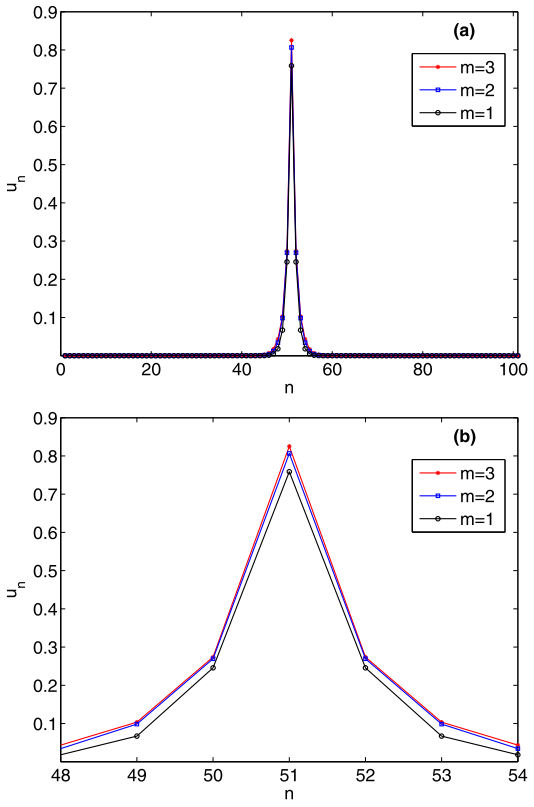

Fig. 5. Dependence of single-hump soliton with next-NNI parameter m. $\widetilde{\eta} = 0.06$, $\mu = 3.6$.

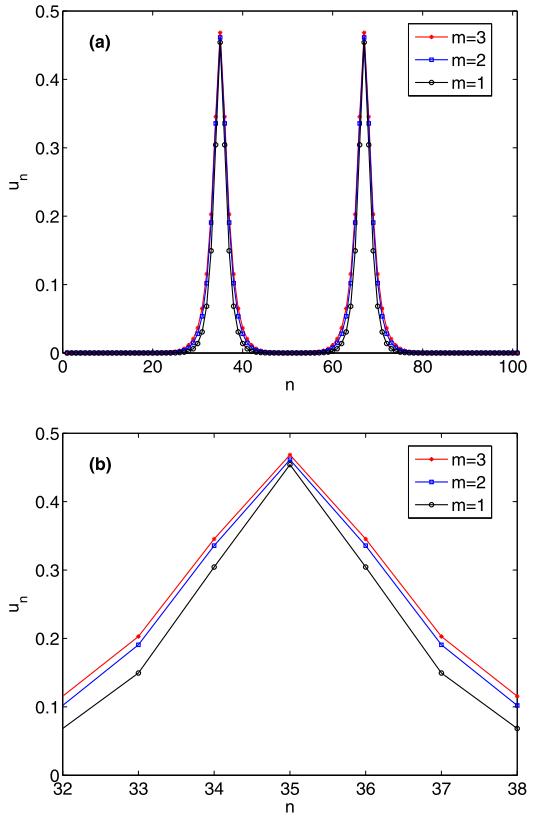

Fig. 6. Dependence of two-hump soliton with next-NNI parameter m. $\widetilde{\eta} = 0.0464$, $\mu = 3.6$.

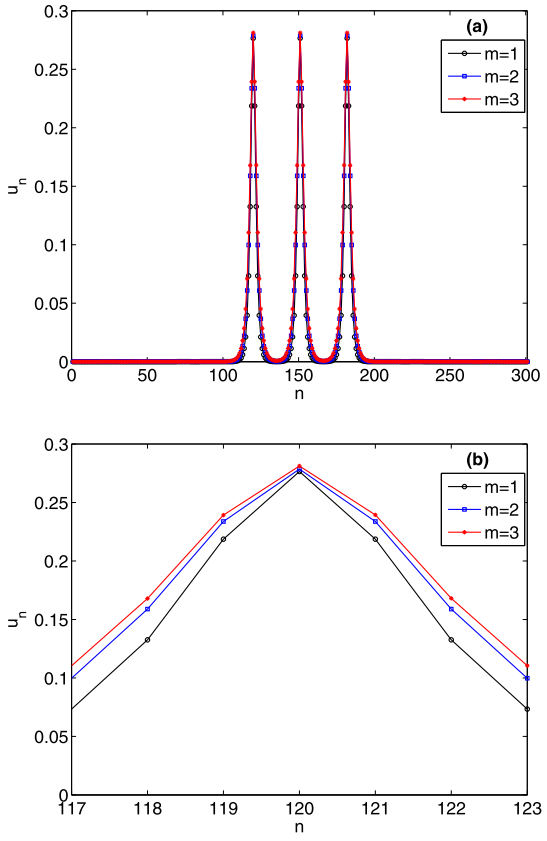

Fig. 7. Dependence of three-hump soliton with next-NNI parameter m. $\widetilde{\eta} = 0.065$, $\mu = 5.63$.

5. Mobility and collisional interactions

We study here numerically the DMHS mobility and the collision between two DMHS taking into account the next-NNI. For performing this, we use as initial condition

$$\phi_{n,\pm}(0) = u_{n,\pm} \exp(\pm i\varpi n) \tag{15}$$

where the subscripts $\pm$ stand for the DMHS coming into collision, u_n is a stationary solution and ϖ represents the relative strength. The numerical simulations presented in this framework use $N = 301$ sites for the mobility and $N = 602$ sites for the collision, a collision center being at $N_0 = 301$.

Following the observations made in previous works [22] where it seems that the mobility is achieved for three-hump and four-hump solitons in short ranged limit, we apply the kick on these modes but this time around we consider the next-NNI. From Fig. 8(a), three-hump soliton ($\mu = 5.635$; $\widetilde{\eta} = 0.065$) has traveled 367 peptide groups for $m = 1$. When m is increased to two (Fig. 8(b)), the number of peptide groups traveled raised to 511. The number of peptide groups is 540 when $m = 3$ (Fig. 8(c)). Regarding four-hump soliton ($\mu = 4.9$ and $\widetilde{\eta} = 0.056$), the number of peptide groups traveled by this wave is 506, 700, 732 for $m = 1$ (Fig. 8(d)), $m = 2$ (Fig. 8(f)) and $m = 3$ (Fig. 8(f)), respectively. The interpretation we draw from this observations is that the inclusion of next-NNI increases the speed of the DMHS and therefore the speed of energy transport along the protein chain. Furthermore, for given m, four-hump soliton is faster than three-hump soliton.

As regards the collision, note that the major part of the studies on collisions of solitons in saturable media was performed in optics. Generally, they are done in multi-component nonlinear systems [30]. Moreover, the study of the collisions of Davydov solitons was carried out [31] in two-component nonlinear systems. We fo-

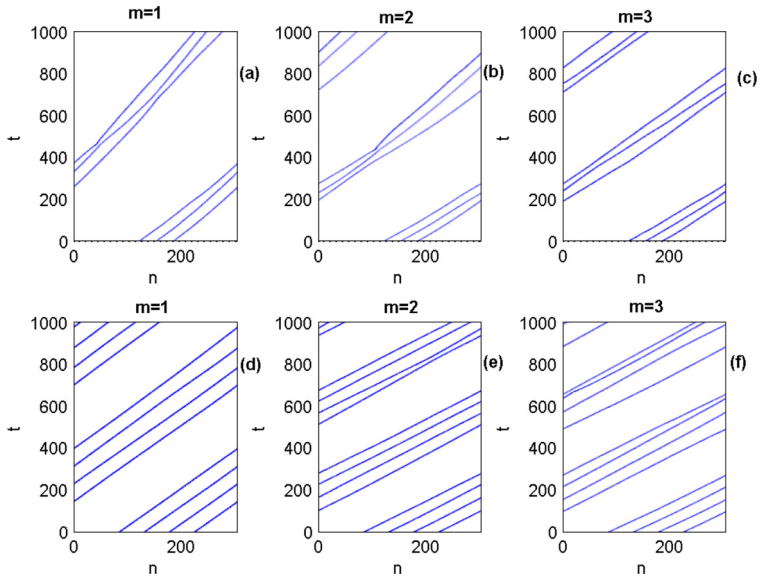

Fig. 8. Density plot $|\phi_n|^2$ for kicked three-hump soliton ((a), (b) and (c)) and four-hump solitons ((d), (e) and (f)) for $\varpi = 0.3$. We have $\mu = 5.635$ and $\widetilde{\eta} = 0.065$ for three-hump soliton while $\mu = 4.9$ and $\widetilde{\eta} = 0.056$ for four-hump soliton.

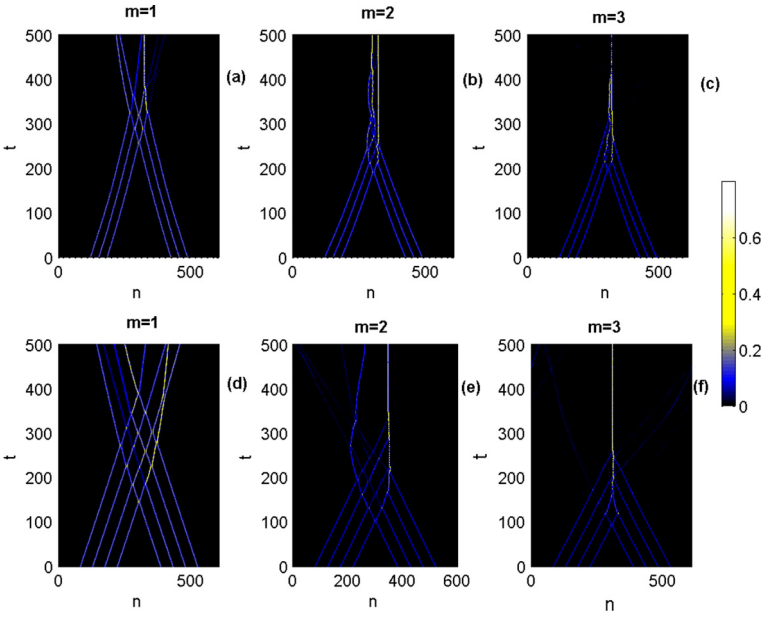

Fig. 9. Head-on collision of two three-hump solitons ((a), (b) and (c)) and two four-hump solitons ((d), (e) and (f)) for $\varpi = 0.3$. We have $\mu = 5.635$ and $\widetilde{\eta} = 0.065$ for three-hump soliton while $\mu = 4.9$ and $\widetilde{\eta} = 0.056$ for four-hump soliton.

cus here, for some examples, on interactions between multihump solitons that propagate in opposite directions with the same kick.

The simulations reveal through Fig. 9(a) the collision between two three-hump solitons. From this collision arises mainly a stationary solution. It was also observed an internal reflection during this collision. This reflection leads a small fraction of energy to continue his career. When we increase the number of nearest neighbors m, this contributes to the formation of a large stationary solution after the collision (Fig. 9(b) and (c)). For the collision of two four-hump solitons, we observe in short ranged limit (Fig. 9(d)), a set of reflection. The inclusion of the second and third nearest neighbors (Fig. 9(e) and (f)) leads to the major reduction of reflections and formation of large stationary solutions. The salient feature that emerges here when considering next-NNI is that the collision between two DMHS leads mainly to the formation of a large stationary soliton.

6. Conclusion

In conclusion, we have studied in detail the discrete modulational instability of DNLS equation with higher order saturable nonlinearities. This equation has been studied in the framework of power dependence r^{-3} on the distance, r, of the dispersive interactions. It appears that the regions of MI of nonlinear plane waves shrink with increasing the number of nearest neighbor m. Furthermore, through the instability growth rate (gain), we note that when m increases, bandwidth of instability decreases. It has also been shown analytically that the higher order saturable nonlinearity can suppress the instability. Besides, the saturation of our model compared to that of Vinetskii–Kukhtarev increases the maximum gain and reduces the bandwidth of amplitudes which can lead to MI. This observation is unchanged when m varies. Using numerical simulations, it appears that the inclusion of second and

third nearest neighbors leads to early onset of MI and this, whatever the value of the amplitude of the nonlinear plane waves. The numerical determination of Discrete Soliton (DS) and Discrete Multihump soliton (DMHS) was accompanied by some remarks: when m increases, the width and height of DS and DMHS increase. However, for a given solution, the corrections decrease as m increases. Moreover, when the number of peaks of solutions increases, the corrections of height to these solutions due to the inclusion of next-NNI decrease. The mobility of DMHS is achieved and we note that the next-NNI increase the speed of energy transfer along the protein molecules mediated by DMHS. Finally, after having carried out a collision between two DMHS, the main feature stands out is that next-NNI contribute significantly to the formation of large stationary solitons.

References

[1] A.S. Davydov, The theory of contraction of proteins under their excitation, J. Theor. Biol. 38 (1973) 559.
[2] W. Forner, Davydov soliton dynamics: temperature effects, J. Phys. Condens. Matter 3 (1991) 4333.
[3] A.V. Savin, A.V. Zolotaryuk, Dynamics of the amide-I excitation in a molecular chain with thermalized acoustic and optical modes, Physica D 68 (1993) 59.
[4] W. Forner, Effects of temperature and interchain coupling on Davydov solitons, Physica D 68 (1993) 68.
[5] L. Cruzeiro-Hansson, V.M. Kenkre, Comparison of quantum Monte Carlo and semiclassical Monte Carlo results in investigations of the thermal stability of Davydov solitons, Phys. Lett. A 203 (1995) 362.
[6] Yi Xiao, One more reason why the Davydov soliton may be thermally stable, Phys. Lett. A 243 (1998) 174.
[7] J. Herrera, M.A. Maza, A.A. Minzoni, N.F. Smyth, A.L. Worthy, Davydov soliton evolution in temperature gradients driven by hyperbolic waves, Physica D 191 (2004) 156.
[8] A.V. Zolotaryuk, P.L. Christiansen, B. Norden, A.V. Savin, Soliton and ratchet motions in helices, Condens. Matter Phys. 2 (1999) 293.
[9] A.V. Zolotariuk, Solitons in molecular chains with intramolecular nonlinear interactions, Physica D 46 (1990) 295.
[10] M. Daniel, M.M. Latha, Soliton in alpha helical proteins with interspine coupling at higher order, Phys. Lett. A 302 (2002) 94.
[11] O.G. Cantu Ros, L. Cruzeiro, M.G. Velarde, W. Ebeling, Eur. Phys. J. B 80 (2011) 545.
[12] L. Cruzeiro-Hansson, Effect of long range and anharmonicity in the minimum energy states of the Davydov–Scott model, Phys. Lett. A 249 (1998) 465.
[13] A.S. Davydov, Theory of Molecular Excitons, Plenum Press, New York, 1971.
[14] S.F. Mingaleev, P.L. Christiansen, Y.B. Gaididei, M. Johansson, K.Ø. Rasmussen, J. Biol. Phys. 25 (1999) 41.
[15] A. Scott, Davydov's soliton, Phys. Rep. 217 (1992) 3.
[16] A. Neuper, Y. Gaididei, N. Flytzanis, F. Mertens, Solitons in atomic chains with long-range interactions, Phys. Lett. A 190 (1994) 165.
[17] P. Woafo, T.C. Kofane, A.S. Bokosah, Kink static properties in a discrete Φ^4 chain with long-range interactions, Phys. Rev. B 48 (1993) 10153.
[18] C. Tatuam Kamga, T.C. Kofane, Gap solitons in anharmonic one-dimensional asymmetrical physical systems with Kac–Baker long-range interactions, Phys. Rev. E 50 (1994) 2257.
[19] C. Tchawoua, T.C. Kofane, A.S. Bokosah, Dynamics of solitary waves in diatomic chains with long-range Kac–Baker interactions, J. Phys. A, Math. Gen. 26 (1993) 6477.
[20] D. Hennig, Next-nearest neighbor interaction and localized solutions of polymer chains, Eur. Phys. J. B 20 (2001) 419.
[21] M. Aguero, R. García-Salcedo, J. Socorro, E. Villagran, Soliton structures in a molecular chain model with saturation, Int. J. Theor. Phys. 48 (2009) 670.
[22] J.D. Tchinang Tchameu, A.B. Togueu Motcheyo, C. Tchawoua, Mobility of discrete multibreather in the exciton dynamics of the Davydov model with saturable nonlinearities, Phys. Rev. E 90 (2014) 43203.
[23] S.K. Burley, G.A. Petsko, Weakly polar interactions in proteins, Adv. Protein Chem. 39 (1988) 125.
[24] K.Ø. Rasmussen, P.L. Christiansen, M. Johansson, Yu.B. Gaididei, S.F. Mingaleev, Localized excitations in discrete nonlinear Schrodinger systems: effects of nonlocal dispersive interactions and noise, Physica D 113 (1998) 134.
[25] Milutin Stepić, Christian E. Rüter, Detlef Kip, Aleksandra Maluckov, Ljupčo Hadžievski, Modulational instability in one-dimensional saturable waveguide arrays: comparison with Kerr nonlinearity, Opt. Commun. 267 (2006) 229.
[26] F.Kh. Abdullaev, A. Bouketirb, A. Messikhc, B.A. Umarova, Modulational instability and discrete breathers in the discrete cubic-quintic nonlinear Schrödinger equation, Physica D 232 (2007) 54.
[27] I. Daumont, T. Dauxois, M. Peyrard, Modulational instability: first step towards energy localization in nonlinear lattices, Nonlinearity 10 (1997) 617.
[28] M. Saha, T.C. Kofane, Nonlinear dynamics of long-ranged protein-helicoidal DNA interactions, Int. J. Mod. Phys. B 26 (2012) 1250101.
[29] M. Laberge, Intrinsic protein electric fields: basic non-covalent interactions and relationship to protein-induced Stark effects, Biochim. Biophys. Acta 1386 (1998) 305.
[30] A. Maluckov, Lj. Hadžievski, B.A. Malomed, Staggered and moving localized modes in dynamical lattices with the cubic-quintic nonlinearity, Phys. Rev. E 77 (2008) 036604.
[31] B. Tan, J.P. Boyd, Davydov soliton collisions, Phys. Lett. A 240 (1998) 282.

Wave Motion 65 (2016) 112–118

Contents lists available at ScienceDirect

Wave Motion

journal homepage: www.elsevier.com/locate/wavemoti

Nonlinear supratransmission of multibreathers in discrete nonlinear Schrödinger equation with saturable nonlinearities

J.D. Tchinang Tchameu, C. Tchawoua *, A.B. Togueu Motcheyo

Laboratory of Mechanics, Department of Physics, Faculty of Science, University of Yaounde I, P.O. Box 812, Yaounde, Cameroon

HIGHLIGHTS

- Numerical and semi-analytical supratransmission threshold of DNSE with higher order nonlinearity have been performed.
- The saturable higher order nonlinearity parameter reduces the threshold amplitude of supratransmission.
- Multibreathers can be transmitted or supratransmitted.

ARTICLE INFO

Article history:
Received 26 January 2016
Received in revised form 4 April 2016
Accepted 5 April 2016
Available online 27 April 2016

Keywords:
Supratransmission
Saturable nonlinearity
Discrete multibreathers

ABSTRACT

We show that the transport of vibrational energy in protein chains modeled by the Discrete Nonlinear Schrödinger equation (DNSE) with saturable nonlinearities can be done through the nonlinear supratransmission phenomenon: we find numerically and semi-analytically threshold amplitudes beyond which the wave propagation takes place within the molecular chains. Subsequently, it is shown that the saturable higher order nonlinearity parameter reduces the supratransmission threshold amplitude. We also prove that the discrete gap multibreathers can be transmitted or supratransmitted according to the frequency belonging to the lower forbidden band gap. More precisely, the discrete gap multibreathers are supratransmitted close to the edge of the lower forbidden band.

1. Introduction

The discrete nonlinear Schrödinger equation (DNSE) in its many versions plays a key role in different fields of science, such as biology [1], nonlinear optics [2], solid-state physics [3], and Bose–Einstein condensates [4]. The version of DNSE with saturable nonlinearity represents a vast class of physical systems, ranging from optical pulse propagation in various doped fibers [5,6], to waveguide arrays in photorefractive strontium barium niobate crystals [7]. Since 1975 where Vinetskii–Kukhtarev model [8] has been introduced, it is recently that a great deal of interest has been drawn to Saturable DNSE [9]. The existence and properties of discrete Solitons (which are also known as intrinsic localized modes) have been considered in preceding studies [9]. Moreover, as an effect of nonlinear modes, gap Solitons in a periodic structure have modeled the wave propagation in the forbidden band of the linear spectrum [10,11]. This phenomenon has been called nonlinear supratransmission and widely used in many models such as coupled pendulum chain [12], discrete nonlinear electrical transmission lattice [13], birefringent quadratic medium [14], waveguide arrays [15,16], Frenkel–Kontorova model [17], granular chains [18] and nanostructured multiferroics [19]. From the perspective of nonlinear supratransmission, this phenomenon has technological applications like terahertz frequency selection devices [20] and binary signal transmissions of information [21]. All the above mentioned works study the gap transmission of single hump breathers. Up to now, no

* Corresponding author.
E-mail addresses: jtchinang@gmail.com (J.D. Tchinang Tchameu), ctchawa@yahoo.fr (C. Tchawoua), abtogueu@yahoo.fr (A.B. Togueu Motcheyo).

http://dx.doi.org/10.1016/j.wavemoti.2016.04.002
0165-2125/

work concerning the study of supratransmission phenomenon using multibreathers has been presented in literature in our knowledge. Study the possibility of supratransmission of the multibreathers is the first purpose of this work.

In more recent years, following Davydov's idea about energy transfer along protein molecules, Tchinang et al. [22,23] showed that the state of amide-I excitations in proteins is modeled by the DNSE with saturable nonlinearities. This was done by taking into account the competition between local compression and local dilatation of the lattice, leading to the interplay between self-focusing and defocusing saturable nonlinearities. Supratransmitted multibreather could presumably bring better understanding of energy transport in the proteins within this model. Accordingly, study the influence of saturable higher order nonlinearity on the threshold amplitude of supratransmission is the second purpose of this work. The presentation is structured as follows. In Section 2, the dynamical model is introduced. We perform numerical integrations to illustrate supratransmission in Section 3 and we examine also the effect of saturable higher order nonlinearity on the threshold amplitude by means of different values of the strength of the nonlinearity. Finally, the results and conclusions are placed in Section 4.

2. The model

Let us consider a one-dimensional ring of peptide groups (H–N–C=O) regularly positioned and coupled by hydrogen bonds. In dimensionless variables (ϕ_n), the state of amide-I excitations associated with this network is described by the DNSE with higher order saturable nonlinearity [22] given by

$$i\frac{\partial \phi_n}{\partial t} = -(\phi_{n+1} + \phi_{n-1} - 2\phi_n) + \eta_1 \frac{\phi_n}{1+|\phi_n|^2} - \eta_2 \frac{|\phi_n|^2 \phi_n}{(1+|\phi_n|^2)^2}, \tag{1}$$

for $n = 0, \ldots, N-1$, where N is the number of peptide groups. The real parameters η_1 and η_2 account for the nonlinearities and t corresponds to temporal coordinate.

There are two integrals of motion in Eq. (1). The first is the Hamiltonian

$$H = \sum_n \left[|\phi_{n+1} - \phi_n|^2 + (\eta_1 - \eta_2)\log(1+|\phi_n|^2) - \frac{\eta_2}{1+|\phi_n|^2} \right]. \tag{2}$$

The second constant is the number of quanta (l^2-*norm*), which is given by

$$P = \sum_n |\phi_n|^2. \tag{3}$$

The interest for Eq. (1) model arises from the fact that it exhibits a competition between local compression and local dilatation of lattice which leads to the interplay between self-focusing and defocusing saturable nonlinearities.

In order to obtain allowed linear band of Eq. (1), we approximate a solution as the discrete plane wave

$$\phi_n = \zeta \exp[i(qn - \omega t)], \tag{4}$$

with ζ, q and ω representing amplitude, wave number, and frequency, respectively. Therefore we obtain the dispersion relation

$$\omega = 4\sin^2\left(\frac{q}{2}\right) + \eta_1, \tag{5}$$

having the phonon band $[\eta_1, \eta_1 + 4]$ in the frequency. For a frequency ω in the forbidden band, the linear theory predicts that a plane wave becomes evanescent.

Moreover, in the case where $\eta_2 = 0$, Eq. (1) reduced to DNSE with saturable nonlinearity for which the existence of supratransmission has been performed by Susanto and Karjanto [15]. Could we obtain the transmission of plane wave in the forbidden band gap when $\eta_2 \neq 0$?

3. Nonlinear supratransmission

3.1. Threshold of supratransmission phenomena

To check supratransmission phenomena in our model, we will impose the launch of the wave by submitting Eq. (1) to the following conditions

$$\phi_0(t) = Ae^{-i\mu t}, \qquad \phi_n(0) = 0 \quad \text{for } n > 0 \tag{6}$$

where A is the driving amplitude and μ is a driving frequency belonging to the lower forbidden band gap. By putting $A \rightarrow A(1 - e^{(-t/50)})$ and adding a damping with intensity linearly varying from 0 to 10 on the last 10 peptide groups, we avoid the initial shock wave and edge reflection respectively [12,24].

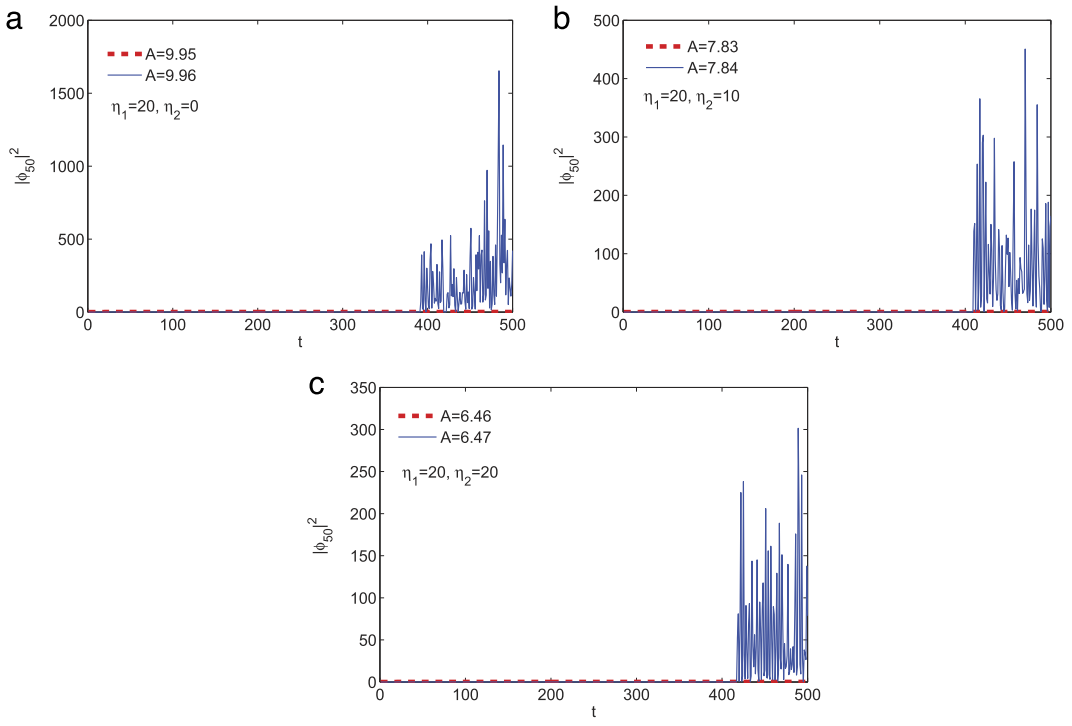

Fig. 1. Plot of $|\phi_{n=50}|^2(t)$ for $\mu = 2$ and $\eta_1 = 20$. The red dashed line corresponds to $A = 9.95$ (a), $A = 7.83$ (b), $A = 6.46$ (c) while the solid blue line corresponds to $A = 9.96$ (a), $A = 7.84$ (b) and $A = 6.47$ (c). Thus the threshold amplitudes for $\eta_2 = 0$ (a), $\eta_2 = 10$ (b), $\eta_2 = 20$ (c) are 9.96, 7.84 and 6.47, respectively. (For interpretation of the references to color in this figure legend, the reader is referred to the web version of this article.)

The numerical integration of Eq. (1), by means fourth-order Runge–Kutta method and boundary conditions seen above, yields Fig. 1. This figure bring out the norm of the fiftieth particle $|\phi_{50}|^2$ for $\mu = 2$ belonging to the lower forbidden band gap and η_1 remaining fixed at 20. Being in the gap, it appears that there is a threshold amplitude beyond which the wave propagation takes place within the molecular chain ($N = 100$). This threshold values decrease gradually as the saturable higher order nonlinearity parameters η_2 increase. Indeed we have the threshold amplitudes 9.96 (Fig. 1(a)), 7.84 (Fig. 1(b)) and 6.47 (Fig. 1(c)) for $\eta_2 = 0$, 10 and 20, respectively. Furthermore, the norm of the complex-valued amplitudes $\phi_{n=50}$ decrease as η_2 increase.

In order to obtain a systematic analysis of the threshold amplitudes versus μ, let us consider stationary solutions to Eq. (1) in the form $\phi_n = u_n e^{-i\mu t}$. We obtain subsequently a set of N coupled algebraic equation for the real-valued function u_n

$$\mu u_n + (u_{n+1} + u_{n-1} - 2u_n) - \eta_1 \frac{u_n}{1 + u_n^2} + \eta_2 \frac{u_n^3}{(1 + u_n^2)^2} = 0. \tag{7}$$

Following Ref. [16] and therefore making the approximation that the system is reduced to a few neighboring site only, Eq. (7) takes the form

$$f = [(\mu - 2)u_1 + A](1 + u_1^2)^2 - \eta_1 u_1 (1 + u_1^2) + \eta_2 u_1^3 = 0. \tag{8}$$

These considerations (Eqs. (7) and (8)) are due to the fact that it has been shown in Ref. [16] using discrete Vinetskii–Kukhtarev equation that a threshold amplitude for supratransmission corresponds to a saddle–node bifurcation in the stationary solution. This bifurcation occurs when the local minimum of the function f for u_1 becomes a root of f with respect to A.

By searching analytically the minimum of f for u_1 and numerically a root of this one for A, we get in Fig. 2 the rule of change of threshold amplitude A_s versus frequency μ in the forbidden band gap. Fig. 2 shows the threshold amplitude A_s above which supratransmission occurs.

In this figure, the solid red line, the solid blue line and solid black line correspond to $\eta_2 = 0$, 10 and 20, respectively. Note that when $\eta_2 = 0$ and η_1 being set to 20, threshold amplitude versus frequency reduces to that found in Ref. [15]. Furthermore, there emerges from Fig. 2 that the saturable higher order nonlinearity parameter η_2 lowers the threshold amplitude A_s for supratransmission. Besides this semi-analytical method, numerical simulations of Eqs. (1) and (6) confirm the above-mentioned observations. In fact, the sequence of cross signs ($\eta_2 = 0$), circle signs ($\eta_2 = 10$) and triangle signs ($\eta_2 = 20$) correspond to numerical simulations. As another observations, we find that the required critical amplitude for supratransmission tends to zero close to the band edge, whatever the value of η_2. This finding joins that made by Leon et al. in Bragg medium under nonlinear continuous wave excitation [25].

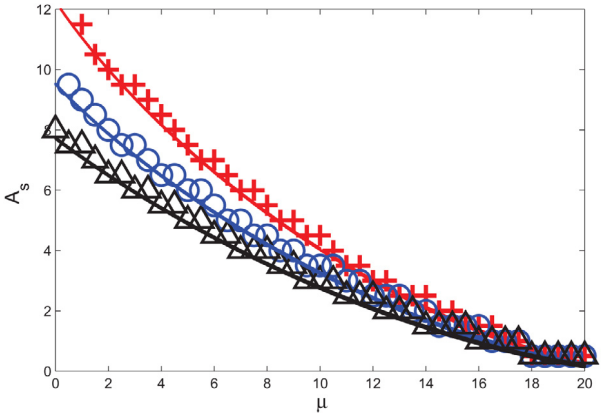

Fig. 2. Threshold amplitude A_s versus driving frequency μ for $\eta_2 = 0$ (solid red line), $\eta_2 = 10$ (solid blue line) and $\eta_2 = 20$ (solid black line). The cross markers ($\eta_2 = 0$), the circle markers ($\eta_2 = 10$) and triangle markers ($\eta_2 = 20$) are relative to numerical method while the solid lines correspond to semi-analytical method. The results of numerical simulation were obtained by computing Eqs. (1) and (6) over the time interval [0, 500] with $N = 100$ and $\eta_1 = 20$. (For interpretation of the references to color in this figure legend, the reader is referred to the web version of this article.)

Recall that above some threshold amplitude, a sequence of nonlinear modes propagating in the medium [26].

On the other hand, it has been shown that our model (Eq. (1)) admits discrete multibreathers solutions as nonlinear modes [22]. The question that emerges from these previous observations is whether among the nonlinear modes propagate in the framework of supratransmission, can discrete multibreathers be one of them?

3.2. Discrete gap multibreathers

Let us start by noticing that it has been experimentally proved that the supratransmission does occur by means of gap soliton trains in Bragg gratings [27]. Here the concern is to show that the supratransmission can occur by means of discrete gap multibreathers that are intrinsic localized modes possessing an arbitrary number of humps. To carry out this work, let us consider Eq. (7) with following constraint

$$\sum_n u_n^2 \simeq \frac{4}{\eta}, \tag{9}$$

representing the normalization condition for a single quantum state when we set $\eta_1 = \eta_2 = \eta$ [22]. The resolution of Eqs. (7) and (9) in order to seek discrete stationary multibreathers solutions, oscillating with frequency belonging to the forbidden band, is done by means of iterative multidimensional Newton–Raphson method with periodic boundary conditions and initial guess produced by the high-confinement approximation [28].

It is worth noticing that, in our model, the mobility of discrete multisoliton is achieved for

$$\mu \simeq \eta_1 \left[1 - \frac{\eta_2 \alpha^2}{\eta_1(1+\alpha^2)}\right] \tag{10}$$

where α is the amplitude of our solutions [22]. Eq. (10) is an extension of what has been done for $\eta_2 = 0$ corresponding to discrete version of the Vinetskii–Kukhtarev equation and using mapping analysis [29]. A comparative study of the threshold amplitude for supratransmission and the mobility condition of discrete multibreathers yields Fig. 3(a) and (b). In these figures, mobility curve of discrete multibreathers has common parts with the area where the supratransmission occurs. Besides that, the discrete gap multibreathers can be transmitted or "supratransmitted" according to the frequency. Moreover, the discrete gap multibreathers are "supratransmitted" when we are close to the edge of the lower forbidden band. It emerges from Fig. 3 that the supratransmission can take the form of a discrete gap multibreather. By the way, the following boundary condition has been used for Eq. (1)

$$\phi_{n=0}(t) = u(\xi t)e^{-i\mu t} \tag{11}$$

where μ is a driving frequency belonging to the lower forbidden band gap. u emulates the discrete stationary multibreathers (breathers with three and four humps) found numerically. Thus, the forcing amplitude u is molded by the shape of the discrete stationary multibreathers. Hence, ξ is the shaken frequency relating to the generation of the humps of the multibreathers. The numerical integration of Eq. (1) with Eq. (11), on a molecular lattice chain consisting of 101 peptide groups, yields Fig. 4(a) and (b) for three-hump soliton ($\xi = 0.27$, $\eta_1 = \eta_2 = 20$, $\alpha = 0.16$, $\mu = 19.50$) and four-hump soliton ($\xi = 0.56$, $\eta_1 = \eta_2 = 20$, $\alpha = 0.12$, $\mu = 19.71$), respectively. The normalization condition, namely Eq. (9), was monitored during the integration procedure.

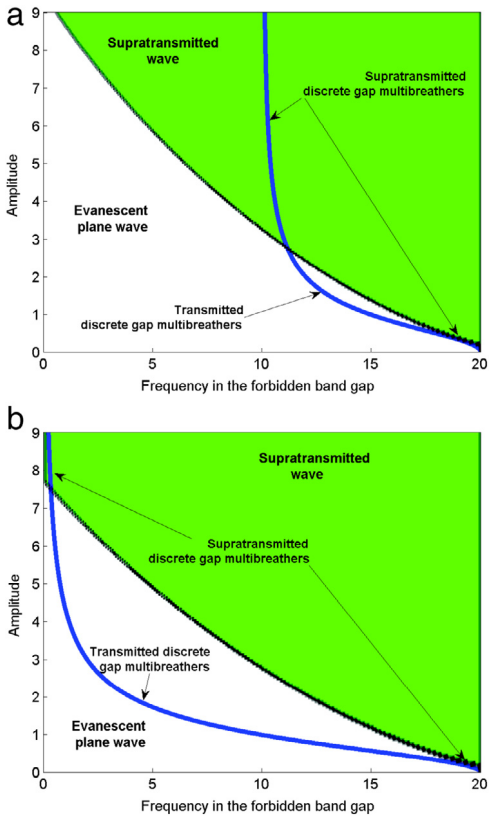

Fig. 3. Graphs of threshold amplitude versus frequency (black line), above which supratransmission occurs (green zone), compared to the mobility curve of discrete multisolitons (blue line) governed by Eq. (10). The saturable higher order nonlinearity parameter is $\eta_2 = 10$ for (a) and $\eta_2 = 20$ for (b), η_1 remaining fixed at 20. (For interpretation of the references to color in this figure legend, the reader is referred to the web version of this article.)

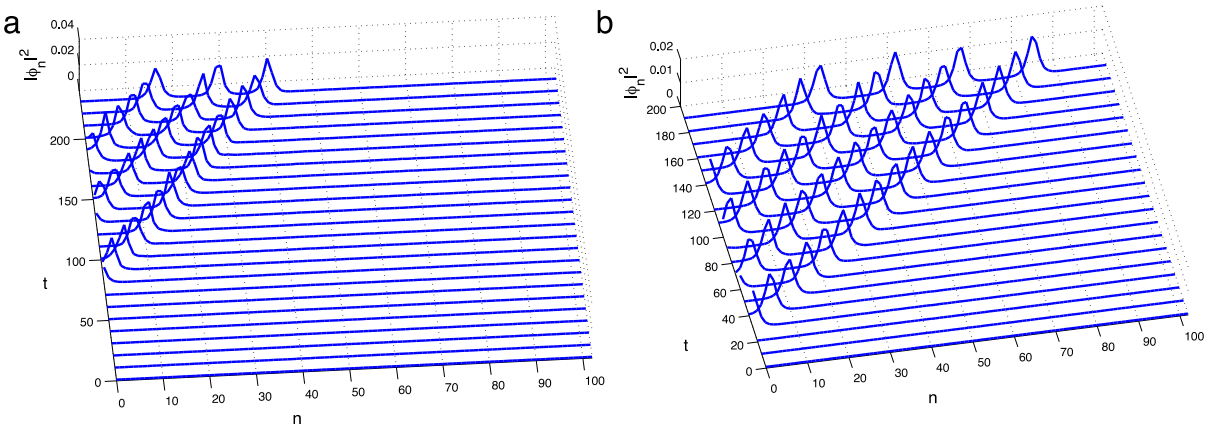

Fig. 4. Propagations of discrete gap three-hump solitons ((a) for ($\xi = 0.27$, $\eta_1 = \eta_2 = 20$, $\alpha = 0.16$, $\mu = 19.50$)) and four-hump soliton ((b) for ($\xi = 0.56$, $\eta_1 = \eta_2 = 20$, $\alpha = 0.12$, $\mu = 19.71$)) in protein chains consisting of 101 peptide groups.

On the other hand, the normalization condition implies that the amplitudes of the discrete multihump solitons decrease as the number of peaks increases. Thus, the discrete multihump solitons require less energy, for frequencies close to the lower band edge, compared to single solitons.

We should also add that during the nonlinear supratransmission, Leon and co-worker [25] think that the one-soliton tail provides an adiabatic deformation of the evanescent plane wave, and that any higher gap soliton trains would require more energy to be generated. This is probably due, besides the fact that Leon were in a continuum limit, to the fact that the discrete multihump soliton is a solution of DNSE while a soliton train is a group of solutions. From that perspective and in the framework where the normalization condition prevails, the nonlinear supratransmission can occur through the discrete gap multibreathers, particularly for frequencies close to the lower band edge.

4. Conclusion

In conclusion, we have highlighted supratransmission phenomena in DNLS equation with saturable nonlinearities modeling the localization and transport of vibrational energy in protein chains. Thus, a threshold amplitude beyond which the wave propagation takes place within the molecular chains were established numerically. A semi-analytical method is also carried out to find this critical value and it follows in accordance with numerical method that the saturable higher order nonlinearity parameter lowers the threshold amplitude for supratransmission, although this critical amplitude tends to zero close to the band edge. In order to see if the supratransmission can occur by means of discrete gap multibreathers, we have drawn for some cases the graph of amplitude vs frequency for which mobility of discrete multisolitons takes place and graph of threshold amplitude vs frequency above which supratransmission occurs. Subsequently, it appears that the discrete gap multibreathers can be transmitted or "supratransmitted" according to the frequency belonging to the lower forbidden band gap. Moreover, the discrete gap multibreathers are "supratransmitted" when we are close to the edge of the lower forbidden band. Interestingly, for some parameter of saturable nonlinearities, the propagation of this type of solution has been emphasized. This shows that the nonlinear supratransmission of discrete gap multibreathers is possibly a mechanism of bio-energy transport in protein chains.

Furthermore, since the cubic–quintic nonlinearity emulates the saturation on the one hand, and on the other, the mobility of discrete solitons in the latter model was studied in detail [30,31]; the investigation of supratransmission in cubic–quintic discrete nonlinear Schrödinger equation may be interesting.

Acknowledgements

The authors would like to thank the anonymous reviewers for their useful comments regarding this manuscript.

References

[1] A.S. Davydov, Solitons and energy transfer along protein molecules, J. Theoret. Biol. 66 (1977) 379.
[2] D.N. Christodoulides, R.I. Joseph, Discrete self-focusing in nonlinear arrays of coupled waveguides, Opt. Lett. 13 (1988) 794.
[3] W.P. Su, J.R. Schieffer, A.J. Heeger, Solitons in polyacetylene, Phys. Rev. Lett. 42 (1979) 1698;
A.J. Sievers, S. Takeno, Intrinsic localized modes in anharmonic crystals, Phys. Rev. Lett. 61 (1988) 970.
[4] A. Trombettoni, A. Smerzi, Discrete solitons and breathers with dilute Bose–Einstein condensates, Phys. Rev. Lett. 86 (2001) 2353.
[5] S. Gatz, J. Herrmann, Soliton propagation in materials with saturable nonlinearity, J. Opt. Soc. Amer. B 8 (1991) 2296.
[6] S. Gatz, J. Herrmann, Soliton propagation and soliton collision in double-doped fibers with a non-Kerr-like nonlinear refractive-index change, Opt. Lett. 17 (1992) 484.
[7] M. Segev, G.C. Valley, B. Crosignani, P. DiPorto, A. Yariv, Steady-state spatial screening solitons in photorefractive materials with external applied field, Phys. Rev. Lett. 73 (1994) 3211.
[8] V.O. Vinetskii, N.V. Kukhtarev, Theory of the conductivity induced by recording holographic gratings in nonmetallic crystals, Sov. Phys.—Solid State 16 (1975) 2414.
[9] M. Stepić, D. Kip, L. Hadžievski, A. Maluckov, One-dimensional bright discrete solitons in media with saturable nonlinearity, Phys. Rev. E 69 (2004) 066618;
L. Hadžievski, A. Maluckov, M. Stepić, D. Kip, Power controlled soliton stability and steering in lattices with saturable nonlinearity, Phys. Rev. Lett. 93 (2004) 033901;
A. Khare, K.Ø. Rasmussen, M.R. Samuelsen, A. Saxena, Exact solutions of the saturable discrete nonlinear Schrödingerbel equation, J. Phys. A 38 (2005) 807;
R.A. Vicencio, M. Johansson, Discrete soliton mobility in two-dimensional waveguide arrays with saturable nonlinearity, Phys. Rev. E 73 (2006) 046602;
T.R.O. Melvin, A.R. Champneys, P.G. Kevrekidis, J. Cuevas, Radiationless traveling waves in saturable nonlinear Schrödinger lattices, Phys. Rev. Lett. 97 (2006) 124101.
[10] W. Chen, D.L. Mills, Gap solitons and the nonlinear optical response of superlattices, Phys. Rev. Lett. 58 (1987) 160.
[11] D.L. Mills, S.E. Trullinger, Gap solitons in nonlinear periodic structures, Phys. Rev. B 36 (1987) 947.
[12] F. Geniet, J. Leon, Energy transmission in the forbidden band gap of a nonlinear chain, Phys. Rev. Lett. 89 (2002) 134102.
[13] A.B. Togueu Motcheyo, C. Tchawoua, M. Siewe Siewe, J.D. Tchinang Tchameu, Supratransmission phenomenon in a discrete electrical lattice with nonlinear dispersion, Commun. Nonlinear Sci. Numer. Simul. 18 (2013) 946;
A.B. Togueu Motcheyo, C. Tchawoua, J.D. Tchinang Tchameu, Supratransmission induced by waves collisions in a discrete electrical lattice, Phys. Rev. E 88 (2013) 040901(R);
K. Tse Ve Koon, J. Leon, P. Marqui, P. Tchofo-Dinda, Cutoff solitons and bistability of the discrete inductance-capacitance electrical line: Theory and experiments, Phys. Rev. E 75 (2007) 066604;
F. Tao, W. Chen, J. Pan, W. Xu, S. Du, Experimental observation on asymmetric energy flux within the forbidden frequency band in the LC transmission line, Chaos Solitons Fractals 45 (2012) 810;
K. Tse Ve Koon, P. Marqui, P. Tchofo Dinda, Experimental observation of the generation of cutoff solitons in a discrete LC nonlinear electrical line, Phys. Rev. E 90 (2014) 052901;
F. Kenmogne, G.B. Ndombou, D. Yemélé, A. Fomethe, Nonlinear supratransmission in a discrete nonlinear electrical transmission line: Modulated gap peak solitons, Chaos Solitons Fractals 75 (2015) 263.
[14] P. Anghel-Vasilescu, J. Dorignac, F. Geniet, J. Leon, M. Taki, Nonlinear supratransmission in multicomponent systems, Phys. Rev. Lett. 105 (2010) 074101.
[15] H. Susanto, N. Karjanto, Calculated threshold of supratransmission phenomena in waveguide arrays with saturable nonlinearity, J. Nonlinear Opt. Phys. Mater. 17 (2008) 159.
[16] H. Susanto, Boundary driven waveguide arrays: Supratransmission and saddle–node bifurcation, SIAM J. Appl. Math. 69 (2008) 111.
[17] J.E. Macías-Díaz, On the controlled propagation of wave signals in a sinusoidally forced two-dimensional continuous Frenkel–Kontorova model, Wave Motion 48 (2011) 13.
[18] J. Lydon, G. Theocharis, C. Daraio, Nonlinear resonances and energy transfer in finite granular chains, Phys. Rev. E 91 (2015) 023208.
[19] R. Khomeriki, L. Chotorlishvili, B.A. Malomed, J. Berakdar, Creation and amplification of electromagnon solitons by electric field in nanostructured multiferroics, Phys. Rev. B 91 (2015) 041408(R).

[20] S. Savel'ev, V.A. Yampol'skii, A.L. Rakhmanov, F. Nori, Layered superconductors as nonlinear waveguides for terahertz waves, Phys. Rev. B 75 (2007) 184503.
[21] J.E. Macías-Díaz, A. Puri, On the propagation of binary signals in damped mechanical systems of oscillators, Physica D 228 (2007) 112;
J.E. Macías-Díaz, A. Puri, An application of nonlinear supratransmission to the propagation of binary signals in weakly damped, mechanical systems of coupled oscillators, Phys. Lett. A 366 (2007) 447.
[22] J.D. Tchinang Tchameu, A.B. Togueu Motcheyo, C. Tchawoua, Mobility of discrete multibreathers in the exciton dynamics of the Davydov model with saturable nonlinearities, Phys. Rev. E 90 (2014) 43203.
[23] J.D. Tchinang Tchameu, C. Tchawoua, A.B. Togueu Motcheyo, Effects of next-nearest-neighbor interactions on discrete multibreathers corresponding to Davydov model with saturable nonlinearities, Phys. Lett. A 379 (2015) 2984.
[24] R. Khomeriki, Nonlinear band gap transmission in optical waveguide arrays, Phys. Rev. Lett. 92 (2004) 063905.
[25] J. Leon, A. Spire, Gap soliton formation by nonlinear supratransmission in Bragg media, Phys. Lett. A 327 (2004) 474.
[26] J.-G. Caputo, J. Leon, A. Spire, Nonlinear energy transmission in the gap, Phys. Lett. A 283 (2001) 129.
[27] D. Taverner, N.G.R. Broderick, D.J. Richardson, R.I. Laming, M. Ibsen, Nonlinear self-switching and multiple gap-soliton formation in a fiber Bragg grating, Opt. Lett. 23 (1998) 328.
[28] Lj. Hadžievski, A. Maluckov, M. Stepić, D. Kip, Power controlled soliton stability and steering in lattices with saturable nonlinearity, Phys. Rev. Lett. 93 (2004) 033901.
[29] A. Maluckov, Lj. Hadžievski, M. Stepić, Bifurcation analysis of the localized modes dynamics in lattices with saturable nonlinearity, Physica D 216 (2006) 95.
[30] C. Mejía-Cortés, R.A. Vicencio, B.A. Malomed, Mobility of solitons in one-dimensional lattices with the cubic-quintic nonlinearity, Phys. Rev. E 88 (2013) 052901.
[31] A. Maluckov, Lj. Hadžievski, B.A. Malomed, Staggered and moving localized modes in dynamical lattices with the cubic-quintic nonlinearity, Phys. Rev. E 77 (2008) 036604.

Physics Letters A 380 (2016) 3057–3060

Contents lists available at ScienceDirect

Physics Letters A

www.elsevier.com/locate/pla

Biological multi-rogue waves in discrete nonlinear Schrödinger equation with saturable nonlinearities

J.D. Tchinang Tchameu, A.B. Togueu Motcheyo, C. Tchawoua *

Laboratory of Mechanics, Department of Physics, Faculty of Science, University of Yaounde I, P.O. Box 812, Yaounde, Cameroon

ARTICLE INFO

Article history:
Received 4 February 2016
Received in revised form 29 June 2016
Accepted 5 July 2016
Available online 14 July 2016
Communicated by A.P. Fordy

Keywords:
Discrete multi-rogue waves
Discrete nonlinear Schrödinger equation

ABSTRACT

The discrete multi-rogue waves (DMRW) as solution of the discrete nonlinear Schrödinger (DNLS) equation with saturable nonlinearities is studied numerically. These biological rogue waves represent the complex probability amplitude of finding an amide-I vibrational quantum at a site. We observe that the growth in the higher order saturable nonlinearity implies the formation of DMRW including an increase in the short-living DMRW and a decrease in amplitude of the long-living DMRW.

1. Introduction

The Discrete Nonlinear Schrödinger (DNLS) equation is involved in the modeling of several phenomena. These phenomena result from interplay between nonlinearity and discreteness such as energy localization in discrete condensed matter and biological systems. Moreover, this energy localization occurs by means of intrinsic localized modes (ILM) or discrete breathers [1–3] which are spatially localized oscillations of large amplitude. Among the classes of localized structure, the rigorous proof of existence of ILM having an arbitrary number of extrema and called multibreathers was done [4]. In this direction the study of their existence has continued in Salerno equation [5], DNLS equation with cubic nonlinearity [6], and Klein–Gordon chain [7]. In addition, multibreathers have been observed in a realistic systems by means of numerical experiment [8], as well as its mobility [10].

Besides these localized modes, it is established that there is mode with a double spatio-temporal localization known as Peregrine soliton and solution of the NLS equation [11]. This solution has a particular characteristic in that it maximum wave amplitude exceeds the background amplitude by a factor of 3, and consequently, is qualified as a Rogue Wave (RW) [12]. The name RW or extreme waves owes its origin to the fact that it was previously met in the ocean and described by fishermen like solid walls of water appearing from nowhere and higher than 30 m. Since then, beyond the hydrodynamics, RW have been mentioned in other systems such as optics [13,14] in order to generate an hight amplitude optical pulse (Optical RW) [15]. In the Bose–Einstein condensates, vector RW have been constructed [16]. Moreover, multi-rogue waves solutions have been obtained analytically for a higher-order nonlinear Schrödinger equation in optical fibers [17].

On the other hand, when the discreteness of the system is taken into account, RW are also noted for Ablowitz–Ladik equation, Hirota equation [18,19], cubic DNLS equation [20] with a small degree of disorder [21]. Recently, it has been shown that the localization and vibrational energy in α-helical protein molecules could be modeled by DNLS equation with saturable nonlinearities in both continuous [9] and discrete medium [10]. Following Bludov's idea who showed that discrete RW can give rise to a localization of all energy into a single (or a few) waveguide(s) of a network [20] and Knowing that RW implies a high nonlinearity of the system [22], questions emerge. Could Discrete Multi-rogue waves (DMRW) be solution of DNLS equation with saturable nonlinearities and randomly distributed molecules around the peptide groups chain? Does biological rogue wave exist in the framework where the dynamic variable is a complex probability amplitude at the nth peptide group? The answers to these questions are the aims of this letter. In the next section, we shall present the DNLS equation with saturable nonlinearities which describes the state of amide-I excitations in proteins. Thereafter, we look for the discrete Multi-rogue waves by means of numerical simulations. In section 3, the results are discussed. Finally, we summarize our main findings in Section 4.

* Corresponding author.
E-mail addresses: jtchinang@gmail.com (J.D. Tchinang Tchameu), abtogueu@yahoo.fr (A.B. Togueu Motcheyo), ctchawa@yahoo.fr (C. Tchawoua).

http://dx.doi.org/10.1016/j.physleta.2016.07.011
0375-9601/

2. Discrete multi-rogue waves

We consider a one-dimensional hydrogen-bonded chain consisting of peptide groups ($H-N-C=O$), regularly spaced, and weakly bound according to the following sequence: $\cdots H-N-C=O\cdots H-N-C=O\cdots H-N-C=O\cdots H-N-C=O\cdots$. In the framework of strong exciton–phonon interaction, the normalized dynamical equations for the complex probability amplitude ϕ_n of finding an amide-I vibrational quantum at site n is given by [10]

$$i\frac{\partial\phi_n}{\partial t} = -(\phi_{n+1}+\phi_{n-1}) + \eta_1\frac{\phi_n}{1+|\phi_n|^2} - \eta_2\frac{|\phi_n|^2\phi_n}{(1+|\phi_n|^2)^2}, \qquad (1)$$

where t is the time coordinate, η_1 and η_2 are the strength of the nonlinearities. Correspondingly, these coefficients exhibit a competition between local compression and local dilatation of lattice which leads to the interplay between self-focusing and defocusing saturable nonlinearities. For $\eta_2 = 0$, Eq. (1) reduces to a discrete version of the Vinetskii–Kukhtarev equation widely used in optics [23].

By taking into account the diagonal disorder ε_n in a site energies [2,24], we can express Eq. (1) as

$$i\frac{\partial\phi_n}{\partial t} = \frac{\varepsilon_n}{J}\phi_n - (\phi_{n+1}+\phi_{n-1}) + \eta_1\frac{\phi_n}{1+|\phi_n|^2} - \eta_2\frac{|\phi_n|^2\phi_n}{(1+|\phi_n|^2)^2}, \qquad (2)$$

where $\varepsilon_n = \varepsilon\beta_n$, β_n is a random sequence, ε is the amide-I site energy without disorder, and J is the dipole–dipole interaction energy. As in Ref. [3] and those included therein, the shift of ground state energy ε_n is due to the interaction of the chain molecules with molecules of the environment. It follows that a random sequence ε_n is centered around the value 0. Notice that Eq. (2) is obtained after carrying a usual gauge transformation allowing us to cancel the term $(\varepsilon/J)\phi_n$ in its right side. Furthermore, Eq. (2) has two conserved quantities: the Hamiltonian H and the total power $P = \sum_n |\phi_n|^2$ which stand for the energy of the system and the total probability, respectively.

For a numerical experiment, the following physical parameters are used [25,26]: $J = 9.67\times10^{-4}$ eV, $\varepsilon = 0.205$ eV. The random quantity β_n is taken as $|\beta_n| \le 10^{-3}$. Our experiments are carried out on a chain with $N = 200$ peptide groups. By using a fourth-order Runge–Kutta method with periodic boundary conditions and taking 10^{-10} as absolute tolerance for the purpose of the conservation of P and H, we integrate Eq. (2). Unlike rational solutions generally used to obtain RW and following the idea of Ref. [21], a uniform probability amplitude is applied as the initial condition of Eq. (2). This is all the more physically relevant since the normalization condition requires $\sum_n |\phi_n|^2 = P$. P being a constant. Therefore $\phi_n(t=0) = \sqrt{\frac{P}{N}}$. Without loss of generality, let $P = 1$. Then the integration of Eq. (2), for $\eta_1 = 102.3$ and $\eta_2 = 0$, leads to Fig. 1(a). We observe that, with a initial uniform probability amplitude ($\phi_n(t=0) \simeq 0.0707$), the system selforganizes as a result of both disorder and nonlinearity. This selforganization is carried out in two ways. Firstly, we note that a short-living peaks appear on different sites. Secondly, as the time evolves, we remark the start (from $t \simeq 401$) of long-living peaks along the chain of peptide groups while the number and intensity of the short-living peaks decrease. Based on the precise definition of RW which stipulates that a wave is seen as extreme if its height is higher than the average wave amplitude plus eight times its corresponding standard deviation (see [22] and references therein), we can analyze the statistical distribution of maximum peak amplitudes. Then, Fig. 2(a) shows that, through each site n, 39.5 percent of absolute maximum amplitudes over time are rogue waves. In addition, the highest value of the maxima is 0.3. Inset of Fig. 2(a) shows the DMRW profile where we can see seven long-living peaks. Recall nevertheless that the normalization condition of amplitude ϕ_n is satisfied ($P \simeq 1$) when $t = 4000$. It therefore follows that the biological rogue waves as complex probability amplitude are not disastrous like rogue waves in the ocean. By increasing the strength of nonlinearity $\eta_2 = 51.15$ in Fig. 1(b), and $\eta_2 = 102.3$ in Fig. 1(c), we observe that the appearance of short-living peaks grows whereas the amplitude of long-living peaks decreases slightly. This is best seen in Fig. 2(b) and Fig. 2(c) where we find that 66.5 percent and 100 percent of absolute (the greatest) maximum peak amplitudes along the lattice, recorded over the time period [0, 4000], are rogue waves, respectively. Subsequently, the higher order saturable nonlinearity promotes the formation of DMRW including an increase in the short-living RW and a decrease in amplitude of the long-living RW. Also indicated in Fig. 2(b) and Fig. 2(c), we have a reduction of the highest value of the maxima which changes from 0.3 to 0.27.

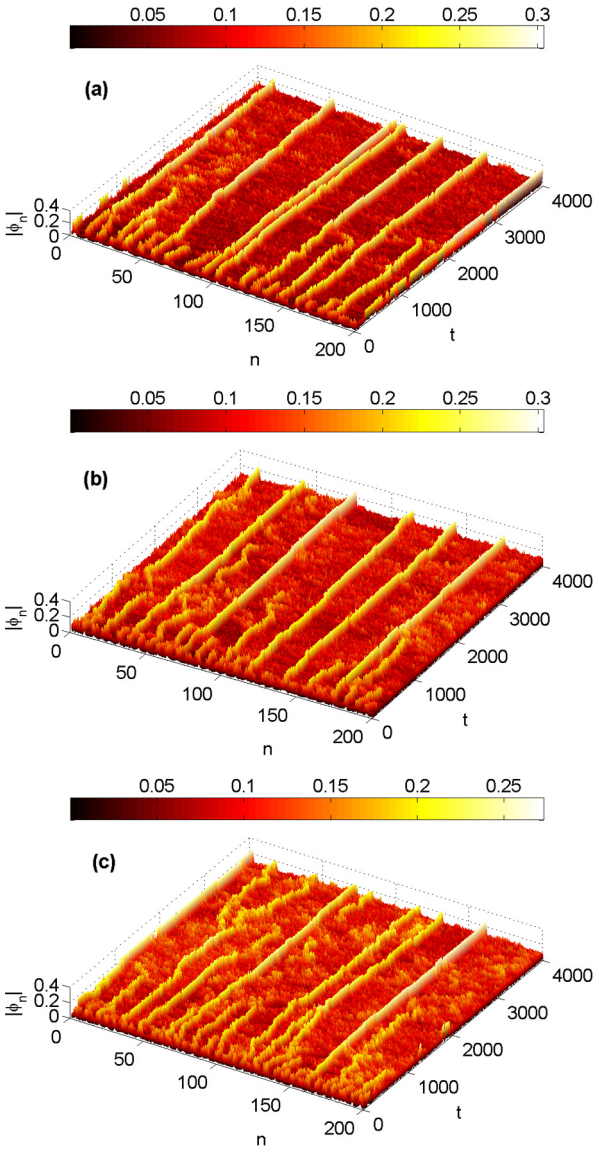

Fig. 1. Discrete multi-rogue waves for $\eta_1 = 102.3$, $\eta_2 = 0$ (a), $\eta_2 = 51.15$ (b), and $\eta_2 = 102.3$ (c). These figures are the results of the integration of Eq. (2) with periodic boundary conditions and a chain of 200 peptide groups. The initial condition of Eq. (2) is taken in the form of uniform probability amplitude $\phi_n(t=0) \simeq 0.0707$. The random sequence β_n has zero-mean distribution in the interval $[-10^{-3}, 10^{-3}]$. (For interpretation of the references to color in this figure legend, the reader is referred to the web version of this article.)

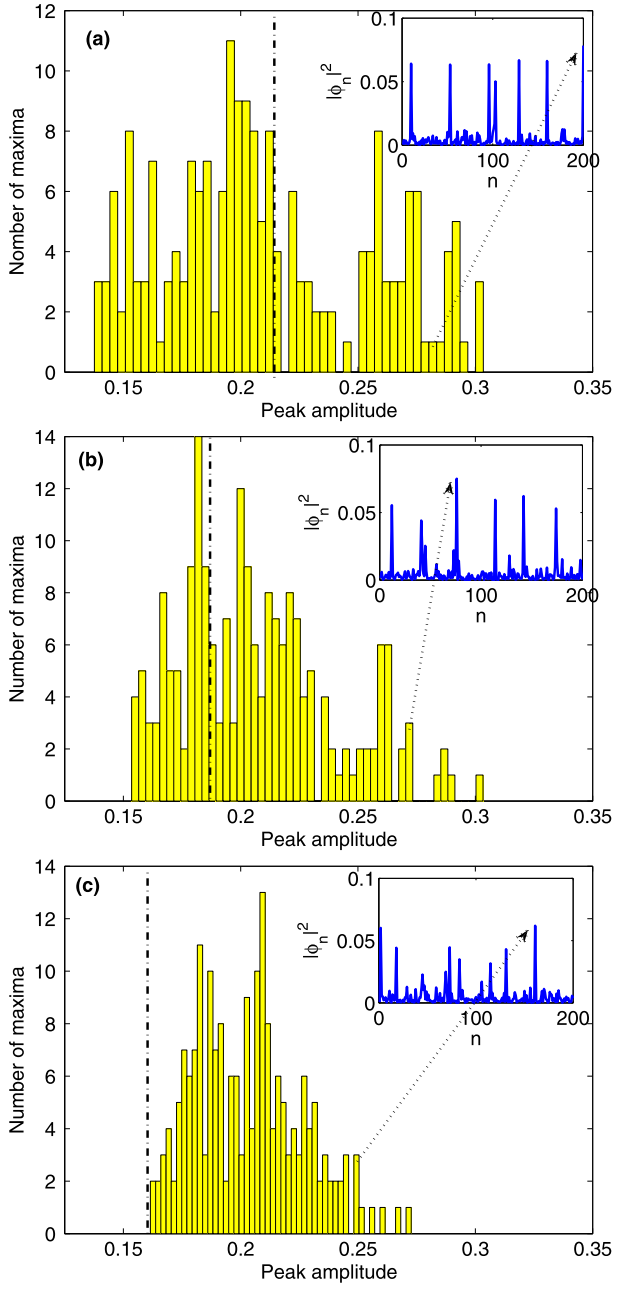

Fig. 2. Statistical distributions of the absolute maximum amplitudes recorded through each peptide group, as a function of their numbers, over the time period [0, 4000] for $\eta_1 = 102.3$, $\eta_2 = 0$ (a), $\eta_2 = 51.15$ (b), and $\eta_2 = 102.3$ (c). For a given peptide group (200 in total), the greatest peak amplitude is retained among 4000 amplitudes after having integrated Eq. (2). The width of the 50 bins is 0.0035 (a), 0.003 (b), and 0.002 (c). The vertical dashed lines stand for a threshold amplitudes beyond which the greatest maximum peak amplitude can be seen as discrete rogue wave. The insets show the DMRW profiles (blue lines) when $t = 4000$. (For interpretation of the references to color in this figure legend, the reader is referred to the web version of this article.)

3. Discussions

Through study of discrete rogue waves in discrete nonlinear Schrödinger lattice with cubic nonlinearity, it has been recently obtained three sharp peaks from uniform initial condition [21]. Here, with saturable nonlinearity which can be emulated by cubic–quintic nonlinearity, we get seven sharp peaks on average. This observation illustrates that the saturable nonlinearity exhibit more extreme events than cubic nonlinearity. Moreover, in light of what has been done in continuum medium of the ocean surface [27], these peaks can be explained as follows. The instability of a uniform initial condition leads first to the creation of a chain of discrete solitons with small amplitudes. As time continues forward, inelastic interactions among each other promote the growth of the larger excitation. Note as well that disorder considerably enhances the instability and, thus, the growth of the larger excitation that could lead to discrete rogue waves when the required criterion in term of the standard deviation is satisfied. As a matter of fact, these explanations join those reported in [21]. DMRW-like mechanism for the localization of vibrational energy in protein chain is therefore possible. On that point, Daumont et al. [28] have presented modulational instability as first step towards energy localization in nonlinear lattices. In the latter work, while taking into account the discreteness, localized modes arising from the modulational instability (MI) have not lead to rogue waves. This is probably because the lack of small disorder which enhances the instability and thus allow for the excitation of discrete rogue waves. As such, the fact that rogue waves are excited when MI develops from noise is consistent with the previous works [29].

As regards the biological nature of our DMRW as probability amplitude of finding a quantum of amide-I, the effect of normalization ($\sum_n \mid \phi_n \mid^2 = 1$) on this solution is of paramount importance. Building on the normalize uniform initial condition, the DMRW is found by means of numerical experiments. This initial condition means that, although low, the probability amplitude is uniform at the beginning on all peptide groups. Thereafter, there is a sudden redistribution of probabilities accompanied by a large one at least two times higher than uniform background probability amplitude in some sites at the expense of other (Fig. 1), due to the conservation of energy which is monitored during the integration procedure. This conservation avoids the system to have unlimited and catastrophic amplitudes and, therefore, to have a great molecular bond distortion that can cause a breakage of the molecular chain (with the understanding that there is a phonon–exciton coupling [2,10]).

Spatiotemporal evolution of the DMRW arising from system depends on the strengths of higher order saturable nonlinearity. By using colormaps which vary smoothly from black through shades of red, orange, and yellow, to white; it appears from Fig. 1(a) that long-living DMRW are promoted. Between crests of DMRW in bright yellow, furrows are red. 39.5 percent of absolute maximum amplitudes of $|\phi_n|$ through each peptide group are RW (Fig. 2(a)). The increasing of the strengths of higher order saturable nonlinearity is associated with a reduction of the amplitude of the long-living DMRW and the short-living DMRW development. The letter appears from nowhere and disappears without a trace as illustrated by the rise of probability "clumps", in yellow, on the furrows (Figs. 1(b) and (c)) when η_2 increases from 51.15 to 102.3. Simultaneously, the percentage of absolute maximum amplitudes of $|\phi_n|$ through each peptide group, recorded over the time period $[0, 4000]$, which are RW increases from 66.5 to 100 (Figs. 2(b) and (c)). The higher order saturable nonlinearity is responsible for the small localization in space of DMRW.

In any event, it appears that DNLS equation with saturable nonlinearities can sustain DMRW as complex probability amplitude. Then DMRW-like mechanism for the localization of vibrational energy in protein chain is possible.

4. Conclusion

It has been shown that discrete nonlinear Schrödinger equation with saturable nonlinearities admits discrete multi-rogue waves (DMRW) as solution. These biological rogue waves stand for the complex probability amplitude ϕ_n of finding an amide-I vibrational quantum at site n. Moreover, it has been observed that the higher order saturable nonlinearity promotes the formation

of DMRW including an increase in the short-living RW and a decrease in amplitude of the long-living RW. Therefore, DMRW opens the way towards a localization of vibrational energy in protein chain.

References

[1] A.S. Davydov, N.I. Kislukha, Phys. Status Solidi (b) 59 (1973) 465.
[2] A.C. Scott, Phys. Rep. 217 (1992) 1.
[3] A.V. Zolotaryuk, K.H. Spatschek, O. Kluth, Phys. Rev. B 47 (1993) 7827.
[4] T. Ahn, Nonlinearity 11 (1998) 965.
[5] T. Bountis, H.W. Capel, M. Kollmann, J.C. Ross, J.M. Bergamin, J.P. van der Weele, Phys. Lett. A 268 (2000) 50.
[6] P.G. Kevrekidis, Discrete Nonlinear Schrödinger Equation: Mathematical Analysis, Numerical Computations and Physical Perspectives, Springer Tracts Mod. Phys., vol. 232, Springer, Berlin, 2009.
[7] V. Koukouloyannis, P.G. Kevrekidis, J. Cuevas, V. Rothos, Physica D 242 (2013) 16.
[8] A.B. Togueu Motcheyo, C. Tchawoua, M. Siewe Siewe, J.D. Tchinang Tchameu, Phys. Lett. A 375 (2011) 1104.
[9] M. Aguero, R. García-Salcedo, J. Socorro, E. Villagran, Int. J. Theor. Phys. 48 (2009) 670.
[10] J.D. Tchinang Tchameu, A.B. Togueu Motcheyo, C. Tchawoua, Phys. Rev. E 90 (2014) 43203.
[11] D.H. Peregrine, J. Aust. Math. Soc. B 25 (1983) 16.
[12] N. Akhmediev, A. Ankiewicz, M. Taki, Phys. Lett. A 373 (2009) 675.
[13] B.G.E. Onana, J. Atangana, F.M. Biya, B. Mokhtari, N.E. Cherkaoui, T.C. Kofane, Phys. Rev. E 90 (2014) 032911.
[14] D.E. Temgoua, T.C. Kofane, Phys. Rev. E 91 (2015) 063201.
[15] D.R. Solli, C. Ropers, P. Koonath, B. Jalali, Nature 450 (2007) 1054.
[16] F. Baronio, A. Degasperis, M. Conforti, S. Wabnitz, Phys. Rev. Lett. 109 (2012) 044102.
[17] F. Yu, Appl. Math. Comput. 220 (2013) 176.
[18] N. Akhmediev, A. Ankiewicz, Phys. Rev. E 83 (2011) 046603.
[19] A. Ankiewicz, N. Akhmediev, J.M. Soto-Crespo, Phys. Rev. E 82 (2010) 026602.
[20] Y.V. Bludov, V.V. Konotop, N. Akhmediev, Opt. Lett. 34 (2009) 3015.
[21] S. Efe, C. Yuce, Phys. Lett. A 379 (2015) 1251.
[22] C. Bonatto, M. Feyereisen, S. Barland, M. Giudici, C. Masoller, J.R. Leite, J.R. Tredicce, Phys. Rev. Lett. 107 (2011) 053901.
[23] A. Maluckov, Lj. Hadžievski, M. Stepić, Physica D 216 (2006) 95.
[24] W. Forner, J. Phys. Condens. Matter 3 (1991) 3235.
[25] K. Kundu, Phys. Rev. E 61 (2000) 5839.
[26] L. MacNeil, A.C. Scott, Phys. Scr. 29 (1984) 284.
[27] A.I. Dyachenko, V.E.E. Zakharov, J. Exp. Theor. Phys. 81 (2005) 255.
[28] I. Daumont, T. Dauxois, M. Peyrard, Nonlinearity 10 (1997) 617.
[29] N. Akhmediev, J.M. Soto-Crespo, A. Ankiewicz, Phys. Lett. A 373 (2009) 2137.

Chaos, Solitons and Fractals 99 (2017) 180–184

Contents lists available at ScienceDirect

Chaos, Solitons and Fractals

Nonlinear Science, and Nonequilibrium and Complex Phenomena

journal homepage: www.elsevier.com/locate/chaos

Review

Multibreathers-impurity interactions in the discrete nonlinear Schrödinger model

J.D. Tchinang Tchameu*, A.B. Togueu Motcheyo, C. Tchawoua

Laboratory of Mechanics, Department of Physics, Faculty of Science, University of Yaounde I, P.O. Box 812, Yaounde, Cameroon

ARTICLE INFO

Article history:
Received 26 September 2016
Revised 27 March 2017
Accepted 4 April 2017

Keywords:
Discrete multibreathers
Impurity
DNLS lattice

ABSTRACT

We report numerical observations of scattering process of moving multibreathers by isolated impurities in the discrete nonlinear Schrödinger lattice representing the vibrational energy transport along the protein chain. It is found that, except for the multibreather passing, internal collision phenomenon support all types of scattering outcomes for both attractive and repulsive impurities. Furthermore, for large strength of attractive impurity the scattering of two-hump soliton can give rise to a trapping on a site other than the one containing the impurity. As concerns three-hump soliton, the passing, trapping and reflection are simultaneously carried out for some parameters. In the case of three-hump soliton introduced between two repulsive impurity sites, back and forth are observed as well as increasingly individualistic behavior of humps over time. Nonetheless, two-hump soliton launched under the same conditions results in large stationary single breather.

1. Introduction

Many problems in solid-state physics are relative to nonlinear localized waves propagation in disordered media (see e.g., Ref. [1] and references therein) because a considerable number of structures in nature are non-crystalline. However, understanding of such problems requires the study of the interaction of soliton with a single impurity. Due to its numerous applications, solitons play a significant role for the dynamics of ferro- and antiferromagnetic materials [2], phase changes in solids [3], dielectric relaxation in crystalline polyethylene [4], dislocations in crystals, fluxons in Josephson contacts and junctions, etc [5]. Moreover, localized inhomogeneity hit by a soliton can correspond to mass discontinuity in lattice [6,7], base-pair inhomogeneity [8], sheath ions in plasma [9], electric or magnetic impurities [10], parity-time-symmetric defects [11–13]. Solitary waves involved in the interaction with localized impurity are governed by a variety of equation such as nonlinear sine-Gordon (SG) equation [14], Discrete Nonlinear Schrödinger (DNLS) equation [15–19]. With particular regard to breather, these equations generally highlight four outcomes in the case of an unexcited impurity: passing, trapping, partial and total reflection [20]. It therefore appears that this outcomes play an important role in transport properties of breathers.

Pointing out the transport in condensed matter systems, Davydov showed that, under adiabatic approximation, Hamilton's equations corresponding to exciton-phonon interaction is reduced to the DNLS equation [21]. In addition, a more realistic modeling of the main polypeptide chain provides the need to take into account diagonal disorder standing for the side groups on the geometry of this chain [21–23].

On the other hand, it has been shown that multibreathers-like mechanism for vibrational energy transport along the protein chain is possible [24]. This was done in a framework of perfect lattice and particularly at a time when a great deal of attention is paid to the study of multibreathers [25,26]. Drawing on this, a question arises. Does the impurity can modify the multibreathers dynamics? If so, in what ways? Indeed, to our knowledge, there is no report on the study of the multibreathers scattering by impurities. Although the topic relating to the interaction of breathers with impurity is old, there is an intrinsic difficulty of the problem in the case of multibreathers-impurity interactions due to the lack of analytical expression of multibreathers in discrete systems at this time. It is in this context that our concern is to explore the problem of multibreathers-impurity interactions in DNLS model from a qualitative standpoint, and to a lesser extent from a quantitative standpoint. Motivated by this, the main objective of the present paper is to analyze the interaction of moving multibreathers with an isolated impurity in the discrete nonlinear Schrödinger model representing the vibrational energy transport along the protein chain. In the next section, we briefly introduce the model. Section 3 is devoted to the numerical studies on scat-

* Corresponding author.
E-mail addresses: jtchinang@gmail.com (J.D. Tchinang Tchameu), abtogueu@yahoo.fr (A.B. Togueu Motcheyo), ctchawa@yahoo.fr (C. Tchawoua).

http://dx.doi.org/10.1016/j.chaos.2017.04.007
0960-0779/

tering of the multibreathers due to a positive or negative impurity. The findings are concluded in Section 4.

2. Model

We consider the DNLS equation which describes a number of phenomena like nonlinear optics, water waves, plasma physics, quantum mechanics, superconductivity, Bose–Einstein condensate theory, biological physics [27,28]. More precisely, this DNLS equation is also useful for the description of the vibrational energy transport in protein chain with on-site potential arising from impurities [21],

$$i\frac{\partial\phi_n}{\partial t} + (\phi_{n+1} + \phi_{n-1}) - \frac{\varepsilon_n}{J}\phi_n + 2\nu|\phi_n|^2\phi_n = 0, \tag{1}$$

where ϕ_n is the probability of finding two amide-I vibrational quanta at nth peptide groups in chain; ε_n is the diagonal disorder; J is the nearest neighbor dipole-dipole coupling energy along a chain and ν is the nonlinear coefficient. For α-helical proteins, we have [29,30]: $J = 9.67 \times 10^{-4}$ eV, $\chi = 3.87 \times 10^{-2}$ eV/Å, $\omega = 0.8125$ eV/Å^2 and $\nu = \frac{\chi^2}{J\omega} = 1.9$.

The model (1) has two conserved quantities: the Hamiltonian

$$E = \sum_n \left[-\frac{\nu}{2}|\phi_n|^4 - (\phi_n\phi^*_{n-1} + \phi_{n-1}\phi^*_n) - \frac{\varepsilon_n}{J}|\phi_n|^2\right], \tag{2}$$

with canonical conjugated variables $\{i\phi_n\}$, $\{\phi^*_n\}$ where the asterisk denotes complex conjugate, and the $l^2 - norm$

$$P = \sum_n |\phi_n|^2 = 1. \tag{3}$$

3. Interaction of a moving discrete multihump soliton with a diagonal disorder

Let us consider stationary solutions to (1) of the form $\phi_n = u_n \exp(i\Omega t)$, Ω being a frequency and u_n, the real-valued amplitudes. The amplitudes u_n satisfy a set of coupled algebraic equations

$$-\Omega u_n + (u_{n+1} + u_{n-1}) - \frac{\varepsilon_n}{J}u_n + \nu u^3 = 0. \tag{4}$$

Use of iterative multidimensional Newton–Raphson method, starting from trivial solutions of the anti-continuous limit depending on the desired localized stationary solution (two-hump and three-hump with the corresponding interpeak separation), and application of the concept of continuation [31] give us the discrete stationary multihump soliton solutions of Eq. (4) [24,32]. In order to check the stability of these solutions, we have added the perturbation

$$\zeta_n = \exp(i\Omega t)(x_n \exp(\lambda t) + y_n \exp(\lambda^* t)) \tag{5}$$

to stationary solutions ϕ_n and linearized Eq. (1) with respect to small perturbation modes x_n and y_n. The ensuing eigenvalue problem was solved by a standard numerical eigenvalue solver. Stationary soliton solutions are linearly unstable if at least one eigenvalue has a strictly positive real part. Once the steps mentioned above is verified, the discrete multihump soliton can be launched along the protein chain with diagonal disorder. In this case, only the central peptide group at n_0 from a chain length of 400 units is disordered. Thus $\varepsilon_n = \varepsilon\sigma_0\delta_{nn_0}$ where δ_{nn_0} is the Kronecker delta symbol, σ_0 is the parameter impurity which can be negative (attractive impurity) or positive (repulsive impurity) and $\varepsilon = 0.205$ eV. Such a diagonal impurity is used for the modeling of different amino acid side groups and local geometric distortions to these groups in proteins [23,33].

In order to get an information about the interaction of discrete multibreathers with a linear point-defect impurity, we perform a

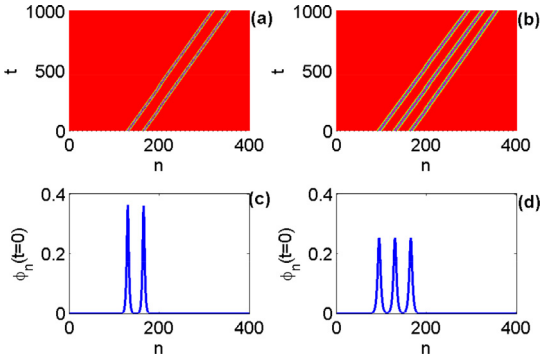

Fig. 1. Discrete (a) two-hump soliton and (b) three-hump soliton passing through the impurity located at $n_0 = 200$ for $\sigma_0 = 0.0001$, $q = 0.1$, $\Omega = 2.24$ (a) and $\Omega = 2.12$ (b). Initial profiles are shown in panels (c) and (d), respectively.

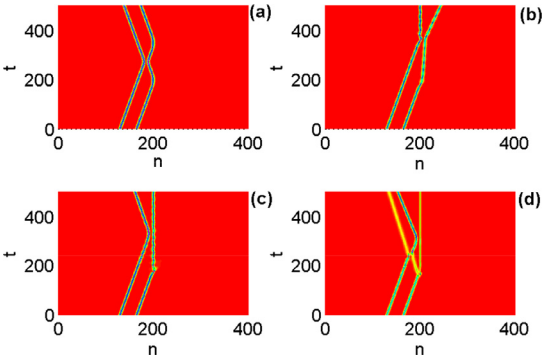

Fig. 2. Typical results of the interaction of two-hump soliton (density plot) with an isolated impurity: reflection (a), partial transmission (b), and partial reflections [(c) and (d)]. The multibreather parameters are: $q = 0.1$, $\Omega = 2.24$, $\sigma_0 = 0.0002$ (a), $\sigma_0 = -0.0005$ (b), $\sigma_0 = -0.0009$ (c), $\sigma_0 = -0.0030$ (d) and the impurity is located at $n_0 = 200$.

numerical integration of Eq. (1) using the 4th order Runge–Kutta scheme with a suitable choice of time step and absolute tolerance (10^{-10}) for the purpose of the conservation of energy and norm.

It is well known that stationary discrete multibreathers can be put into mouvement by adding a thrust q to it so that $\phi_n(0) = u_n \exp(iqn)$(see [24] and references therein). During the propagation, the interaction of moving discrete multihump soliton with a linear point-defect impurity is observed. Well before that, it should be noted that the stability of propagating discrete multihump soliton has been checked. Indeed, with discrete multibreathers, it has been shown that the intensity of instability decreases as interpeak separation increases [24,32]. It seems that for interpeak separation of 35, two-hump solitons and three-hump soliton becomes stable with frequencies $\Omega = 2.24$ and $\Omega = 2.12$, respectively. Therefore, we can achieve the mobility of discrete multibreathers. For $\sigma_0 = 0.0001$ and $q = 0.1$, we observe a smooth propagation of the incident two-hump soliton passing through the impurity site located at $n_0 = 200$ (Fig. 1(a) and (c)). A similar observation is made for three-hump soliton in Fig. 1(b) and (d). However, for $\sigma_0 = 0.0002$ and the same thrust, the discrete multibreather is reflected. Fig. 2(a) indicates also the quasi-elastic character of the collision of this one with the impurity. Another striking effet of multibreather-impurity interactions is what may be called *internal collision* of discrete two-hump soliton that leaves reflected multibreather which is identical to the incident one. In the case of attractive impurity ($\sigma_0 = -0.0005$) and kick $q = 0.1$, we obtain an unusual *partial transmission* where the impurity capture a part of the discrete multibreather and allows the other part of it to escape (Fig. 2(b)). Even in this case, it should be noted that collision phenomenon is an inherent element of the multibreather scattered by

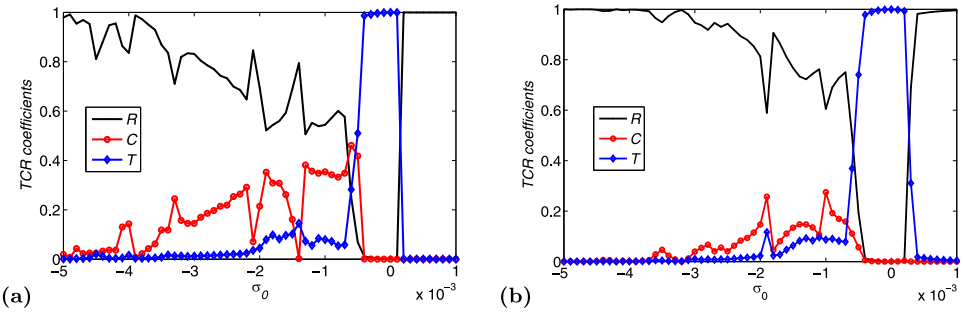

Fig. 3. Reflection (black line), transmission (blue line), and capture (red line) diagrams for discrete two-hump (a) and three-hump (b) soliton solutions. The thrust is $q = 0.1$, the frequencies are $\Omega = 2.24$ (a), and $\Omega = 2.12$ (b). (For interpretation of the references to colour in this figure legend, the reader is referred to the web version of this article.)

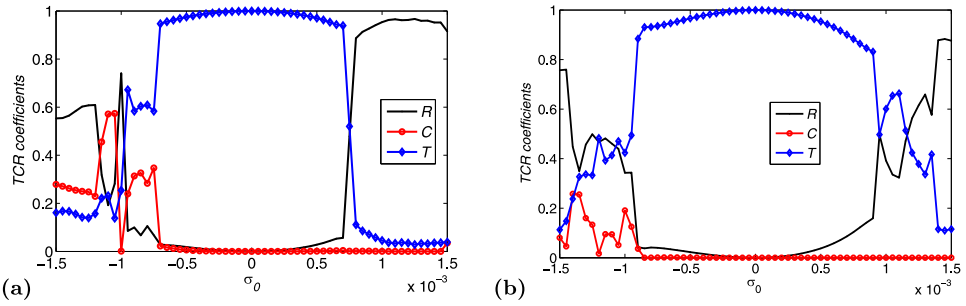

Fig. 4. Reflection (black line), transmission (blue line), and capture (red line) diagrams for discrete two-hump (a) and three-hump (b) soliton solutions. The thrust $q = 0.2$ and the frequency $\Omega = 2.24$ (a), and $\Omega = 2.12$ (b). (For interpretation of the references to colour in this figure legend, the reader is referred to the web version of this article.)

impurity. Taking $\sigma_0 = -0.0009$ and $q = 0.1$, we get a partial reflection as shown in Fig. 2(c). Increasing the value of σ_0 to -0.0030, we still get a partial reflection (Fig. 2(d)). But this time the multibreather scattered by an attractive impurity gives rise to the formation of a complex pattern involving multiple collisions.

In order to better understand the role of σ_0 and q, we define the reflection coefficient R, capture (trapping) coefficient C, and transmission coefficient T as follows

$$R = \sum_{n=1}^{197} |\phi_n(t_f)|^2, \tag{6}$$

$$C = \sum_{n=198}^{202} |\phi_n(t_f)|^2, \tag{7}$$

and

$$T = \sum_{n=203}^{400} |\phi_n(t_f)|^2, \tag{8}$$

where t_f is the time chosen long after the multibreather-impurity interactions has taken place. After calculation of these coefficients, it appears that for σ_0−values of the same absolute values but opposite signs the behaviors of discrete two-hump soliton with regard to impurity are not the same. This result is contrary to those obtained by Förner [23]. Our findings are evidenced by Figs. 3(a) and 4(a) for $q = 0.1$ and $q = 0.2$, respectively. We can also see that the interval of the strength of inhomogeneity σ_0 for sharp transmission increases as q increases. Therefore, this interval jumps from $[-0.0004, 0.0001]$ to $[-0.0007, 0.0007]$ as the thrust q changes from 0.1 to 0.2. Furthermore, for $q = 0.3$, the interval of sharp transmission is $[-0.0012, 0.0011]$. This is expected since q acts like the velocity. Therefore, the increase of the kinetic energy of multibreathers leads to the increase of sharp transmission window. Another highlight has drawn our attention. For large strength of attractive impurity ($\sigma_0 = -0.0060$ for example), in contrast to the discrete one-hump soliton, the scattering of a discrete

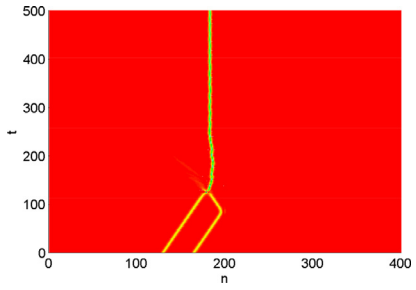

Fig. 5. Density plot of the multibreather-impurity interactions giving rise to a trapping on a site ($n = 183$) other than the one containing the impurity ($n_0 = 200$). The thrust $q = 0.2$, the parameter of inhomogeneity $\sigma_0 = -0.0060$ and the frequency $\Omega = 2.24$.

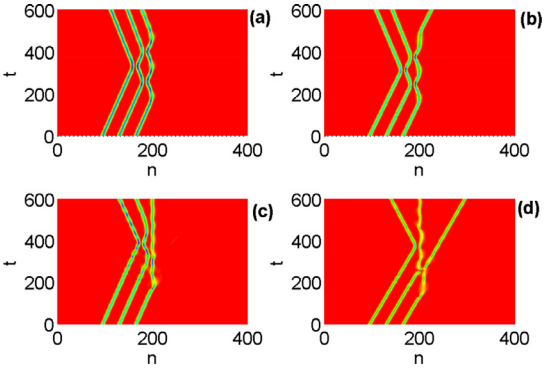

Fig. 6. Typical results of the interaction of three-hump soliton (density plot) with an isolated impurity: reflection (a), reflection and transmission (b), and partial reflection (c), and reflection-capture-transmission (d). The multibreather parameters are: $\Omega = 2.12$; $q = 0.10, \sigma_0 = 0.0004$ (a); $q = 0.11$, $\sigma_0 = 0.0004$ (b); $q = 0.100$, $\sigma_0 = -0.0007$ (c); and $q = 0.133$, $\sigma_0 = -0.0007$ (d). The impurity is located at $n_0 = 200$.

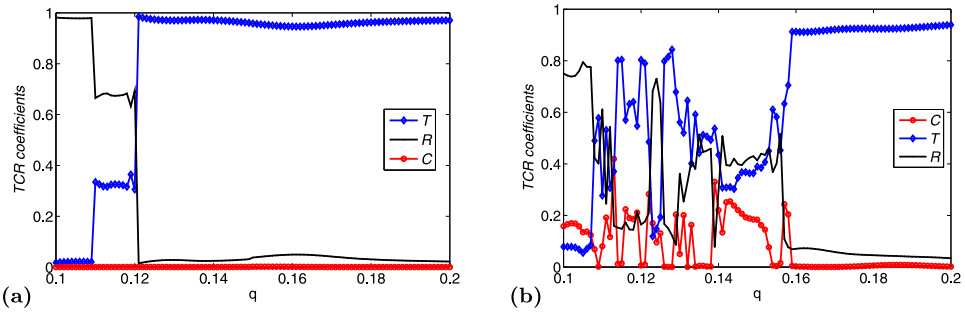

Fig. 7. Reflection (black line), transmission (blue line), and capture (red line) coefficients versus thrust q for discrete three-hump soliton solutions. The parameters of inhomogeneity $\sigma_0 = 0.0004$ (a) and $\sigma_0 = -0.0007$ (b), the frequency $\Omega = 2.12$. (For interpretation of the references to colour in this figure legend, the reader is referred to the web version of this article.)

two-hump soliton can gives rise to a trapping on a site ($n = 183$) other than the one containing the impurity ($n_0 = 200$), as Fig. 5 shows. Given this observation for large strength of attractive impurity, the calculation of the reflection coefficient, capture coefficient, and transmission coefficient is strenuous by means of Eqs. (6)–(8).

Concerning in particular three-hump soliton, they can interact in various ways among which, those present in Fig. 6. Clearly, the three-hump soliton can be reflected by an impurity as shown in Fig. 6(a) for $q = 0.1$ and $\sigma_0 = 0.0004$. The main feature of this interaction is that the reflection is accompanied by *internal collision* phenomenon, like for two-hump soliton. *Internal collision* phenomenon described here, leading to multiple collisions, feels like what is happening in Ref.[34] where we have collisions between two supersolitons. With $\sigma_0 = -0.0007$, we observe that the three-hump soliton hitting the impurity is partially captured, allowing two-hump soliton to be reflected (see Fig. 6(c)). Systematically, the transmission window as function of the parameter impurity is presented in Fig. 3(b) for $q = 0.1$. Compared to the scattering of two-hump soliton, it appears that the sharp transmission window for three-hump soliton is slightly higher: $-0.0004 \leq \sigma_0 \leq 0.0002$. Moreover, the increase in the thrust to $q = 0.2$ of three-hump soliton involves the expansion of this sharp transmission window (see Fig. 4(b)). Although the role played by thrust q is obvious, the transmission window as function of it in Fig. 7 reveals that the transition from reflection to sharp transmission over the increase in thrust is done without having a capture for repulsive impurity (see, e.g., Figs. 6(a), (b), and 7(a) with $\sigma_0 = 0.0004$). This observation is known in literature for a single breather. This is not the case for attractive impurity where this transition comes with an unusual pattern (see, e.g., Figs. 6(c), (d), and 7(b) with $\sigma_0 = -0.0007$). It follows from these multibreather-impurity interactions new outcomes as shown in Fig. 6(d). This figure describes simultaneously a reflection (41%), a capture (19%) and transmission (40%) with a very small loss of radiation. This kind of interaction has not been reported in previous works relating to single-hump soliton [16]. In order to understand this interaction of three-hump breathers with an impurity, recall that it is well known that trapping of single-hump breathers on a potential well is observed when the resonant transfer of translational energy from this wave to the linear impurity mode arises [15,16]. The Fourier spectra (see Fig. 8) of the incident three-hump breather and the captured one-hump breather may confirm the resonant transfer, since the frequency responses contain a spike at $\Omega = 2.129$ and $\Omega = 2.108$, respectively. Qualitatively, this new outcome can be explained, in addition, by the fact that the well defect is deep enough to hold a part of the miltibreather, thus leaving another part transmitted and reflected. However, for large values of strength of local impurity potential, the multibreather trapping decreases, just like for the single-hump breathers [15].

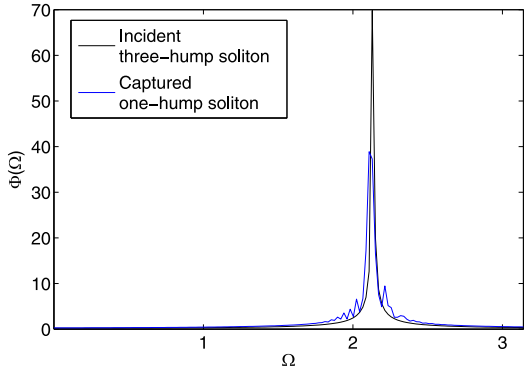

Fig. 8. Fourier spectra $\Phi(\Omega)$ of the incident three-hump breather (black) and the captured one-hump breather (blue) involved in the interaction shown in Fig. 6(d). (For interpretation of the references to colour in this figure legend, the reader is referred to the web version of this article.)

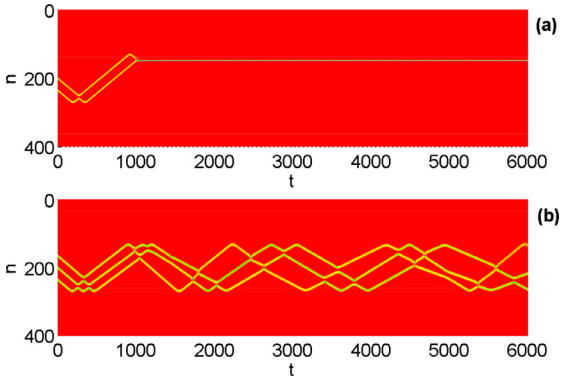

Fig. 9. Traping of two-hump soliton (a) and three-hump soliton (b) between two impurity sites located at $n = 130$ and $n = 270$ for $\sigma_0 = 0.0001$, $q = 0.1$, $\Omega = 2.24$ (a) and $\Omega = 2.12$ (b).

Knowing that single breather can be trapped between two repulsive impurity sites in the form of multiple reflections [35], what about multibreathers? Fig. 9(a) and (b) try to provide answers to this question. A multiple reflections are found for the case of three-hump soliton (Fig. 9(b)) with $\sigma_0 = 0.0001$, $q = 0.1$ and $\Omega = 2.12$. On top of that, we note an increasingly individualistic behavior of three-hump soliton's hump over time. Fig. 9(a) rather reveals a large stationary single breather when we introduce two-hump soliton between two repulsive impurity sites with $\sigma_0 = 0.0001$, $q = 0.1$ and $\Omega = 2.24$. This is likely due to the parity of the multibreather.

4. Conclusion

In sum, the influence of impurities on moving multibreathers in DNLS lattice was numerically analyzed. It emerged from this analysis that, excluding the transmission case, the phenomenon of internal collision of multibreathers accompanies all types of scattering outcomes, regardless of sign of the impurity. We have also recorded the formation of a complex pattern involving multiple collisions for the case of two-hump soliton scattered by an attractive impurity. Moreover, contrary to previous studies related to breather-impurity interactions, the scattering of a discrete two-hump soliton can lead to a trapping on a site other than the one containing the impurity, after one collision. In particular with regard to three-hump soliton, numerical simulations demonstrate for attractive impurity a reflection, a capture, a transmission with a very small loss of radiation and all this at the same time. A multiple reflections have been found for the case of three-hump soliton introduced between two repulsive impurity sites, including an increasingly individualistic behavior of humps over time. However, for two-hump soliton, we have not seen the solution moving back and forth between repulsive impurities but rather a large stationary single breather.

References

[1] Kivshar YS, Gredeskul SA, Sanchez A, Vázquez L. Localization decay induced by strong nonlinearity in disordered systems. Phys Rev Lett 1990;64:1693.
[2] Braun OM, Kivshar YS. Nonlinear dynamics of the Frenkel–Kontorova model. Phys Rep 1998;306:1.
[3] Aubry S. A unified approach to the interpretation of displacive and order-disorder systems. II. Displacive systems. J Chem Phys 1976;64:3392.
[4] Wahlstrand KJ. Computer simulation studies of soliton models for dielectric relaxation in crystalline polyethylene and related polymers. I. Continuum and pinned limits. J Chem Phys 1985;82:5247.
[5] Cuevas-Maraver J., Kevrekidis P.G., Williams F., editors. The sine-Gordon model and its applications: from Pendula and Josephson junctions to gravity and high-energy physics. Springer, Berlin; 2014.
[6] Iizuka T, Amie H, Hasegawa T, Matsuoka C. Numerical studies on scattering of the NLS soliton due to an impurity. Phys Lett A 1996;220:97.
[7] Shadkhoo S, Bruinsma R. Impurities in Bose–Einstein condensates: from polaron to soliton. Phys Rev Lett 2015;115:159903.
[8] Palmero F, Archilla JFR, Hennig D, Romero FR. Effect of base-pair inhomogeneities on charge transport along the DNA molecule, mediated by twist and radial polarons. New J Phys 2004;6:13.
[9] Watanabe T, Kanamori Y, Yajima N. Reflection of ion-acoustic waves and solitons. J Phys Soc Jpn 1989;58:1273.
[10] Tong D, Wong K. Instantons, Wilson lines, and D-branes. Phys Rev D 2015;91:026007.
[11] Chen Z, Huang J, Chai J, Zhang X, Li Y, Malomed BA. Discrete solitons in self-defocusing systems with PT-symmetric defects. Phys Rev A 2015;91:053821.
[12] Suchkov SV, Sukhorukov AA, Dmitriev SV, Kivshar YS. Scattering of the discrete solitons on the PT-symmetric defects. Europhys Lett 2012;100:54003.
[13] Abdullaev FK, Brazhnyi VA, Salerno M. Scattering of gap solitons by PT-symmetric defects. Phys Rev A 2013;88:043829.
[14] Saadatmand D, Dmitriev SV, Borisov DI, Kevrekidis PG. Interaction of sine–Gordon kinks and breathers with a parity-time-symmetric defect. Phys Rev E 2014;90:052902.
[15] Morales-Molina L, Vicencio RA. Trapping of discrete solitons by defects in nonlinear waveguide arrays. Opt Lett 2006;31:966.
[16] Palmero F, Carretero-Gonzalez R, Cuevas-Maraver J, Kevrekidis PG, Krolikowski W. Solitons in one-dimensional nonlinear Schrödinger lattices with a local inhomogeneity. Phys Rev E 2008;77:036614.
[17] Al-Marzoug SM. Scattering of a discrete soliton by impurity in dipolar Bose–Einstein condensates. Int J Mod Phys B 2014;28:1450214.
[18] Yue H, Molina MI, Kevrekidis PG, Karachalios NI. Self-trapping transition for a nonlinear impurity within a linear chain. J Math Phys 2014;55:102703.
[19] Brazhnyi VA, Jisha CP, Rodrigues AS. Interaction of discrete nonlinear Schrödinger solitons with a linear lattice impurity. Phys Rev A 2013;87:013609.
[20] Adamatzky A. Computing in nonlinear media and automata collectives. IoP Publishing; 2001.
[21] Scott AC. Davydov's soliton. Phys Rep 1992;217:1.
[22] Förner W. Quantum and disorder effects in Davydov soliton theory. Phys Rev A 1991;44:2694.
[23] Förner W. Davydov soliton dynamics: two-quantum states and diagonal disorder. J Phys 1991;3:3235.
[24] Tchameu JDT, Motcheyo ABT, Tchawoua C. Mobility of discrete multibreathers in the exciton dynamics of the Davydov model with saturable nonlinearities. Phys Rev E 2014;90:43203.
[25] Motcheyo ABT, Tchawoua C, Siewe MS, Tchameu JDT. Multisolitons and stability of two hump solitons of upper cutoff mode in discrete electrical transmission line. Phys Lett A 2011;375:1104.
[26] Mitchell M, Segev M, Christodoulides DN. Observation of multihump multimode solitons. Phys Rev Lett 1998;80:4657.
[27] Flach S, Willis CR. Discrete breathers. Phys Rep 1998;295:181.
[28] Davydov AS. Soliton and energy transfer along protein molecules. J Theor Biol 1977;66:379.
[29] Kundu K. Perturbative study of classical Ablowitz-Ladik type soliton dynamics in relation to energy transport in a-helical proteins. Phys Rev E 2000;61:5839.
[30] MacNeil L, Scott AC. Launching a Davydov soliton: II. Numerical studies. Phys Scr 1984;29:284.
[31] Marín JL, Aubry S. Breathers in nonlinear lattices: numerical calculation from the anticontinuous limit. Nonlinearity 1996;9:1501.
[32] Kalosakas G. Multi-peaked localized states of DNLS in one and two dimensions. Physica D 2006;216:44.
[33] Xiao-feng P. Improvement of the Davydov theory of bioenergy transport in protein molecular systems. Phys Rev E 2000;62:6989.
[34] Li P, Li L, Malomed BA. Multisoliton Newton's cradles and supersolitons in regular and parity-time-symmetric nonlinear couplers. Phys Rev E 2014;89:062926.
[35] Homma S, Takeno S. Soliton scattering by an impurity on a nonlinear lattice. Phys Lett A 1992;169:355.